The non-motor protein RHAMM locates TPX2 to coordinate spindle assembly and balance motor forces needed to segregate chromosomes and complete cell division

by

Helen Chen

B.Sc., The University of British Columbia, 2010

A THESIS SUBMITTED IN PARTIAL FULFILLMENT OF

THE REQUIREMENTS FOR THE DEGREE OF

DOCTOR OF PHILOSOPHY

in

THE FACULTY OF GRADUATE AND POSTDOCTORAL STUDIES

(Experimental Medicine)

THE UNIVERSITY OF BRITISH COLUMBIA

(Vancouver)

December 2016

Abstract

Cell division requires the assembly and organization of a microtubule-based mitotic spindle. Microtubule assembly at multiple sites is dependent on Aurora kinase A activity, which is promoted through a complex with TPX2 (targeting protein for XKlp2). Subsequent organization of these microtubules and progression into anaphase requires balance between forces orchestrated by antagonistic motor complexes. My studies show that the non-motor protein RHAMM (receptor for hyaluronan mediated motility) integrates structural and biochemical pathways to ensure the fidelity of cell division.

Silencing RHAMM in HeLa cells delayed the kinetics of spindle assembly. I located RHAMM to centrosomes and non-centrosome sites for microtubule nucleation and found it necessary for TPX2 localization and Aurora A activity at kinetochores. The RHAMM-TPX2 complex requires a conserved leucine zipper motif in RHAMM and a domain that includes the nuclear localization signal in TPX2. These findings indicate RHAMM is needed for spatially-regulated activation of Aurora A by TPX2, which coordinates spindle assembly.

I monitored mouse embryonic fibroblasts deficient for RHAMM through division and identified defects progressing through the spindle checkpoint. In RHAMM-silenced HeLa cells, I identified sustained activation of the checkpoint with unfocused spindles and unattached kinetochores, implicating unbalanced motor activities mediated by kinesins. In metaphase-delayed cells, the abundance or location of checkpoint proteins was not altered. Moreover, aberrant spindle orientation could not account for each delayed division. In RHAMM-silenced cells, I found that the reciprocal immunoprecipitation of Eg5-TPX2, an inhibitory complex, was reduced and that the concurrent inhibition of Eg5-generated force recovered division kinetics. I

also observed a prolonged metaphase delay in a proportion of RHAMM-silenced cells, which resolved through cohesion fatigue. Together, my findings indicate that RHAMM-mediated attenuation of Eg5-dependent outward forces is needed to align chromosomes and progress through division.

Lastly, I identified defects in spindle structure and function in redundant models for RHAMM over-expression. Collectively, my studies demonstrate that RHAMM coordinates Aurora A signaling and balances motor forces that are needed for cell division. These findings provide novel insights into processes that are essential for mammalian cell division and the maintenance of genome stability.

Preface

I performed the majority of the experiments and data analyses presented in Chapters 3-5, with the following exceptions:

Parts of the work presented in Chapter 3 were published in: **H. Chen**, P. Mohan, J. Jiang, O. Nemirovsky, D. He, M. Fleisch, D. Niederacher, L. Pilarski, C.J. Lim, and C.A. Maxwell. Spatial regulation of Aurora A activity during mitotic spindle assembly requires RHAMM to correctly localize TPX2. *Cell Cycle* 2014; 13(14):2248-61. Dr. Maxwell and I designed the study and wrote the manuscript. Dr. Lim and DH assisted in FRET imaging. Dr. Fleisch, Dr. Niederacher and Dr. Pilarski provided reagents and expertise. PM made the lentivirus containing shRNA against TPX2. JJ and ON assisted in data analysis.

HeLa cells with inducible GFP-RHAMM expression were generated by Dr. Brian Taylor in Dr. Linda Pilarski's laboratory (Cross Cancer Institute, Canada). Mouse embryonic fibroblasts were collected from RHAMM-deficient embryos generated in the Maxwell lab through a collaboration with the Mouse Animal Production Service (CMMT, Canada).

Table of Contents

List of Tables

List of Figures

List of Abbreviations

APC/C	anaphase promoting complex/cyclosome
BRCA1	Breast cancer 1, early onset protein
BSA	bovine serum albumin
bZip	basic leucine zipper
cDNA	complementary DNA
CENPA	Centromere protein A
CC	Coriell Cell
DAPI	4’,6-diamidino-2-phenylindol
DMEM	Dulbecco’s modified Eagle medium
DMSO	dimethyl sulfoxide
DNA	deoxyribonucleic acid
FBS	fetal bovine serum
FRET	fluorescence resonance energy transfer
GAPDH	Glyceraldehyde 3-phosphate dehydrogenase
GDP	guanine diphosphate
GFP	green fluorescence protein
GTP	guanine triphosphate
Hklp2	Human kinesin-like protein 2
HMMR	Hyaluronan mediated motility receptor (gene)
Kt-MT	kinetochore-microtubule
NHP	non-hairpin

MAP	microtubule-associated proteins
MEF	mouse embryonic fibroblast
MCC	mitotic checkpoint complex
MVA	mosaic variegated aneuploidy
PCM	pericentriolar material
PBS	phosphate buffered saline
PLK1	Polo-like kinase 1
qPCR	quantitative polymerase chain reaction
qRT-PCR	quantitative reverse-transcription polymerase chain reaction
RHAMM	Receptor for hyaluronan mediated motility (protein)
RNA	ribonucleic acid
SAF	spindle assembly factor
SD	standard deviation
SDS	sodium dodecyl sulfate
SEM	standard error of the mean
shRNA	small hairpin RNA
siRNA	small interfering RNA
TBP	TATA-binding protein
TPX2	Targeting protein for Xklp2
TuRC	γ-tubulin ring complex
XRHAMM	*Xenopus* RHAMM
XKlp2	*Xenopus* kinesin-like protein 2

Acknowledgements

This dissertation is made possible with the help and support of many wonderful people. Foremost, I would like to express my deepest gratitude to my supervisor, Dr. Christopher Maxwell for his guidance, support and kindness. I thank him for recognizing my strengths and weaknesses, and for providing me with a rewarding graduate school experience that led to both personal and professional growth. I am forever grateful for this opportunity. I would also like to thank my supervisory committee, Dr. C. James Lim, Dr. Catherine Pallen and Dr. Nelly Panté for their input and advice on my research, and for constantly challenging me.

To members of the Maxwell lab, both past and present, I am grateful for their help and support, especially for letting me use their microscope times. I would also like to thank all the trainees at CFRI for lending me an ear on a rough day, or an antibody on a Saturday night.

Last but not least, I would like to thank my family and friends for their patience and understanding during challenging times. To my parents, everything is made possible because of you.

Dedication

This work is dedicated to my parents for their unwavering support and unconditional love.

Chapter 1: Introduction

1.1 Mitosis

There are 37 trillion (estimated) cells in the human body (Bianconi et al., 2014). Through multiple rounds of coordinated cell division, or mitosis, one zygote cell develops into a multicellular organism. Mitosis occurs throughout an organism's life: during development and growth, cell numbers increase to form a specialized multicellular organism; during adulthood, regulated mitosis ensures cell replacement and regeneration. Successful mitosis is characterized by the faithful segregation of duplicated chromosomes from the mother cell into two daughter cells.

1.1.1 Chromosome organization during mitosis

The packaging of genetic information differs dramatically between interphase and mitosis. During interphase, individual chromosomes and complexed proteins (i.e. chromatin) occupy discrete territories. As the cell enters mitosis, chromatin condenses into visible loops and coils, and individual chromosomes become distinguishable. Mitosis is divided into five distinct stages: prophase, prometaphase, metaphase, anaphase and telophase/cytokinesis (Fig. 1.1). These phases are characterized by the physical state of both the chromosomes and the mitotic spindle, a microtubule-based machine that captures, aligns and segregates chromosomes during division.

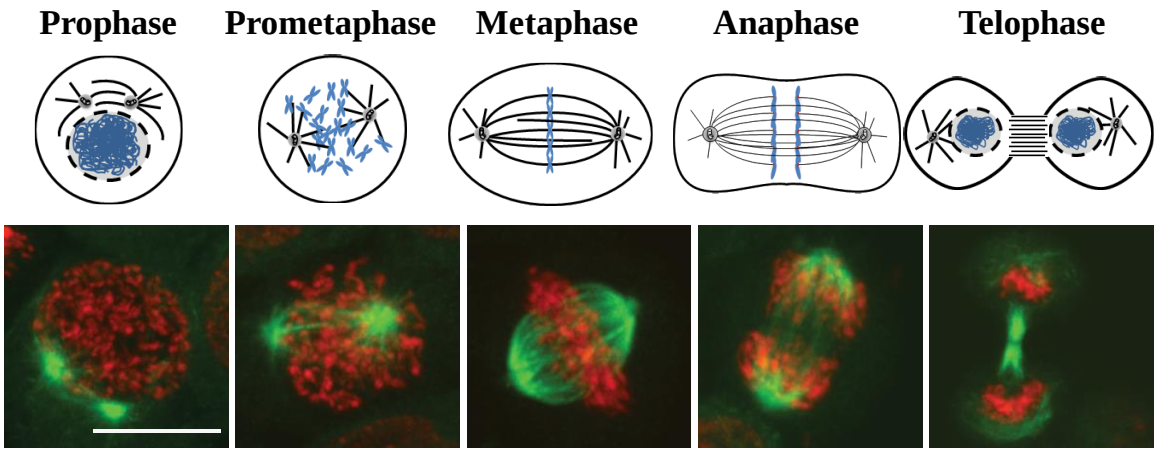

Figure 1.1 Phases of mitosis in HeLa cells.

Schematics and the corresponding fluorescence microscopy images showing the different phases of mitosis. In the fluorescent images (bottom row), DNA (DAPI) is labelled in red and the mitotic spindle (tubulin) is labelled in green. During prophase, the DNA starts to condense, while duplicated centrosomes, which are the major microtubule nucleation structures, start to move apart to opposite sides of the nucleus. At the end of prophase, the nuclear envelope begins to breakdown, which allows microtubules to interact with the chromosomes. During prometaphase, -microtubule nucleation surges throughout the cell to build the mitotic spindle. During metaphase, each sister chromatid is attached to microtubules originating from opposing sides of the spindle. As a consequence, all chromosomes are aligned in the middle of the cell. During anaphase, the cohesion that holds the sister chromatids together is cleaved. Sister chromatids are pulled towards opposite sides of the cell so that both daughter cell ends up with an identical set of chromosomes. During telophase, the final stage of mitosis, chromosomes decondense and the nuclear membrane reforms. Concurrently, the cell membrane ingresses between the two nuclei, which is followed by abscission to physically separate the two daughter cells. Scale bar= 10 μm.

1.1.2 Chromosome cohesion during early mitosis

Prior to mitosis, the entire genome is duplicated during S-phase, and the duplicated sister chromatids are held together by the cohesin complex at the centromere. The cohesin complex is composed of four subunits of the SMC (structural maintenance of chromosomes) family of proteins: Smc1, Smc3, Scc1 and Scc3 (Dej and Orr-Weaver, 2000; Hirano, 2000; Kschonsak and Haering, 2015; Nasmyth et al., 2000; Naumova et al., 2013). The cohesin complex forms a "V" shaped structure, which functions as a physical bridge that holds sister chromatids together at centromeres (Akhmedov et al., 1998). During prophase, condensin, another member of the SMC family of proteins, promotes the looping of linear chromatin segments, which will facilitate subsequent chromosome movement (Hirano, 2000; Koshland and Strunnikov, 1996; Kschonsak and Haering, 2015; Nasmyth et al., 2000; Naumova et al., 2013). Together, these two distinct processes, sister cohesion and DNA condensation, forms the iconic "X" shaped chromosomes visible during mitosis.

The cohesin complex will hold sister chromatids together until anaphase when the action of an E3 ubiquitin ligase known as the anaphase-promoting complex/cyclosome (APC/C) severs the cohesion between sister chromatids. The APC/C recognizes its substrates via degradation motifs, such as the D-box and the KEN-box, and marks substrates to be degraded by the 26S proteasome through the ubiquitination pathway (Townsley and Ruderman, 1998). During cohesion release, the APC/C promotes the degradation of securin (Nasmyth, 2002) and cyclin B (Kraft et al., 2003). Securin binds to and inhibits the enzymatic activity of separase, which is able to cleave the cohesin complex (Ciosk et al., 1998). Separase activity can also be inhibited by

cyclin B/Cdk1-mediated phosphorylation. Thus, degradation of cyclin B and securin by APC/C is needed for optimal separase activity and subsequent cleavage of the cohesion complex and entry into anaphase (Castro et al., 2005; Clute and Pines, 1999; Zur and Brandeis, 2001).

Prior to anaphase, chromosomes must first be aligned at the cell equator during metaphase. To accomplish this, each chromosome is attached to microtubules originating from the opposing poles of the mitotic spindle. This process involves highly accurate interactions between chromosomes and mitotic microtubules originating from multiple sites in the dividing cell, including the spindle poles and the chromosomes. At the metaphase to anaphase transition, a highly conserved checkpoint mechanism, known as the spindle checkpoint, monitors chromosome attachments and suppresses APC/C activity until all chromosomes are aligned, which is described in more detail in section 1.3.

1.1.3 Chromosome segregation during mitotic exit

During anaphase, the loss of chromosome cohesion enables the movement of each chromatid to opposite sides of the dividing cell. Anaphase is further separated into two stages: anaphase A and anaphase B. During anaphase A, microtubules proximal to chromosomes shorten and pull the two subsets of daughter chromatids apart and towards opposite sides of the cell (Gadde and Heald, 2004; Tanenbaum and Medema, 2010; Walczak and Heald, 2008; Wittmann et al., 2001). In anaphase B, longer microtubules slides past each other and, as a result, the spindle poles further separate and the cell elongates (Gadde and Heald, 2004; Tanenbaum and Medema, 2010; Walczak and Heald, 2008; Wittmann et al., 2001). Moreover, the central region

of the mitotic spindle is reorganized to form the midzone spindle, which determines the site of the cytokinesis furrow (Tanenbaum and Medema, 2010; Walczak and Heald, 2008; Wittmann et al., 2001).

During telophase/cytokinesis, the final act of mitosis, the cell membrane ingresses to form a cleavage furrow at the equatorial cortex, where cytoplasmic contents are partitioned between two daughter cells (Fededa and Gerlich, 2012; Rappaport, 1971). The cleavage furrow will continue to constrict until the contractile ring, composed of actin filaments and myosin II, reaches a diameter between 1 - 2 μm (Fededa and Gerlich, 2012; Rappaport, 1971), after which, Golgi- and endosome-derived vesicles accumulate at the midbody to promote membrane abscission (Goss and Toomre, 2008; Gromley et al., 2005; Schiel et al., 2011). At the completion of mitosis, the nuclear envelope is reformed from membrane vesicles of the mother cell's nuclear envelope and the chromosomes decondense (Kschonsak and Haering, 2015; Naumova et al., 2013).

1.1.4 Outstanding questions

Walther Flemming (1878) first coined the term “mitosen” due to the threadlike appearance of chromosomes observed during salamander egg cell division. I have only briefly summarized our current knowledge of mitosis in order to highlight two key points: 1) chromosome movement is highly dynamic and dictated by microtubules and associated proteins that compose the mitotic spindle; and, 2) multiple mechanisms are at play to ensure equal segregation of the genome. While we understand many aspects of mitosis, this thesis aims to address key outstanding questions related to how the mitotic spindle is built and stabilized at specific sites in the dividing cell (reviewed in Section 1.2); and, what proteins coordinate the spindle checkpoint and protect genome fidelity by monitoring and enabling (or disabling) entry into anaphase (reviewed in Section 1.3).

1.2 Building and stabilizing the mitotic spindle

The mitotic spindle is the macromolecular machine responsible for capturing, aligning and segregating duplicated chromosomes. The mitotic spindle is primarily composed of antiparallel arrays of microtubules, which are hollow cylinders composed of 13 protofilaments assembled from α/β-tubulin heterodimers arranged in a head-to-tail fashion. The organization of microtubules produces an intrinsic polarity within each protofilament, defined by a plus-end (where β-tubulin is exposed for the addition of new tubulin subunits and microtubule elongation) and a minus-end (where α-tubulin is exposed for tubulin removal and microtubule shrinkage) (Mitchison and Kirschner, 1984). This intrinsic polarity enables the directional movement of molecular motors, which in turn enable directed force generation (Desai and Mitchison, 1997). During mitosis, microtubule nucleation occurs at various locations in the dividing cell (Duncan and Wakefield, 2011; Meunier and Vernos, 2012; Walczak and Heald, 2008) and these newly made microtubules must be: 1) stable enough to maintain the overall structure of the spindle; and, 2) dynamic enough to direct chromosome movement. These two attributes (i.e., stability and movement) are ensured by microtubule-associated proteins and protein complexes, including molecular motor proteins and non-motor adapter proteins.

1.2.1 Centrosomes separate during prophase to generate a bipolar spindle

In a typical somatic mammalian cell, the formation of a bipolar spindle is initiated by the separation of duplicate centrosomes during prophase. The centrosome is a non-membrane enclosed organelle composed of a pair of centrioles surrounded by a cloud of proteinous material

called the pericentriolar material (PCM). The centrosome nucleates and organizes microtubule arrays (Bornens, 2012; Doxsey, 2001; Nigg, 2002) and is duplicated along with the chromosomes during S-phase (Meraldi and Nigg, 2002; Nigg and Stearns, 2011). During prophase, the two duplicated centrosomes separate by moving along the nuclear envelope to form the opposing poles of the mitotic spindle (Tanenbaum and Medema, 2010). This movement is enabled by molecular motor complexes that slide microtubules relative to each other (Fig. 1.2).

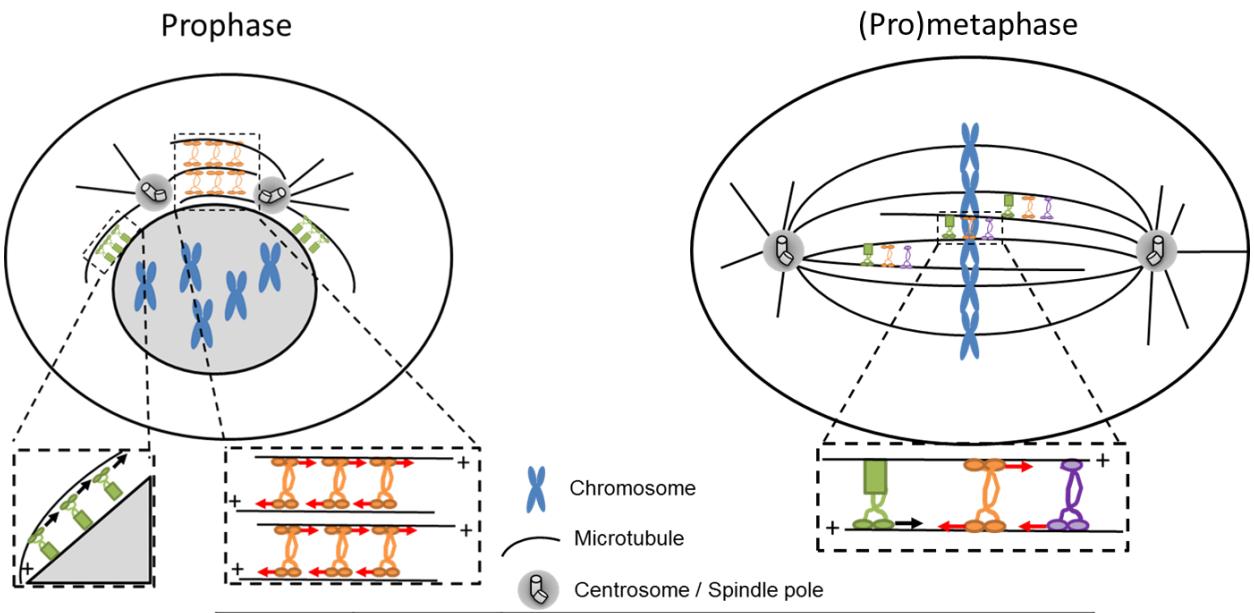

	Name	Directionality	Description
	Dynein	- (minus end)	Dynein is a multisubunit motor. Dynein is located at specific regions of the cell cortex, as well as spindle poles, spindle microtubules and near kinetochores. Dynein functions and locations are dependent on interactions with adapter proteins.
	Eg5	+ (plus end)	Eg5 is a member of the kinesin 11 family. Eg5 is a homotetramer that cross-links two anti-parallel microtubules simultaneously and slides them apart. This feature allows Eg5 to participate in centrosome separation and spindle bipolarity maintenance.
	Kif15/Hklp2	+ (plus end)	Kif15 is a member of the kinesin 15 family. Kif15 exists as a dimer, thus can only bind to one microtubule at a time. However, Kif15 can interact with TPX2 and use TPX2 to bind one microtubule while also sliding another microtubule with the Kif15 motor domain.

Figure 1.2 Motor protein movements during spindle assembly.

During prophase, centrosome separation is driven by Eg5- and dynein-mediated forces along the nuclear envelope. During prometaphase and metaphase, dynein activity is antagonized by Eg5 and Kif15 to establish a balance of force along the mitotic spindle. Adapted with permission from J. Raaijmakers (Raaijmakers, 2014).

Kinesin-5 (aka Eg5) is a highly conserved plus-end motor that acts as a tetramer and drives centrosome separation (Cole et al., 1994; Kapitein et al., 2005; Kashina et al., 1996). When the two centrosomes are in close proximity, microtubules emanating from each organelle will overlap and Eg5 tetramers will cross-link and slide these microtubules to push the duplicated centrosomes apart (Kapitein et al., 2005; Kashina et al., 1996). While Eg5 is the main driver for centrosome separation, and its loss of function results in monopolar spindles (Tanenbaum et al., 2008; Whitehead et al., 1996; Woodcock et al., 2010), other motor proteins may be involved in this process. In *Drosophila,* inhibition of Eg5/Klp61F does not affect centrosome separation in prophase, although it is essential for subsequent spindle assembly (Sharp et al., 1999). In both *Xenopus* and mammalian cells, the plus-end directed motor *Xenopus* kinesin-like protein 2 (Xklp2/Hklp2/Kif15) cooperates with Eg5 and is sufficient to fully separate centrosomes (Tanenbaum et al., 2009; Vanneste et al., 2009). Unlike Eg5, Kif15 exists as a dimer and requires an adapter protein, termed targeting protein for *Xenopus* kinesin-like protein 2 (TPX2), to cross-link and slide microtubules (Raaijmakers et al., 2012; Tanenbaum et al., 2009; Vanneste et al., 2009; Wittmann et al., 1998). Interestingly, TPX2 targets Kif15, a plus-end-directed motor, to microtubule minus ends located at the spindle poles by forming a complex with dynein, a minus-end directed motor (Wittmann et al., 1998). Dynein may also promote centrosome separation through two proposed mechanisms. First, dynein that is anchored at the cortex may act on centrosome-anchored microtubules to pull and separate centrosomes (Sharp et al., 2000). Second, dynein that is recruited to the nuclear envelope may pull along the nuclear membrane to direct the two centrosomes towards opposite sides of the cell (Salina et al., 2002; Splinter et al., 2010). Thus, centrosome separation requires the balanced and antagonistic activities of plus-end directed and minus-end directed motor protein complexes acting along mitotic microtubules.

1.2.2 Mitotic microtubules assemble at centrosomes to form the spindle

After nuclear envelope break down, mitotic microtubules are rapidly assembled at various sites within the cell and organized into a distinct bipolar array termed the mitotic spindle (Bornens, 2012; Meunier and Vernos, 2012; Tanenbaum and Medema, 2010; Walczak and Heald, 2008). Different subclasses of microtubules contribute to different spindle functionality and the overall success of cell division (Duncan and Wakefield, 2011; Meunier and Vernos, 2012; Walczak and Heald, 2008).

In a typical mammalian somatic cell, the centrosome is the main microtubule organizing center and the duplicated, separate mitotic centrosomes constitute the spindle poles and facilitate the bipolar nature of the mitotic spindle (Nigg and Stearns, 2011). Microtubule nucleation at centrosomes is initiated by a specialized type of tubulin called γ-tubulin. Structures known as the γ-tubulin ring complex (γ-TuRC) at the centrosome provide a template for the initial addition of α/β tubulin heterodimers (Zheng et al., 1995). Nucleation capacity at the centrosomes surges during prophase and prometaphase through recruitment of more γ-TuRC to centrosomes, as well as other spindle assembly factors (SAFs) (Bornens, 2012; Compton, 2000; Duncan and Wakefield, 2011; Meunier and Vernos, 2012; Walczak and Heald, 2008). Different mitotic kinase complexes, from the families of Aurora kinases (Aurora A, B, and C), NEKs [NIMA (never in mitosis in *Aspergillus nidulans*)-related kinases] and Polo-like kinases (PLK1-4), are recruited to centrosomes and their activities promote centrosome duplication, microtubule nucleation and cell cycle progression. Thus, the proper regulation of these kinases is crucial in ensuring successful cell division.

Centrosome-derived, or astral, microtubules establish a directional bias; that is, the density of microtubule fibers emanating from the centrosome towards the chromosomes is greater than those emanating towards the cell cortex (Bird and Hyman, 2008; Wang et al., 2014). This density bias requires the action of scaffolding proteins (i.e., non-motor adapters and motor complexes) and plays an important role in positioning the spindle during chromosome segregation and cytokinesis. Astral microtubules probe the cytoplasm and capture individual chromosomes on a specialized protein structure called the kinetochore (Chan et al., 2005). The attached chromosome will have a mono-oriented configuration, because it is attached to only one spindle pole, and will oscillate within the cytoplasm until the sister chromatid becomes attached to the opposite spindle pole (Kirschner and Mitchison, 1986). This process is known as the "search and capture" model (Kirschner and Mitchison, 1986). According to the model, successful "search and capture" depends on the dynamic nature of astral microtubules, which allow the microtubules to sample a large area in search of a chromosome; if it fails to capture a chromosome, that particular microtubule is rapidly depolymerized (Walczak et al., 2010). However, computational analysis demonstrates the "search and capture" model is restricted by the size of the cell as well as the number of chromosomes (Wollman et al., 2005), suggesting that additional mechanisms ensure bipolar chromosome attachment.

Analysis of various systems that lack centrosomes, such as oocyte divisions in mice (Calarco-Gillam et al., 1983), *Drosophila* (Matthies et al., 1996) and *Xenopus* (Heald et al., 1996), indicate alternative or additional pathways contribute to mitotic spindle assembly. Furthermore, functional spindles can be built after laser ablation or physical displacement of both centrosomes (Khodjakov et al., 2000; Steffen et al., 1986). In *Drosophila,* Centrosomin (*cnn)*-

null mutants fail to initiate microtubule nucleation at centrosomes, however, a bipolar spindle is still observed and these larvae are able to reach adulthood with few observable defects in morphology or developmental timing (Megraw et al., 2001). In monkey CVG-2 cells, laser ablation of both centrosomes does not disrupt bipolar spindle assembly (Khodjakov et al., 2000). These findings demonstrate that non-centrosomal microtubules are sufficient to construct a bipolar mitotic spindle.

1.2.3 Mitotic microtubules assemble at/near kinetochores to form the spindle

A second model, termed "self-organization", was hypothesized to explain bipolar spindle assembly in the absence of centrosomes. The first experimental evidence that suggests chromosomes may have a role in microtubule nucleation came from Karsenti and Kirschner, when they showed that injecting *E. coli* DNA into *Xenopus* oocytes was sufficient to trigger microtubule nucleation (Karsenti et al., 1984). Subsequent investigations demonstrate that DNA-coated beads can induce bipolar spindle assembly in *Xenopus* egg extracts, which supports the idea that chromosomes are self-sufficient in mitotic spindle assembly and organization (Heald et al., 1996).

Chromosome-mediated microtubule nucleation involves a small GTPase termed Ran, which also regulates nucleo-cytoplasmic transport during interphase via the importin α/β complex (Clarke and Zhang, 2008). In the nucleus during interphase, a high concentration of the GTP- bound form of Ran (Ran-GTP) liberates newly imported cargos from importin-β (Ohtsubo et al., 1989, 1987). During interphase, Ran GTPase-activating protein 1 (RanGAP1) in the

cytoplasm catalyzes the hydrolysis of GTP to GDP and promotes binding between the importin α/β complex and its cargo (Ohtsubo et al., 1989, 1987). Near chromosomes during prometaphase, a chromatin-bound guanine exchange factor (GEF), called regulator of chromosome condensation 1 (RCC1), locally establishes a high concentration of Ran-GTP (Ohtsubo et al., 1989, 1987). During the process of spindle assembly, the high concentration of Ran-GTP near the chromosomes establishes a gradient that triggers the local release of SAFs from the importin α/β complex (Gruss et al., 2002; Ribbeck et al., 2006; Wittmann et al., 2000; Wong and Fang, 2006). As an example, the Ran-GTP gradient liberates TPX2, which triggers spindle assembly around chromosomes (Gruss et al., 2002, 2001; Tulu et al., 2006). Subsequent studies show that TPX2 may also promote microtubule bundling to organize these kinetochore fibers, or K-fibers (Schatz et al., 2003). Injection of importin-β and depletion of TPX2 reduces microtubule nucleation at kinetochores and increases microtubule depolymerization (Tulu et al., 2006). While additional SAFs have been shown to stabilize/organize microtubules in response to Ran-GTP (eg. HURP, NuSAP, MCRS1) (Koffa et al., 2006; Meunier and Vernos, 2011; Ribbeck et al., 2006; Santarella et al., 2007; Wong and Fang, 2006), TPX2 is unique for its microtubule nucleation capacity.

Bipolar spindle assembly in systems lacking centrosomes takes much longer, and the spindle fibers undergo a number of intermediate structures before being organized into a bipolar structure (Duncan and Wakefield, 2011). For example, motor proteins must cross-link antiparallel K-fibers and sort these microtubules into bipolar arrays, similar to the process observed during centrosomal spindle assembly (Compton, 1998).

1.2.4 Motor protein complexes cross-link microtubules and maintain spindle bipolarity

Once assembled, microtubules must be focused at spindle poles to maintain spindle bipolarity in cells with and without centrosomes. The minus-ends of newly formed microtubules are stabilized and cross-linked at spindle poles by microtubule associated proteins (MAPs), including motor and non-motor proteins.

TPX2, which accumulates at metaphase spindle poles in a dynein-dynactin dependent manner, cross-links microtubules through high affinity binding (Garrett et al., 2002; Wittmann et al., 2000) and is critical to focus the spindle. In mitotic *Xenopus* egg extracts, TPX2 depletion reduced microtubule density and resulted in abnormal fragmented poles, whereas addition of excess TPX2 resulted in dense monopolar spindles and ectopic microtubule asters (Wittmann et al., 2000). TPX2 function at spindle poles is regulated by partner proteins, including Kif15 (Wittmann et al., 1998), Eg5 (Uteng et al., 2008), Aurora A (Kufer et al., 2002) and another MAP called RHAMM (receptor for hyaluronan mediated motility) (Maxwell et al., 2005, 2003). For example, expressing a C-terminal truncation of TPX2, which interrupts the Eg5 interaction domain within TPX2, results in spindle fragmentation and multipolarity (Ma et al., 2011). The importance of TPX2-RHAMM and TPX2-Aurora A interactions will be discussed in detail in later sections.

The actions of all non-motor proteins during spindle assembly (eg. MCRS1-MCAK (Meunier and Vernos, 2011), TACC3/ch-TOG/clathrin (Booth et al., 2011)) will not be reviewed, but I will briefly outline the role of nuclear mitotic apparatus protein (NuMA), an adapter for the minus-end motor dynein. NuMA is a large coiled-coil protein located at mitotic

spindle poles (Gaglio et al., 1996, 1995; Merdes et al., 1996). Cytoplasmic dynein and NuMA complex with dynactin to anchor one microtubule relative to an adjacent sliding microtubule (Gaglio et al., 1996; Merdes et al., 1996), and tether centrosomes to the microtubule matrix (Khodjakov et al., 2003). In cultured cells, the disruption of NuMA function results in unfocused spindles and delays mitotic progression (Gaglio et al., 1996, 1995). In mice, genetic deletion of NuMA displaces the centrosome from microtubules at spindle poles and results in unfocused K-fibers (Silk et al., 2009). Together, these findings highlight the important role non-motor microtubule-associated proteins play in regulating motor activities and maintaining spindle integrity.

For over 35 years, it has been appreciated that chromosomes can initiate microtubule nucleation independent of centrosomes in mammalian tissue culture cells. It is now widely accepted that microtubules can nucleate at different sites within the dividing mammalian cell, and different subsets of microtubules may play different roles within the functional spindle. The relative contribution from the "search-and-capture" and "self-organization" pathways vary in different systems: abolishing or perturbing the Ran-GTP gradient results in more severe spindle defects in egg extracts (Caudron et al., 2005) than in mammalian cells (Kaláb et al., 2006). While spatial and temporal regulation of the Ran-mediated spindle assembly pathway is best described in *Xenopus* egg extracts, an important goal for cell biology is to uncover the molecular regulators of this process in mammalian cells. Chapter 3 reveals RHAMM as a critical determinant of Aurora A-mediated microtubule assembly near kinetochores through the stabilization and localization of TPX2.

1.3 Bipolar chromosome segregation is safeguarded by the assembly checkpoint

It is vital to maintain genome stability during cell division. Genome instability refers to increased tendency of alterations to the genome, a characteristic of all cancer cells (Negrini et al., 2010). Most cancer cells harbor a form of genome instability called chromosome instability, which refers to changes in chromosome structure and number resulting from abnormal mitoses (Negrini et al., 2010). For this reason, multiple cellular processes ensure equal segregation of chromosomes, including safeguards during chromosome duplication prior to mitosis and chromosome alignment (ie. the spindle checkpoint) prior to mitotic exit. Equal chromosome segregation requires each sister chromatid within a pair to form stable kinetochore-microtubule (Kt-MT) attachment to opposing spindle poles, which will produce tension across sister kinetochores due to pulling forces exerted by spindle microtubules (Zhou, 2002). Satisfaction of the spindle assembly checkpoint relies on these two criteria: the attachment of chromosomes to kinetochores and the tension exerted across kinetochores.

1.3.1 Chromosome attachment at kinetochores is monitored to ensure bipolarity

The kinetochore, a multi-protein platform, is the site on centromeric DNA where mitotic microtubules attach with chromosomes. These attachments involve a complex interplay between motor proteins, kinetochore proteins and spindle microtubules. K-fibers are the main sub-class of microtubules involved in chromosome attachment (Khodjakov et al., 2003). The kinetochore uses a conserved KNL1-Mis12-NDC80 (KMN) network to attach to the plus end of K-fiber

microtubules and form bipolar or amphitelic attachments (Cheeseman and Desai, 2008; Joglekar et al., 2010).

The KMN network is critical to the maintenance and satisfaction of the spindle assembly checkpoint. First, the KMN network enables microtubule attachments to the kinetochore, which can be lateral or end-on (Joglekar et al., 2010). Lateral attachment refers to when a kinetochore encounters a microtubule lattice, while end-on attachments occur when a kinetochore attaches to microtubule ends. Lateral attachments are initially made during prometaphase, but are then converted to end-on attachments during metaphase to ensure 20-30 microtubules are attached to each mature kinetochore within the bipolar spindle (Shrestha and Draviam, 2013). The NDC80 complex is the main component involved in microtubule binding, with high affinity for straight microtubules and low affinity for curled microtubules, suggesting attachments are made preferentially with stabilized microtubules (Alushin et al., 2010). The Mis12 and KNL1 complexes serve as the platform for assembly of kinetochore proteins (Cheeseman et al., 2006; Kline et al., 2006) and recruitment of spindle checkpoint proteins (Cheeseman and Desai, 2008; Kiyomitsu and Cheeseman, 2012), respectively, but have low affinity for microtubules (Cheeseman et al., 2006). NDC80 molecules on adjacent microtubules can also cluster together to serve as microtubule cross-linkers (Alushin et al., 2012, 2010).

The final end-on Kt-MT attachment must be strong and dynamic. Kt-MT attachments must transduce forces exerted by spindle microtubules and motors during chromosome alignment and segregation. Simultaneously, Kt-MT attachments need to be dynamic enough to be depolymerized in the event of misattachment, which are not amphitelic attachments. The robust, yet flexible nature of Kt-MT attachment is achieved by antagonistic motor proteins at the

kinetochore. In particular, cytoplasmic dynein located at kinetochores has been implicated in the initial microtubule capturing and fast-gliding prior to end-on attachment formation (Pfarr et al., 1990; Rieder and Alexander, 1990; Varma et al., 2008). A high concentration of dynein is found on unattached kinetochores, and these complexes are released once kinetochores acquire a sufficient number of K-fibers (Hoffman et al., 2001; King et al., 2000). Conversely, the plus-end directed motor MCAK opposes dynein (Abrieu et al., 2000; Maney et al., 1998; Rieder and Alexander, 1990; Shrestha and Draviam, 2013; Yao et al., 2000). MCAK (mitotic centromere-associated kinesin), is a member of the kinesin-13 family, unlike the other kinesins, MCAK utilizes the ATP turnover to function as a microtubule depolymerase, rather than a motor (Abrieu et al., 2000; Maney et al., 1998; Rieder and Alexander, 1990; Shrestha and Draviam, 2013; Yao et al., 2000). MCAK is necessary for the correct Kt-MT attachment, where depletion or inhibition of kinesin activity resulted in misaligned chromosomes during metaphase and lagging chromosomes during anaphase (Maney et al., 1998; Walczak et al., 2002, 1996).

MCAK is located at both centromeres and kinetochores (Desai et al., 1999; Wordeman and Mitchison, 1995), but it becomes more closely associated with kinetochores, thereby moving away from the centromere as chromosomes achieve bi-oriented attachment (Andrews et al., 2004). This spatial segregation of MCAK determines its catalytic activity, such that chromosomes without bi-orientation (checkpoint ON) will have a higher concentration of MCAK on the centromere and a higher rate of microtubule depolymerization (Andrews et al., 2004; Hunter et al., 2003). This balance of motor forces establishes tension, which is a major signal for chromosome alignment needed to satisfy the spindle assembly checkpoint and progress into anaphase.

1.3.2 Activation of the checkpoint delays anaphase onset and protects genome integrity

The spindle checkpoint is a highly conserved quality control mechanism that can transiently delay anaphase until all chromosomes are stably attached to the spindle in a bipolar fashion (Foley and Kapoor, 2013; Lara-Gonzalez et al., 2012; Musacchio and Salmon, 2007). The spindle checkpoint signal is generated at kinetochores. In the presence of an unattached or a misattached kinetochore, a "wait anaphase" signal is generated. This signal can be rapidly extinguished through laser ablation of the last unattached kinetochore (Rieder et al., 1995). The checkpoint is an "all-or-none" response (Rieder et al., 1995) that is exquisitely sensitive and titratable by increasing concentration of key mitotic checkpoint complex proteins at kinetochores (Vink et al., 2006).

As mentioned previously, anaphase onset is initiated by the degradation of cyclin B (Kraft et al., 2003) and securin (Nasmyth, 2002), resulting in the deactivation of Cdk1 (Chang et al., 2003) and the activation of separase (Ciosk et al., 1998), respectively (Fig. 1.3). The spindle checkpoint functions by inhibiting APC/C activity. This inhibition is established through the formation of the mitotic checkpoint complex (MCC), which is composed of four key proteins: Mad2, BubR1, Bub3 and cdc20 (Chao et al., 2012; Sudakin et al., 2001). Upon formation, Cdc20, an activator of the APC/C, is sequestered in the MCC, thus preventing localized activation of the E3 ubiquitin ligase (Acquaviva and Pines, 2006; Clute and Pines, 1999; Hardwick et al., 2000; Sudakin et al., 2001; Tang et al., 2004). Formation of the MCC is catalyzed on unattached kinetochores (Acquaviva and Pines, 2006; Clute and Pines, 1999; Hardwick et al., 2000; Sudakin et al., 2001; Tang et al., 2004). These MCC proteins are

important tumor suppressors. For example, silencing BubR1 results in precocious anaphase onset and chromosome segregation errors. Moreover, mutations in BubR1 are causal for a cancer predisposition syndrome, termed Mosaic Variegated Aneuploidy (MVA; OMIM 257300) (Bohers et al., 2008; Chan et al., 1999; Fang, 2002; Hanks et al., 2004; Hanks and Rahman, 2005; Kajii et al., 2001; Kawame et al., 1999; Lampson and Kapoor, 2005; Limwongse et al., 1999; Matsuura et al., 2006; Suijkerbuijk et al., 2010).

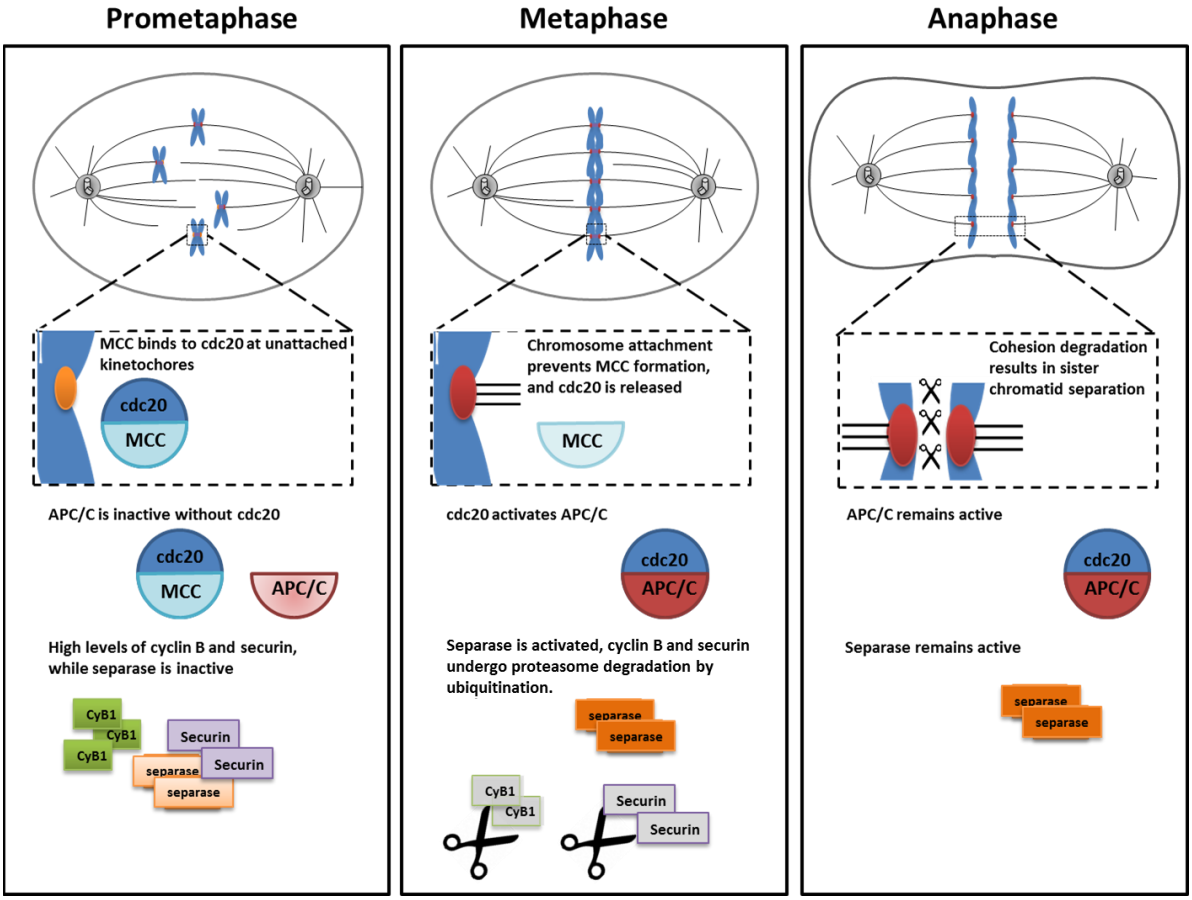

Figure 1.3 The spindle checkpoint.

Schematic representation of the spindle checkpoint. The checkpoint prevents anaphase initiation until all kinetochores are properly attached to the mitotic spindle. In prometaphase, unattached kinetochores catalyze the formation of the MCC. The MCC binds to the APC/C activator cdc20, thereby preventing APC/C activation. As a consequence, cyclin B and securin (inhibitor of separase) are stabilized. In metaphase, when all kinetochores are stably attached to the mitotic spindle, MCC cannot form and releases cdc20, which activates the APC/C and leads to the ubiquitination and degradation of cyclin B and securin. As a result, separase cleaves sister chromatid cohesion and initiates anaphase. Adapted with permission from J. Raaijmakers (Raaijmakers, 2014).

1.3.3 Inactivation of the checkpoint promotes anaphase onset

To promote entry into anaphase, the cell must first detect and distinguish between correct and incorrect chromosome attachment. Bipolar attachment of a chromosome generates tension across sister chromatids due to pulling forces exerted on the mitotic spindle (Gadde and Heald, 2004; Khodjakov and Pines, 2010; Maresca and Salmon, 2010; Zhou, 2002). Aurora kinase B senses this tension and phosphorylates MCAK to promote the protein's microtubule depolymerizing activities (Andrews et al., 2004; Ems-McClung et al., 2013). Upon bipolar orientation, the distance between sister centromeres increases and separates MCAK from Aurora B allowing the dephosphorylation of MCAK by protein phosphatase 1 (PP1) (Andrews et al., 2004; Ems-McClung et al., 2013; Gorbsky, 2004; Hsu et al., 2000; Hunter et al., 2003; Sassoon et al., 1999). Thus, tension modulates MCAK activity, and subsequent microtubule depolymerization (Andrews et al., 2004), and stabilizes Kt-MT attachments providing a positive feedback loop that ensures incorrect attachments are severed while correct attachments are maintained. Kt-MT attachments also enable the dynein-dependent removal of MCC components and the local activation of APC/C (Howell et al., 2001; Wojcik et al., 2001). Inhibition of dynein activity, in turn, accumulates key checkpoint proteins at kinetochores and promotes arrest during metaphase (Howell et al., 2001; Wojcik et al., 2001).

The mitotic delay imposed by the spindle checkpoint is transient. Cells can slip past an active spindle checkpoint and undergo premature sister chromatid separation (Gorbsky, 2013; C. L. Rieder and Maiato, 2004; Rossio et al., 2010; Weaver and Cleveland, 2005). Alternatively, if the checkpoint signal is sustained for a prolonged period of time, the cell may undergo

unscheduled mitotic exit without chromosome separation and produce a single tetraploid cell, known as “adaptation” or “mitotic slippage” (C. L. Rieder and Maiato, 2004; Weaver and Cleveland, 2005). The newly made tetraploid cell may undergo apoptosis, p53-dependent G1 arrest or enter a new round of the cell cycle (C. L. Rieder and Maiato, 2004; Weaver and Cleveland, 2005). Prolonged checkpoint activation can also induce a phenomenon known as “cohesion fatigue” (Gorbsky, 2013). Cohesion fatigue describes the asynchronous separation of single chromatids in cells that are arrested at metaphase (Gorbsky, 2013). Cohesion fatigue initiates with separation of chromosomes at the centromere and then spreads outward along the chromosome arms (Gorbsky, 2013). The separated chromatid may oscillate between two spindle poles, which tends to cause chromosome fragmentation (Gorbsky, 2013). Interestingly, there is a resurgence of spindle checkpoint signal on kinetochores of separated chromatids, detected by high concentration of BubR1 (Daum et al., 2012, 2009; Lara-Gonzalez and Taylor, 2012). The exact mechanism behind cohesion fatigue is not well known.

Both the functionality and kinetics of the spindle checkpoint are vital to the maintenance of genome stability. Chapter 4 identifies RHAMM as a new regulator of the spindle checkpoint that is needed to balance motor forces during chromosome congression and separation.

1.4 Aurora kinase A signaling regulates mitotic spindle assembly

The activities of mitotic kinases are regulated both temporally and spatially and their deregulation results in mitotic catastrophe, genome instability, and cancer. There are four main mitotic kinase families: aurora kinases, polo-like kinases, cyclin-dependent kinases and NEKs. As Chapter 3 describes a new mechanism responsible for Aurora kinase A mediated mitotic spindle assembly, this section will review Aurora kinase A biology.

1.4.1 Aurora kinase A: discovery, structure, expression and subcellular localization

Aurora A is a serine/threonine kinase. *Aurora* refers to Aurora Borealis, as mutations of *aurora* that were identified in *Drosophila* prevented centrosome separation and the resulting monopolar microtubule aster resembled the atmospheric phenomenon (Glover et al., 1995). Since its initial discovery, the following homologs of Aurora have been identified: *S. cerevisiae* has a single Aurora kinase, known as Ipl1 (increase in ploidy 1) (Chan and Botstein, 1993); *C. elegans* (Schumacher et al., 1998a, 1998b), *Drosophila* (Glover et al., 1995) and *Xenopus* (Roghi et al., 1998) each have two types of aurora kinases: Aurora A and Aurora B; and, the Aurora kinase family is composed of three members in mammals: Aurora A, B and C. In mammals, Aurora A regulates centrosome and mitotic spindle assembly, Aurora B regulates the spindle checkpoint and cytokinesis, while less is known about the testis-specific, Aurora kinase C (Carmena et al., 2009).

Aurora kinases are comprised of two domains: a regulatory domain in the N-terminus and a catalytic domain in the C-terminus (Dodson et al., 2010). The regulatory domain is variable between the three members, whereas the catalytic domain shares >70% sequence homology between Aurora A and B (Carmena et al., 2009). Several degradation motifs have been identified in Aurora A, including the D-box, A-box and KEN-box, recognized by the ubiquitination pathway (Castro et al., 2002; Crane et al., 2004). Aurora A activation requires autophosphorylation of the threonine residue T288 (Bayliss et al., 2003; Dodson and Bayliss, 2012; Eyers et al., 2005), which is achieved through binding with different co-activators (Bayliss et al., 2003; Eyers and Maller, 2004; Hirota et al., 2003; Ouchi et al., 2004; Satinover et al., 2004).

Northern blot analysis showed high expression of Aurora A in thymus, testis and fetal liver and low expression in bone marrow, lymph node and spleen (Bischoff et al., 1998). Aurora A expression is cell cycle regulated, with peak expression during late G2 to metaphase (Katayama et al., 2004). Kinase expression decreases in an APC/C dependent manner during mitotic exit and is barely detected after mitosis (Castro et al., 2002; Crane et al., 2004; Giubettini et al., 2011). Aurora A localizes to duplicated centrosomes during G2 phase, decorates the spindle poles and fibers from prophase to metaphase, and remains on the central spindle from anaphase to telophase (Bischoff et al., 1998). During interphase, Aurora A was reported to localize at the nucleus and the centrosome (Rannou et al., 2008).

1.4.2 The functions of Aurora A during mitosis

Aurora A has cell cycle specific substrates and functions. In G2 phase, Aurora A is part of the PCM and is activated by the LIM protein, Ajuba, to promote centrosome maturation (Hirota et al., 2003). Active Aurora A phosphorylates SAFs, which is required for their recruitment to the centrosome (Barros et al., 2005; Berdnik and Knoblich, 2002; Giet et al., 2002; Kinoshita et al., 2005; Mori et al., 2007; Terada et al., 2003). At the G2-M transition, Aurora A phosphorylates CDC25B, which localizes cyclin B to the nucleus and promotes mitotic entry (Cazales et al., 2005). Depletion of Aurora A by RNA interference (RNAi) results in G2-M arrest and subsequent apoptosis (Cazales et al., 2005).

During prophase, Aurora A promotes centrosome separation (Giet et al., 1999; Glover et al., 1995; Roghi et al., 1998). In *Xenopus*, Aurora A phosphorylates the motor protein Eg5, but the significance of this phosphorylation remains unknown (Giet et al., 1999). Interestingly, the inhibition of either Aurora A or Eg5 prevents centrosome separation (Glover et al., 1995; Roghi et al., 1998; Sawin et al., 1992). Eg5 is also a substrate of Cdk-1 and this phosphorylation event strongly increases Eg5 binding to microtubules in *Xenopus* egg extract spindle (Cahu et al., 2008). Thus, it is reasonable to speculate that Aurora A may drive centrosome separation through Eg5, and this process may be phosphorylation dependent.

After nuclear envelope breakdown, TPX2 becomes the chief activator of Aurora A (Bayliss et al., 2003; Eyers et al., 2003; Tsai et al., 2003). TPX2 activation of Aurora A is multifaceted. The first 43 amino acids in the N-terminus of TPX2 binds to Aurora A (Bayliss et al., 2003), which promotes its autophosphorylation on T288 (Bayliss et al., 2003; Dodson and

Bayliss, 2012; Xu et al., 2011). Moreover, TPX2 binding induces a conformational change in Aurora A that renders T288 inaccessible to the PP1 and PP6 phosphatases (Satinover et al., 2004; Zeng et al., 2010), thus stabilizing Aurora A in its active form (Bayliss et al., 2003; Eyers et al., 2003; Tsai et al., 2003). TPX2 binding is also necessary to target Aurora A to spindle microtubules and poles (De Luca et al., 2006; Giubettini et al., 2011; Kufer et al., 2002). Furthermore, TPX2 prevents the degradation of Aurora A through the action of APC/C, thus stabilizing kinase expression in both interphase and mitotic cells (Giubettini et al., 2011). Lastly, Shim *et al* identified a highly conserved phosphorylation site at the T72 residue in TPX2 that may regulate Aurora A activity (Shim et al., 2015). Abolishment of phosphorylation of the T72 residue, through the use of the T72A mutant, upregulated Aurora A activity and resulted in the elongation of spindle length (Shim et al., 2015). Furthermore, the T72A mutant preferentially concentrates on the spindle, whereas wildtype TPX2 localized to both spindle and cytosol, suggesting accumulation of the T72A mutant on the spindle may lock Aurora A in an active state at this location (Shim et al., 2015). Thus, during mitosis, TPX2 binds, activates, protects, locates and stabilizes Aurora A to promote mitotic spindle assembly.

Active Aurora A promotes microtubule nucleation and assembly by recruiting SAFs to the centrosomes (Barros et al., 2005; Berdnik and Knoblich, 2002; Giet et al., 2002; Kinoshita et al., 2005; Mori et al., 2007; Terada et al., 2003). For example, Aurora A phosphorylates Cnn, a core component of the centrosome, and promotes its ability to anchor γ-tubulin during spindle assembly (Terada et al., 2003). In addition to promoting their recruitment, active Aurora A also protects SAFs from degradation. That is, Aurora A phosphorylates BRCA1 (breast cancer 1) and inactivates the E3 ubiquitin ligase complex, BRCA1-BARD1 (BRCA1 associated ring domain

protein 1) (Pujana et al., 2007; Sankaran et al., 2007, 2006, 2005). Aurora A also regulates chromosome-mediated microtubule assembly (Koffa et al., 2006; Tsai and Zheng, 2005). As demonstrated in *Xenopus* egg extracts, Aurora A promotes the formation of a protein complex containing TPX2, Eg5, and other proteins to stimulate microtubule nucleation and stabilize K-fibers (Koffa et al., 2006). It has been postulated but not yet confirmed that Aurora A promotes microtubule assembly at non-centrosomal sites in mammalian cells, as well.

Aurora A may also be involved in the satisfaction of the spindle checkpoint response and the completion of cytokinesis. CENP-A, a variant of histone H3, was identified in a two-hybrid screen and found to be a substrate for Aurora A (Kunitoku et al., 2003). Inhibition of Aurora A-mediated phosphorylation of CENP-A results in chromosome misalignment during metaphase and segregation errors during anaphase (Kunitoku et al., 2003). MCAK and Aurora B destabilize erroneous Kt-MT attachments during the spindle checkpoint response (Andrews et al., 2004; Hunter et al., 2003) (section 1.3.3), however, MCAK is also a substrate of Aurora A (Zhang et al., 2008). MCAK phosphorylation by Aurora A appears to inhibit the depolymerizing action of MCAK (Zhang et al., 2008). Aurora A overexpression may override the spindle checkpoint and promote anaphase entry with defective Kt-MT attachments (Anand et al., 2003). These findings highlight the importance of activating Aurora A at the correct time and location to promote spindle assembly and to prevent genome instability.

1.4.3 Aurora A is an important molecular target in many cancers

Genomic amplification of *Aurora A* has been identified in a variety of cancers, including breast (Tanaka et al., 1999), ovarian (Gritsko et al., 2003), bladder (Fraizer et al., 2004; Sen et al., 2002) and gastric (Kamada et al., 2004; Sakakura et al., 2001). Moreover, two polymorphism in Aurora A associate with human tumor susceptibility: the F31I variant associates with elevated risk to develop human colon and ovarian cancers (Dicioccio et al., 2004; Ewart-Toland et al., 2003); and, the combination of F31I and V57I associate with increased breast cancer risk (Cox et al., 2006; Egan et al., 2004). Overexpression of Aurora A transformed NIH 3T3 cells (Bischoff et al., 1998; Zhou et al., 1998) and Rat1 fibroblast cells (Anand et al., 2003) and promoted tumor formation in nude mice (Wang et al., 2006; Zhang et al., 2004). Importantly, *Aurora A* is located on human chromosome 20q13 in close proximity to *TPX2* (20q11), and 20q amplification often occurs in tumors (Beroukhim et al., 2010; Scotto et al., 2008). Tumors with co-amplification of *Aurora A* and *TPX2* have been classified as having poor overall or progression-free survival (Kadara et al., 2009). Indeed, the Aurora A-TPX2 complex has been termed an oncogenic holoenzyme (Asteriti et al., 2010). Therefore, the process of tumorigenesis may be augmented or attenuated through molecules and pathways that regulate the Aurora A-TPX2 complex.

1.5 Molecular motors produce and balance forces needed for chromosome alignment

The mitotic spindle must be dynamic to accommodate chromosome movement and changes in cell size. Initially, it was thought that microtubule assembly and disassembly generated the force needed for chromosome alignment and segregation (Inoué and Salmon, 1995). This model was proven incomplete with the discovery of motor proteins, which are mechanochemical ATPases (adenosine triphosphatase) that walk along microtubules to move cargo and generate force. During mitosis, chromosomes are transported as cargos along the microtubules composing the mitotic spindle, and force is generated as motors slide adjacent spindle microtubules apart.

1.5.1 Plus-end directed kinesins vs. minus-end directed dynein

Motor proteins are classified based on their direction of travel: dyneins exhibit retrograde movement toward the minus ends of the microtubule while kinesins exhibit antegrade movement toward the plus ends of the microtubule (Goldstein, 2001; Vale, 2003), Fig. 1.2. Dyneins are classified as either cytoplasmic or axonemal, while 14 members of the kinesin superfamily have been identified and each are classified based on their sequence and cellular functions (Marx et al., 2009).

Most kinesins are dimeric, with each monomer composed of three domains: 1) a highly conserved motor head with ATPase activity that binds to microtubules; 2) a coiled-coil stalk that mediates dimerization; and, 3) a non-conserved tail that binds to cargo (Marx et al., 2009). The most notable kinesin in the dividing cell belongs to the kinesin-5 family, and is referred to as Eg5

in mammalian cells. Eg5 was first identified in a genetic screen in *A. nidulans* and named BimC, as one of the "blocked in mitosis" genes (Enos and Morris, 1990). Eg5 functions as a homotetramer such that each unit has two motor heads at either end of an elongated stalk, similar to a dumbbell (Blangy et al., 1995; Kashina et al., 1996; Sharp et al., 1999). This conformation allows Eg5 to bind to two microtubules simultaneously, which mediates cross-linking and sliding, and it is thus referred to as a sliding motor.

Eg5 is located diffusely throughout the cytoplasm during interphase but localizes to spindle microtubules and enriches at spindle poles during mitosis (Groen et al., 2008; Kapoor, 2001; Kwok et al., 2004; Sawin et al., 1992). Eg5 establishes spindle bipolarity and its inhibition, via siRNA or small molecule inhibition, induces prometaphase-like cells with unseparated centrosomes (Groen et al., 2008; Kapoor, 2001; Kwok et al., 2004; Sawin et al., 1992). However, in pre-formed metaphase spindles, Eg5 inhibition does not disrupt spindle integrity or bipolarity but rather perturbs chromosome alignment and congression (Ferenz et al., 2009; Tanenbaum et al., 2009; van Heesbeen et al., 2014; Vanneste et al., 2009). The latter findings suggest that other kinesin family members may play a redundant or compensatory role in the establishment of spindle bipolarity.

A member of the kinesin-12 family, Kif15 (*H. sapien*) or Xklp2 (*Xenopus*), functions in concert with Eg5 to promote centrosome separation (Tanenbaum et al., 2009; Vanneste et al., 2009). Unlike Eg5, Kif15 is a dimer and can therefore only walk on one microtubule at a time. But, when bound by its adapter protein TPX2, the Kif15-TPX2 complex can function as a sliding motor, allowing it to crosslink two microtubules simultaneously and slide them apart (Boleti et al., 1996; Wittmann et al., 2000, 1998). Through an interaction with TPX2 and dynein, Kif15 is

located at the centrosome throughout the cell cycle (Wittmann et al., 1998). Kif15 is also present on spindle microtubules and enriched at the poles during mitosis (Wittmann et al., 1998).

Kif15/Xklp2 is not essential for the assembly of a bipolar spindle. The removal of >98% of Xklp2 from egg extracts (Wittmann et al., 2000), or RNAi mediated knockdown of Kif15 in HeLa cells (Zhu et al., 2005), did not affect bipolar assembly. However, in the absence of Eg5 activity, high expression of Kif15 is needed to restore bipolar spindle assembly and to replace all the essential functions of Eg5 (Tanenbaum et al., 2009; Vanneste et al., 2009). This suggests that the Kif15-TPX2 complex cooperates with the tetrameric Eg5 complex to mediate microtubule sliding and produce outward-directed force on the mitotic spindle.

The outward-directed forces produced by Eg5 and Kif15 are antagonized by inward-directed forces produced by cytoplasmic dynein (Ferenz et al., 2009; Florian and Mayer, 2012; Mitchison et al., 2005; Tanenbaum et al., 2008). Cytoplasmic dynein is a homodimer composed of two heavy chains, two intermediate chains, four light intermediate chains and three different light chain dimers (Kardon and Vale, 2009; Pfister et al., 2006). The ATPase is located within the heavy chain, while the additional subunits are required to link dynein to its cargos, as well as to provide structural support and maintain complex integrity (Trokter et al., 2012). Dynein can be found at various locations in the dividing cell, including the nuclear envelope, centrosomes, kinetochores, spindle microtubules and cell cortex (Kiyomitsu and Cheeseman, 2012; Maxwell et al., 2003; Pfarr et al., 1990; Steuer et al., 1990; Tanenbaum et al., 2008; Tanenbaum and Medema, 2010). Various studies have implicated dynein in the control of spindle organization, spindle positioning, chromosome attachment and movement, and spindle checkpoint signaling (Dunsch et al., 2012; Howell et al., 2001; Maxwell et al., 2003; Varma et al., 2013, 2008).

Dynein interacts with various adapters, which in turn affects the motor's subcellular localization, cargo specificity, and motor processivity (Kardon and Vale, 2009). For example, dynactin is a multi-subunit protein complex that links dynein together with a microtubule and its cargo, and enhances dynein processivity *in vitro* (Kardon and Vale, 2009). At the kinetochore, non-motor adapters (i.e. NdeL1 and LIS1) target dynein to microtubule minus ends and stabilize Kt-MT attachments (Liang et al., 2007; Stehman et al., 2007). Upon spindle checkpoint completion, dynein transports these checkpoint proteins poleward to initiate anaphase onset (Howell et al., 2001; Wojcik et al., 2001). During spindle assembly and positioning, dynein is also present on the cell cortex; asymmetric distribution of dynein on the cortex, which is established by a Ran-GTP gradient from chromosomes (Kiyomitsu and Cheeseman, 2012), exerts pulling forces on the astral microtubules emanating from spindle poles (Grill and Hyman, 2005) to define spindle orientation (Glotzer, 1997). Lastly, dynein located at spindle poles and along spindle fibers antagonizes the forces generated by opposing kinesin motors, such as Eg5 and Kif15, to stabilize the spindle and ensure the correct alignment of chromosomes.

1.5.2 Balancing forces along the mitotic spindle

Antagonistic actions between mitotic kinesins (ie, Eg5 and Kif15) and dynein produce opposing forces along the mitotic spindle, but, this antagonism is more complicated than a simple "push-pull" model. After Eg5 inhibition by small molecule inhibitors, either Kif15 overexpression or dynein depletion can restore centrosome separation (Ferenz et al., 2009; Florian and Mayer, 2012; Mitchison et al., 2005; Sharp et al., 2000; Tanenbaum et al., 2008). However, in the absence of both Eg5 and Kif15, centrosome separation is completely blocked

regardless of the presence or absence of dynein activity (van Heesbeen et al., 2014). These findings show that a net outward force is required during centrosome separation. However, the removal of individual antagonistic motors during metaphase changed mitotic spindle length, which could be recovered by removing opposing motors in combination (Mitchison et al., 2005; Sharp et al., 2000; Syrovatkina et al., 2013). Thus, balanced motor forces are favored during metaphase and imbalances in force alter spindle architecture. In each of these studies, perturbation of force affected downstream chromosome segregation. While these studies provide insights into the coordination of antagonistic motors during spindle assembly and maintenance, they fail to explain why chromosome segregation is affected.

1.5.3 Non-motors adapters modulate motor activities: TPX2 as the example

Dynein behavior is modulated by its adapters (Kardon and Vale, 2009); kinesin activities, as well, are tightly regulated through partner proteins. For example, TPX2 is able to downregulate the motor activity of both Eg5 (Balchand et al., 2015; Ma et al., 2011) and Kif15 (Drechsler et al., 2014). The C-terminus of TPX2 is required for its interaction with either Kif15 (Wittmann et al., 1998) or Eg5 (Eckerdt et al., 2008). Depletion of TPX2 (RNAi), or disruption of the interaction between TPX2 and Eg5 (using a dominant negative, truncated form of TPX2), increases Eg5 activity on antiparallel microtubules and causes these microtubules to buckle (Ma et al., 2011). Single molecule tracking experiments reveal that Eg5 motor stepping is reduced as long as TPX2 is bound to microtubules, even without a TPX2-Eg5 interaction (Balchand et al., 2015). A similar inhibitory mechanism has been described for the TPX2-Kif15 interaction

(Drechsler et al., 2014). Thus, TPX2 can act as a brake on outward force generated through Eg5 or Kif15.

Collectively, TPX2 appears to play both biochemical and structural roles during mitosis [reviewed by (Neumayer et al., 2014; Wadsworth, 2015)]. As an activator of Aurora A, TPX2-Aurora A complexes influence microtubule nucleation at centrosomes via phosphorylation of SAFs (Bayliss et al., 2003; Dodson and Bayliss, 2012; Eyers et al., 2003; Eyers and Maller, 2004). As a partner protein of kinesins, TPX2 regulates Kif15 localization and inhibits Kif15 and Eg5 activity (Kufer et al., 2002; Wittmann et al., 1998). But, how is TPX2 regulated during mitosis? And, does the Aurora A-TPX2 complex also promote spindle assembly at non-centrosomal sites in mammalian cells (when centrosomes/spindle poles are present) as it does in acentrosomal *Xenopus* egg extracts? Moreover, what proteins regulate the structural regulation of motor proteins by TPX2 and how do these proteins alter chromosome alignment and anaphase entry?

1.6 The non-motor, spindle assembly factor receptor for hyaluronan mediated motility

In both human and *Xenopus* mitotic cells, 40–60% of TPX2 is in a complex with receptor for hyaluronan mediated motility (RHAMM) (Groen et al., 2004; Joukov et al., 2006; Maxwell et al., 2005, 2003). RHAMM is a cell cycle regulated, microtubule associated protein, and an important cell division gene product in both mammalian (Neumann et al., 2010) and *Xenopus* (Groen et al., 2004; Joukov et al., 2006) cells. However, the discovery, localization, function and specific role of RHAMM in cancer and other pathologic states is controversial.

1.6.1 The discovery and brief history of extracellular RHAMM

RHAMM was originally isolated from supernatants of mouse NIH-3T3 and mouse sarcoma virus transformed 3T3 cells as part of the hyaluronan (HA) binding protein (HABP) complex (Turley et al., 1987). HA is a non-branched polysaccharide located in the extracellular matrix (Lee and Spicer, 2000). Gel electrophoresis resolved the HA affinity-purified fraction and identified three major protein bands at 70 kDa, 66 kDa and 56 kDa, respectively (Turley et al., 1987). A follow-up study demonstrated that HABP and HA upregulated cell locomotion in 10T1/2 cells, which could be blocked by a monoclonal antibody raised against the 56 kDa peptide (Turley et al., 1991). The first attempt to clone mouse RHAMM identified a 58 kDa protein (designated RHAMM2) encoded by 340 amino acids (Hardwick et al., 1992). Polyclonal antibodies raised against the amino acid sequence predicted by the cDNAdemonstrated cell surface localization and these antibodies inhibited *ras*-regulated increased locomotion (Hardwick et al., 1992). Consequently, the gene product was named RHAMM (Hardwick et al., 1992).

Subsequent studies, using antibodies generated against the cDNA clone sequence from RHAMM2, identified various protein isoforms ranging from 52 to 125 kDa (Entwistle et al., 1995; Hall et al., 1995; Hardwick et al., 1992). These findings suggested the cDNA sequence for RHAMM2, as described by Hardwick *et al.*, was not the full length transcript. Indeed, Entwistle *et al.* identified two transcripts, a major 70 kDa transcript termed RHAMM1, which did not contain exon 4 (note: exon 8 of the full-length transcript), and a minor 73 kDa transcript that contained exon 4 (exon 8), designated RHAMM1v4 (Entwistle et al., 1995). Overexpression of the RHAMM1v4 isoform was then shown to induce and maintain *ras* transformation in mice (Hall et al., 1995). Importantly, these studies used a cDNA that corresponds to exon 6 – 18 of the gene (*hyaluronan mediated motility receptor*, *HMMR*) that encodes RHAMM.

The full length mouse RHAMM was identified as a single 95 kDa protein, translated from a transcript with 18 exons encoding 794 amino acids in both immortalized mouse cells and primary tissues (Fieber et al., 1999; Hofmann et al., 1998). Thus, the RHAMM2 variant (Hardwick et al., 1992) (exons 10-18), the minor RHAMM1v4 variant (Entwistle et al., 1995) (exons 6-18) and the major RHAMM1 variant (Entwistle et al., 1995) (exons 6-18, lacking exon 8) are incomplete transcripts of unknown physiological relevance. Expression of the full-length RHAMM transcript was detectable in all mouse tissues examined with elevated mRNA levels in testis, thymus and spleen (Fieber et al., 1999).

Human RHAMM was identified in a breast cDNA expression library using the mouse RHAMM1 cDNA sequence (Wang et al., 1996). Human RHAMM is an 85 kDa protein with 725 amino acids encoded by 18 exons (Wang et al., 1996). No splice variant for exon 8 was identified in human RHAMM, but two other splice variants have been detected. RHAMM

lacking exon 13 (RHAMM$^{-exon13}$) was identified in breast carcinoma (Wang et al., 1998) and multiple myeloma samples (Crainie et al., 1999). RHAMM lacking exon 4 (RHAMM^{-exon4} or RHAMM B) was identified in various cell lines and cancer tissues, including breast, myeloma and colorectal (Assmann et al., 1998; Crainie et al., 1999; Line et al., 2002). Subcellular fractionation and immunofluorescence showed human RHAMM as an intracellular protein (Assmann et al., 1998). Concurrently, antibodies were raised against the 95 kDa protein for the full-length mouse RHAMM and these antibodies showed intracellular localization exclusively (Hofmann et al., 1998). Thus, it was proposed to rename the protein intracellular hyaluronic acid binding protein (IHABP) (Hofmann et al., 1998). RHAMM is also designated as CD168.

1.6.2 Structural domains contained in RHAMM

RHAMM is encoded by *HMMR*, which is located on human chromosome 5q33.2-qter (Spicer et al., 1995). RHAMM contains three key regions (Fig. 1.4): 1) a basic N-terminus, within which exon 4 mediates a direct interaction with microtubules (Assmann et al., 1999); 2) an extensive coiled-coil stalk that serves as a potential dimerization domain at aa 69-681 (Assmann et al., 1999); and 3) a basic leucine zipper at the C-terminus, which is highly conserved across species (~45% and 80% identical to murine and *Xenopus* RHAMM (XRHAMM), respectively (Groen et al., 2004; Maxwell et al., 2003). RHAMM interacts with the spindle protein CHICA through a region within the stalk region (aa 365-546) (Dunsch et al., 2012). In addition, a calcium-dependent calmodulin binding domain (aa 574-602) has been identified, although the functional significance of this domain remains unknown (Assmann et al., 1999).

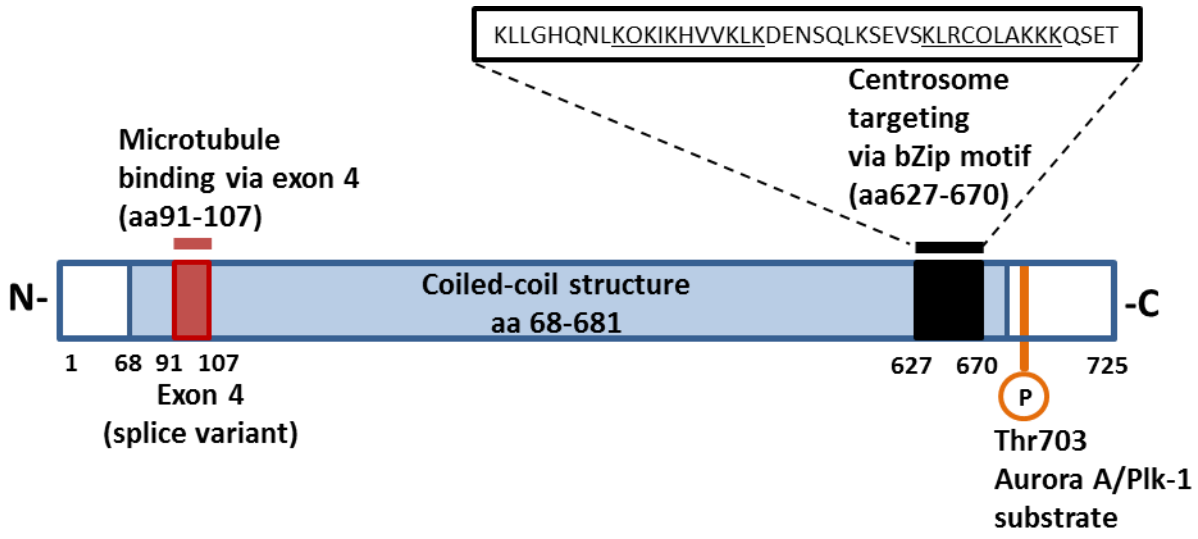

Figure 1.4 Structural domains and regions of RHAMM.

The amino-terminus binds to microtubules via exon 4. The central stalk of the protein is a predicted coiled-coil structure. The carboxy-terminus contains a basic leucine zipper motif (bZip), which mediates the localization of the protein to spindle poles and interactions with the dynein motor complex. The HA-binding $B(X)_7B$ domains of RHAMM are underlined. Threonine 703 (Thr703) is phosphorylated by Aurora A.

Two HA binding motifs were identified in the C-terminus of RHAMM, corresponding to aa 636-646 and aa 658-667 (Yang et al., 1993). The amino acids within these motifs are basic residues such as lysine or arginine, which allow RHAMM to interact with HA in an ionic manner (Yang et al., 1994, 1993). This motif was labelled as the Basic (B) $(X)_7$ Basic (BX_7B) motif (Yang et al., 1994, 1993), and was postulated to be a novel HA binding domain. Members of the HA receptor complex on the cell surface (eg. CD44) use a large link module motif for HA binding (Toole, 2004, 2001). RHAMM does not contain a link module and contains no sequence homology with members of the HARC (HA receptor complex) family (Toole, 2004, 2001). Moreover, the BX_7B motifs bind to both acidic HA and heparin via an ionic interaction (Yang et al., 1994, 1993). Sequence alignments and structural prediction revealed 72% homology between the BX_7B motifs in RHAMM (aa 627-670) and the basic leucine zipper (bZip) motif in Kif15/hKlp2 (aa 1342-1388), including conservation of the leucines (Maxwell et al., 2003). The bZip motif in Kif15 interacts with TPX2, which seeded the studies of RHAMM-TPX2 biology. In RHAMM, a phosphorylation site just C-terminal to the bZip motif (T703) is recognized by Aurora A (Maxwell et al., 2011) and PLK1 (Grosstessner-Hain et al., 2011). In the next section, I will review the evidence supporting an intracellular role for RHAMM during cell division.

1.6.3 RHAMM expression and intracellular functions

Human RHAMM is differentially expressed in healthy tissues with significant mRNA levels detected in the testis, spleen, placenta, and thymus (Greiner et al., 2002). RHAMM mRNA and protein expression are cell cycle regulated with peak expression between late G2 to early M

phases (Maxwell et al., 2005; Yang et al., 2005). RHAMM degradation is facilitated through ubiquitination by the APC/C (Song and Rape, 2010) and BRCA1/BARD1 (Joukov et al., 2006) through D, KEN, and TEK boxes located in the C-terminus of RHAMM (Song and Rape, 2010). These degrons are within or in close proximity to the bZip motif and the C-terminal T703 phosphorylation site. In *Xenopus* oocytes, proper XRHAMM levels along the mitotic spindle are established through regulated degradation by BRCA1/BARD1, which is vital for spindle pole focusing (Joukov et al., 2006).

During interphase, RHAMM localizes to microtubules (Assmann et al., 1999) with accumulation at the centrosome (Maxwell et al., 2003). The truncated mouse isoform, RHAMM$^{\Delta 163}$ (aa 163-794, aka RHAMM1v4) (Hall et al., 1995) also binds to microtubules and modifies their stability through ERK1/2 activity (Tolg et al., 2010). During mitosis, RHAMM promotes microtubule cross-linking via direct binding of microtubules at the N-terminus and indirectly through an interaction with dynein at the C-terminal bZip motif (Maxwell et al., 2005, 2003; Tolg et al., 2010). The interaction between RHAMM and dynein maintains spindle pole stability during metaphase (Maxwell et al., 2005, 2003) and depletion of RHAMM (siRNA or microinjection of antibodies) delays mitotic progression and results in aberrant spindle architecture, with an elevated proportion of multipolar spindles (Maxwell et al., 2003). In *Xenopus*, XRHAMM promotes anastral spindle pole focusing, which also relies on the bZip motif (Groen et al., 2004; Joukov et al., 2006). With respect to other filament systems, RHAMM interacts specifically with polymerized actin (Assmann et al., 1999). RHAMM does not display any canonical actin-binding motifs, however, it does show sequence and structural similarities to tropomyosin, which is known to stabilize actin filaments (Ayscough, 1998). The exact manner of

binding approach and the sequence involved in the interaction between RHAMM and actin filaments remain unknown.

1.6.4 RHAMM in cancer

RHAMM was identified as a *bona fide* breast cancer susceptibility gene (OMIM: 600936) (Pujana et al., 2007). Haplotypes that either augment or reduce RHAMM germline expression can elevate breast cancer risk (Pujana et al., 2007). In breast tumors, enhanced expression of RHAMM at trabeculae and tumor island edges suggested involvement in tumor cell invasion and motility (Assmann et al., 2001). Moreover, elevated RHAMM expression is strongly associated with disease progression and overall survival in mammary carcinoma (Wang et al., 1998), stomach (Li et al., 2000), pancreatic (Rein et al., 2003), colon (Yamada et al., 1999), prostate (Gust et al., 2009) and head and neck cancers (Shigeishi et al., 2014). Thus, elevated RHAMM expression has been identified as a poor prognostic marker in a variety of cancers (Akiyama et al., 2001; Gust et al., 2009; Hall et al., 1995; Ishigami et al., 2011; Yamano et al., 2008; Zlobec et al., 2008). On the other hand, hemizygous deletion of *HMMR*/RHAMM has been identified in 46% of Neurofibromatosis-1 (NF1) associated Malignant Peripheral Nerve Sheath Tumors (MPNSTs) (Mantripragada et al., 2008); in these tumors, as well as in myeloma cancers, sensitivity to Aurora kinase A inhibition is dependent on gene dosage and expression of *HMMR*/RHAMM (Mohan et al., 2013; Shi et al., 2007). Moreover, RHAMM expression is absent in 96% of human seminomas, which may misorient germ cell divisions and underlie tumor initiation (Li et al., 2016). From the COSMIC (Catalogue of Somatic Mutations in Cancer) and CCLE (Cancer Cell Line Encyclopedia) datasets, the bZip motif in RHAMM is a hotspot for

mutations. This motif contains a stretch of 9 alanines (encoding 3 lysine residues) and 24 out of 34 mutations identified in these datasets involve the insertion of an additional A to induce frameshifts that may alter the stability of the protein. In addition, the alternative splicing of exon 4, which disrupts the protein's binding to microtubules, correlates with poor progression of multiple myeloma (Maxwell et al., 2004) and breast cancer (Venables et al., 2008). Moreover, the expression of RHAMM^{-exon4} was sufficient to promote tumor growth and metastasis to lymph nodes and liver of pancreatic islet tumors (Du et al., 2011). Taken together, it is difficult to classify RHAMM as a tumor suppressor or an oncogene but it is clear that the expression of RHAMM is strictly monitored and its over- or under-expression is associated with pathologies.

1.7 Rationale, hypothesis and significance of study

1.7.1 Summary of rationale

Cell division relies upon the assembly of a microtubule-based mitotic spindle apparatus that captures, aligns and segregates duplicated chromosomes. Assembly of the mitotic spindle is spatially regulated by the localized activation of Aurora A, mediated by its co-activator TPX2 (Barros et al., 2005; Giet et al., 2002; Mori et al., 2007; Terada et al., 2003). To ensure equal division of the genetic material, each sister chromatid within a pair needs to attach to microtubules originating from opposing spindle poles; this process is monitored by the spindle checkpoint and requires a balance of forces generated by opposing motor proteins (Ferenz et al., 2009; Sharp et al., 2000, 1999, Tanenbaum et al., 2009, 2008; van Heesbeen et al., 2014). Motor activities are regulated, in part, by non-motor adapter proteins, such as TPX2 and RHAMM (Balchand et al., 2015; Drechsler et al., 2014; Dunsch et al., 2012; Ma et al., 2011; Maxwell et al., 2003). In both human and *Xenopus* dividing cells, RHAMM is a partner protein of TPX2. In *Xenopus* dividing cells, both depletion of Xenopus RHAMM as well as accumulation of Xenopus RHAMM, through the loss of BRCA1, disrupts TPX2 localization and spindle organization (Groen et al., 2004; Joukov et al., 2006). Thus, the interaction between RHAMM and TPX2 may influence structural cues mediated by molecular motors and modulate biochemical signaling pathways that ensure bipolar spindle assembly and mitotic progression.

1.7.2 Hypothesis and aims of study

Hypothesis:

The interaction between RHAMM and TPX2 is necessary for Aurora kinase A mediated mitotic spindle assembly at centrosome and non-centrosome sites, and balances the motor forces needed to align chromosomes and complete the spindle checkpoint.

Aims:

1. Determine the necessity of RHAMM for Aurora kinase A activity during spindle assembly.
2. Determine the necessity of RHAMM for balanced motor forces that align and segregate chromosomes.
3. Determine the consequences of RHAMM overexpression on mitotic outcomes.

1.7.3 Significance

Mitosis is under tight regulation to preserve genome stability. Cancer cells are often highly proliferative, making mitosis an attractive intervention point for chemotherapy, and exhibit genome instability, which has been defined as an enabling characteristic of cancer. Anti-tumor drugs, such as Aurora A inhibitors, interfere with either the assembly or stability of the mitotic spindle, thus inducing programmed cell death. My studies identify RHAMM as a novel regulator of Aurora A-TPX2 and the Eg5-TPX2 complexes, which control the assembly of the mitotic spindle and balance motor forces along the spindle that are needed for chromosome attachment and segregation, respectively. Collectively, the findings from my studies outline critical steps in the construction and organization of the mitotic spindle and preservation of genome stability, which benefits our understanding of the tumorigenic process and may assist the design or best use of the next-generation of anti-tumor drugs.

Chapter 2: Materials and methods

2.1 Cell culture

2.1.1 Maintenance of HeLa cells

HeLa cells were purchased from American Type Culture Collection (ATCC) and cultured in Dulbecco's modified eagle medium (DMEM, Thermo-Fisher) supplemented with 10% fetal bovine serum (FBS, Invitrogen), 20 U/ ml penicillin (Invitrogen) and 20 μg/ ml streptomycin (Invitrogen). HeLa cells that stably express eGFP-alpha-Tubulin and mCherry-Histone-H2B (Gruneberg lab, University of Liverpool) were cultured in DMEM supplemented with 10% FBS, and maintained with 0.3 μg/ ml puromycin (Invitrogen) and 0.5 μg/ ml blasticidin S (Invitrogen). HeLa tet-on cells that express elevated GFP-RHAMM following induction (see below) were cultured in DMEM supplemented with 10% tetracycline-free FBS (Clontech), 10mM HEPES (Invitrogen), 1 mM Na pyruvate (Invitrogen), 4 mM L-glutamax (Invitrogen), 200 μg/ ml hygromycin B (Invitrogen), and 200 μg/ ml Geneticin (Fisher). All cell lines were grown at 37°C in a 5% (v/v) CO_2 incubator. Cells were passaged at 80% density, and reseeded at 15-20% density.

2.1.2 Maintenance of RPMI 8226 cells

RPMI 8226 cells were purchased from ATCC and cultured in ATCC-formulated RPMI-1640 Medium (ATCC) supplemented with 10% FBS. Cells were grown at 37°C in a 5% (v/v) CO_2 incubator.

2.1.3 Maintenance of fibroblast cells

BJ fibroblast cells were purchased from ATCC and cultured in DMEM:F12 medium (Invitrogen) supplemented with 15% FBS, 20 U/ ml penicillin and 20 μg/ ml streptomycin. Primary human fibroblasts with a t(12q32.31-5q33) were purchased from the Coriell Biorepository and maintained in MEM (Invitrogen) supplemented with 15% FBS, 20 U/ ml penicillin and 20 μg/ ml streptomycin. For all experiments, Coriell fibroblast cells were only cultured for four passages after thawing.

Primary mouse embryonic fibroblasts (MEFs) with genetic disruption of *Hmmr* were isolated from embryonic day 13.5 mice (C57/BL6N). Tissues were homogenized using an 18-gauge needle and a 10cc syringe, and cultures were seeded and incubated for two days, trypsinized on day 3, and frozen once confluent. MEFs were cultured in DMEM supplemented with 10% FBS (Invitrogen), 4 mM L-glutamax and 0.1 mM Non-Essential Amino Acids (Invitrogen). For all experiments, MEFs were only cultured for two passages after thawing. All cell lines were grown at 37°C in a 5% (v/v) CO_2 incubator.

2.1.4 Generation of tetracycline-inducible (tet-on) GFP-RHAMM in HeLa Cells

This cell line was generated by Dr. B.J. Taylor in Dr. L.M. Pilarski's laboratory (Cross Cancer Institute, Canada). Enhanced green fluorescent protein (eGFP) fused in frame with full-length RHAMM (GFP-RHAMM) was amplified by polymerase chain reaction (PCR) to contain 5' Mlu I and 3' Not sites, and inserted into Mlu I/ Not I digested pTre2HyG tetracycline response vector (Clontech). Ten micrograms of this plasmid and $1x10^7$ HeLa tet-on cells were mixed together in 0.4 ml OPTI-MEM (Gibco) and electroporated in 4 mm gap cuvettes (GenePulser set at 260 V, 960 uF; BioRad, Hercules, CA). Electroporated cells were grown in standard HeLa media. After 48 hours, fresh media was added containing 400 μg/ ml Geneticin (Invitrogen) and 200 μg/ ml hygromycin-B (Invitrogen) for selection of stable transfectants. The cells were grown with media changes every 2-3 days. Distinct colonies began to form after 10 days. RHAMM expression was induced with 1 μg/ml doxycycline (Clontech) and colonies were visualized by fluorescence microscopy. Colonies demonstrating fluorescence before induction were marked as leaky expressers and avoided; those demonstrating fluorescent spindle staining upon induction were picked and expanded under non-inducing condition in standard HeLa media with selection. For subsequent experiments, the cells were treated with 1 μg/ml doxycycline to induce GFP-RHAMM expression.

2.1.5 Lentivirus mediated shRNA knockdown and generation of shTPX2 sub-lines

This cell line was generated by P. Mohan in Dr. C. Maxwell's laboratory. To produce lentivirus containing small-hairpin RNA (shRNA) against TPX2, virus was packaged in HEK-

293FT cells using psPAX2 (packaging plasmid), pMD2.G (envelope plasmid) (Addgene), and pLKO.1- based vectors targeting TPX2 or a non-hairpin (NHP) negative control (shRNA sequences are described in Table 1). Plasmids were transfected into HEK293FT cells using Lipofectamine2000™ (Invitrogen). Virus was harvested every 24 hours and kept at 4°C. Virus was concentrated with the Lenti-X concentrator (Clontech) and stored at -20°C in phosphate buffered saline (PBS). To transduce cell lines, cells were seeded in antibiotic-free media and, after 9 hours, switched to OPTI-MEM for 24 hours. Next, 50 µl of virus and 8 µg/ ml Polybrene (Sigma) were added to cells and incubated for 16 hours. Virus containing media was removed and replaced with fresh antibiotic-free media. After 24 hours, 0.5 µg/ ml puromycin was added to select for transduced cells for 1 week. Transduced cell lines were maintained with 0.3 µg/ ml puromycin.

2.1.6 Transfection (siRNA and plasmids)

Small interfering RNA (siRNA) sequences are listed in Table 1. HeLa cells were seeded at 80% density in 6-well plates and allowed to adhere overnight. Media was then changed to OPTI-MEM and incubated for 8 hours prior to transfection. To transfect the cell-lines, each siRNA construct was incubated in 250 µl OPTI-MEM for 5 minutes at room temperature to make up a final concentration of 40 nM. Concurrently, 5 µl Lipofectamine 2000™ was added to 250 µl OPTI-MEM. For plasmid transfections, 2 ng of each plasmid was added. After the incubation period, the two mixtures were added together and incubated for 20 minutes at room temperature and then added drop-wise to cells. After 16 hours, cells were washed twice with PBS and seeded for analyses. Expression of mRNA or protein was measured 72 hours post

transfection. Cells were fixed for analysis 72 hours post transfection or living cells were imaged between 72- 96 hours post transfection.

2.1.7 Cell synchronization

For synchronization, cells were treated with 200 ng/ ml nocodazole (Sigma) for 16 hours, or subjected to a double thymidine block with 2 mM thymidine (Sigma). For double thymidine block, the cells were incubated with thymidine for 16 hours and then released into drug-free media for 10 hours, which was followed by a second incubation (16 hours) with thymidine. Cells were collected or fixed at designated times after synchronization in accordance with each experiment.

2.2 Reagents and antibodies

MG132 (Sigma), Hoechst (Invitrogen), MLN8237 (Selleck Chemicals) and BI2536 (Selleck Chemicals) were used as indicated. Primary antibodies used are listed in Table 2.3. Secondary antibodies were conjugated to IR Dye (Rockland), HRP (Sigma) or to Alexa Fluor 488, 594 or 679 (Invitrogen). DAPI was purchased from Sigma.

2.3 Molecular cloning and site directed mutagenesis

Truncation variants of RHAMM and TPX2 were constructed using the Gateway cloning system (Invitrogen). DNA fragments of RHAMM (1- 623), RHAMM (1- 679) and RHAMM

(623- 724) were amplified from eGFP-RHAMM (1- 724). TPX2 (1- 319) was amplified from mCherry-TPX2 (Origene) while TPX2 (40- 783) and TPX2 (319- 783) were amplified from TPX2-GFP (Origene). Products were first cloned into pDONR223 (Invitrogen), and then transferred into pLenti6/V5-DEST or pDEST57 expression vectors (Invitrogen). Site-directed mutagenesis was performed using the QuikChange II kit (Agilent). All clones sequences were validated by sequencing (ABI Prism 3130xl Genetic Analyzer). Primer sequences used for PCR are listed in Table 2.1.

2.4 Genomic and reverse-transcription (RT) PCR and quantitative PCR

Genomic DNA was extracted with the DNeasy extraction kit (Qiagen) and RNA was extracted from cells using RNeasy mini kit (Qiagen). Preparations were measured with a NanoDrop (Thermo-Fisher). RT reaction conditions were: 1 cycle at 22°C for 5 minutes, followed by 1 cycle at 42°C for 20 minutes, followed by 1 cycle at 85°C for 5 minutes, and held at 4°C. RT reaction was carried out using the SuperScript VILO MasterMix reaction (Invitrogen). Quantitative PCR (qPCR) reactions were run in triplicate in a 7000 series machine (Applied Biosystems), using the Fast SYBR Green Master Mix reaction (Applied Biosystems). qPCR cycling conditions were: 95°C for 5 minutes (initial holding stage), followed by 40 amplification cycles at 95°C for 60 seconds (denaturing stage) and 60°C for 30 seconds (annealing/extension stage), followed by 72°C for 5 minutes (final extension stage), followed by the generation of the melting curve, and held at 4°C until analysis. Analysis of qPCR results was done using the delta delta Ct method. Expression of RHAMM mRNA was normalized to the level of TATA box binding protein (TBP), while the level of *HMMR* gDNA was normalized to

the level of *glyceraldehyde 3-phosphate dehydrogenase* (*GAPDH*). Primers are listed in Table 2.2.

2.5 Microtubule regrowth assay

Microtubules were depolymerized by treating cells with 5 μM nocodazole for 1 hour at 37°C. Cells were then washed three times with PBS and incubated in pre-warmed drug-free media at 37°C to allow microtubule regrowth. Cells were fixed at specified time points or living cells were imaged.

2.6 Immunofluorescence and image acquisition

Cells were grown on coverslips and fixed with cold methanol for 15 minutes at -20°C. Cells were permeabilized with PBS-0.25% Triton X-100 (Sigma) for 5 minutes, washed with PBS three times, and then blocked in PBS with 0.1% Triton X-100 and 3% BSA for 1 hour at room temperature. Antibodies were diluted in PBS with 0.1% Triton X-100 and 3% BSA. Primary antibodies were diluted, and incubated with coverslips for 2 hours at room temperature. Secondary antibodies were diluted, and incubated with coverslips for 1 hour in the dark at room temperature. Cells were washed before and after incubations three times in PBS-0.5% Tween-20. Coverslips were mounted with ProLong Gold Antifade Reagent containing DAPI (Invitrogen).

Fixed cells were imaged using a 60X 1.2 NA oil objective with the Fluoview software (Olympus) on the Olympus Fluoview FV10i confocal microscope (Olympus). Image stacks of 15 optical sections with a spacing of 0.7 μm through the cell volume were taken. Maximum

intensity projection of the fluorescent channels was performed in ImageJ v1.46j (National Institute of Health).

2.7 Fluorescence resonance energy transfer (FRET) biosensor

The FRET-based biosensor for PLK1 activity is as described by Liu et al., 2012. Briefly, the biosensor was modified from a protein kinase C sensor (Violin et al., 2003) to include a CFP (cyan fluorescent protein)/ YFP (yellow fluorescent protein) fluorophore pair with a substrate peptide and an FHA2 phospho-Thr-binding domain in between. The PLK1 FRET biosensor is fused to the kinetochore protein Hec1 (Liu et al., 2012) to specifically measure kinase activity at kinetochores. PLK1 activity is high in prometaphase cells and decreases by metaphase alignment, which is reflected by the increasing FRET ratio of the probe (reflecting a decreasing level of phosphorylated substrate) as the cell progresses towards metaphase (Liu et al., 2012).

2.8 Live cell imaging

Cells were grown on glass coverslips, mounted in a silicone gasket (Chamlide CMM), and placed in a 37°C and 5% CO_2 environmental chamber (Precision Control). Images were taken using the Olympus IX81 epifluorescence microscope (Olympus) with a 40X 0.75 NA dry objective and a cooled charge coupled device camera (CoolSNAP HQ2; Photometrics) controlled by the MetaMorph 7.5 software (Molecular Devices Inc.). For analysis of mitosis, images were taken every 15 minutes using 350-ms exposures, 2x2 binned resolution, with 20% of full lamp intensity for each channel, and 7 optical sections spaced 1.0 μm apart. For

microtubule regrowth analyses, images were taken every 2 minutes using 350-ms exposures, 2x2 binned resolutions, with 20% of full lamp intensity, and 7 optical sections spaced 1.0 µm apart. Maximum intensity projection of the fluorescence channels was performed in MetaMorph 7.5 software.

Cells grown in a 96 well plate (Corning) were placed in a 37°C and 5% CO_2 environmental chamber (ImageXpress Micro XL). Images were taken using a 40X 0.75 NA dry objective with the MetaXpress 5.0.2.0 software (Molecular Devices Inc.) on the ImageXpress Micro XL epifluorecence microscope (Molecular Devices Inc.). Images were taken every 15 minutes using 100-ms exposures, 2x2 binned resolution, with 25% of full lamp intensity per channel. Movies of the fluorescence channels were made in the MetaXpress 5.0.2.0 software.

Live imaging of the PLK1 FRET biosensor was performed using the Olympus IX81 epifluorescence microscope equipped with a 60X 1.35NA oil objective and a cooled charge coupled device camera (CoolSNAP HQ2; Photometrics) controlled by the MetaMorph 7.5 software. TFP (teal fluorescent protein) and YFP (yellow fluorescent protein) emissions were acquired simultaneously with a 505DCXR beam splitter (Dual-View; Optical Insights, LLC) with the following optical filters: 438/24 for TFP excitation; 480/30 for TFP and 535/40 for YFP emission, respectively. Images were taken every 2 minutes using 300-ms exposures at 2x2 binned resolution for 30 minutes after nocodazole washout, with 45% of lamp intensity and 5 optical sections spaced 1.0 µm apart. Post-acquisition processing of images was performed using ImageJ v1.46j (National Institute of Health), as follows: The TFP and YFP emission images were background corrected by subtracting the value obtained from the cytoplasm, which does not include the kinetochore regions. The YFP/TFP FRET emission ratio value was then calculated as an average for the region of interest that was demarcated by the whole cell. Pseudocolored FRET

images were generated by viewing the ratiometric data using the Ratio LUT (Look Up Table) plugin in ImageJ.

2.9 Western blot and immunoprecipitation analyses

Cells were lysed at 0.5 - 1.0 x 10^7 cells/ ml in RIPA buffer (25 mM Tris, pH 7.8, 150 mM NaCl, 0.1% SDS, 1.0% NP-40, 0.5% sodium deoxycholate) or 0.5% NP-40 immunoprecipitation buffer (50 mM Tris-HCl, pH 7.4, 150 mM NaCl, 1 mM EDTA, 0.5% NP-40) supplemented with protease inhibitors (Roche). Cell lysates were clarified by centrifugation at 16,000 X *g* for 20 minutes at 4°C and protein concentration was determined using the BCA protein assay kit (Pierce).

For immunoprecipitation experiments, cell lysates were precleared with protein A/G PLUS-Agarose beads (Santa Cruz) and rotated for 2 hours at 4°C. Protein complexes were isolated following the incubation of pre-cleared lysates with antibodies for 6 hours at 4°C, and then the addition of protein A/G PLUS-Agarose beads for another 4 hours at 4°C during which the mixtures were rotated. Isolated complexes were washed three times with lysis buffer. Samples were mixed with SDS sample buffer, separated by SDS-PAGE, transferred to nitrocellulose, and blotted with indicated primary antibodies and detected by HRP (horseradish peroxidase)- or IR (infrared) Dye-conjugated antibodies and enhanced chemiluminescence (GE Healthcare) or Odyssey IR imaging (LI-COR) system, respectively. Precleared lysates and post-immunoprecipitation fractions were analyzed to determine the efficiency of the immunoprecipitation.

Low adhesive mitotic cells are dislodged by shaking at high speed on an orbital shaker for five minutes, cells are collected along with media after shake-off.

2.10 Statistics

Data were expressed as mean ± standard deviation (s.d.) or as mean ± standard error of mean (SEM) as indicated in each figure. Statistical analysis was performed by unpaired two-tailed Student's t-test or ANOVA as indicated in each figure. The results were considered significant at $P < 0.05$.

Table 2.1 Cloning primers and siRNA and shRNA sequences

Truncation	Sequence
$RHAMM^{FL}$	Forward (F1): 5' GGGGACAAGTTTGTACAAAAAAGCAGGCTCCACCATGGTGAGCAAGGGCGAG 3' Reverse: 5' GGGGACCACTTTGTACAAGAAAGCTGGGTCTTACTTCCATGATTCTTGAC 3'
$RHAMM^{1-623}$	F1 R:5'GGGGACCACTTTGTACAAGAAAGCTGGGTCCTATCTTATTTTATTTAGCTGTTCCTGAGCTGCACC3'
$RHAMM^{1-679}$	F F1 R:5'GGGGACCACTTTGTACAAGAAAGCTGGGTCCTATGGTGTTTGGTACCTAGAACTTAATTCAAT 3'
$RHAMM^{623-724}$	F:5'GGGGACAAGTTTGTACAAAAAAGCAGGCTTGAAGGAGATAGAACCATGAGAGATTCATATGCTAAATTATTGG 3' R: 5' GGGGACCACTTTGTACAAGAAAGCTGGGTCTTACTTCCATGATTCTTGAC 3'
$TPX2^{FL}$	F (F2): 5' GGGGACAAGTTTGTACAAAAAAGCAGGCTCCACCATGGTGAGCAAGGGCGAG 3' R: 5' GGGGACCACTTTGTACAAGAAAGCTGGGTCGTTTAAACTCTTTCTTCACCGGCA 3'
$TPX2^{1-319}$	F: F2 R: 5' GGGGACCACTTTGTACAAGAAAGCTGGGTCTAATTCATCAAATGTTCTTTTCTTTCCT 3'
$TPX2^{40-783}$	F:5'GGGGACAAGTTTGTACAAAAAAGCAGGCTCGAAGGAGATAGAACCATGAATTTGGAGAATAAGTTACTGGGG 3' R (R1): 5' GGGGACCACTTTGTACAAGAAAGCTGGGTCGTTTAAACTCTTTCTTCACCGGCA 3'
$TPX2^{319-783}$	F:5'GGGGACAAGTTTGTACAAAAAAGCAGGCTCGAAGGAGATAGAACCATGGAAACAGTTTCTACATATGTGCCC 3' R: R1
Mutagenesis	
$RHAMM^{L629R}$	F: 5' GATTCATATGCTAAAcgATTGGGTCATCAGAATTTG 3' R: 5' TCTTATTTTATTTAGCTGTTCCTGAGCTGCACC 3'
$RHAMM^{L645R}$	F: 5' AAGCATGTTGTGAAGcgGAAAGATGAAAATAGCCAACTC 3' R: 5' GATTTTTTGTTTCAAATTCTGATGACCCAATcgTTTAGC 3'
$RHAMM^{L663R}$	F: 5' AAACTCCGCTGTCAGCgTGCTAAAAAAAAACAAAGTGAG 3' R: 5' TGATACTTCCGATTTGAGTTGGCTATTTTCATCTTTCcg 3'
siRNA	
siHMMR 1	Sense: 5' GAAAUAAGGACAAGCCUAAUU 3' Antisense: 5' PUUAGGCUUGUCCUUAUUUCUU 3'
siHMMR 2	S: 5' GCAAAUACCUCCUCCCUAAUU 3' AS: 5' UUAGGGAGGAGGUAUUUGCUU 3'
siHMMR 3	S: 5' UGGCUUUCCAAUUGGCUAAUU 3' ASe: 5' PUUAGCCAAUUGGAAAGCCAUU 3'
siKif15	5' GAGCUUCAGUCUUUGCAAA3'
Control	AllStars Negative Control siRNA (proprietary), Qiagen
shRNA	
TPX2	5' CCGAGCCTATTGGCTTTGATT 3'
Control	pLKO.1 - TRC control (Plasmid 10879), Addgene

Table 2.2 PCR primers

	Sequence
qRT-PCR	
Human HMMR cDNA	Forward: 5' TGTGCTTCAGATCAAGTGG 3' Reverse: 5' CGTTGTGTTCTCTATTCCTG 3'
TBP cDNA	Forward: 5`TGCACAGGAGCCAAGAGTGAA 3' Reverse: 5`CACATCACAGCTCCCCACCA 3'
qPCR	
Human HMMR gDNA E2 – I3	Forward: 5' TTGTGCACCATCTCCAGG 3' Reverse: 5' CTGAAGCAGGCAAGGTAGT 3'
Human HMMR gDNA E10 – I10	Forward: 5' CAGGAATAGAGAACACAACG 3' Reverse: 5' GAAATCTTTCCAGGTCAGTGTA 3'
Human HMMR gDNA E13 – I14	Forward: 5' TATAAAGCGTTAACAGCCAGTG 3' Reverse: 5' CTTCTAAGTTCCAAAATCAGCA 3'
Human TBP gDNA	Forward: 5' TGGCGTGTGAAGATAACCCAAG 3' Reverse: 5' GTAGAGATGAGGTTTCACCACG 3'
Mouse HMMR gDNA	Forward: 5' AACAACTGGATGCCTTTGAAGCCG 3' Reverse: 5' AGCCTTGGAAGGGTCAAAGTGTCT 3'
Mouse GAPDH gDNA	Forward: 5' AGGTCGGTGTGAACGGATTTG 3' Reverse: 5' TGTAGACCATGTAGTTGAGGTCA 3'

Table 2.3 Primary antibodies dilutions

Antibodies	Company	Host	Dilution
Actin	Sigma	Rb	WB: 1:2000
Aurora A	Cell Signaling	Rb	WB: 1:500, IF:75
Aurora B	Abcam	Rb	WB: 1:5000, IF: 1:100
BubR1	Abcam	Mo	WB: 1:100, IF: 1:200
CENPA	Abcam	Mo	IF: 1:100,000
Cyclin B1	Cell Signaling	Mo	WB: 1:500
Eg5	Abcam	Mo	WB: 1:500, IP: 1:100, IF: 1:1000
GAPDH	Fitzgerald	Mo	WB: 1:90,000
GFP	Abcam	Mo	WB: 1:500, IP: 1:50
NDC80	Abcam	Rb	WB: 1:10,000, IF: 1:100
Kif15	Abcam	Mo	WB: 1:200, IF: 1:100, IP: 1:50
Mad2	Milliport	Mo	WB: 1:200, IF:1:100
mCherry	Abcam	Rb	WB: 1:1000, IP:1:100
Phopho-Aurora A	Cell Signaling	Rb	WB: 1:200, IF: 1:1500
PLK1	Cell Signaling	Rb	WB: 1:500
Ran	Cell Signaling	Rb	WB: 1:1000
RHAMM	Abcam	Rb	WB: 1:10,000, IF: 1:250, IP: 1:100
RHAMM	Abcam	Rb	WB: 1:10,000, IF: 1:100, IP: 1:50
TPX2	Novus Biologicals	Mo	WB: 1:1000, IF: 1:750, IP:1:100
TPX2	Novus Biologicals	Rb	WB: 1:1000, IF: 1:1000, IP: 1:100
β-tubulin	Cell Signaling	647 Conjugated	IF: 1:750
TUBG1	Sigma	Mo	IF: 1:7500

Chapter 3: Spatial regulation of Aurora A activity during mitotic spindle assembly requires RHAMM to correctly localize TPX2

Aspects of this chapter were published as:

Chen H, Mohan P, Jiang J, Nemirovsky O, He D, Fleisch MC, Niederacher D, Pilarski LM, Lim CJ, Maxwell CA. Spatial regulation of Aurora A activity during mitotic spindle assembly requires RHAMM to correctly localize TPX2.

Cell Cycle 2014; 13(14): 2248- 61. Doi: 10.4161/cc.29270. Epub 2014 May 29.

PMID: 24875404

3.1 Rationale and hypothesis

Cell division relies upon the assembly of a microtubule-based mitotic spindle apparatus that captures, aligns and segregates duplicated chromosomes. The major sites for microtubule assembly are the centrosomes, which form the spindle poles, but assembly also occurs near kinetochores (Walczak et al., 2010). Microtubule assembly is spatially regulated by the localized activation of the mitotic kinase, Aurora A (Barros et al., 2005; Giet et al., 2002; Mori et al., 2007; Terada et al., 2003). In both human and *Xenopus* dividing cells, RHAMM is a partner protein of TPX2, the principal co-activator of Aurora A during mitosis. Thus, a regulatory role for RHAMM in Aurora A activity during spindle assembly has been postulated (Groen et al., 2004; Joukov et al., 2006; Pujana et al., 2007), but not yet demonstrated.

RHAMM was identified as a mitotic hit in the MitoCheck RNAi screen, in which automated live cell analysis identified strange interphase nuclear shape, aberrant mitotic figures

and kinetics following the treatment of cells with siRNA targeting RHAMM (Neumann et al., 2010). Loss of function phenotypes that followed the inhibition of RHAMM, Aurora A or TPX2 showed substantial overlap (Fig. 3.1), which suggested shared functions. Since Aurora A activity is dependent on and limited by TPX2 availability and location (Bayliss et al., 2003; Dodson and Bayliss, 2012), I hypothesize that RHAMM interacts with and locates TPX2 in mitotic cells, which promotes the localized activation of Aurora A kinase and spindle assembly at these sites.

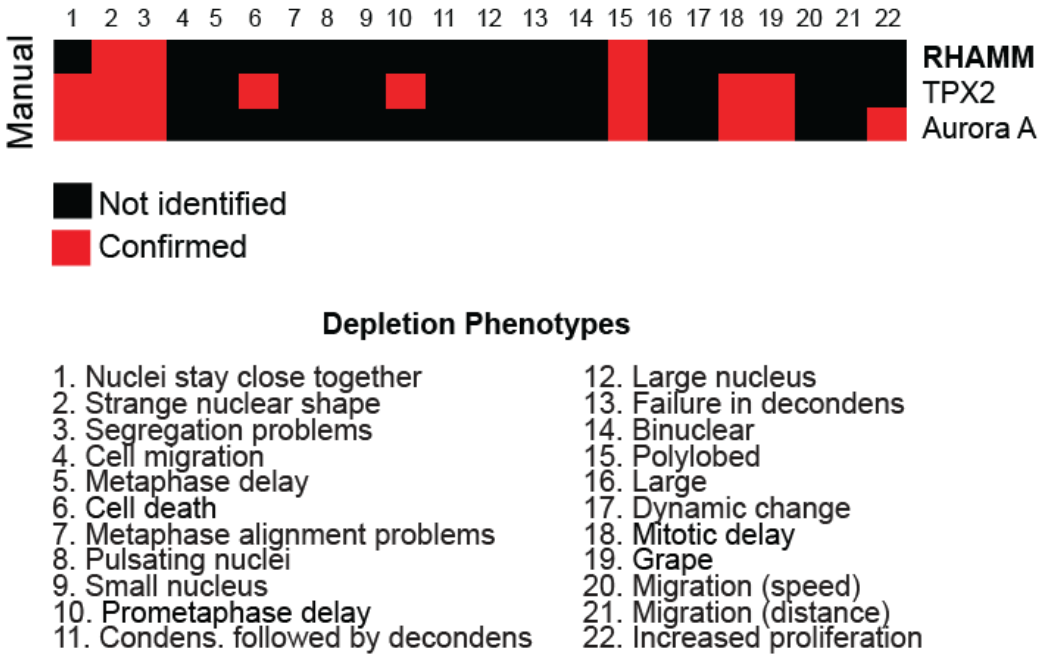

Figure 3.1 Manual comparison of RHAMM, TPX2 and Aurora A depletion phenotypes identified in the MitoCheck screen.

In a dataset published by the MitoCheck consortium (Neumann et al., 2010), manual comparison of the depletion phenotypes associated with RNAi treatments targeting RHAMM, Aurora A or TPX2 revealed similar morphological abnormalities, such as strange nuclear shape and chromosome segregation problems.

3.2 Results

3.2.1 RHAMM localization throughout mitosis

I first examined RHAMM localization by immunofluorescence throughout mitosis in HeLa cells (Fig. 3.2). During prophase, RHAMM concentrated at the center of two microtubule asters and co-localized with microtubules (β-tubulin, TUBB) growing between the two asters. During prometaphase and metaphase, RHAMM intensified at spindle poles and was present along the entire metaphase spindle. During anaphase and telophase, RHAMM was also located at the spindle midzone.

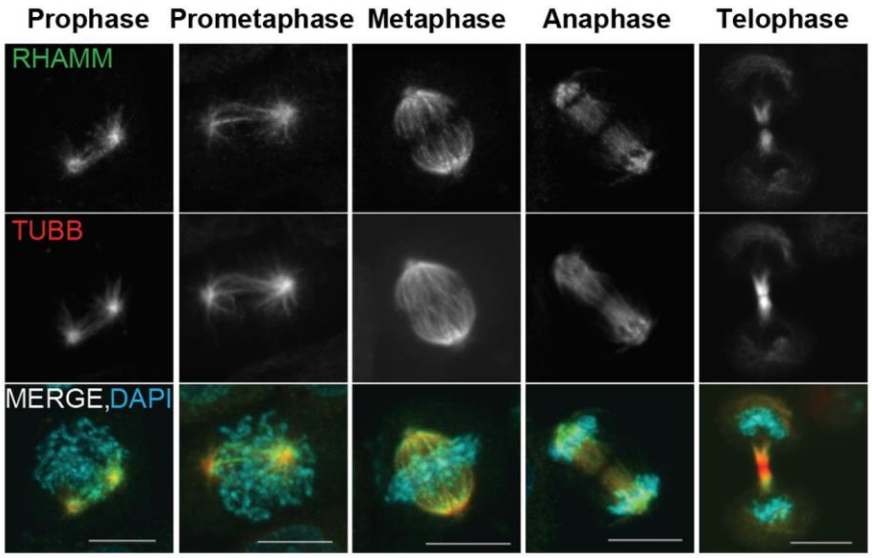

Figure 3.2 RHAMM localization during mitosis.

Fluorescence microscopy images show mitotic localization of RHAMM and the microtubule marker beta-tubulin (TUBB) in asynchronous HeLa cells. Scale bar= 10 μm.

3.2.2 RHAMM localized to both centrosome and non-centrosome sites of microtubule assembly

To study a putative role for RHAMM during spindle assembly, I used immunofluorescence to track RHAMM localization in prophase cells and found that it colocalized with a centrosome marker (γ-tubulin, TUBG1) (Fig. 3.3A). I also noted RHAMM localized to discrete foci within the chromosome volumes. I then used a kinetochore marker, BubR1, to show that RHAMM localized to punctate, non-centrosomal sites near the kinetochores. This localization was more pronounced with the expression of GFP-RHAMM in the hematopoietic cell line, RPMI-8226 (Fig. 3.3B).

To determine whether RHAMM may be involved in microtubule nucleation at centrosomes and near kinetochores, I used a regrowth assay to analyze microtubule nucleation at these foci (Fig. 3.3C). The microtubules were first depolymerized with nocodazole, then the drug was washed away and microtubule regrowth was analyzed during a recovery phase in drug-free media. Following one minute of recovery, microtubule regrowth had not occurred. At two minutes of recovery, microtubules began to assemble at centrosomes, demarked by TUBG1. By six minutes of recovery, mitotic microtubules were assembled at centrosomes as well as non-centrosome sites, which co-localized with BubR1. In these microtubule regrowth experiments, RHAMM localized to both centrosome and non-centrosome sites of microtubule assembly during mitosis.

Collectively, these data indicate that RHAMM is located at spindle poles and fibers throughout mitosis. During early mitosis, RHAMM localizes to microtubule assembly sites at both centrosomes and near kinetochores.

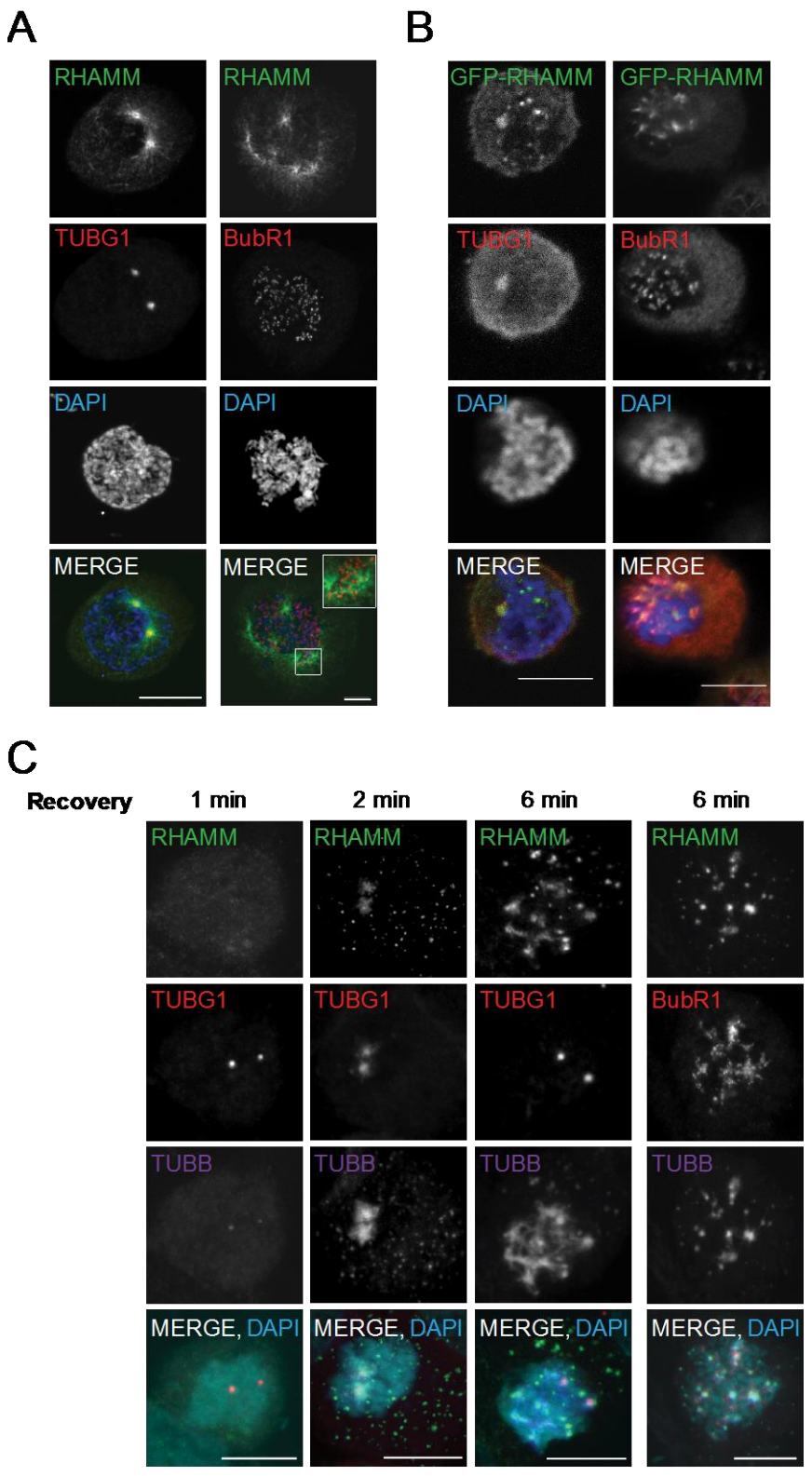
A
RHAMM
RHAMM
TUBG1
BubR1
DAPI
DAPI
MERGE
MERGE
B
GFP-RHAMM
GFP-RHAMM
TUBG1
BubR1
DAPI
DAPI
MERGE
MERGE
C
Recovery
1 min
2 min
6 min
6 min
RHAMM
RHAMM
RHAMM
RHAMM
TUBG1
TUBG1
TUBG1
BubR1
TUBB
TUBB
TUBB
TUBB
MERGE, DAPI
MERGE, DAPI
MERGE, DAPI
MERGE, DAPI

Figure 3.3 RHAMM localizes to centrosome and non-centrosomal spindle assembly sites

A) In prophase HeLa cells, RHAMM was located at the centrosomes (identified by TUBG1) as well as non-centrosomal sites near kinetochores (identified by BubR1) within nuclear volumes (identified by DAPI). Scale bars= 10 μm.

B) In prophase RPMI 8226 cells, exogenous GFP-RHAMM colocalized with TUBG1 at the centrosomes and BubR1 at the kinetochores within nuclear volumes. Scale bars= 10 μm.

C) In mitotic HeLa cells treated with nocodazole to depolymerize the mitotic spindle and released into fresh media to allow microtubule assembly, RHAMM localization at microtubule assembly sites was tracked at indicated times following release. Microtubule assembly (identified by TUBB) initiated at two minutes around the centrosomes (indicated by TUBG1). By six minutes, microtubule assembly sites included centrosomes and non-centrosomal sites near the kinetochores (indicated by BubR1). RHAMM was located at both centrosomes and non-centrosomal microtubule assembly sites. Images are representative of two experiments. Scale bars= 10 μm.

3.2.3 RHAMM is required for normal mitotic spindle architecture

To query whether RHAMM is needed for microtubule assembly or is simply a passenger microtubule associated protein at these sites, cells were separately treated with three siRNA duplexes that target the untranslated regions (UTRs) of RHAMM mRNA. In cell populations treated with siRNA targeting RHAMM (hereafter termed RHAMM-silenced), the endogenous RHAMM mRNA levels were reduced by 40-70% (Fig. 3.4A), which translated to a 70-80% reduction in the levels of RHAMM protein as measured by quantitative Western blot analysis using infrared (IR) detection (Fig. 3.4B). Cells were treated with a pool of all three siRNA targeting RHAMM for subsequent experiments, and compared to cells treated with a scrambled siRNA control. I observed a significant increase in both the proportion of cells with mitotic spindle defects, such as multipolar spindles and disorganized spindles (Fig. 3.4C), and multinucleated interphase cells in RHAMM-silenced cell populations (Fig. 3.4D). Moreover, in RHAMM-silenced cell populations, there was a significant increase in the proportion of mitotic cells, which suggested either the induction of a mitotic arrest and/or the delay of mitotic kinetics (Fig. 3.4E).

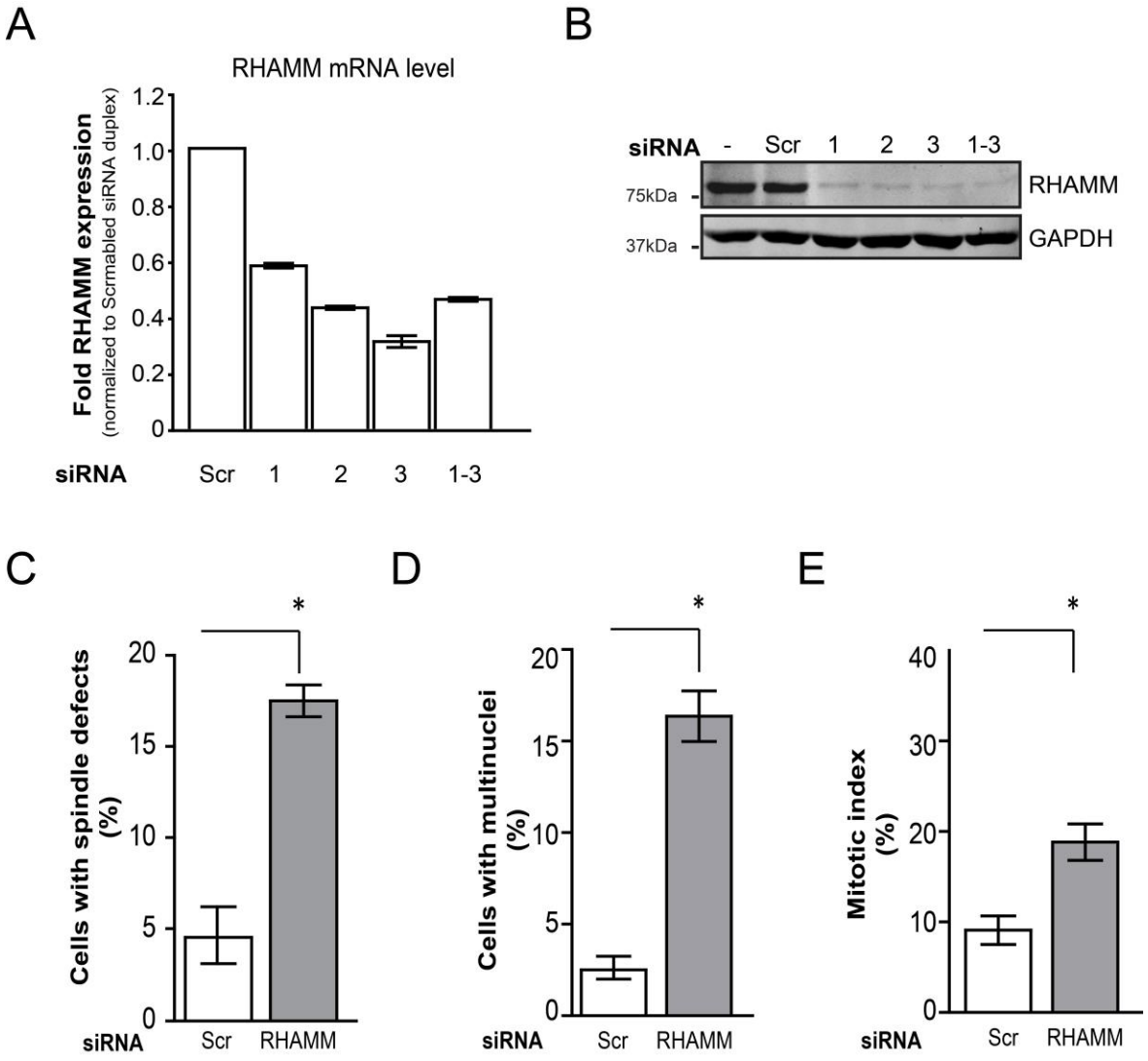
A
RHAMM mRNA level
Fold RHAMM expression
(normalized to Scrmabled siRNA duplex)
1.2
1.0
0.8
0.6
0.4
0.2
0
siRNA
Scr
1
2
3
1-3
B
siRNA
-
Scr
1
2
3
1-3
75kDa
RHAMM
37kDa
GAPDH
C
Cells with spindle defects (%)
20
15
10
5
0
*
siRNA
Scr
RHAMM
D
Cells with multinuclei (%)
20
15
10
5
0
*
siRNA
Scr
RHAMM
E
Mitotic index (%)
40
30
20
10
0
*
siRNA
Scr
RHAMM

Figure 3.4 RHAMM is required for normal mitotic spindle architecture

A) HeLa cells were treated with scrambled (Scr) siRNA control or siRNA duplexes targeting RHAMM. Quantitative PCR indicated the following expression of endogenous RHAMM at 72 hours following transfection: 42% loss following 3' UTR-A (#1), 57% loss following 3'UTR-B (#2), 69% loss following 5' UTR (#3) and 54% loss following pooled siRNA (1-3). Expression fold differences were normalized to endogenous RHAMM levels observed in control-treated cell populations. (mean ± s.d., n= 3, ANOVA)

B) HeLa cells were treated with scrambled siRNA or siRNA duplexes targeting RHAMM. RHAMM expression was measured by quantitative Western blot analysis at 72 hours following transfection. Protein bands were visualized by Licor imaging using IR fluorophore tagged secondary antibodies. Equal loading was confirmed by probing for GAPDH.

C) Aberrant spindle figures (multipolar spindle, disorganized spindle and unattached chromosomes) were significantly more frequent in RHAMM-silenced cells. Asynchronized HeLa cells were stained for beta-tubulin (TUBB) to visualize the spindle. (mean ± s.d., n= 3, >100 cells/treatment, **P*< 0.05, t-test)

D) Multinucleated cells were significantly more frequent in RHAMM-silenced cells. Asynchronized HeLa cells were stained with DAPI to visualize nuclei. (mean ± s.d., n= 3, >100 cells/treatment, **P*< 0.05, t-test)

E) Mitotic cells were identified by DAPI and TUBB immunofluorescence and the ratio between the number of mitotic cells and the total number of cells (mitotic index) was determined. The mitotic index was significantly higher in RHAMM-silenced cells. (mean ± s.d., n= 3, >100 cells/treatment, **P*< 0.05, t-test)

3.2.4 RHAMM is required for normal spindle assembly kinetics

To help distinguish between mitotic arrest and delayed kinetics, non-synchronized HeLa cells that stably express eGFP-alpha tubulin (TUBA) and mCherry-Histone H2B were followed by time-lapse microscopy as they transited through mitosis (Fig. 3.5A). I quantified the time necessary for spindle assembly and completion of mitosis by tracking the progression of mitotic cells (Fig. 3.5B and C). Spindle assembly duration was defined as the time necessary to transit from the onset of prophase (chromosome condensation) to the onset of metaphase (chromosome alignment), and mitosis duration was defined as the time necessary to transit from the onset of prophase to the end of telophase (disappearance of the midzone spindle). In control cells pretreated with scrambled siRNA, the average duration for spindle assembly was 26 ± 9 minutes and these cells completed mitosis in 106 ± 17 minutes (Fig. 3.5B), which are similar kinetics to those of untreated cells (27 ± 13 minutes and 118 ± 24 minutes, respectively). In RHAMM-silenced cells, however, I observed a significant delay in both the time needed to assemble a bipolar spindle and the time needed to complete mitosis (51 ± 17 minutes and 185 ± 32 minutes, respectively); indeed, 43% of RHAMM-silenced mitotic cells were unable to complete mitosis during the imaging time and these cells were excluded from the quantification of mitosis completion (Fig. 3.5C).

RHAMM-silenced cells exhibit delayed spindle assembly kinetics and mitosis completion. Immunofluorescence analysis demonstrated a significant increase in aberrant spindle morphology and multinucleated cells in RHAMM-silenced relative to control-treated cells.

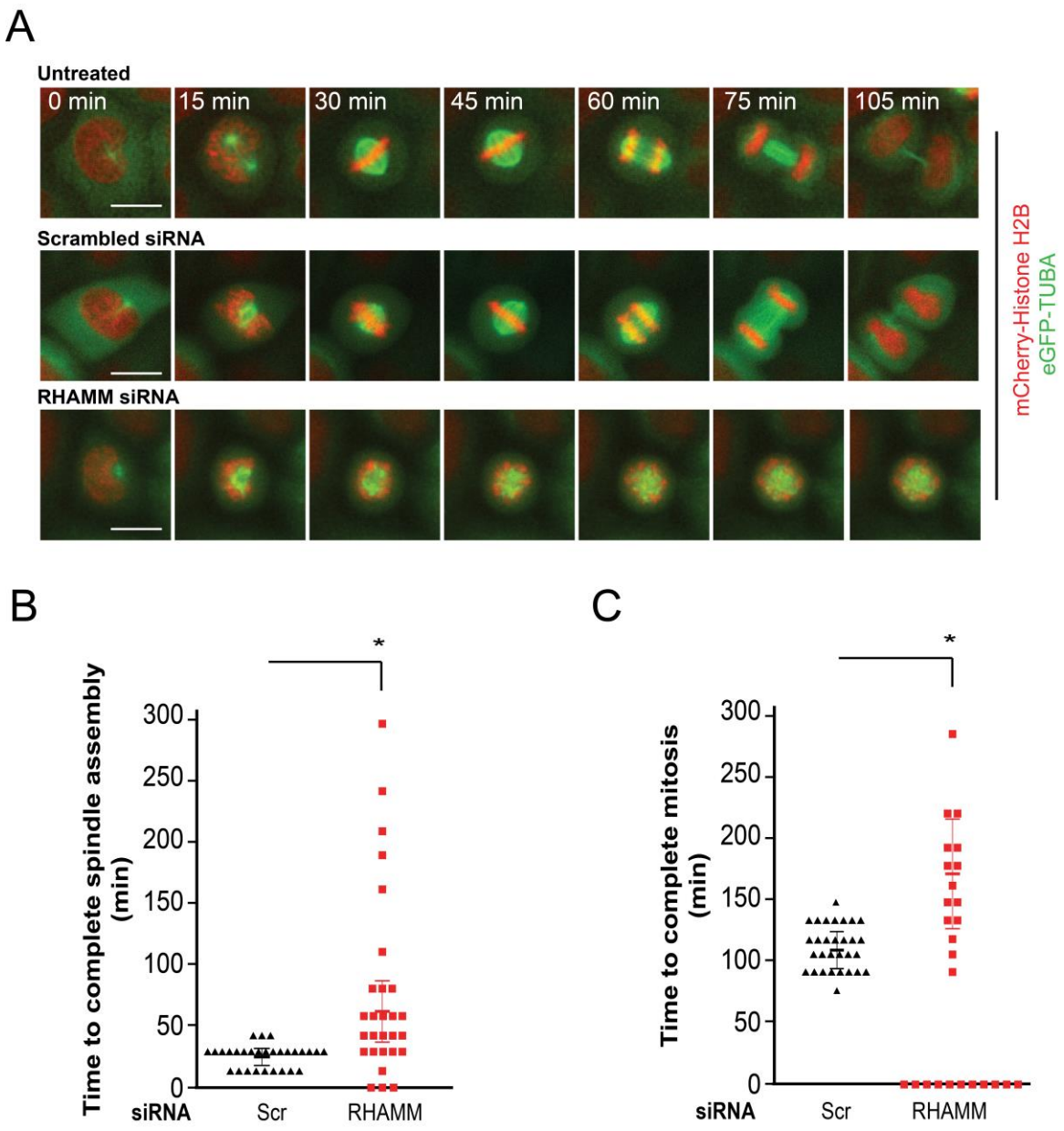

Figure 3.5 Proper mitotic kinetics and microtubule assembly kinetics depend on RHAMM

A) Living HeLa cells were pre-treated with either scrambled siRNA or siRNA duplexes targeting RHAMM and followed through mitosis by time-lapse microscopy. Scale bars= 10 μm.

B) Spindle assembly duration is significantly delayed in RHAMM-silenced cells. Cells that arrested in prometaphase during imaging were plotted at 0 minutes. (mean ± s.d., 30 cells/treatment, n= 6, **P*< 0.05, t-test).

C) Mitosis duration is significantly delayed in RHAMM-silenced cells. Cells that did not complete mitosis during imaging were plotted at 0 minutes and were not included in the quantification of mitosis duration. (mean ± s.d., 30 cells/treatment, n= 6, **P*< 0.05, t-test).

3.2.5 GFP-RHAMM rescues aberrant spindle phenotypes in RHAMM-silenced cells

To demonstrate that the aberrant mitotic phenotypes observed in the population of RHAMM-silenced cells are due to the loss of RHAMM expression, I transiently transfected a wild-type transgene tagged with GFP at the amino (N)-terminus (GFP-RHAMM) into RHAMM-silenced cells, following the protocol outlined in Fig. 3.6A. This transgene lacks the 5'- and 3'-UTR and resists the siRNA targeted to these regions such that GFP-RHAMM was expressed at levels that approximated endogenous RHAMM levels (top band is GFP-RHAMM in Fig. 3.6B). GFP-RHAMM decorated the spindle poles and fibers during early mitosis, similar to the localization of the endogenous protein (Fig. 3.6C). After treatment with siRNA targeting RHAMM, transient expression of GFP-RHAMM reduced the proportion of cells with mitotic spindle defects (Fig. 3.6D) and multinucleated cells (Fig. 3.6E).

3.2.6 GFP-RHAMM rescues aberrant mitotic kinetics in RHAMM-silenced cells

Next, I used time-lapse microscopy to analyze the kinetics of division in RHAMM-silenced cells expressing GFP-RHAMM. Time-lapse microscopy was performed during optimal GFP-RHAMM expression, 24 - 48 hours post transfection, and a Hoechst stain was added to the media to visualize DNA (Fig. 3.7A). Analysis of time-lapsed videos revealed that transient expression of GFP-RHAMM was able to reduce both the duration of spindle assembly and the time needed to complete mitosis (32 ± 17 minutes and 131 ± 29 minutes, respectively) (Fig. 3.7B and C). Moreover, only 17% of the cells did not complete mitosis after GFP-RHAMM rescue, compared to the 43% of RHAMM-silenced cells that did not complete mitosis.

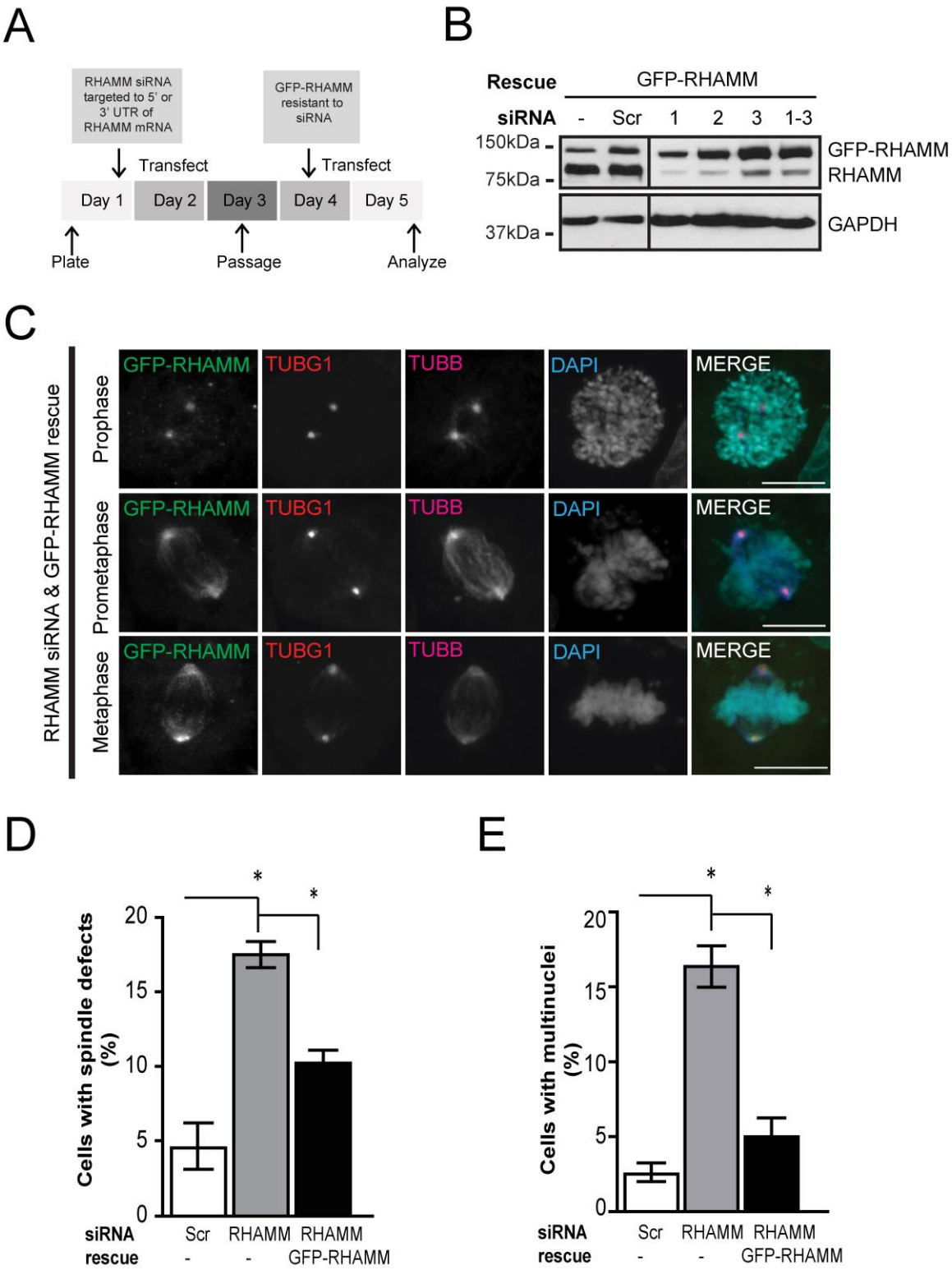
A
RHAMM siRNA targeted to 5' or 3' UTR of RHAMM mRNA
GFP-RHAMM resistant to siRNA
Transfect
Transfect
Day 1
Day 2
Day 3
Day 4
Day 5
Plate
Passage
Analyze
B
Rescue
GFP-RHAMM
siRNA
- Scr 1 2 3 1-3
150kDa
75kDa
37kDa
GFP-RHAMM
RHAMM
GAPDH
C
RHAMM siRNA & GFP-RHAMM rescue
Prophase
Prometaphase
Metaphase
GFP-RHAMM
TUBG1
TUBB
DAPI
MERGE
D
Cells with spindle defects (%)
siRNA
rescue
Scr
RHAMM
RHAMM
GFP-RHAMM
E
Cells with multinuclei (%)
siRNA
rescue
Scr
RHAMM
RHAMM
GFP-RHAMM

Figure 3.6 Expression of GFP-RHAMM rescues aberrant spindle phenotypes in RHAMM-silenced cells

A) Experimental protocol for silencing endogenous RHAMM and expressing GFP-RHAMM.

B) GFP-RHAMM was transfected into HeLa cells that were initially treated with scrambled siRNA or siRNA duplexes targeting RHAMM for 48 hours. GFP-RHAMM then was transfected into these cells. After a further 48 hours, the expression of RHAMM, and GFP-RHAMM (shifted by 27 kDa), were measured by Western blot analysis. Equal loading was confirmed by probing for GAPDH.

C) GFP-RHAMM localized along the spindle fibers and at the spindle poles in RHAMM-silenced cells. Scale bars= 10 μm.

D) Proportion of aberrant spindle figures were significantly reduced with expression of GFP-RHAMM in RHAMM-silenced cells. (mean ± s.d., >100 cells/treatment, n= 3, *P< 0.05, t-test)

E) Multinucleated cells were significantly reduced with expression of exogenous GFP-RHAMM in RHAMM-silenced cells. (mean ± s.d., >100 cells/treatment, n= 3, *P< 0.05, t-test)

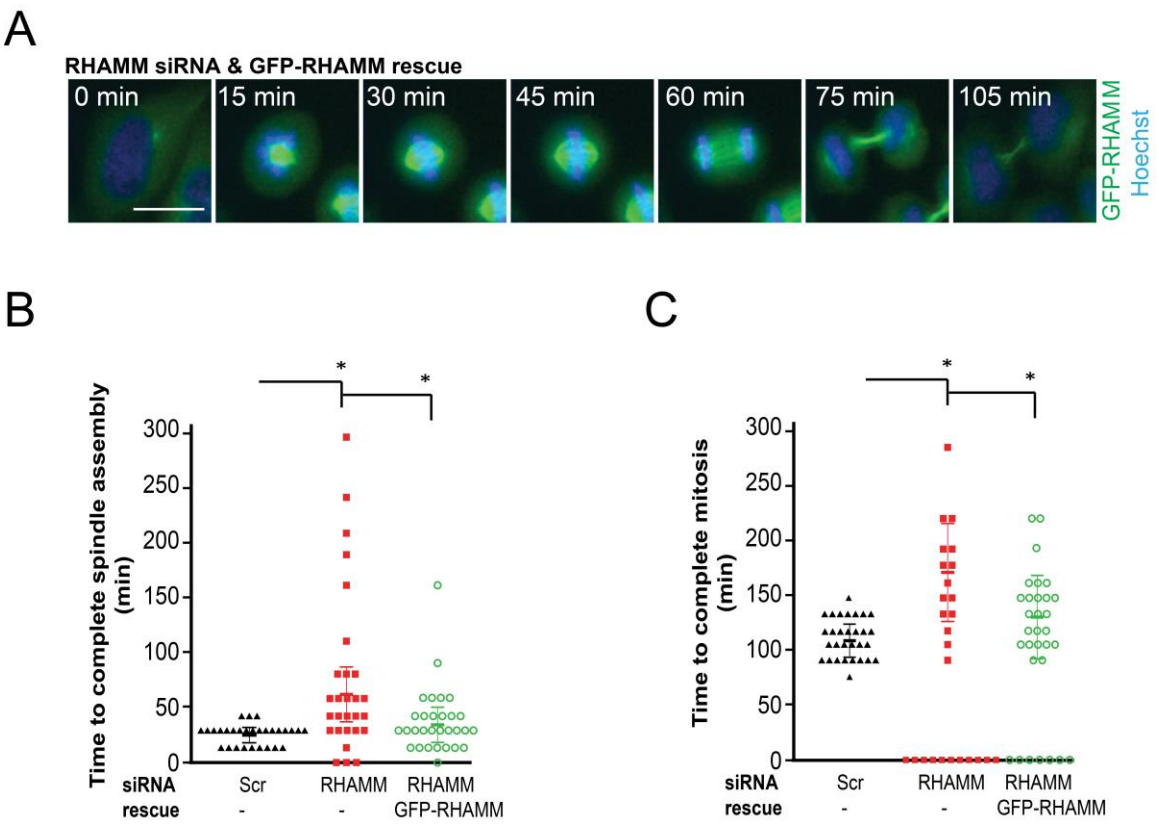

Figure 3.7 Expression of GFP-RHAMM rescues aberrant mitotic kinetics in RHAMM-silenced cells

A) HeLa cells were treated with siRNA duplexes targeting RHAMM and rescued with exogenous GFP-RHAMM. Cells were labelled with Hoechst to visualize DNA and followed through mitosis by time-lapse microscopy. Scale bars= 10 μm.

B) Transient expression of exogenous GFP-RHAMM significantly reduced the time needed for spindle assembly in RHAMM-silenced cells (as quantified in Fig. 3.5). Cells that arrested in prometaphase during imaging were plotted at 0 minutes. No significant differences were observed between control cells and GFP-RHAMM rescued cells. (mean ± s.d., 30 cells/treatment, n= 6, **P*< 0.05, t-test)

C) Transient expression of exogenous GFP-RHAMM significantly reduced the time to transit through mitosis in RHAMM-silenced cells (as quantified in Fig. 3.5). Cells that did not complete mitosis during imaging were plotted at 0 minutes and were not included in the quantification of mitosis duration. No significant differences were observed between control cells and GFP-RHAMM rescue cells. (mean ± s.d., 30 cells/treatment, n= 6, **P*< 0.05, t-test)

3.2.7 RHAMM depletion attenuates non-centrosomal microtubule assembly

To determine the role of RHAMM during the assembly of a bipolar mitotic spindle, I measured the kinetics of microtubule regrowth after nocodazole depolymerization in living mitotic cells. HeLa cells expressing eGFP-TUBA were first treated either with a scrambled siRNA or siRNA targeting RHAMM, and then subjected to nocodazole-mediated microtubule depolymerization. In comparison to scrambled siRNA- treated control cells, microtubule nucleation and the formation of a bipolar spindle was delayed in RHAMM-silenced cells (Fig. 3.8A). Specifically, in control-treated cells, multiple nucleation sites were present at 4 minutes of recovery, whereas RHAMM-silenced cells only contained two nucleation sites (Fig. 3.8B), suggesting that RHAMM may seed or establish microtubule assembly at non-centrosome sites. To investigate this, I quantified the number of microtubule regrowth foci in fixed cells at six minutes following recovery, when both centrosome and non-centrosome assembly sites should be present, as observed previously in Fig. 3.3C. I observed a significant reduction in the number of microtubule foci assembled at non-centrosome sites in RHAMM-silenced cells and the expression of GFP-RHAMM was sufficient to recover the number of these sites (Fig. 3.8B). Further analysis of both live and fixed cells showed non-centrosomal spindle assembly was not eliminated with RHAMM depletion, but rather was significantly attenuated and delayed to later time points in the microtubule regrowth assay.

A

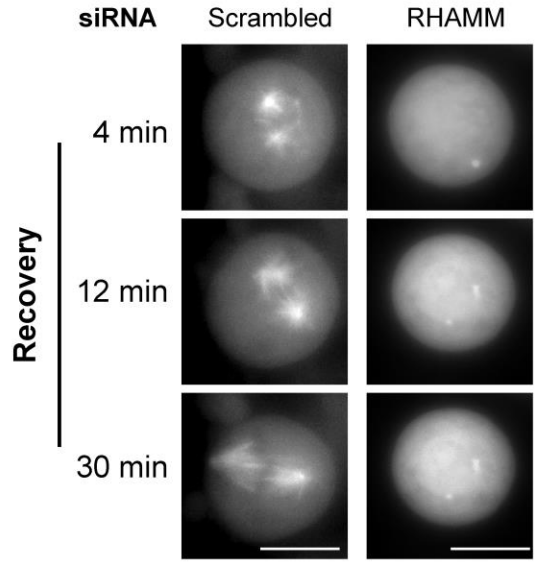
siRNA
Scrambled
RHAMM
Recovery
4 min
12 min
30 min

B

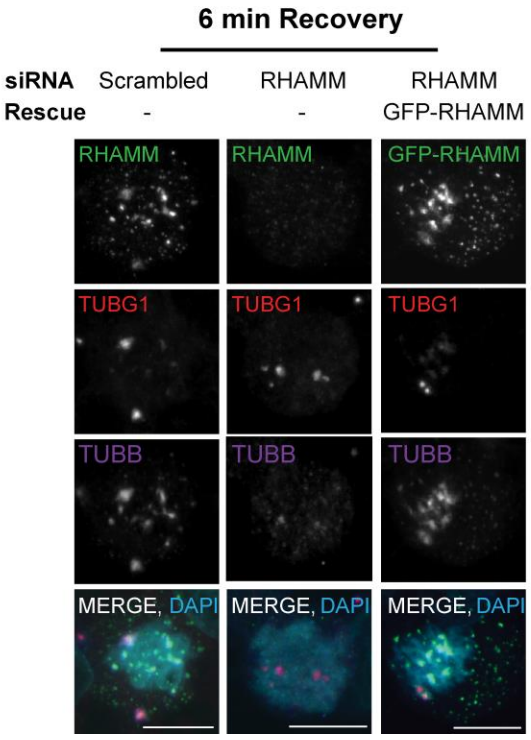
6 min Recovery
siRNA
Scrambled
RHAMM
RHAMM
Rescue
-
-
GFP-RHAMM
RHAMM
RHAMM
GFP-RHAMM
TUBG1
TUBG1
TUBG1
TUBB
TUBB
TUBB
MERGE, DAPI
MERGE, DAPI
MERGE, DAPI

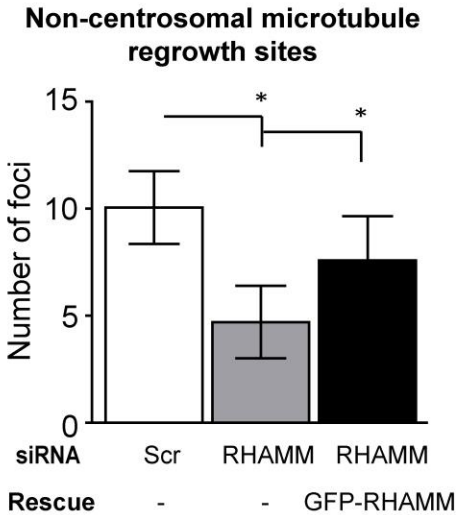
Non-centrosomal microtubule regrowth sites
Number of foci
15
10
5
0
*
*
siRNA
Scr
RHAMM
RHAMM
Rescue
-
-
GFP-RHAMM

Figure 3.8 RHAMM depletion attenuates microtubule assembly at non-centrosome sites

A) In living RHAMM-silenced HeLa cells expressing eGFP-TUBA, microtubule assembly and the formation of a bipolar spindle following nocodazole treatment were disrupted in comparison to control-treated cells. Scale bars= 10 μm.

B) In mitotic RHAMM-silenced cells that had recovered for six minutes following nocodazole treatment, microtubule assembly at non-centrosome sites was attenuated and the expression of GFP-RHAMM was sufficient to re-establish microtubule assembly at these sites. TUBG1 marks the centrosomes. Scale bars= 10 μm. (mean ± s.d., n= 4, > 40cells/ treatment *P< 0.05, t-test).

3.2.8 RHAMM localizes TPX2 at microtubule assembly sites and is needed for TPX2 stability

In *Xenopus* egg extracts, the XRHAMM -TPX2 complex may stabilize microtubules and focus spindle poles; specifically, immunodepletion of XRHAMM prevented TPX2 concentration at spindle poles (Groen et al., 2004). However, these experiments did not distinguish microtubule nucleation from microtubule stabilization (Groen et al., 2004). To distinguish these two events, I used a mitotic microtubule regrowth assay to examine the localization of TPX2 to sites of microtubule assembly in control-treated and RHAMM-silenced mitotic cells. I noted significantly fewer TPX2-positive microtubule regrowth sites in RHAMM-silenced cells, which were restored by subsequent rescue with GFP-RHAMM expression (Fig. 3.9A). Next, I localized TPX2 by immunofluorescence in non-synchronized mitotic HeLa cells and found that TPX2 was lost from spindle poles (i.e., regions of interest identified by TUBG1) in RHAMM-silenced mitotic cells (Fig. 3.9B). These findings suggest TPX2 localization at microtubule assembly sites is dependent on the presence of RHAMM.

In both of the described assays, the abundance of TPX2 appeared reduced in RHAMM-silenced cells. To test the possibility that the specific loss of RHAMM reduced the stability of TPX2, I determined the abundance of these proteins in lysates from G2/M synchronized cell populations. Synchronized populations of RHAMM-silenced cells showed reduced abundance of RHAMM and TPX2, but not the GTP binding protein Ran, which is also involved in spindle assembly at non-centrosome sites (Fig. 3.9C). Pre-treatment of cells with the proteasome inhibitor MG132 recovered TPX2 levels in RHAMM-silenced cells (Fig. 3.9C), which implies that the loss of RHAMM augments proteasome-dependent turnover of TPX2.

Given that Aurora A stability is regulated by TPX2 binding (Giubettini et al., 2011), I next measured the levels of Aurora A and active, autophosphorylated Aurora A (pAurora A) in these lysates (Fig. 3.9D). Like TPX2, the abundance of Aurora A and the levels of pAurora A were reduced in RHAMM-silenced G2/M synchronized cell lysates. Addition of a proteasome inhibitor to RHAMM-silenced cells (fourth lane, Fig. 3.9D) resulted in a total level of Aurora A greater than that seen in control-treated cells (first lane, Fig 3.9D). However, the pAurora A levels were attenuated in RHAMM-silenced, proteasome inhibited cells (fourth lane, Fig. 3.9D) relative to control-treated cells (first lane, Fig 3.9D) despite elevated levels of total Aurora A and total TPX2 (fourth lane, Fig. 3.9C). The reduced levels of pAurora A observed in lysates collected from MG132-treated, RHAMM-silenced cells, suggest that activation of Aurora A may be sub-optimal, in spite of appropriate levels of total Aurora A and TPX2, due to mislocalization of TPX2 in the absence of RHAMM.

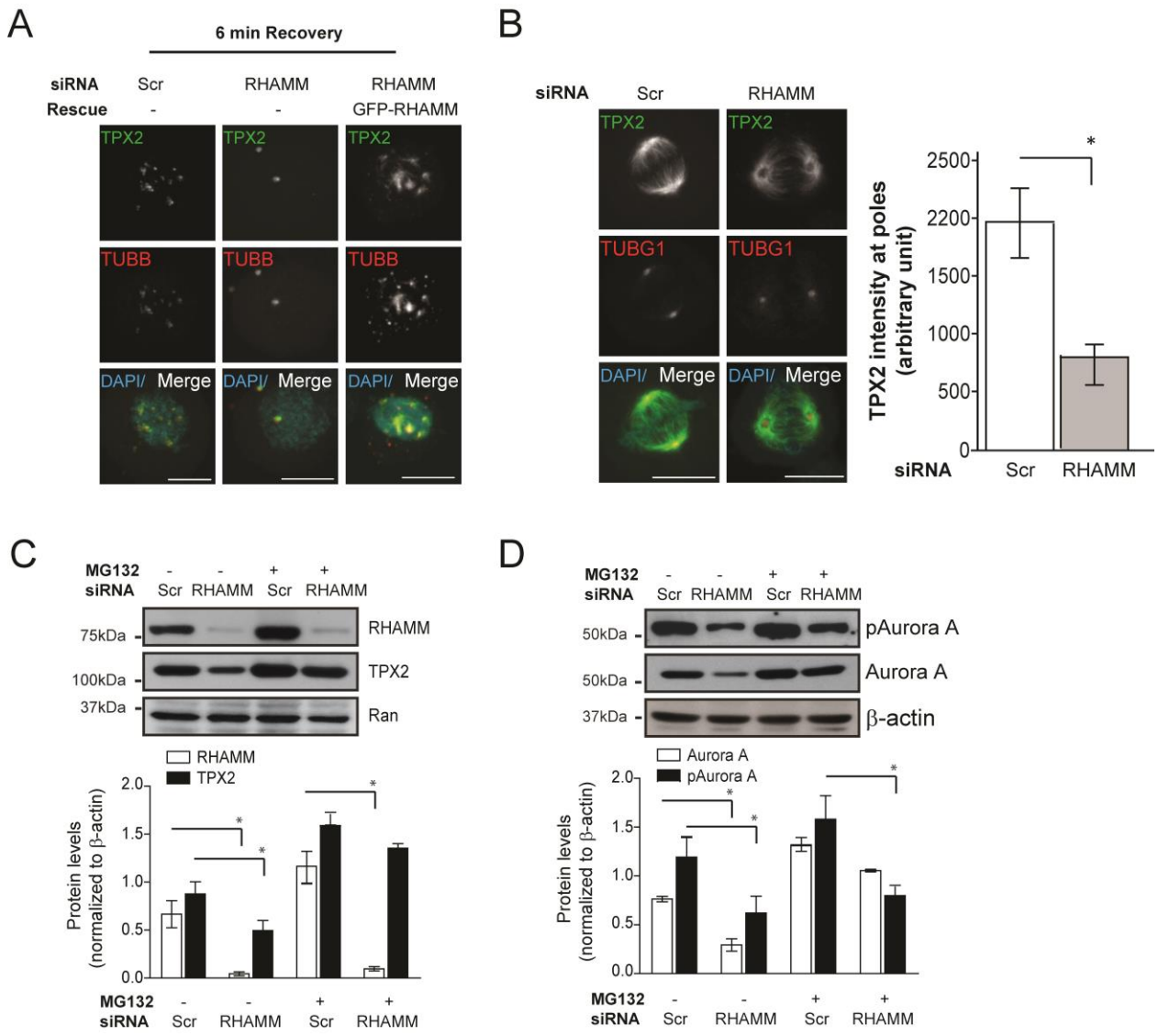
A
6 min Recovery
siRNA Scr RHAMM RHAMM
Rescue - - GFP-RHAMM
TPX2
TUBB
DAPI/ Merge
B
siRNA Scr RHAMM
TPX2
TUBG1
DAPI/ Merge
TPX2 intensity at poles (arbitrary unit)
2500
2200
1500
1000
500
0
*
siRNA Scr RHAMM
C
MG132 - - + +
siRNA Scr RHAMM Scr RHAMM
75kDa
100kDa
37kDa
RHAMM
TPX2
Ran
RHAMM
TPX2
Protein levels (normalized to β-actin)
2.0
1.5
1.0
0.5
0.0
*
*
*
MG132 - - + +
siRNA Scr RHAMM Scr RHAMM
D
MG132 - - + +
siRNA Scr RHAMM Scr RHAMM
50kDa
50kDa
37kDa
pAurora A
Aurora A
β-actin
Aurora A
pAurora A
Protein levels (normalized to β-actin)
2.0
1.5
1.0
0.5
0.0
*
*
*
MG132 - - + +
siRNA Scr RHAMM Scr RHAMM

Figure 3.9 RHAMM is required for TPX2 stability and localization at microtubule assembly sites

A) In mitotic RHAMM-silenced cells that had recovered for six minutes following nocodazole treatment, TPX2 did not locate to non-centrosome sites of microtubule assembly. GFP-RHAMM expression re-established microtubule assembly and TPX2 at these sites. Scale bars= 10 μm.

B) Spindle pole (identified by TUBG1) - localized TPX2 was significantly reduced in RHAMM-silenced cells. Scale bars= 10 μm. (mean ± s.d., 75 cells/treatment, n= 3, *P< 0.05, t-test).

C) HeLa cells were treated with indicated siRNA and synchronized in early mitosis. RHAMM and TPX2 abundance were reduced in lysates obtained from RHAMM-silenced populations. Treatment of cells with a proteasome inhibitor (MG132, 15 μM for 2 hours) recovered TPX2 abundance in RHAMM-silenced cell lysates. Ran served as a related protein that was unaffected in lysates obtained from RHAMM-silenced cells. Protein bands were visualized by Licor imaging using IR fluorophore tagged secondary antibodies. Protein levels were normalized to β-actin. (mean ± SEM., n= 2, *P< 0.05, ANOVA).

D) HeLa cells were treated with indicated siRNA and synchronized in early mitosis. Aurora A and pAurora A were reduced in lysates obtained from RHAMM-silenced populations. Treatment of cells with a proteasome inhibitor (MG132, 15 μM for 2 hours) recovered the level of Aurora A, but not pAurora A, in RHAMM-silenced cell lysates. Protein bands were visualized using IR fluorophore tagged secondary antibodies. Protein levels were normalized to β-actin. (mean ± SEM., n= 2, *P< 0.05, ANOVA).

3.2.9 RHAMM temporally and spatially regulates Aurora A activity

The results described in section 3.2.8 suggest a regulatory relationship between RHAMM and Aurora A activity during mitotic spindle assembly. To test this, I employed both fixed and live cell experiments that examined Aurora A activity in RHAMM-silenced cells. In asynchronous mitotic cells, I used immunofluorescence to measure the levels of pAurora A at mitotic spindle poles marked by TUBG1 (Fig. 3.10A); as a positive control to reduce kinase activity, mitotic cells were pretreated with an Aurora A-specific small-molecule inhibitor, MLN8237, or the delivery vehicle, DMSO. In RHAMM-silenced cells, or cells pre-treated with MLN8237, I observed significantly reduced levels of pAurora A at spindle poles. To analyze Aurora A activity at non-centrosome sites of assembly, I used mitotic microtubule regrowth experiments and immunofluorescence to measure pAurora A abundance at these sites after six minutes for recovery as described previously (Fig. 3.8). In scrambled siRNA-treated cells, or vehicle control-treated cells, non-centrosome sites for assembly were strongly positive for pAurora A (Figs. 3.10B). In RHAMM-silenced cells, or cells pre-treated with MLN8237, the intensity of pAurora A was reduced at these sites.

A complicating issue for the measurements of assembly at non-centrosome sites in RHAMM-silenced cells was the fact that these sites were significantly reduced when measured six minutes after release from nocodazole. To overcome this deficiency, and to add kinetic information to my analysis, I utilized a FRET-based probe for Polo-like kinase 1 (PLK1) activity that is specifically targeted to kinetochores (Liu et al., 2012) to indirectly measure Aurora A activity at these sites (see section 2.7). PLK1 is a substrate for Aurora A and depletion of Aurora A by siRNA is sufficient to attenuate PLK1 activity (Bruinsma et al., 2013; De Luca et al., 2006;

Macurek et al., 2008). PLK1 activity is high in prometaphase cells and decreases by metaphase alignment; I used the iteration of the probe (Liu et al., 2012) that increases the FRET ratio (reflecting a decreasing level of phosphorylated substrate) as the cell progresses towards metaphase (Fig. 3.10C). I modified the protocol outlined in Fig. 3.6A and transfected cells with the FRET probe rather than with the GFP-RHAMM construct. During optimal expression of FRET probe, cells were treated with nocodazole for 6 hours to depolymerize mitotic microtubules. Small molecule inhibitors, or DMSO vehicle control, were added for the final 2 hours of nocodazole treatment. Drugs and/or nocodazole were removed, cells were provided fresh media (with or without drug) and mitotic cells expressing the FRET probe were imaged as they recovered from nocodazole treatment (Fig. 3.10C). The FRET emission ratio was significantly higher (indicative of lower kinase activity) in prometaphase cells pre-treated with a PLK1-specific inhibitor, BI2531, or an Aurora A-specific inhibitor, MLN8237 (Fig. 3.10D). Similarly, the FRET emission ratio was augmented in RHAMM-silenced prometaphase cells. The level of PLK1 activity is low in metaphase cells ant the pretreatment with either a PLK1 inhibitor or an Aurora A-specific inhibitor, or silencing RHAMM did not further reduce kinase activity, as would be indicated by an augmented emission ratio (Fig. 3.10D).

Collectively, the findings presented in Figures 3.9 and 3.10 suggest that RHAMM is needed to target TPX2 to non-centrosome sites, prevent proteasome-dependent turnover of TPX2, and promote microtubule assembly. In the absence of RHAMM, even when the abundance of TPX2 and Aurora A was restored through proteasome inhibition, the level of active pAurora A is sub-optimal at non-centrosome sites and kinetochores presumably due to the mislocalization of TPX2.

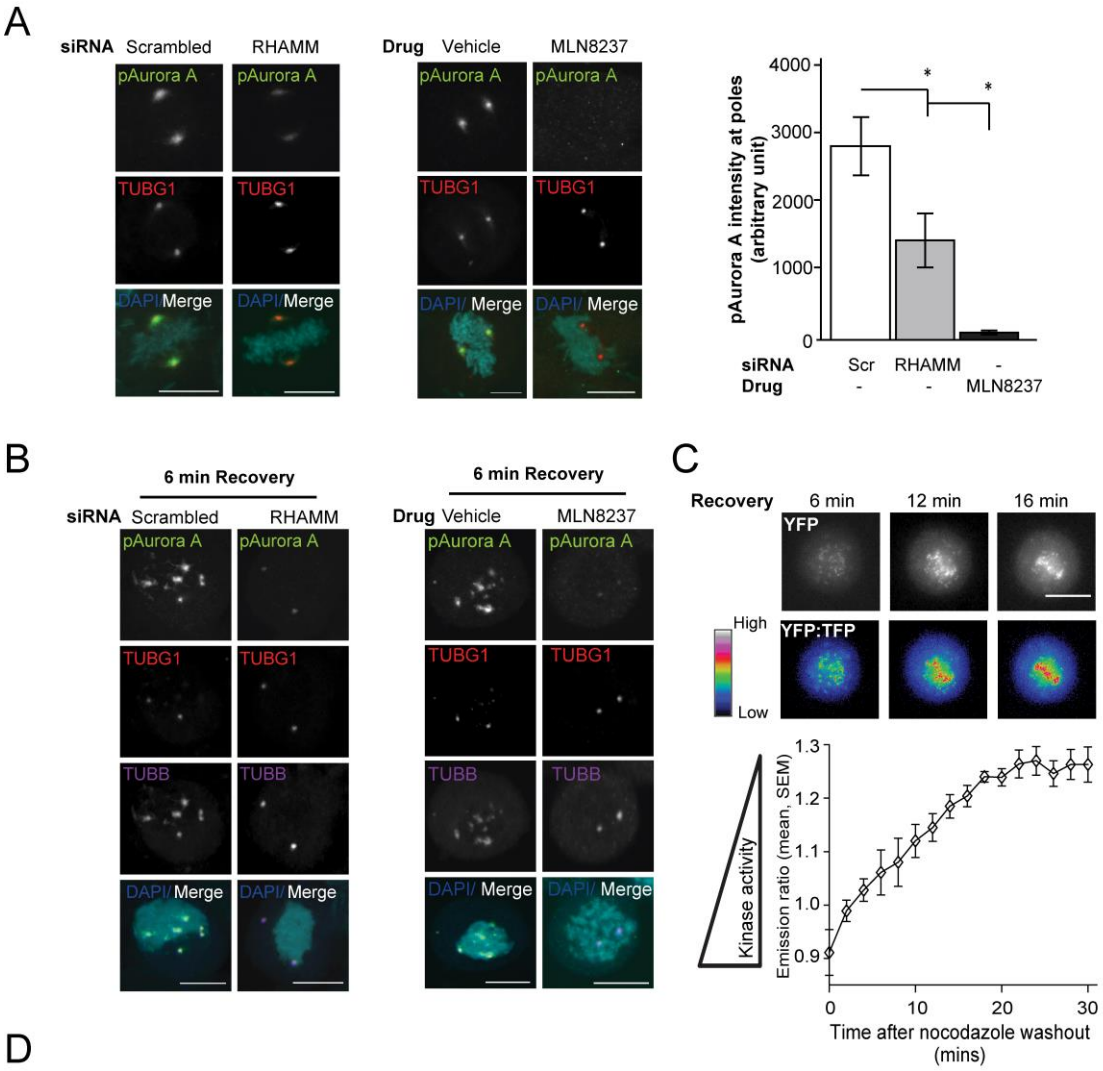
A
siRNA Scrambled RHAMM
Drug Vehicle MLN8237
pAurora A
TUBG1
DAPI/ Merge
pAurora A intensity at poles (arbitrary unit)
4000
3000
2000
1000
0
siRNA Scr RHAMM -
Drug - - MLN8237
B
6 min Recovery
siRNA Scrambled RHAMM
Drug Vehicle MLN8237
TUBB
C
Recovery 6 min 12 min 16 min
YFP
YFP:TFP
High
Low
Kinase activity
Emission ratio (mean, SEM)
1.3
1.2
1.1
1.0
0.9
0 10 20 30
Time after nocodazole washout (mins)
D
Prometaphase
Metaphase
0.6
DMSO
Plk inhibitor
Aurora A inhibitor
Scrambled siRNA
RHAMM siRNA

Figure 3.10 RHAMM is required for the temporally- and spatially- regulated activity of Aurora A

A) In asynchronous mitotic HeLa cells, pAurora A at spindle poles (regions of interest identified by TUBG1) was significantly reduced in cells pretreated with MLN8237 (Aurora A specific inhibitor, 1 μM for 2 hour) or in RHAMM-silenced cells. Scale bars= 10 μm. (mean ± s.d., >50 cells/treatment, n= 3, **P*< 0.05, t-test)

B) In mitotic HeLa cells treated with nocodazole to depolymerize microtubules and released to allow microtubule assembly, pAurora A localization to non-centrosome assembly sites was abolished in RHAMM-silenced cells or cells pre-treated with MLN8237 (1 μM for 2 hour). Scale bars= 10 μm.

C) HeLa cells expressing a Hec-1(kinetochore) targeted PLK1 FRET sensor were imaged during recovery from nocodazole treatment. Phosphorylation of the kinetochore-targeted sensor was highest in early prometaphase (0-18 minutes) and diminished to background levels by metaphase (18-20 minutes) as indicated by the increasing YFP:TFP emission ratio. Scale bars= 10 μm. (mean ± SEM., n= 3, 6 cells/treatment)

D) Relative to measurements in cells incubated with DMSO vehicle control, FRET ratios for the Hec-1 targeted PLK1 substrate were significantly higher in cells incubated with either a PLK1-specific inhibitor (BI2536, 20 nM for 2 hour) or an Aurora A- specific inhibitor (MLN8237, 1 μM for 2 hour) during prometaphase (2 minutes after nocodazole washout). Pretreatment of cells with siRNA targeting RHAMM, but not with scrambled siRNA, also significantly augmented the FRET emission ratio in prometaphase cells. No significant change in the FRET ratio was observed in metaphase cells 20 minutes after nocodazole washout (mean ± SEM., n= 3, 6 cells/treatment, **P*< 0.05, ANOVA).

3.2.10 The C-terminal bZip motif of RHAMM binds near the nuclear localization signal of TPX2

To better define the RHAMM-TPX2 protein complex and map the domains necessary for this interaction, truncation mutants were constructed for the C-terminus of RHAMM (Fig. 3.11A). GFP-RHAMM mutants were transiently expressed in cells depleted of endogenous RHAMM and the ability of these variants to co-precipitate TPX2 was tested through immunoprecipitation with antibodies to GFP, or IgG control antibodies. TPX2 was efficiently co-precipitated by RHAMM mutants that contained a minimal necessary binding domain of amino acids 623-679 (i.e. Full-length, 1-679, and 623-724), which contains the bZip motif (Fig. 3.11B). TPX2 was not found in immunoprecipitates of GFP-RHAMM mutants lacking the bZip motif [i.e. 1-623 and the ΔbZip, in which three leucines were mutated to arginines, L629R, L644R and L662R (refer to Fig. 1.4 for amino acid sequence in the bZip motif)].

Reciprocal studies were performed with transient expression of truncation variants for human TPX2. Since there are essential protein-binding domains in both the N- and C-termini of TPX2, I designed various truncation mutants from the wild-type transgene tagged with either mCherry at the N- terminus (mCherry-TPX2) or GFP at the C-terminus (TPX2-GFP) to map the domains necessary for the RHAMM interaction. mCherry-TPX2 and TPX2-GFP truncation mutants were transiently expressed in HeLa cells (Fig. 3.11C), and immunoprecipitated with antibodies to GFP, mCherry, or IgG control antibodies. mCherry-TPX2 (FL) co-precipitated RHAMM and Aurora A, which was included as a positive control (Fig. 3.11D). The Kif15/hKlp2 targeting domain [aa 319-783(Brunet et al., 2004)] was not sufficient to co-precipitate RHAMM (Fig. 3.11D). The N-terminus of TPX2 (aa 1-319), however, was sufficient, and the deletion of

the Aurora A binding domain (aa 1-40 (Bayliss et al., 2003; Brunet et al., 2004)) did not alter RHAMM-TPX2 binding. Together, these data localize the RHAMM-binding domain in TPX2 to amino acids 40- 319, which also contains an importin-α binding motif (Giesecke and Stewart, 2010).

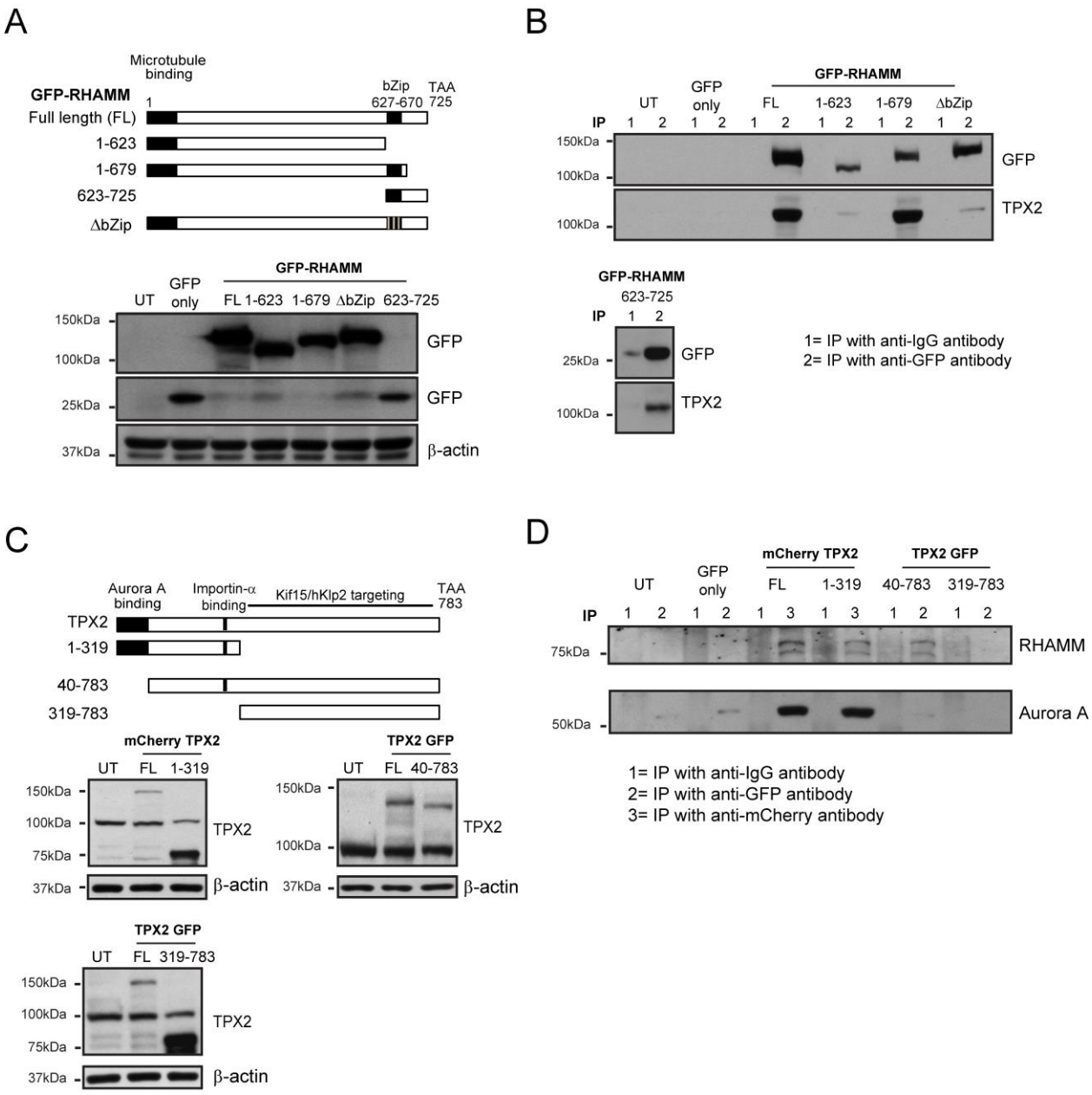
A
Microtubule binding
GFP-RHAMM
1
bZip 627-670
TAA 725
Full length (FL)
1-623
1-679
623-725
ΔbZip
GFP-RHAMM
UT
GFP only
FL 1-623 1-679 ΔbZip 623-725
150kDa
100kDa
25kDa
37kDa
GFP
GFP
β-actin
B
GFP-RHAMM
UT
GFP only
FL 1-623 1-679 ΔbZip
IP 1 2 1 2 1 2 1 2 1 2 1 2
150kDa
100kDa
GFP
100kDa
TPX2
GFP-RHAMM
623-725
IP 1 2
25kDa
GFP
100kDa
TPX2
1= IP with anti-IgG antibody
2= IP with anti-GFP antibody
C
Aurora A binding
Importin-α binding
Kif15/hKlp2 targeting
TAA 783
TPX2
1-319
40-783
319-783
mCherry TPX2
UT FL 1-319
150kDa
100kDa
75kDa
37kDa
TPX2
β-actin
TPX2 GFP
UT FL 40-783
150kDa
100kDa
37kDa
TPX2
β-actin
TPX2 GFP
UT FL 319-783
150kDa
100kDa
75kDa
37kDa
TPX2
β-actin
D
mCherry TPX2
TPX2 GFP
UT
GFP only
FL 1-319 40-783 319-783
IP 1 2 1 2 1 3 1 3 1 2 1 2
75kDa
RHAMM
50kDa
Aurora A
1= IP with anti-IgG antibody
2= IP with anti-GFP antibody
3= IP with anti-mCherry antibody

Figure 3.11 Characterization of the functional domains involved in RHAMM-TPX2 interaction

A) Schematic diagram of domains in RHAMM. The three grey lines in the ΔbZip construct represent the leucines that were mutated to arginines. Western blot analysis confirmed the expression of GFP-RHAMM constructs. β-actin levels confirmed equal loading. UT: untreated.

B) Immunoprecipitation of GFP-RHAMM constructs from cell lysates with either an IgG control antibody (lanes marked 1) or antibodies against eGFP (lanes marked 2). Co-precipitation of TPX2 identified the bZip motif as a necessary domain for the RHAMM-TPX2 interaction.

C) Schematic diagram of domains in TPX2. Western blot analysis confirmed the expression of endogenous TPX2 (100 kDa) and mCherry-TPX2 or TPX2-GFP truncation variants. The mCherry-TPX2 variants are probed with a TPX2 antibody that recognized the N-terminus of the protein, while the TPX2-GFP variants are probed with a TPX2 antibody that recognized the C-terminus of the protein. β-actin levels confirmed equal loading.

D) Immunoprecipitation of mCherry-TPX2, or TPX2-GFP, constructs from cell lysates with IgG control antibody (lanes marked 1), antibodies against eGFP (lanes marked 2) or mCherry (lane marked 3). Co-precipitation of RHAMM identified amino acids 40-319 as necessary for the TPX2-RHAMM interaction.

3.2.11 The C-terminal bZip of RHAMM is required to correctly locate TPX2 to sites of microtubule assembly and control spindle length

To map the minimal necessary domain in RHAMM required for TPX2 targeting and retention at spindle poles, I analyzed TPX2 localization at spindle poles in RHAMM-silenced cells transiently transfected with one of various GFP-RHAMM truncation variants. Loss of TPX2 attenuates kinetochore-mediated microtubule assembly and results in compression of the mitotic spindle and reduced spindle length (Bird and Hyman, 2008; Greenan et al., 2010). Therefore, I also analyzed mitotic spindle length. I observed, consistent with the published literature (Dunsch et al., 2012), that mitotic spindle orientation was disturbed in RHAMM-silenced cells. As mitotic spindles that are a normal length but are also rotated along the Z-axis may appear compressed when viewed along the Z-axis, I confirmed that both spindle poles (marked by TUBG1) were visible in one focal plane prior to measuring the pole-to-pole distance. In RHAMM-silenced cells expressing GFP-RHAMM (full-length) or GFP-RHAMM (1-679) mutants, TPX2 localized to spindle poles and decorated phenotypically normal mitotic spindles (Fig. 3.12A) of typical lengths (Fig. 3.12B). However, expression of GFP-RHAMM (1-623), which lacks the bZip motif, or GFP-RHAMM (623-724) was not sufficient to correctly localize TPX2 (Fig. 3.12A) and, consistently, mitotic spindle lengths were significantly compressed (Fig. 3.12B). Thus, the bZip motif in RHAMM is required, but is not sufficient, for the correct targeting and retention of TPX2 at spindle poles. Additional motifs in RHAMM, likely the microtubule binding domain in the N-terminus, are needed for the correct targeting and retention of TPX2 at spindle poles.

To define the necessary domains in TPX2 that may target RHAMM, reciprocal targeting experiments were performed in HeLa cells treated with shRNA targeting TPX2 (stable TPX2-silenced cell line generated as described in section 2.1.5) (Fig. 3.12C). RHAMM remains localized to spindle poles in TPX2-silenced mitotic cells (Fig. 3.12C). Spindles appeared compressed in TPX2-silenced cells, in a fashion similar to RHAMM-silenced mitotic cells. These compressed phenotypes were rescued only by the expression of full-length mCherry-TPX2 and not by truncation variants (Fig. 3.12D and E). Thus, TPX2 is not required for the correct targeting and retention of RHAMM at spindle poles.

Collectively, findings presented in Figures 3.11 and 3.12 suggest the C-terminal bZip motif in RHAMM binds a region in TPX2 that contains a nuclear localization signal and an importin-α binding motif. The bZip motif in RHAMM is required, but not sufficient, for the targeting and retention of TPX2 to spindle pole, while RHAMM localization at spindle poles does not depend on TPX2. A proper interaction between RHAMM and TPX2 is required to establish a metaphase spindle with the correct length.

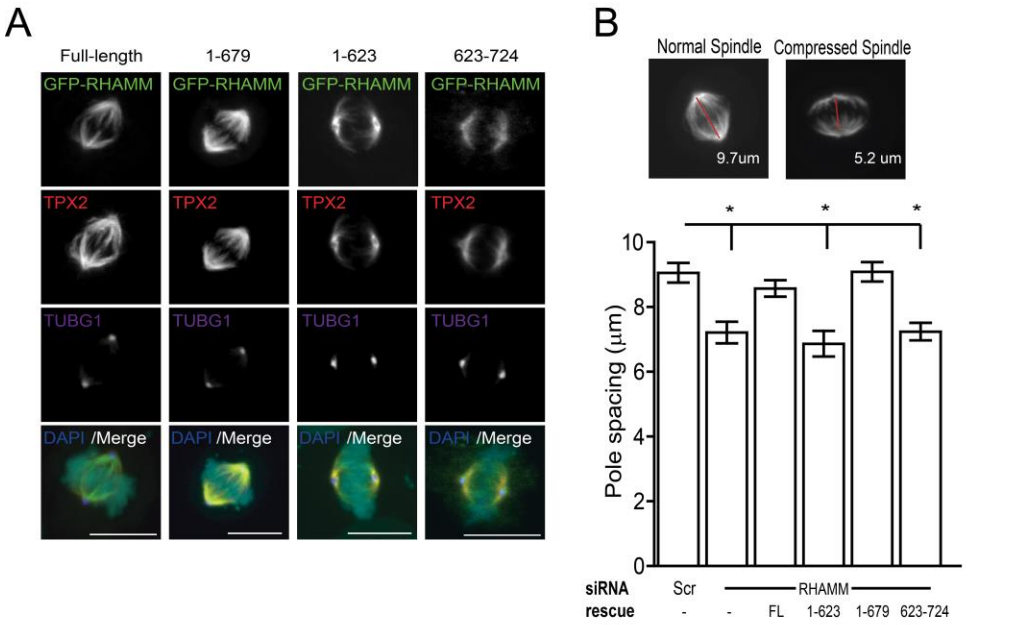
A
Full-length
1-679
1-623
623-724
GFP-RHAMM
TPX2
TUBG1
DAPI /Merge
B
Normal Spindle
Compressed Spindle
9.7um
5.2 um
Pole spacing (μm)
siRNA
rescue
Scr
RHAMM
FL
1-623
1-679
623-724
C
shRNA
Scr
TPX2
100kDa
37kDa
TPX2
β-actin
RHAMM
TUBB
TUBG1
MERGE, DAPI
Scrambled
D
Full-length
1-319
40-783
319-783
mCherry-TPX2
TPX2-GFP
E
shRNA
rescue
TPX2
FL
1-319
40-783
319-783

Figure 3.12 Mitotic spindle length requires that RHAMM targets TPX2 to the spindle poles

A) RHAMM-silenced cells were transfected with the indicated GFP-RHAMM constructs and asynchronous metaphase cells were analyzed by immunofluorescence. Amino acids 623-679 of RHAMM were the minimal required domain for TPX2 localization to spindle poles (identified by TUBG1). (Representative of 3 experiments, 30 cells/treatment) Scale bars= 10 μm.

B) RHAMM-silenced cells were transfected with the indicated GFP-RHAMM and spindle length was measured in mitotic cells with both spindle poles (based on TUBG1 staining) within one confocal slice. Measurements were made in a 3D projection along a plane perpendicular to the chromosomes. The bZip motif (623-679) was necessary, though not sufficient, to establish proper mitotic spindle length (mean ± SEM, n= 3, 30 cells/treatment, **P*< 0.05, ANOVA).

C) TPX2 was efficiently silenced in cells treated with shRNA targeting TPX2, compared to scrambled shRNA (Scr) or untreated cells. β-actin levels confirmed equal loading. RHAMM remained localized at the spindle poles in TPX2-silenced cells. (Representative of 4 experiments, 40 cells/treatment) Scale bars= 10 μm.

D) TPX2-silenced cells were transfected with the indicated mCherry-TPX2 or TPX2-GFP constructs and asynchronous metaphase cells were analyzed by immunofluorescence. (Representative of 2 experiments, 20 cells/treatment) Scale bars= 10 μm.

E) Spindle length was measured in mitotic cells with both spindle poles (based on TUBG1 staining) within one confocal slice. Cells were pre-treated with either scrambled shRNA or shRNA targeting TPX2, and followed by rescue with the indicated mCherry-TPX2 or TPX2-GFP constructs. Measurements were made in a 3D projection along a plane perpendicular to the chromosomes. (mean ± SEM, n=1, >15 cells/ treatment, **P*< 0.05, ANOVA)

3.2.12 Germline loss of RHAMM expression in MEF cells results in aberrant spindle figures and mitosis kinetics

The preceding studies of the RHAMM-TPX2-Aurora A pathway were performed in HeLa cells. HeLa cells are widely used for the study of cell division as they double every 20 hours, they tolerate various experimental manipulations such as DNA/siRNA transfections, and a variety of HeLa sub-lines with stable expression of fluorescently-tagged marker proteins are available for live cell imaging. However, despite these advantages, HeLa are cancer cells that display extensive genomic rearrangements, including hypertriploid chromosomes (Landry et al., 2013; Macville et al., 1999). Thus, to validate our findings, I examined MEF (mouse embryonic fibroblast) cells obtained from matings of *HMMR*$^{+/-}$ mice (C57/BL6N) generated in the Maxwell lab. MEFs were isolated at E13.5, genotyped, and *HMMR*$^{-/-}$ (KO, knock-out), *HMMR*$^{+/-}$ (Het, heterozygous), and *HMMR*$^{+/+}$ (WT, wildtype) MEF cells were analyzed. Genomic DNA was isolated and qPCR analysis revealed a dose dependent reduction in the wild-type *HMMR*/RHAMM allele (Fig. 3.13A). Western blot analysis of cell lysates using an antibody that recognizes mouse RHAMM showed a protein expression pattern that reflected the genomic qPCR results (Fig. 3.13B). Next, I used the same antibody to perform immunofluorescence experiments, and quantified the proportion of cells displaying aberrant metaphase and anaphase phenotypes within each MEF population (Fig. 3.13C). In both the Het and KO MEF cells, I noted a significant reduction in normal mitotic spindle figures. Specifically, more cells displayed multipolar spindle and disorganized bipolar spindle phenotypes. I observed a dose response correlating *HMMR* expression and the percentage of cells with abnormal mitotic figures, where abnormal mitotic figures increased with decreasing *HMMR* expression. Using time-lapse

microscopy, I analyzed the kinetics of cell division in the different genotypes (Fig. 3.13D). Similar to my observations in RHAMM-silenced HeLa cells, the duration of spindle assembly and mitosis was significantly longer in KO MEF cells. I also noted an increase in time needed to complete the checkpoint (transition from pro-/metaphase to anaphase) in KO MEF cells, which suggested a potential role for RHAMM during the spindle checkpoint response. For the Het MEF cells, I noted small increases in the duration of different mitotic events compared to the WT MEF cells, although these changes were not statistically significant.

In conclusion, MEF cells with germline loss of the *HMMR* gene product served as an additional model to study the loss of RHAMM function during cell division. Analysis of fixed cells showed a dose response correlating *HMMR* expression and the percentage of cells with abnormal mitotic figures. Analysis of cell division kinetics revealed a delay during spindle assembly and in the completion of the spindle checkpoint in KO compared to WT MEF cells.

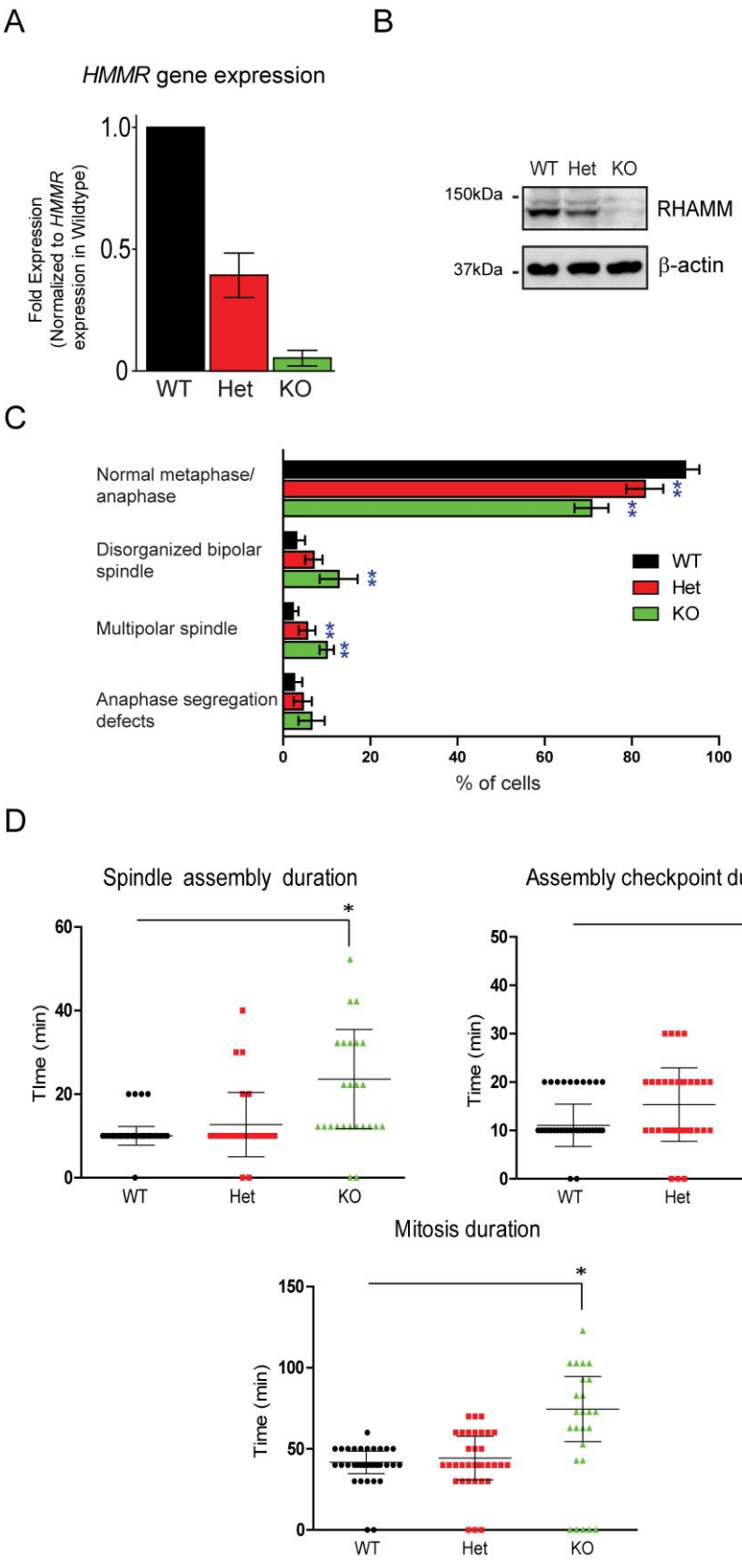
A
B
HMMR gene expression
Fold Expression (Normalized to HMMR expression in Wildtype)
1.0
0.5
0
WT Het KO
WT Het KO
150kDa
RHAMM
37kDa
β-actin
C
Normal metaphase/ anaphase
Disorganized bipolar spindle
Multipolar spindle
Anaphase segregation defects
WT
Het
KO
0 20 40 60 80 100
% of cells
D
Spindle assembly duration
Time (min)
Assembly checkpoint duration
Time (min)
Mitosis duration
Time (min)
WT Het KO

Figure 3.13 Germline deletion of *HMMR*/RHAMM results in abnormal mitotic figures and kinetics

A) Genomic DNA was extracted from mouse embryonic fibroblasts (MEFs) and the germline loss of *HMMR* was confirmed by qPCR. Expression fold differences were normalized to expression in the WT cells. (mean ± s.d., n= 3)

B) RHAMM expression was measured by Western blot analysis in nocodazole synchronized MEF cells. Equal loading was confirmed by probing for β-actin.

C) Quantification of aberrant metaphase and anaphase spindle figures in MEFs. (mean ± s.d., n= 3, >30 cells/treatment, ***P*< 0.05 compared to WT, ANOVA)

D) The kinetics of mitosis in different MEF genotypes. Cells that arrested at a particular stage of mitosis were plotted at 0 minutes and were not included in the quantification of mitosis duration. (mean ± s.d., >20 cells/treatment, n= 4, **P*< 0.05, t-test).

3.3 Key findings

1. RHAMM is located at sites of microtubule assembly (centrosomes and near kinetochores) during early mitosis.
2. Silencing RHAMM mislocalizes TPX2 and attenuates the activation of Aurora A with a consequent reduction in mitotic spindle length and an increase in the time needed to complete the process of spindle assembly.
3. The RHAMM-TPX2 complex requires a C-terminal bZip motif in RHAMM and a domain that includes the nuclear localization signal in TPX2.
4. RHAMM$^{-/-}$ MEF cells display aberrant mitotic spindle figures and delayed cell division kinetics compared to their wildtype counterparts.

3.4 Discussion

Construction of the mitotic spindle is a multi-step process that relies on microtubule assembly at various sites within the cell. RHAMM is a key cell division gene product (Neumann et al., 2010) that maintains spindle pole stability (Maxwell et al., 2005, 2003). Consistently, studies with *Xenopus* egg extracts showed that *Xenopus* RHAMM was critical for anastral (i.e., no centrosomes) spindle assembly through the Ran-GTP pathway (Groen et al., 2004; Joukov et al., 2006; Sharp et al., 2011). In addition, these studies mechanistically bridged the actions of the tumor-suppressor BRCA1-BARD1 complex, which targets RHAMM for degradation (Joukov et al., 2006; Pujana et al., 2007), to the oncogenic Aurora A-TPX2 complex during spindle assembly. However, both depletion of XRHAMM as well as the accumulation of XRHAMM,

through the loss of BRCA1, disrupted TPX2 localization to spindle poles and resulted in aberrant spindle morphology (Groen et al., 2004; Joukov et al., 2006). Thus, it was not clear whether RHAMM promotes or prevents the correct localization of TPX2 to spindle poles. Moreover, prior experiments did not distinguish spindle microtubule nucleation and spindle microtubule organization, which together are usually termed as mitotic spindle assembly. Thus, the putative contribution of RHAMM to TPX2 localization and biochemical signaling through Aurora A, and the contradictory effects of XRHAMM on TPX2 location, were unresolved.

Here, I located RHAMM to sites of microtubule assembly at centrosomes and near kinetochores in asynchronous cells and during microtubule regrowth assays. RHAMM localization to kinetochores was restricted to mitotic stages prior to chromosome alignment, and was more pronounced when GFP-RHAMM was transiently expressed in asynchronous cells. This transient localization of RHAMM to kinetochores during prometaphase may explain why Dunsch and colleagues found that RHAMM (termed HMMR) was not robustly immune-localized at cold-stable kinetochore fibers in metaphase cells (Dunsch et al., 2012). In RHAMM-silenced cells, I found that TPX2 failed to locate to non-centrosome assembly sites near kinetochores, and local Aurora A activity was severely reduced. These findings are consistent with the initial study of anastral spindle assembly in *Xenopus* cells, which showed that XRHAMM is needed to ensure correct TPX2 localization (Groen et al., 2004). Moreover, I showed that proteasome-mediated proteolysis of TPX2 and Aurora A was augmented in RHAMM-silenced cells. As the TPX2-Aurora A complex prevents the proteasome-mediated proteolysis of Aurora A (Giubettini et al., 2011; Stewart and Fang, 2005), my findings suggest that RHAMM mediated localization of TPX2 promotes a TPX2-Aurora A interaction and protects each component of the holoenzyme from proteolysis. Indeed, chemical inhibition of the

proteasome restores Aurora A and TPX2 abundance during early mitosis in RHAMM-silenced cells. However, RHAMM must be important for more than the stability of TPX2 and Aurora A as kinase activity remains sub-optimal in RHAMM-silenced cells even when the abundance of these proteins are augmented through proteasome inhibition. Indeed, I find that the location of TPX2 is disrupted in the absence of RHAMM implying that optimal Aurora kinase A activity requires both the correct abundance and location of its co-activator, TPX2. RHAMM is a necessary regulator for these interdependent processes.

Scrofani *et al* (2015) used acentrosomal *Xenopus* egg extracts to study XRHAMM during spindle assembly and validated my finding that RHAMM was a necessary enabler of TPX2-mediated Aurora A activation (Scrofani et al., 2015). Similar to my studies, Scrofani *et al* demonstrated that the TPX2-RHAMM complex performs both biochemical and structural roles (Scrofani et al., 2015). We both find that the TPX2-RHAMM complex activates Aurora A, but Scrofani *et al* (2015) also showed this complex acts as a scaffold to recruit various microtubule nucleation complexes, including the γ-tubulin ring complex and its adapter protein, NEDD1 (Neural precursor cell expressed developmentally down-regulated protein 1) (Scrofani et al., 2015). Within this multi-protein complex, Aurora A then phosphorylates NEDD1 although the precise role of this modification remains uninvestigated (Scrofani et al., 2015). Along with my studies, these findings indicate the RHAMM-TPX2-Aurora A mediated microtubule nucleation pathway is conserved between human and *Xenopus* mitotic cells and plays an important role in the nucleation of K-fibers near chromosomes.

Maxwell *et al* (2003) suggested the highly conserved bZip motif within the C-terminus of RHAMM may be involved in the formation of a trimeric protein complex that contained RHAMM, TPX2 and dynein, and that this complex was vital for spindle pole stability (Maxwell

et al., 2003). Sequence alignment shows *Xenopus*, mouse and human RHAMM are all highly homologous at their C-termini (Groen et al., 2004). Subsequently, Joukov *et al* speculated that a C-terminal fragment of XRHAMM (aa 1038-1075, containing the bZip motif) may be involved in the formation of XRHAMM homodimers or heterodimers with other SAFs and that these interactions are important for XRHAMM mitotic functions that are regulated by BRCA1/ BARD1 (Joukov et al., 2006). Indeed, my findings show the bZip motif in RHAMM as a contributor to spindle assembly, specifically this motif is required for the localization of TPX2 to the spindle poles, and associated downstream functions. To date, it remains unclear if the bZip motif is necessary for an interaction with dynein. Furthermore, I demonstrate the minimal necessary binding domain for RHAMM (aa 40-319 in TPX2) overlaps with a primary nuclear localization signal and contains the motif recognized by importin-α for nuclear import (Giesecke and Stewart, 2010). The proximity of these binding domains in TPX2 suggests that RHAMM may compete with importin-α for complexes with TPX2. If so, RHAMM may provide additional regulation of TPX2 by liberating TPX2 from the importin complex as required for spindle assembly through the Ran-GTP pathway. Previous findings show importin-α prevents TPX2-induced microtubule formation in *Xenopus* egg extracts, while a TPX2 mutant that cannot bind importin-α is constitutively active in the induction of microtubule aster formation, both conditions were shown to be detrimental for spindle assembly (Schatz et al., 2003). Thus, competitive binding to TPX2 between RHAMM and importin-α may ensure an appropriate level of TPX2-induced microtubule formation occurs during mitosis, since both the depletion of TPX2 and excess TPX2 result in abnormal spindle morphology and mitotic failure (Gruss et al., 2002, 2001; Wittmann et al., 2001).

The pathway of K-fiber production during anastral spindle assembly is not well defined in mammalian cells. This is due in part to the fact that multiple spindle assembly mechanisms exist in parallel within a single dividing cell. While these compensatory pathways ensure a functional spindle is made under most circumstances, this redundancy makes investigation of a single pathway challenging. My work, along with those presented by Scrofani *et al* (2015), provides a cohesive mechanism by which RHAMM promotes anastral spindle microtubule nucleation by regulating the Aurora A-TPX2 complex in both human and *Xenopus* dividing cells. I demonstrate that the regulation of TPX2 by RHAMM is twofold: 1) RHAMM targets TPX2 to spindle assembly sites; and, 2) RHAMM maintains TPX2 stability, which is reduced through proteasome-dependent degradation. Both actions are necessary to ensure proper activation of Aurora kinase A.

Chapter 4: RHAMM balances motor forces needed to satisfy the spindle assembly checkpoint

4.1 Rationale and hypothesis

Time-lapsed image analysis of RHAMM$^{-/-}$ MEF cells (Fig. 3.2.12) revealed a delay in time needed to transition from metaphase to anaphase suggesting that RHAMM may promote this transition. Completion of the spindle checkpoint requires that all chromosomes reach bipolar attachment, and this is achieved when antagonistic motors establish force balance along the spindle microtubules (Ferenz et al., 2009; Sharp et al., 2000, 1999, Tanenbaum et al., 2009, 2008; van Heesbeen et al., 2014). Outward forces generated by plus-end directed motors, Eg5 and Kif15, are opposed by inward forces generated by dynein. Motor activities are regulated, in part, by non-motor adapter proteins, such as TPX2 and RHAMM (Balchand et al., 2015; Drechsler et al., 2014; Dunsch et al., 2012; Ma et al., 2011; Maxwell et al., 2003). Dunsch and colleagues identified RHAMM as a partner protein of dynein light chain 1 (DYNLL1) by immunoprecipitation and mass spectrometry analysis, and demonstrated that RHAMM, along with a protein termed CHICA, served as an adapter complex for DYNLL1 to correctly orient spindles during mitosis (Dunsch et al., 2012). In addition, TPX2 directly influences kinesin motor activity (Balchand et al., 2015; Ma et al., 2011). Thus, I hypothesize that RHAMM may help to balance motor forces directly, or indirectly through TPX2, and that these balanced forces along the spindle control chromosome behavior and mitotic progression.

4.2 Results

4.2.1 RHAMM-silenced cells exhibit sustained checkpoint activation

To investigate whether RHAMM function is required for progression into anaphase, I first treated mCherry-histone H2B HeLa cells with siRNA targeting RHAMM, and then performed time-lapse microscopy to follow mitotic progression in the RHAMM-silenced cells. Quantification of time-lapse images revealed that the transition from chromosome alignment (metaphase) to chromosome segregation (anaphase) was 27 ± 10 minutes in scrambled siRNA (control)-treated cells, with no observable segregation errors (Fig. 4.1A and B). The average duration for this transition was prolonged to 57 ± 26 minutes in RHAMM-silenced cells. Approximately 55% of RHAMM siRNA-treated cells spent >30 minutes prior to transition from metaphase to anaphase (Fig. 4.1C). Interestingly, a subset of RHAMM-silenced cells (~10%) exhibited extensive metaphase arrest (>60 minutes) (Fig. 4.1C). Of note, only metaphase cells with phenotypically normal bipolar spindles were included in this analysis.

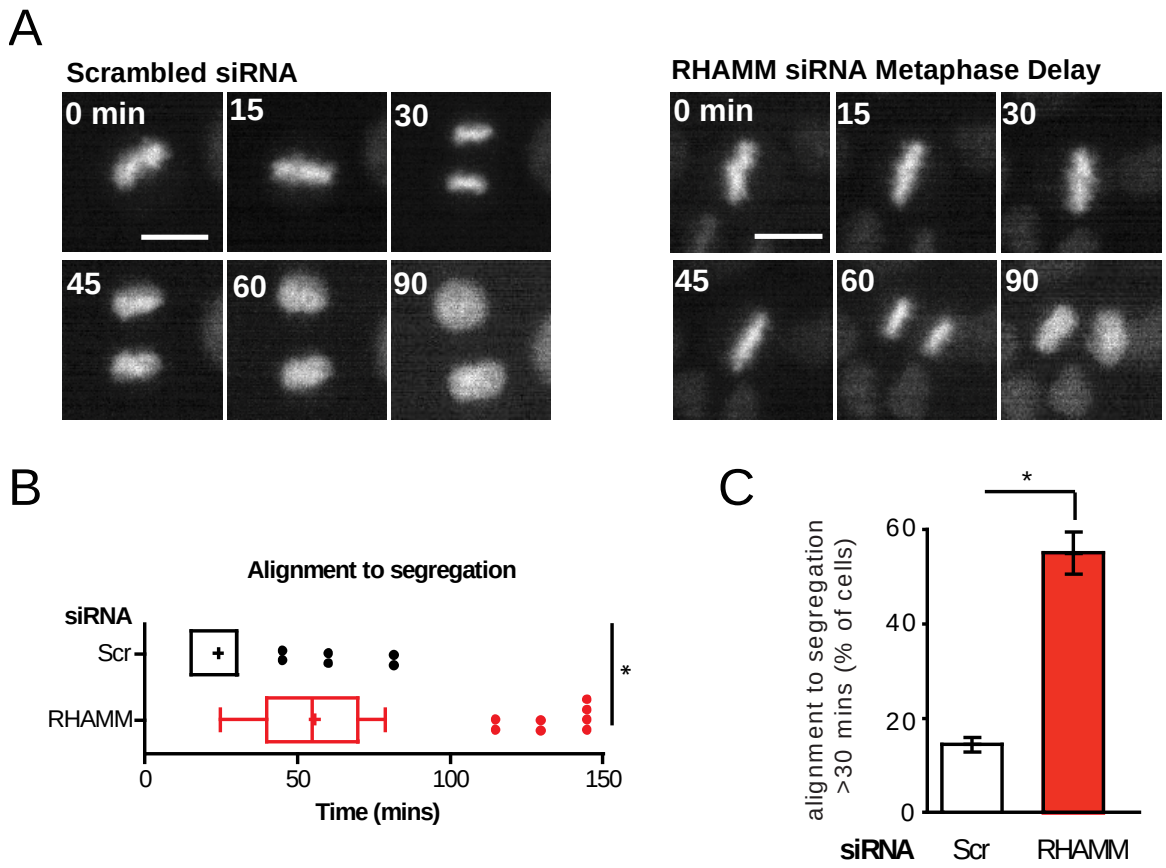

Figure 4.1 RHAMM-silenced HeLa cells are delayed in metaphase

A) HeLa cells expressing mCherry Histone-H2B were treated with either scrambled siRNA or RHAMM targeting siRNA. Asynchronous cells were followed through mitosis by time-lapse microscopy. Scale bars= 10 μm.

B) HeLa cells expressing mCherry Histone-H2B were treated with either scrambled siRNA or RHAMM targeting siRNA. Asynchronous cells were imaged and the time needed to transition from chromosome alignment (metaphase) to chromosome segregation (anaphase) was quantified. Only cells with phenotypically normal bipolar spindles were analyzed. Box-and-whisker plots display the median flanked by 10th, 25th, 75th, and 90th percentiles. (4 experiments, >90 cells/bar, +: mean, *P<0.05, t-test)

C) The percentage of mitotic cells that took >30 minutes to transition from metaphase to anaphase is graphed. (mean ± s.d., n=4, 50 cells/bar, *P<0.05, t-test)

Anaphase onset depends on completion of the spindle checkpoint, which will activate the APC/C and promote the degradation proteins such as cyclin B and securin (Acquaviva and Pines, 2006; Castro et al., 2005; Chang et al., 2014; Ciosk et al., 1998; Clute and Pines, 1999; Nasmyth, 2002; Peters, 2002; Simpson-Lavy et al., 2015). Cyclin B expression peaks between prometaphase and metaphase, and must be degraded prior to chromosome segregation (Chang et al., 2003; Clijsters et al., 2014; van Zon et al., 2010). Thus, the kinetics of cyclin B degradation serves as a biochemical marker for satisfaction of the assembly checkpoint. I followed the kinetics of cyclin B1 degradation in HeLa cells following a single thymidine block by collecting mitotic fractions (shake-off method) every 20 minutes starting 9 hours after release (Fig. 4.2A). In control-treated cells, degradation of cyclin B1 began at 10 hours (9 hours + 60 minutes) and was completed roughly 80 minutes later (Fig. 4.2B). In the RHAMM-silenced population, however, the initiation of degradation was delayed by 20 minutes and complete loss occurred 120 minutes later (Fig. 4.2B). Interestingly, cyclin B1 degradation appeared to be biphasic in the RHAMM-silenced population, suggesting a moderate delay in all cells and an extensive delay in a subset of cells (Fig. 4.2B).

The transition from metaphase to anaphase, and therefore the satisfaction of the spindle checkpoint, is delayed in RHAMM-silenced cells.

A

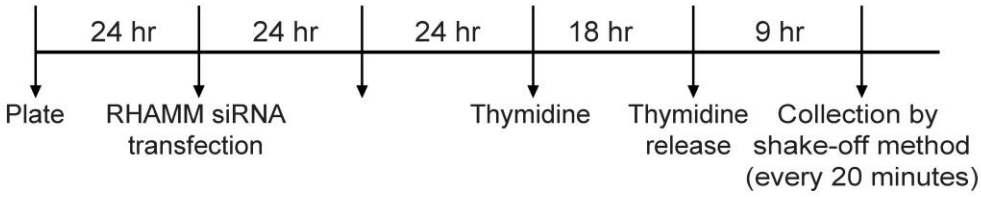
24 hr
24 hr
24 hr
18 hr
9 hr
Plate
RHAMM siRNA transfection
Thymidine
Thymidine release
Collection by shake-off method (every 20 minutes)

B

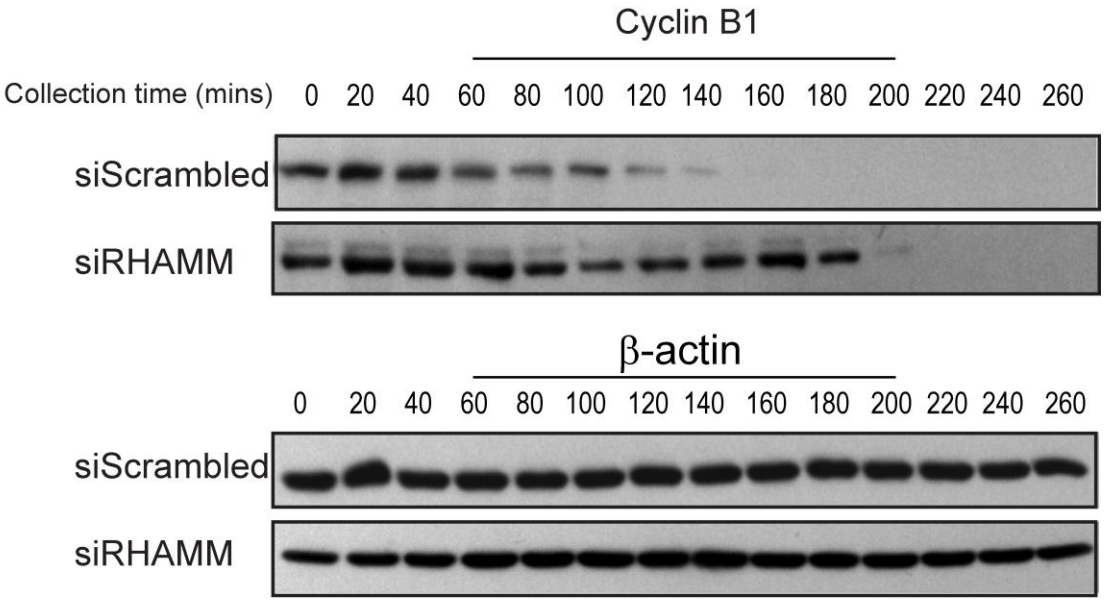
Cyclin B1
Collection time (mins) 0 20 40 60 80 100 120 140 160 180 200 220 240 260
siScrambled
siRHAMM
β-actin
0 20 40 60 80 100 120 140 160 180 200 220 240 260
siScrambled
siRHAMM

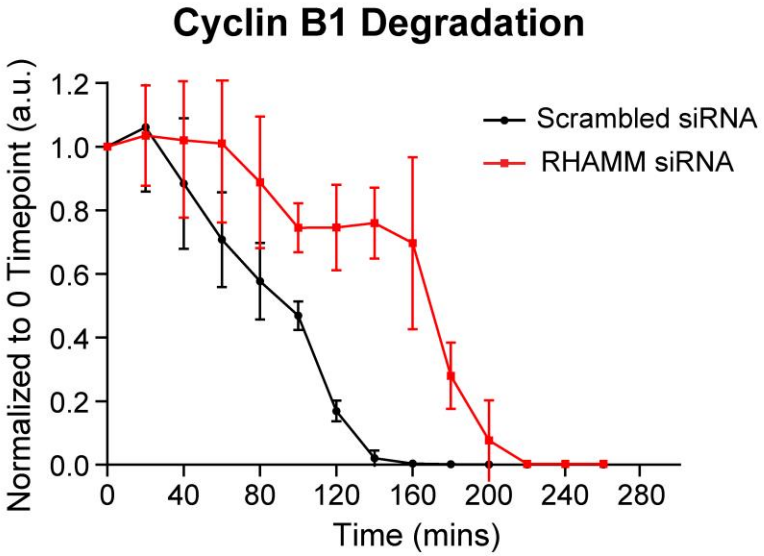
Cyclin B1 Degradation
Normalized to 0 Timepoint (a.u.)
1.2
1.0
0.8
0.6
0.4
0.2
0.0
0 40 80 120 160 200 240 280
Time (mins)
Scrambled siRNA
RHAMM siRNA

Figure 4.2 Cyclin B1 degradation is delayed in RHAMM-silenced cells

A) Timeline showing the experimental strategy. HeLa cells were synchronized at S-phase with a single thymidine block and then released into the cell cycle. Mitotic cells were collected by the shake-off method at indicated times after thymidine release for protein analysis.

B) Lysates were analyzed for cyclin B1 levels. Equal loading was confirmed by probing for β-actin. Cyclin B1 level was quantified first by normalizing to the level of β-actin at each corresponding time point, then normalizing to the levels at the t=0 time point (9 hours post release). 3 experiments, mean ± s.d.

4.2.2 Delayed checkpoint completion is not solely due to spindle rotation in RHAMM-silenced cells

A subset of RHAMM-silenced cells misorient the mitotic spindle (Dunsch et al., 2012), which could delay the spindle checkpoint due to altered spindle geometry. To examine this possibility, I took advantage of the fact that HeLa cells align their mitotic spindle parallel to the growth surface, and divide along that axis. In standard fluorescence microscopy, I imaged fixed cells at different focal positions along the z-axis, and then generated 2D maximum intensity projections of those series rotated to reveal both spindle poles (Fig. 4.3A). In control-treated cells, both spindle poles were typically visible on the same plane parallel to the coverslip surface. In RHAMM-silenced cells, however, about 48% of mitotic cells demonstrated a rotated spindle relative to the coverslip surface, compared to 15% of cells in the control population (Fig. 4.3B). The observed proportion of rotated cells in RHAMM-silenced population (48%, Fig. 4.3B) is comparable to previous findings (Dunsch et al., 2012). I then examined the kinetics of cell division in RHAMM-silenced cells with and without rotated spindles. Time-lapse images showed that a fraction of RHAMM-silenced cells displayed a "tumbling" spindle and these cells arrested in metaphase, possibly, due to this rotation (Fig. 4.4A). In other RHAMM-silenced metaphase cells (53%), however, the spindle oriented correctly and the cell underwent a "stationary" metaphase arrest (Fig. 4.4A). I quantified metaphase to anaphase transition for cells that displayed rotated or stationary spindles and found that roughly half of metaphase-arrested RHAMM-silenced cells showed no evidence of spindle rotation (Fig. 4.4B).

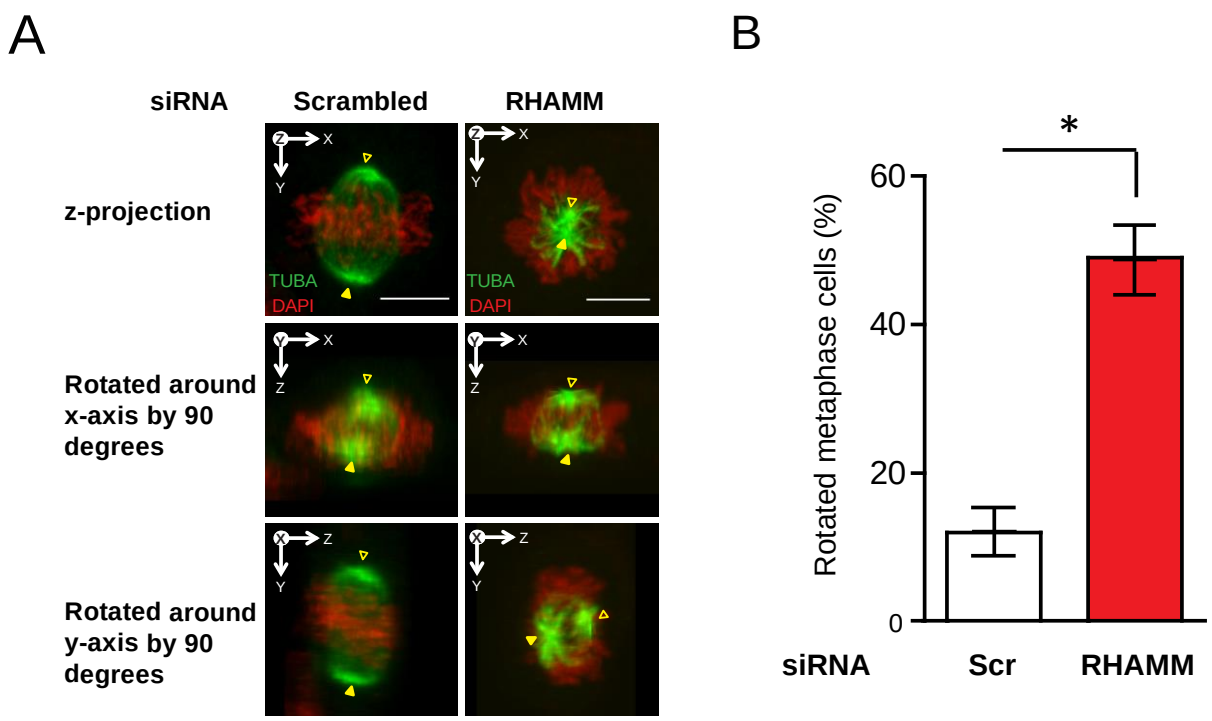

Figure 4.3 Spindle orientation is perturbed in RHAMM-silenced cells

A) Confocal maximum intensity projections (z-axis) of metaphase cells are shown in the top row. The full 3D z-projections are rotated to view the spindle from various planes, arrow heads are used to track individual spindle pole. In RHAMM siRNA treated cells, the bipolar spindle failed to align parallel to the coverslip, unlike the scrambled siRNA treated cells. Arrow heads mark individual spindle pole. Scale bars= 10 μm.

B) The percentage of metaphase cells with rotated spindles were quantified from fixed confocal images. (mean ± s.d., n= 2, 145 cells, *P< 0.05, t-test).

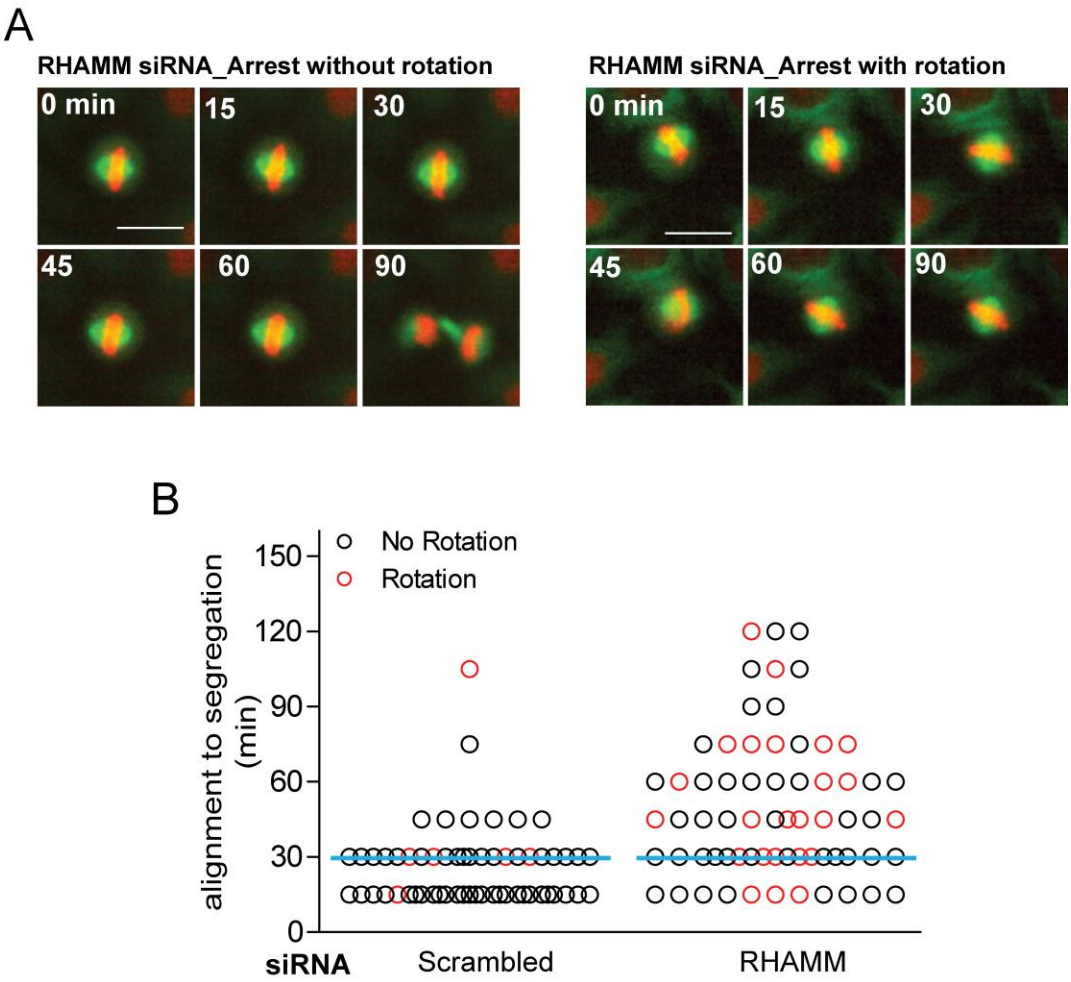

Figure 4.4 Delayed checkpoint in RHAMM-silenced cells is not solely due to spindle rotation

A) Time-lapse microscopy of spindle rotation in RHAMM-silenced metaphase arrested HeLa cells expressing mCherry Histone-H2B and eGFP-TUBA. Scale bars= 10 μm.

B) Scatter plot of checkpoint duration in individual HeLa cells treated with either scrambled siRNA or RHAMM targeting siRNA. In the RHAMM-silenced population, 47% of metaphase arrested cells exhibited spindle rotation. Blue line indicates the median quantified from the scrambled siRNA population. (n= 4, 65 cells/treatment).

4.2.3 RHAMM silencing does not affect the abundance of checkpoint proteins

The spindle checkpoint response correlates with the expression level of key checkpoint proteins, such as BubR1 (Bohers et al., 2008), Mad2 (Niault et al., 2007) and CENPA (Amato et al., 2009). To test whether the prolonged checkpoint response in RHAMM-silenced cells corresponded with augmented expression of these proteins, I examined the abundance of key checkpoint proteins in synchronized cells. Western blot analysis showed no difference in the expression of key kinetochore proteins such as Aurora B, PLK1, BubR1 and Mad2 between populations of control-treated and RHAMM-silenced cells (Fig. 4.5).

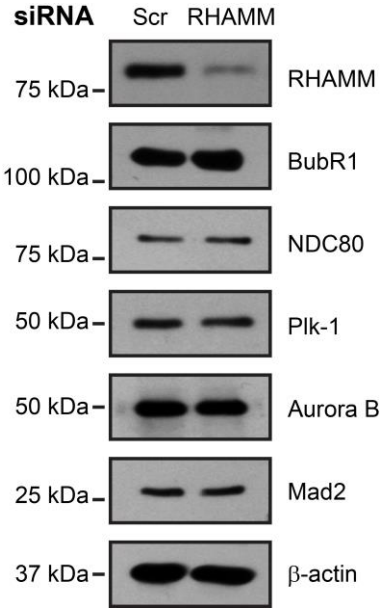

Figure 4.5 The abundance of checkpoint proteins is not affected in RHAMM-silenced cells.

The expression of key checkpoint proteins was measured 96 hours following transfection with control siRNA or siRNA targeting RHAMM. Cells were synchronized by a double thymidine block and released into early mitosis. Equal loading was confirmed by probing for β-actin.

4.2.4 RHAMM silencing does not affect the localization of checkpoint proteins

I also examined the location of key checkpoint proteins in intact metaphase spindles (Fig. 4.6). In control-treated cells, I observed the expected localization of several checkpoint proteins during metaphase: BuBR1 localized to individual kinetochore as discrete puncta (Fig. 4.6A); Aurora kinase B localized throughout chromosome arms (Fig. 4.6B); PLK1 localized throughout chromosome arms, as well as decorated the spindle poles (Fig. 4.6C); and Mad2 only located to kinetochores of unattached chromosomes (Fig. 4.6D). These patterns of localization were unaffected in RHAMM-silenced cells.

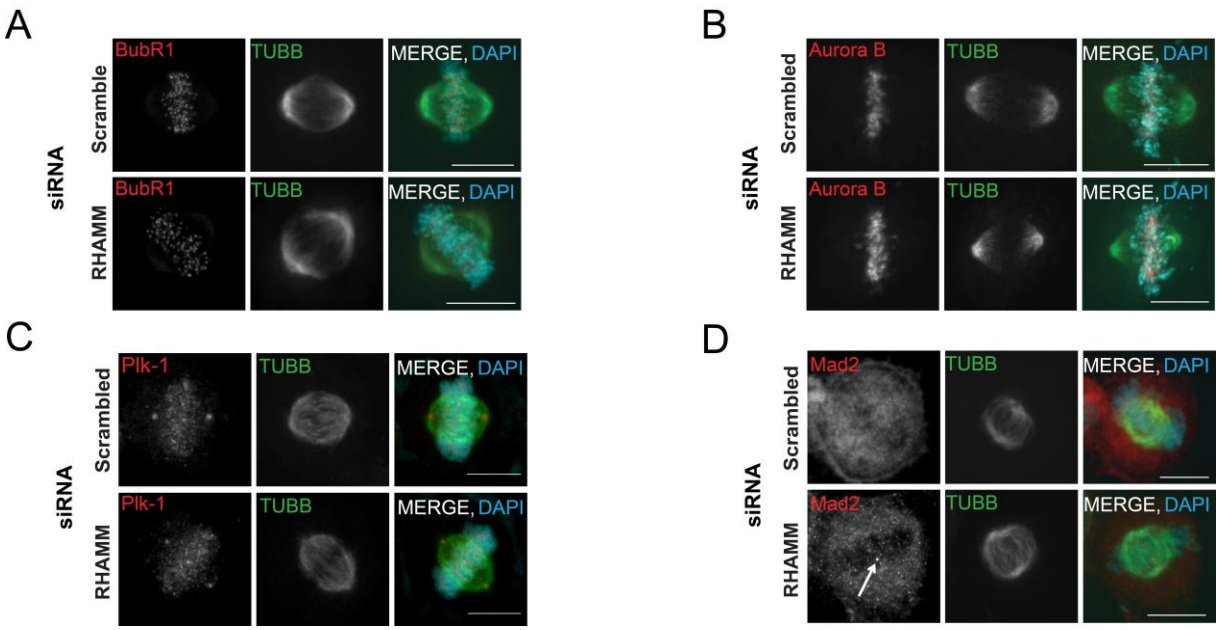

Figure 4.6 Localization of checkpoint proteins is not affected in RHAMM-silenced cells.

A) In asynchronous HeLa cells treated with the indicated siRNA, BubR1 localizes to chromosomes. Scale bar= 10 μm.

B) In asynchronous HeLa cells treated with the indicated siRNA, Aurora B localizes to chromosomes. Scale bar= 10 μm.

C) In asynchronous HeLa cells treated with the indicated siRNA, PLK1 localizes to chromosomes and spindle poles. Scale bar= 10 μm.

D) In asynchronous HeLa cells treated with the indicated siRNA, Mad2 localizes to unattached chromosomes indicated by arrow. Scale bar= 10 μm.

Next, I examined the loading of these proteins onto kinetochores after nocodazole treatment to disrupt the spindle network and activate the spindle checkpoint prior to fixation (Fig. 4.7A-D). All four proteins co-localized with CENPA, a marker for the inner kinetochore plate, in both control-treated and RHAMM-silenced cells. Aurora B, however, appeared to be slightly more diffuse within the chromosome volume in both control-treated and RHAMM-silenced cells. These findings suggest that RHAMM is not needed to locate key checkpoint proteins.

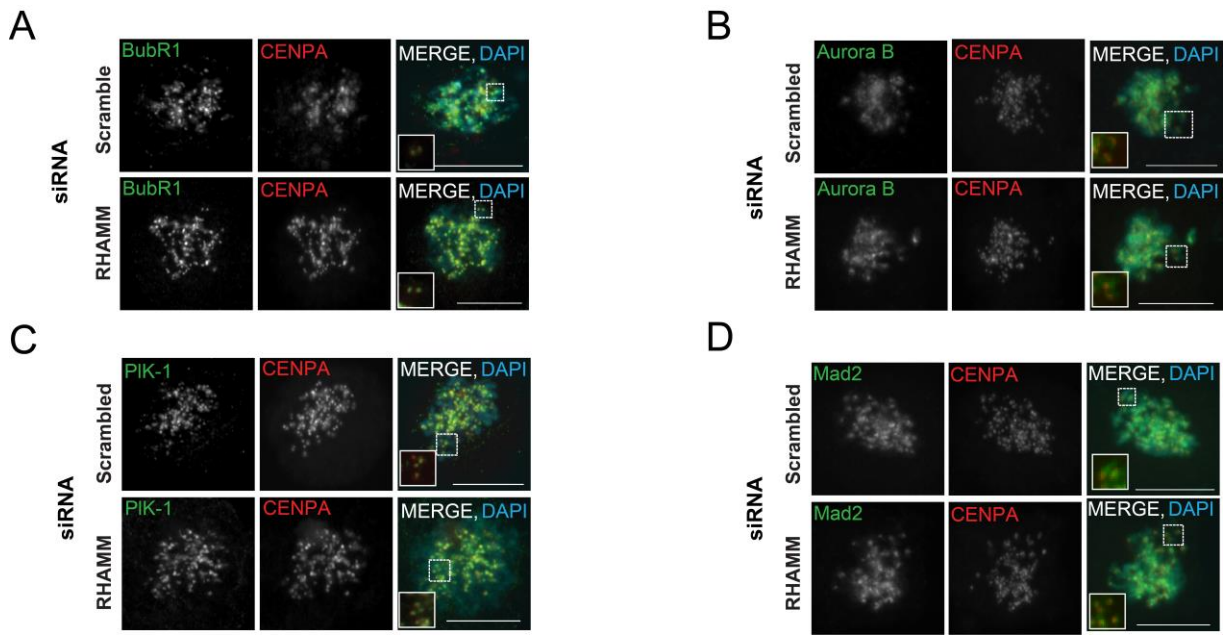

Figure 4.7 RHAMM silencing does not affect loading of checkpoint proteins

A) Control-treated and RHAMM-silenced cells were treated with nocodazole to activate the checkpoint, BubR1 co-localizes with CENPA at kinetochores. Scale bar= 10 μm.

B) Control-treated and RHAMM-silenced cells were treated with nocodazole to activate the checkpoint, Aurora B co-localizes with CENPA at kinetochores. Scale bar= 10 μm.

C) Control-treated and RHAMM-silenced cells were treated with nocodazole to activate the checkpoint, PLK1 co-localizes with CENPA at kinetochores. Scale bar= 10 μm.

D) Control-treated and RHAMM-silenced cells were treated with nocodazole to activate the checkpoint, Mad2 co-localizes with CENPA at kinetochores. Scale bar= 10 μm.

4.2.5 RHAMM is required for chromosome attachment and tension across kinetochores

Checkpoint completion requires bipolar attachment of all chromosomes to the spindle. Mad2 localizes exclusively to unattached kinetochores and, as part of the mitotic checkpoint complex (MCC), prevents anaphase entry. I analyzed kinetochore-microtubule (Kt-MT) attachments in RHAMM-silenced cells and found significantly more Mad2-positive (unattached) kinetochores in comparison to control- treated cells (Fig. 4.8A). In addition, the number of Mad2-positive kinetochores within individual RHAMM-silenced cells was significantly higher (Fig. 4.8A). I also measured the tension across kinetochores for insight into the type of Kt-MT attachments; bi-oriented chromosomes are subjected to poleward forces exerted by motors, which generates tension (Li and Nicklas, 1997; McIntosh, 1991) that is apparent as an increase in the distance between paired sister kinetochores. As a control for loss of Kt-MT tension, I treated cells with vincristine, a microtubule destabilizing drug, and observed a dose-dependent reduction in inter-kinetochore distance (Fig. 4.8B). Consistent with a loss of tension, inter-kinetochore distance was significantly reduced in RHAMM-silenced cells (Fig. 4.8B). To ensure that the measurement of inter-kinetochore distance was not skewed due to the rotation of spindles in RHAMM-silenced cells, I measured inter-kinetochore distances in images viewed through the z-axis as well as in images rotated along the z-axis, similar to Fig. 4.3A. Both quantification methods revealed similar results (Fig. 4.8C).

Silencing RHAMM does not appear to affect the abundance or localization of key checkpoint proteins but does reduce stable Kt-MT attachments. Spindle rotation only partially accounts for the delay in metaphase to anaphase transition seen in RHAMM-silenced cells.

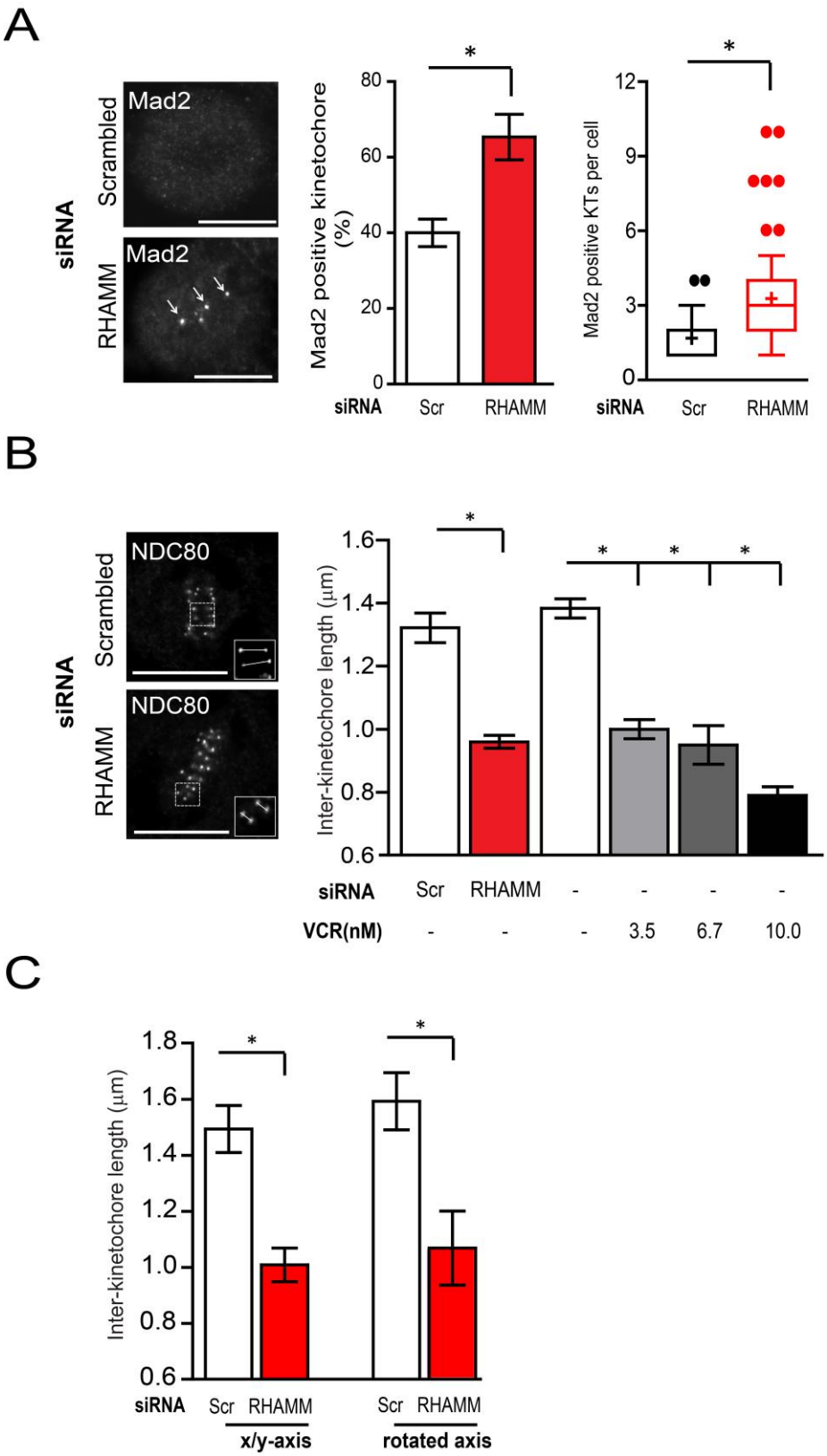
A
siRNA
Scrambled
RHAMM
Mad2
Mad2
Mad2 positive kinetochore (%)
siRNA
Scr
RHAMM
Mad2 positive KTs per cell
siRNA
Scr
RHAMM
B
siRNA
Scrambled
RHAMM
NDC80
NDC80
Inter-kinetochore length (μm)
siRNA
Scr
RHAMM
VCR(nM)
3.5
6.7
10.0
C
Inter-kinetochore length (μm)
siRNA
Scr
RHAMM
Scr
RHAMM
x/y-axis
rotated axis

Figure 4.8 RHAMM is required for chromosome attachment and tension at kinetochores

A) Mad2-specific immuno-staining was significantly increased in RHAMM-silenced metaphase cells. Only cells with phenotypically normal bipolar spindles were included in the quantification. Scale bars= 10 μm. (mean ± s.d., n= 4, >150 cells/bar, **P*< 0.05, t-test).

B) Inter-kinetochore distance was quantified based on fluorescence intensity profile of paired NDC80 foci and was found to be decreased in RHAMM-silenced metaphase cells as well as cells treated with different doses of vincristine (diluted in water) for 1hr prior to fixation. Only cells with phenotypically normal bipolar spindles were included in the quantification. More than 500 kinetochores from 150 cells were quantified for each treatment. Scale bars= 10 μm. (mean ± s.d., n= 4, **P*< 0.05, t-test).

C) Inter-kinetochore distance was quantified based on fluorescence intensity profile of paired NDC80 foci in metaphase cells. Measurements were first performed in the x/y-axis, and then measurements were repeated along a rotated axis where both spindle poles were visible in the same focal plane. Only cells with phenotypically normal bipolar spindles were included in the quantification. More than 120 kinetochores from 60 cells were quantified for each treatment. (mean ± s.d., n= 3, **P*< 0.05, t-test).

4.2.6 Eg5 inhibition rescues checkpoint kinetics and inter-kinetochore tension in RHAMM-silenced cells

In RHAMM-silenced cells, I observed a delay in the progression to anaphase with no associated changes in the location and abundance of key checkpoint proteins. Moreover, I observed compressed mitotic spindles and the improper formation or stability of Kt-MT attachments. In mitotic cells depleted of dynein, spindles appear unfocused and chromosome alignment is delayed due to unbalanced outward forces that can be rescued through concurrent inhibition of Eg5 (van Heesbeen et al., 2014). Moreover, the transport of checkpoint proteins, such as KMN network components Mad1/2, Bub1 and BubR1, is impaired leading to their accumulation at kinetochores (Silva et al., 2015). While I observed no changes in loading/stripping of checkpoint proteins in RHAMM-silenced cells, the observed alterations in spindle architecture, metaphase to anaphase kinetics and Kt-MT attachments are consistent with those observed when motor forces are unbalanced. I reasoned, therefore, that excess outward force along the spindle may explain the phenotypes I observed in RHAMM-silenced cells.

To test my hypothesis, I dampened outward Eg5-dependent forces by treating cells with a small molecule Eg5 inhibitor, termed S-trityl-L-cystein (STLC). As expected, the frequency of monopolar spindles was significantly increased after 2 hours of STLC treatment (Fig. 4.9A). Time-lapse image analysis of single mitotic cells expressing mCherry-H2B as they transited through division (Fig. 4.9B) revealed that STLC treatment alleviated the metaphase delay observed in RHAMM-silenced cells (representative images labelled as RHAMM 1 in Fig. 4.9B). Importantly, few RHAMM-silenced cells underwent a prolonged (>60 minutes) metaphase

phenotype (representative images labelled as RHAMM 2 in Fig. 4.9B) when Eg5 was concurrently inhibited (Fig. 4.9C). Eg5 inhibition also significantly reduced the time needed for metaphase to anaphase transition (Fig. 4.9D) and restored kinetochore tension in RHAMM-silenced cells (Fig. 4.9E).

4.2.7 Silencing Kif15 does not rescue checkpoint kinetics in RHAMM-silenced cells

Kif15 exerts outward forces on the spindle during centrosome separation (Tanenbaum et al., 2009; van Heesbeen et al., 2014; Vanneste et al., 2009) and contains a C-terminal bZip domain that is homologous to the conserved bZip motif in RHAMM (Maxwell et al., 2003). To test whether augmented Kif15 activity may occur and explain the phenotypes observed in RHAMM-silenced cells, I used a double siRNA approach to deplete endogenous Kif15 and RHAMM in HeLa cells expressing mCherry-H2B. Western blot analysis confirmed the silencing of Kif15 and/or RHAMM (Fig. 4.10A). Time-lapse image analysis of single mitotic cells expressing mCherry-H2B as they transited through division (Fig. 4.10B), however, showed that Kif15 silencing failed to reduce the prolonged metaphase observed in RHAMM-silenced cells (Fig. 4.10C) and did not significantly impact the kinetics of the metaphase to anaphase progression (Fig. 4.10D). Thus, augmented activity of Eg5, but not Kif15, is at least partially responsible for the compressed spindles, reduced Kt-MT attachments and inter-kinetochore tension, and delayed metaphase to anaphase kinetics observed in RHAMM-silenced cells. Note, Kif15 silencing is less efficient in HeLa cells treated with both siRNA targeting Kif15 and RHAMM, potentially due to less siRNA added during transfection as required by the protocol.

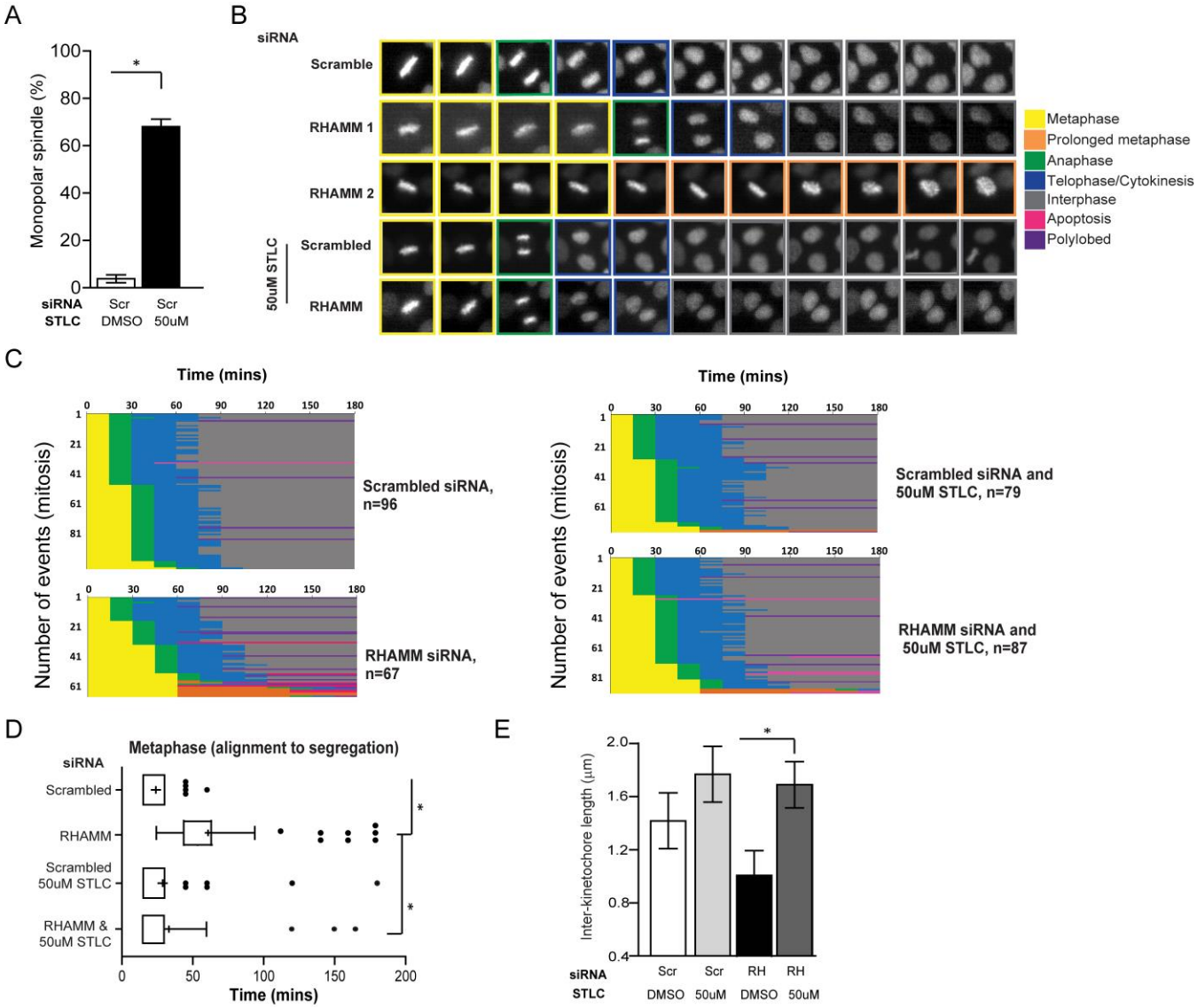
A
Monopolar spindle (%)
100
80
60
40
20
0
*
siRNA
STLC
Scr
DMSO
Scr
50uM
B
siRNA
Scramble
RHAMM 1
RHAMM 2
Scrambled
RHAMM
50uM STLC
Metaphase
Prolonged metaphase
Anaphase
Telophase/Cytokinesis
Interphase
Apoptosis
Polylobed
C
Time (mins)
Number of events (mitosis)
Scrambled siRNA, n=96
RHAMM siRNA, n=67
Scrambled siRNA and 50uM STLC, n=79
RHAMM siRNA and 50uM STLC, n=87
D
Metaphase (alignment to segregation)
siRNA
Scrambled
RHAMM
Scrambled 50uM STLC
RHAMM & 50uM STLC
Time (mins)
E
Inter-kinetochore length (μm)
siRNA
STLC
Scr
DMSO
Scr
50uM
RH
DMSO
RH
50uM

Figure 4.9 Eg5 inhibition rescues mitotic kinetics and inter-kinetochore tension in RHAMM-silenced cells

A) HeLa cells expressing mCherry Histone-H2B and eGFP-TUBA were treated with scrambled control siRNA and either 50μM STLC, or equivalent DMSO vehicle control, for 2hr prior to fixation. The percentage of mitotic cells with monopolar spindle was scored (n=3, >75 cells/bar, +: mean, *P<0.05, t-test)

B) HeLa cells expressing mCherry Histone-H2B were treated as indicated and followed through mitosis. Only bipolar metaphase cells were included in the analysis and the different mitotic phases, as indicated by chromosome morphologies, were extracted from the imaging data.

C) Extraction of mitotic phases and alignment, based upon time spent in metaphase, for the indicated treatments.

D) Quantification of the time needed to progress from chromosome alignment (metaphase) to chromosome segregation (anaphase). Only cells with bipolar spindles were included in the quantification. Box-and-whisker plots display the median flanked by 10th, 25th, 75th, and 90th percentiles. (3 experiments, +: mean, *P<0.05, t-test)

E) Inter-kinetochore distance was quantified based on fluorescence intensity profile of paired NDC80 puncta. This distance was found to be decreased in RHAMM-silenced metaphase cells and was recovered following 2 hours of treatment with 50μM STLC relative to DMSO vehicle control treatment. More than 100 kinetochores from 60 cells were quantified for each treatment. (mean ± s.d., n= 3, *P< 0.05, t-test)

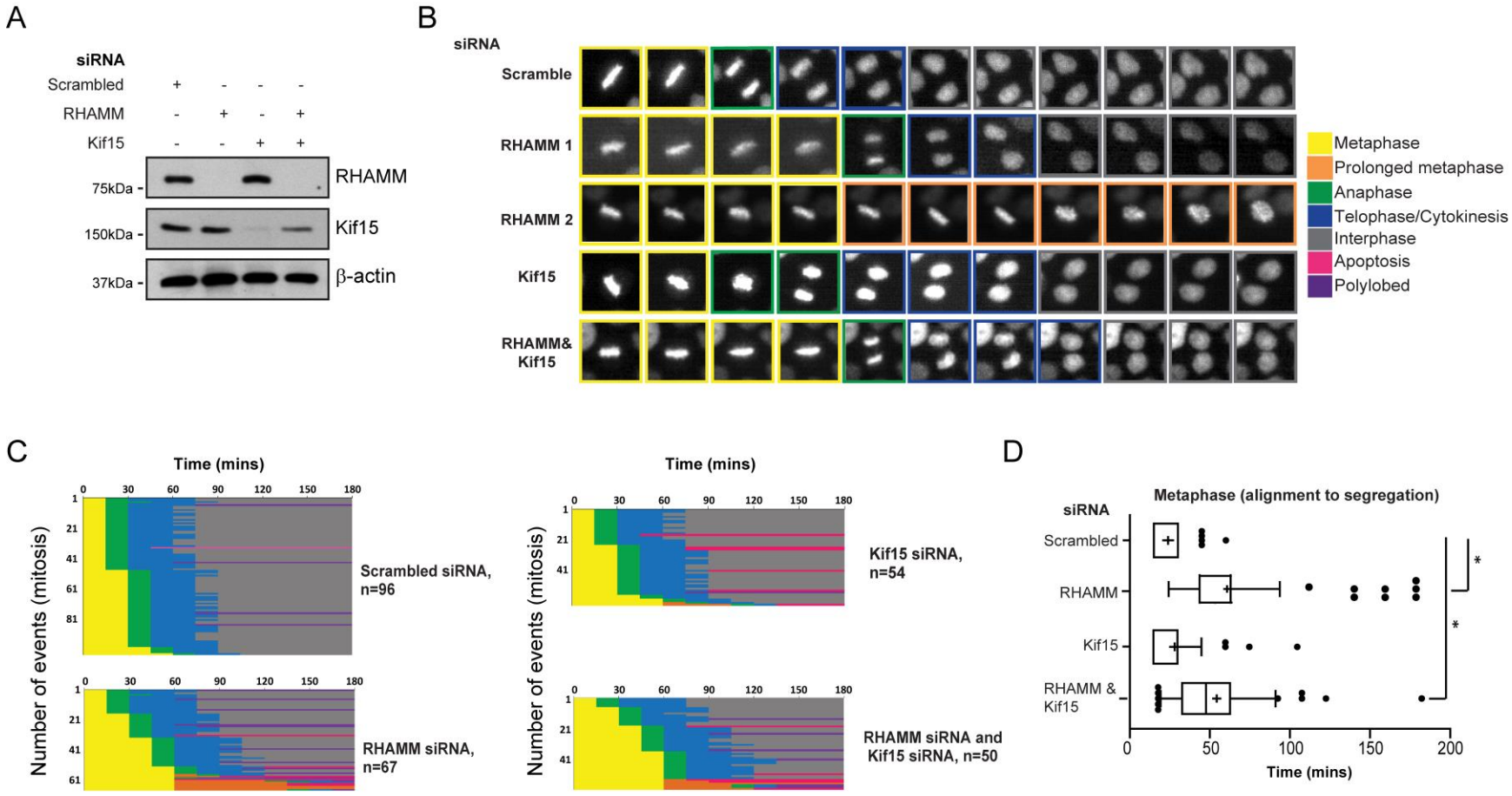
A
siRNA
Scrambled + - - -
RHAMM - + - +
Kif15 - - + +
75kDa
RHAMM
150kDa
Kif15
37kDa
β-actin
B
siRNA
Scramble
RHAMM 1
RHAMM 2
Kif15
RHAMM& Kif15
Metaphase
Prolonged metaphase
Anaphase
Telophase/Cytokinesis
Interphase
Apoptosis
Polylobed
C
Time (mins)
Number of events (mitosis)
Scrambled siRNA, n=96
RHAMM siRNA, n=67
Kif15 siRNA, n=54
RHAMM siRNA and Kif15 siRNA, n=50
D
Metaphase (alignment to segregation)
siRNA
Scrambled
RHAMM
Kif15
RHAMM & Kif15
Time (mins)

Figure 4.10 Silencing Kif15 does not rescue checkpoint kinetics in RHAMM-silenced cells

A) HeLa cells expressing mCherry Histone-H2B were transfected with the indicated siRNA and, 96 hours later, synchronized in prometaphase by nocodazole treatment and lysed. RHAMM or Kif15 abundance was measured by Western blot analysis with β-actin serving as a loading control.

B) HeLa cells expressing mCherry Histone-H2B were treated as indicated and followed through mitosis. Only bipolar metaphase cells were included in the analysis and the different mitotic phases, as indicated by chromosome morphologies, were extracted from the imaging data.

C) Extraction of mitotic phases and alignment, based upon time spent in metaphase, for the indicated treatments.

D) Quantification of the time needed to progress from chromosome alignment (metaphase) to chromosome segregation (anaphase). Only cells with bipolar spindles were included in the quantification. Box-and-whisker plots display the median flanked by 10th, 25th, 75th, and 90th percentiles. (3 experiments, +: mean, *P<0.05, t-test)

4.2.8 Eg5 inhibition does not affect the kinetics of other mitotic stages in RHAMM-silenced cells

I examined whether a putative motor imbalance observed during metaphase may also alter the kinetics of spindle assembly (prophase and prometaphase) (Fig. 4.11A) or mitotic exit (anaphase to telophase) (Fig. 4.11B). Consistent with my prior findings (section 3.2.4), I observed that RHAMM-silenced cells required more time transiting through prophase and prometaphase (Fig. 4.11A). Silencing Kif15, alone or in combination with silencing RHAMM, did not significantly alter the kinetics of spindle assembly (Fig. 4.11A). Importantly, Eg5 inhibition induced monopolar spindles in the majority of mitotic cells (Fig. 4.9A). Therefore, I measured the kinetics in the few Eg5-inhibited cells that formed bipolar spindles, which displayed altered spindle assembly kinetics only in combination with RHAMM depletion, but not Eg5 inhibition alone (Fig. 4.11A). However, the kinetics of mitotic exit were not altered in any of the conditions measured (Fig. 4.12B).

In summary, inhibition of Eg5, the major generator of outward forces exerted on the mitotic spindle, restored spindle checkpoint kinetics and recovered inter-kinetochore tension in RHAMM-silenced cells; however, silencing Kif15 did not alter kinetics or tension. Thus, motor force balance along the metaphase spindle may be disturbed in the absence of RHAMM resulting in excess outward forces produced by Eg5 that reduce inter-kinetochore tension and delay the completion of the checkpoint and the transition to anaphase.

A

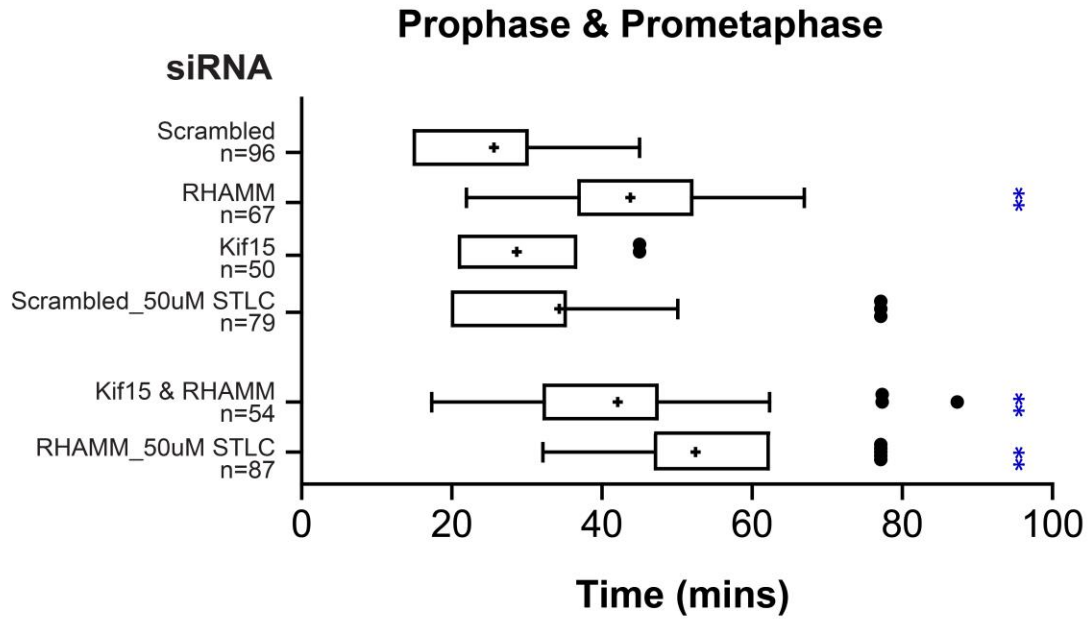
Prophase & Prometaphase
siRNA
Scrambled n=96
RHAMM n=67
Kif15 n=50
Scrambled_50uM STLC n=79
Kif15 & RHAMM n=54
RHAMM_50uM STLC n=87
0
20
40
60
80
100
Time (mins)

B

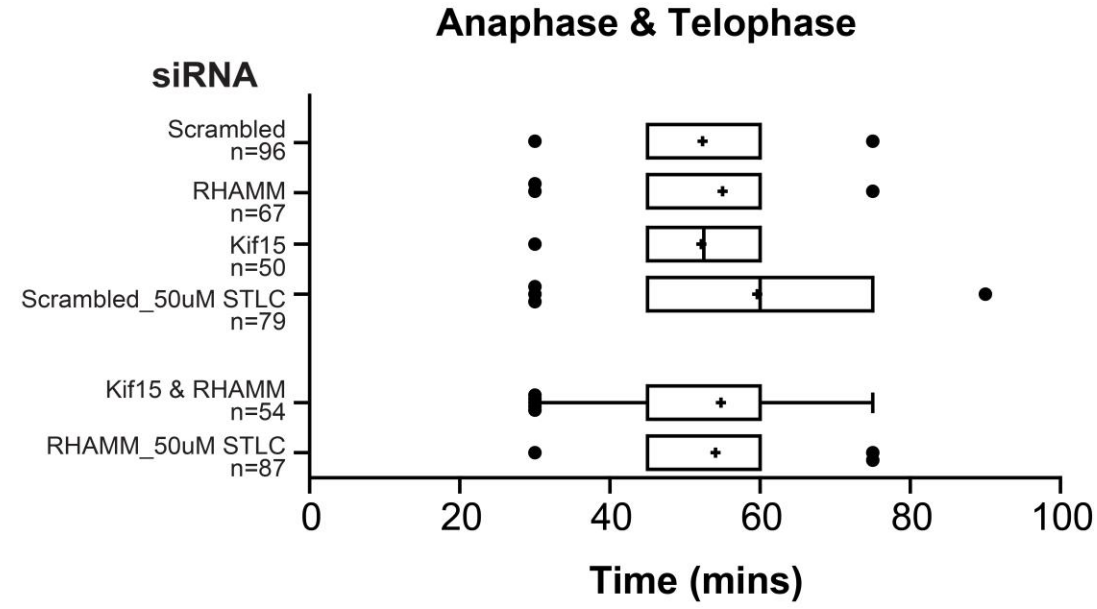
Anaphase & Telophase
siRNA
Scrambled n=96
RHAMM n=67
Kif15 n=50
Scrambled_50uM STLC n=79
Kif15 & RHAMM n=54
RHAMM_50uM STLC n=87
0
20
40
60
80
100
Time (mins)

Figure 4.11 In cells with bipolar spindles, the inhibition of outward motor forces does not alter the kinetics of early or late mitotic stages in the presence or absence of RHAMM.

A) HeLa cells expressing mCherry Histone-H2B were treated as indicated and followed through mitosis. Only bipolar metaphase cells were included in the analysis. The time needed to transit from prophase (chromosome condensation) through prometaphase (prior to chromosome alignment) was quantified. Box-and-whisker plots display median flanked by 10th, 25th, 75th, and 90th percentiles. (3 experiments, +: mean, number of cells quantified as indicated**P<0.05 compared to scrambled siRNA, ANOVA)

B) HeLa cells expressing mCherry Histone-H2B were treated as indicated and followed through mitosis. Only bipolar metaphase cells were included in the analysis. The time needed to transit from anaphase (chromosome segregation) through telophase/cytokinesis (prior to loss of central spindle) was quantified. Box-and-whisker plots display median flanked by 10th, 25th, 75th, and 90th percentiles. (3 experiments, +: mean, number of cells quantified as indicated **P<0.05 compared to scrambled siRNA, ANOVA)

4.2.9 Silencing RHAMM does not affect motor protein abundance

To understand the mechanism that underly augmented Eg5 activity in RHAMM-silenced cells, I first examined the abundance of Eg5, along with other motors such as p150 (the intermediate chain for dynein) (Fig. 4.12). The abundance of RHAMM was efficiently reduced (NOTE: the doublet represents the full-length, 724 aa, and –exon 4, 708 aa, variants) as was the abundance of TPX2 (Chen et al., 2014), which was restored by inhibiting the proteasome with MG132 (Fig. 4.12). However, the abundance of kinesin motors, Eg5 and Kif15, and the p150 component of dynein were not affected (Fig. 4.12).

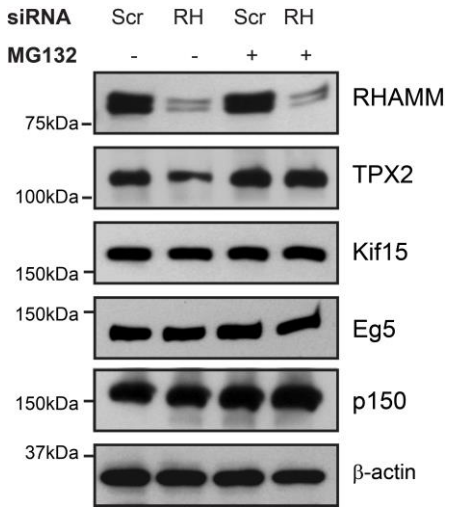

Figure 4.12 TPX2, but not Kif15, Eg5, or p150, is reduced in RHAMM-silenced cells.

HeLa cells were treated with scrambled control siRNA or siRNA targeting RHAMM and, 48 hours later, synchronized to early mitosis by a double thymidine treatment and subsequently lysed. Prior to lysis, cells were treated with either proteasome inhibitor (MG132, 15 μM) or DMSO vehicle control for 2 hours. The abundance of indicated proteins was determined through western blot analysis and equal loading was confirmed by probing for β-actin. Images are representative of two experiments.

4.2.10 Silencing RHAMM alters spindle morphology but not Eg5 and Kif15 localization.

Nest, I assessed the localization of Eg5 or Kif15 in control-treated and RHAMM-silenced cells. In control-treated cells, the spindle was focused with bilaterally equal half spindles; Eg5 localized along spindle microtubules while Kif15 concentrated at spindle poles (Fig. 4.13). In RHAMM-silenced cells, however, the spindle appeared compressed with unfocussed poles, in accordance with my previous findings (section 3.2.11) and consistent with augmented Eg5 activity (Ma et al., 2011; Uteng et al., 2008). Despite this aberrant, unfocused spindle morphology, Eg5 remained localized along spindle microtubules (Fig. 4.13A) while the localization of Kif15 was consistent with the minus ends of mitotic microtubules (Fig. 4.13B).

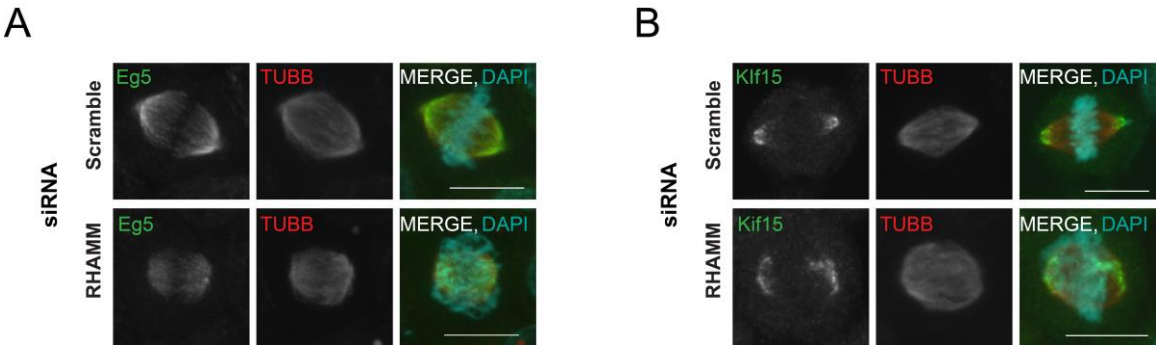

Figure 4.13 Kinesin localization is not affected in RHAMM-silenced cells

A) Confocal images of Eg5 localization along the metaphase spindle (indicated by beta-tubulin, TUBB) in cells treated with scrambled siRNA or siRNA targeting RHAMM. Images are representative of four experiments. Scale bars= 10 μm.

B) Confocal images of Kif15 localization along the metaphase spindle (indicated by beta-tubulin, TUBB) in cells treated with scrambled siRNA or siRNA targeting RHAMM. Images are representative of four experiments. Scale bars= 10 μm.

4.2.11 Silencing RHAMM attenuates the TPX2-Eg5 but not the TPX2-Kif15 interaction

TPX2 interacts with both Eg5 and Kif15 and these interactions alter their respective motor activities (Balchand et al., 2015; Drechsler et al., 2014; Gable et al., 2012; Ma et al., 2011). As the abundance and location of TPX2 is altered in RHAMM-silenced cells (Chen et al., 2014; Scrofani et al., 2015), I hypothesized that interactions between TPX2 and kinesins may be attenuated as a result. To test this, I first examined protein interactions in untreated cells using immunoprecipitation experiments. I used two different RHAMM antibodies targeting either the N- or C-terminus of the protein to immuno-isolate RHAMM complexes from early mitotic cells (Fig. 4.14A). These antibodies efficiently depleted RHAMM from post-IP lysates (Fig. 4.14A). I probed the precipitates for TPX2, a known interacting protein, and NuMA, a spindle assembly factor that is known to not interact with RHAMM (Fig. 4.14A). I identified Kif15, but not Eg5, in precipitates isolated by either RHAMM antibody. This suggested that the augmented Eg5 activity in RHAMM-silenced cells was not a direct effect of RHAMM on Eg5 but rather an indirect effect.

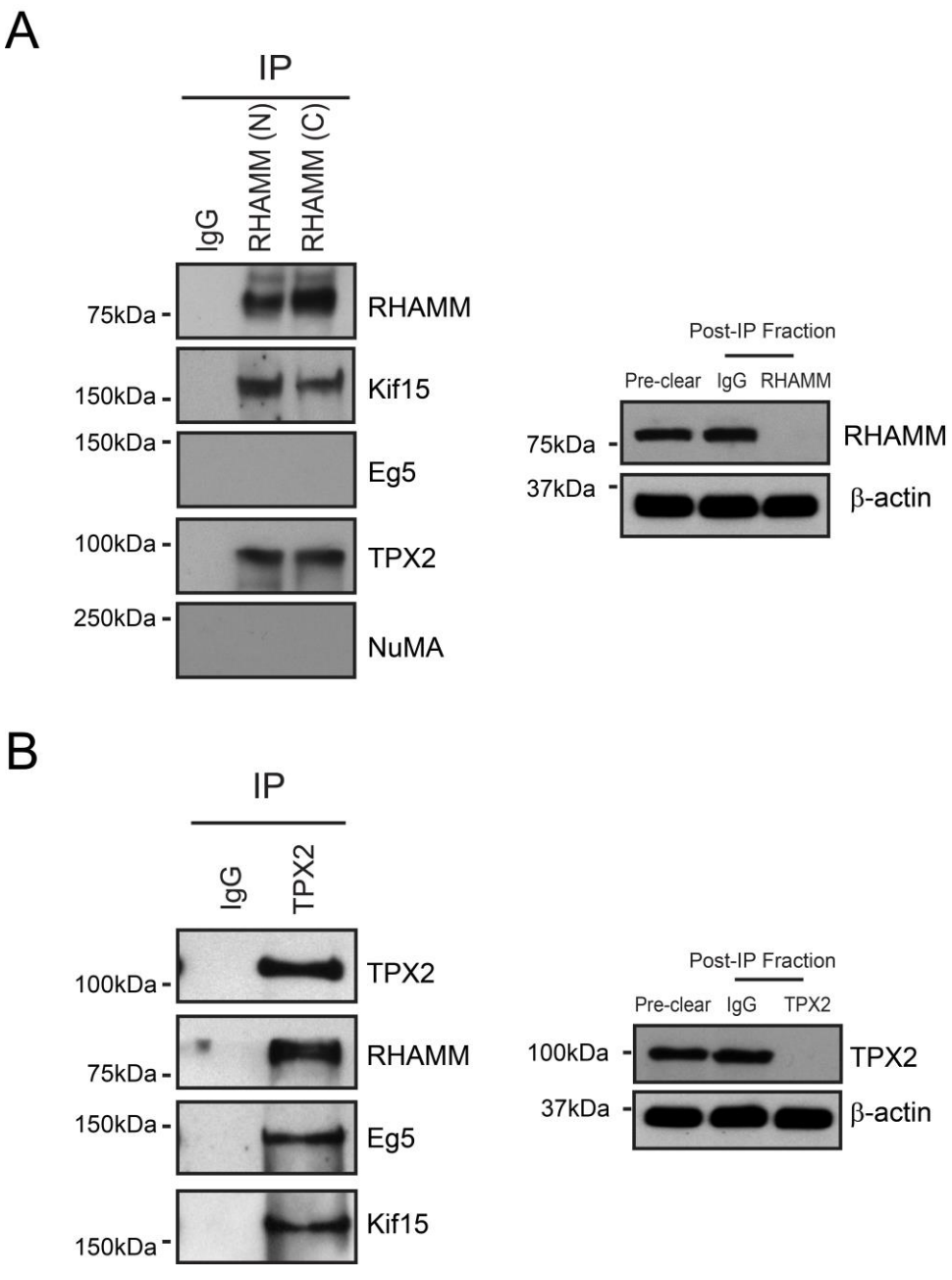
A
IP
IgG
RHAMM (N)
RHAMM (C)
75kDa
RHAMM
150kDa
Kif15
150kDa
Eg5
100kDa
TPX2
250kDa
NuMA
Post-IP Fraction
Pre-clear
IgG
RHAMM
75kDa
RHAMM
37kDa
β-actin
B
IP
IgG
TPX2
100kDa
TPX2
75kDa
RHAMM
150kDa
Eg5
150kDa
Kif15
Post-IP Fraction
Pre-clear
IgG
TPX2
100kDa
TPX2
37kDa
β-actin

Figure 4.14 Precipitates isolated from synchronized HeLa cells reveal a new RHAMM-Kif15 interaction and confirm known TPX2 interactions.

A) Antibodies raised against either the N- or C-terminus of RHAMM precipitated Kif15, but not Eg5, from double thymidine synchronized mitotic HeLa lysates. TPX2 was included as a positive control, whereas NuMA was included as a negative control. RHAMM was efficiently precipitated, as indicated by comparisons of pre-cleared and post-immunoprecipitation lysates. Equal loading was confirmed by probing for β-actin.

B) Antibodies raised against TPX2 precipitated Kif15, Eg5, and RHAMM from double thymidine synchronized mitotic HeLa lysates. TPX2 was efficiently precipitated, as indicated by comparisons of pre-cleared and post-immunoprecipitation lysates. Equal loading was confirmed by probing for β-actin.

To determine whether TPX2-kinesin interactions were altered in RHAMM-silenced cells, I first evaluated precipitates isolated from synchronized HeLa cell lysates using an antibody raised against TPX2. These precipitates of endogenous proteins contained both kinesins as well as RHAMM (Fig. 4.14B). To determine the necessity of RHAMM for either the Eg5-TPX2 or the Kif15-TPX2 interaction, I precipitated complexes from lysates prepared from HeLa cells pretreated with control (scrambled) siRNA or with siRNA targeting RHAMM (Fig. 4.15 and Fig. 4.16). As the abundance of TPX2 is reduced in RHAMM-silenced cells, I also treated cells with either a vehicle (DMSO) control or a proteasome inhibitor (MG132) to equalize the levels of TPX2, as described in section 4.2.9. To analyze the abundance of precipitated proteins, I utilized IR detection, which afforded two benefits: 1) protein abundance is linear to detection levels, and 2) co-precipitated kinesins (Eg5 or Kif15) could be detected on the same membrane as the precipitated TPX2. In lysates generated from RHAMM-silenced cells, the amount of Eg5 precipitated with TPX2 antibodies is less than 50% of that in control-treated cell lysates, despite the equivalent levels of TPX2 (Fig. 4.15A). Reciprocal precipitates using Eg5 antibodies revealed similarly attenuated levels of co-precipitated TPX2 in lysates generated from RHAMM-silenced cells (Fig. 4.15B). I used a similar reciprocal co-precipitation strategy to analyze the TPX2-Kif15 complex in lysates generated from control-treated or RHAMM-silenced cells; however, I did not detect differences in TPX2-Kif15 interactions between these cell populations (Fig. 4.16A and B). Lastly, the high efficiency of each of these immunoprecipitations was confirmed by the reduced protein abundance in the post-IP fractions relative to the pre-cleared (pre-IP) fractions (Fig. 4.16C).

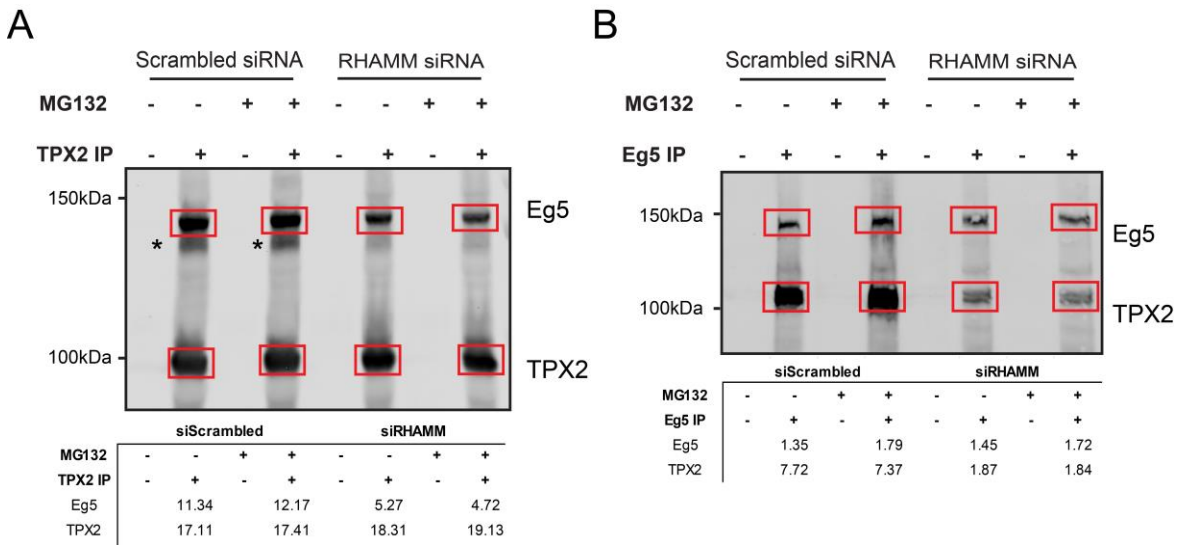

Figure 4.15 RHAMM silencing attenuates TPX2-Eg5 interaction

A) HeLa cells (treated as indicated) were synchronized by a double thymidine treatment and released into early mitosis. Prior to lysis, cells were treated with either proteasome inhibitor (MG132, 15 µM) or DMSO vehicle control for 2 hours. Quantitative Western blot analysis of immunoprecipitates for TPX2 antibodies revealed decreased abundance of Eg5 in RHAMM-silenced populations. Protein bands were visualized by Licor imaging using IR fluorophore tagged secondary antibodies. The asterisk marks a non-specific band.

B) HeLa cells (treated as indicated) were synchronized by a double thymidine treatment and released into early mitosis. Prior to lysis, cells were treated with either proteasome inhibitor (MG132, 15 µM) or DMSO vehicle control for 2 hours. Quantitative Western blot analysis of immunoprecipitates for Eg5 antibodies revealed decreased abundance of TPX2 in RHAMM-silenced populations. Protein bands were visualized by Licor imaging using IR fluorophore tagged secondary antibodies.

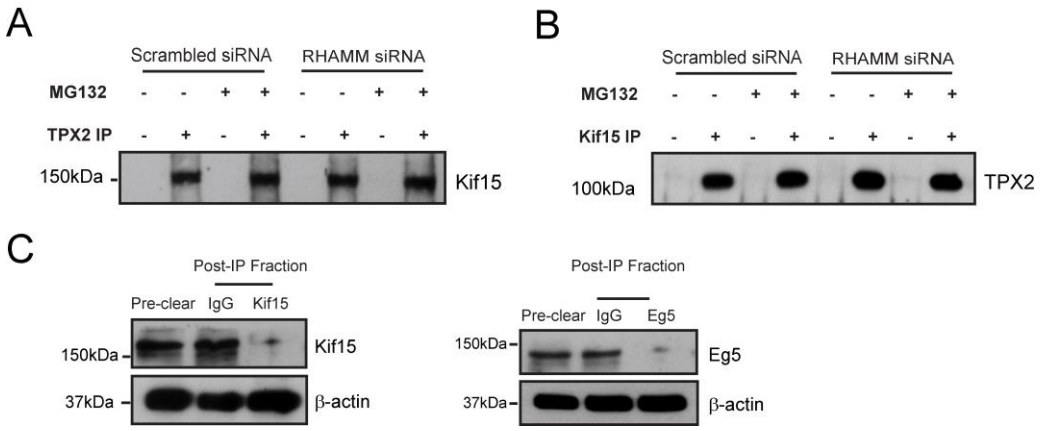

Figure 4.16 RHAMM silencing does not affect TPX2-Kif15 interaction

A) HeLa cells (treated as indicated) were synchronized by a double thymidine treatment and released into early mitosis. Prior to lysis, cells were treated with either proteasome inhibitor (MG132, 15 μM) or DMSO vehicle control for 2 hours. Western blot analysis of immunoprecipitates for TPX2 antibodies revealed similar levels of Kif15 in control and RHAMM-silenced populations.

B) HeLa cells (treated as indicated) were synchronized by a double thymidine treatment and released into early mitosis. Prior to lysis, cells were treated with either proteasome inhibitor (MG132, 15 μM) or DMSO vehicle control for 2 hours. Western blot analysis of immunoprecipitates for Kif15 antibodies revealed similar levels of TPX2 in control and RHAMM-silenced populations.

C) Examination of immunoprecipitation efficiency for antibodies targeting Kif15, TPX2 or Eg5. Equal loading was confirmed with actin.

4.2.12 RHAMM is required for concentrating TPX2 on spindle poles

Results described in section 4.2.11 suggest that formation of an inhibitory TPX2-Eg5 complex is attenuated in RHAMM-silenced mitotic cell lysates. I reasoned that this effect may be due to TPX2 mislocalization along the mitotic spindle, given I observed no difference in Eg5 location in RHAMM-silenced cells (Fig. 4.13). To test this, I compared the location of TPX2 and Eg5 along the mitotic spindle in control and RHAMM-silenced cells by immunofluorescence (Fig. 4.17). In control cells, TPX2 and Eg5 colocalize along the entire mitotic spindle, however, in RHAMM-silenced cells, TPX2 is greatly reduced at the poles but remains present on microtubules in the half-spindle, which is defined as the region between the pole and equator. Intensity profile by linescan analysis reveal in RHAMM-silenced cells that TPX2 and Eg5 fail to colocalize at the spindle poles, demonstrated by intensity peaks that no longer overlap at these sites.

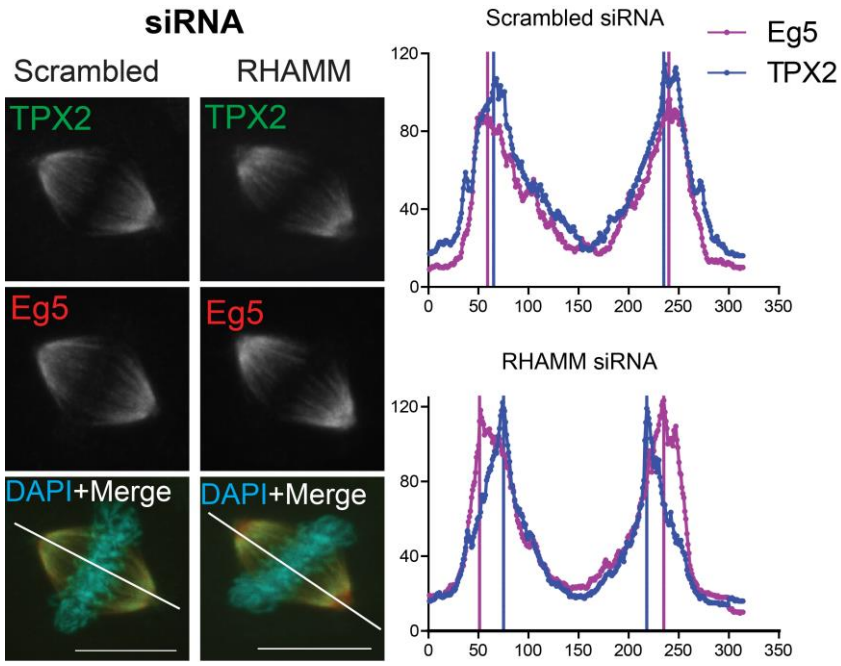

Figure 4.17 RHAMM is required to concentrate TPX2 at spindle poles.

Confocal images of TPX2 and Eg5 localization along the metaphase spindle in cells treated with scrambled siRNA or siRNA targeting RHAMM. Corresponding fluorescence intensity profiles were analyzed by linescan as indicated by the white line. Notice that shift of the intensity peaks for TPX2 in the RHAMM-silenced cell. Images are representative of three experiments. Scale bars= 10 μm.

4.2.13 The RHAMM-TPX2 interaction is required for spindle checkpoint completion

Having demonstrated that silencing RHAMM reduces the formation of (inhibitory) TPX2-Eg5 complexes potentially at spindle poles, and inhibition of Eg5 activity restores tension and anaphase progression in RHAMM-silenced cells, I reasoned that a RHAMM-TPX2 interaction may be needed to establish tension and promote mitotic progression. To test this hypothesis, I introduced siRNA-resistant GFP-RHAMM truncation mutants into RHAMM-silenced cells and measured the kinetics of anaphase progression and inter-kinetochore tension (Fig. 4.18A and B). These GFP-RHAMM truncation mutants were designed to investigate the functional significance of the TPX2 binding domain: the C-terminal bZip motif (described in section 3.2.10). Live cell analysis was performed during optimal GFP-RHAMM expression, which was determined to be 48 hours post transfection. Time-lapse image analysis revealed that rescue with GFP-RHAMM constructs that contained the bZip motif (full-length and aa 1-679) were able to alleviate the metaphase arrest (Fig. 4.18B) and recover tension (Fig. 4.18C) in cells depleted of endogenous RHAMM. GFP-RHAMM$^{1\text{-}623}$, which lacks the bZip motif, and GFP-RHAMM (ΔbZip), where three conserved leucines were mutated to arginines, were not able to alleviate the metaphase arrest or establish tension.

A

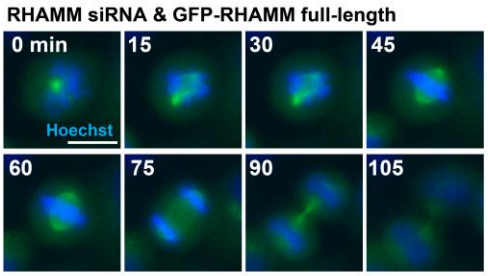
RHAMM siRNA & GFP-RHAMM full-length
0 min
15
30
45
Hoechst
60
75
90
105

B

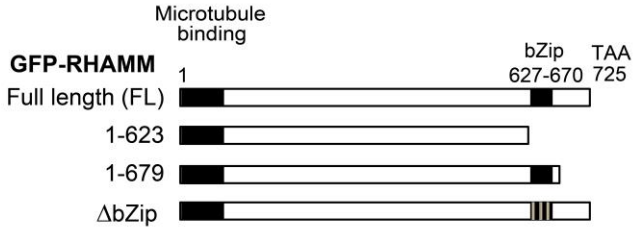
Microtubule binding
GFP-RHAMM
1
bZip 627-670
TAA 725
Full length (FL)
1-623
1-679
ΔbZip

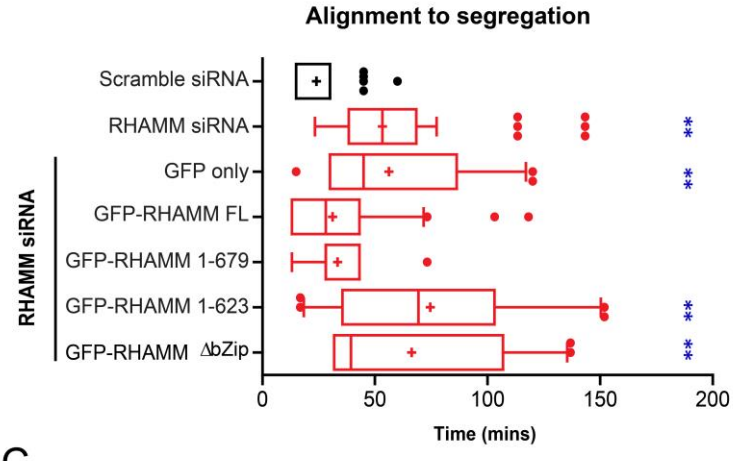
Alignment to segregation
Scramble siRNA
RHAMM siRNA
GFP only
GFP-RHAMM FL
GFP-RHAMM 1-679
GFP-RHAMM 1-623
GFP-RHAMM ΔbZip
RHAMM siRNA
0
50
100
150
200
Time (mins)

C

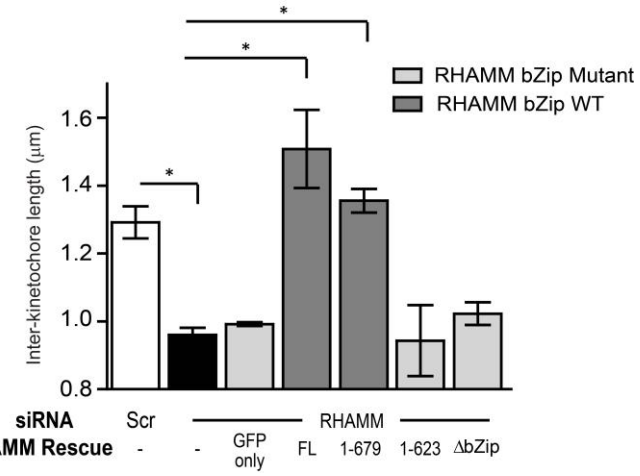
RHAMM bZip Mutant
RHAMM bZip WT
Inter-kinetochore length (μm)
1.6
1.4
1.2
1.0
0.8
siRNA
Scr
RHAMM
GFP-RHAMM Rescue
-
-
GFP only
FL
1-679
1-623
ΔbZip

Figure 4.18 The C-terminal bZip motif in RHAMM is required for spindle checkpoint completion

A) GFP-RHAMM (full-length), or variants thereof, were transfected into RHAMM-silenced cells. The cells were labelled with Hoechst to visualize DNA, and mitotic kinetics were followed by time-lapse microscopy. Scale bar= 10 μm.

B) Schematic diagram of domains in RHAMM. The three grey lines in the ΔbZip construct represent leucines mutated to arginines. The time needed to progress from chromosome alignment (metaphase) to chromosome segregation (anaphase) was quantified in cells with phenotypically normal bipolar spindles from experiments as shown in (A). Box-and-whisker plots display the median flanked by 10th, 25th, 75th, and 90th percentiles. (3 experiments, >30 cells/bar, mean: "+", **P<0.05 compared to scrambled siRNA, ANOVA)

C) GFP-RHAMM (full-length), or variants thereof, were transfected into RHAMM-silenced cells and inter-kinetochore tension was measured based on NDC80 staining in metaphase cells with phenotypically normal bipolar spindles. More than 100 kinetochores from 60 cells were quantified per treatment. Scale bars= 10μm. (mean ± s.d., n= 3, *P< 0.05, t-test)

Collectively, these findings demonstrate that RHAMM depletion resulted in compressed and unfocused metaphase spindles. The following endogenous complexes were identified: RHAMM-Kif15; RHAMM-TPX2; TPX2-Kif15; and, TPX2-Eg5. In lysates generated from RHAMM-silenced cells, the abundance of TPX2-Eg5 complexes was attenuated as demonstrated in reciprocal immune-precipitates. The depletion of RHAMM, however, did not affect the abundance of TPX2-Kif15 complexes. Thus, TPX2 does not require RHAMM to interact with Kif15 (NOTE: both Kif15 and RHAMM contain a C-terminal bZip motif that directs TPX2 binding). While RHAMM does not form an endogenous complex with Eg5, the depletion of RHAMM does reduce the TPX2-Eg5 interaction. Specifically, localization analysis revealed TPX2 no longer colocalized with Eg5 at spindle poles in the absence of RHAMM. Thus, a fraction of the mitotic pool of TPX2 requires RHAMM to interact with Eg5, or the efficiency of the TPX2-Eg5 interaction is augmented in the presence of RHAMM. Speaking to the latter point, the bZip motif in the C-terminus of RHAMM, which is needed to bind TPX2, is needed to generate tension across sister kinetochores and complete the spindle checkpoint. Thus, RHAMM-TPX2 complexes promote the formation of inhibitory TPX2-Eg5 complexes, which reduce outward forces on the spindle, maintain spindle bipolarity, promote tension and enable the completion of the spindle checkpoint and progression into anaphase.

4.2.14 RHAMM-silenced cells exhibit cohesion fatigue phenotype

A subset of RHAMM-silenced metaphase cells (~10%) exhibit extensive arrest during metaphase (>60 mins) when followed by time-lapsed image analysis (Fig. 4.1B). But, when mitotic progression is followed in cell lysates, cyclin B1 degradation occurs (Fig. 4.2) even in the presence of the reduced inter-kinetochore tension that characterizes RHAMM-silenced cells. When I examined RHAMM-silenced cells undergoing a prolonged bipolar metaphase arrest, I noted a scatter chromosome phenotype (Fig. 4.19A), consistent with a phenomenon previously described as cohesion fatigue (Daum et al., 2012; Stevens et al., 2011).

Cohesion fatigue is the asynchronous separation of chromatids in cells that exhibit a prolonged metaphase arrest (Gorbsky, 2013). Asynchronous separation of chromatids may contribute to both numerical and structural chromosome abnormalities, as well as trigger the reactivation of the spindle checkpoint and checkpoint induced apoptosis (Gorbsky, 2013). To examine this phenomenon in RHAMM-silenced cells, I first classified cohesion fatigue by the presence of chromosome scattering (Fig. 4.19B). In the RHAMM-silenced population, 14% of mitotic cells underwent cohesion fatigue followed predominantly by an abnormal anaphase and mitotic exit. Expression of GFP-RHAMM was only able to partially reduce the frequency of cohesion fatigue, specifically, the level of mitotic death was not attenuated.

Previous studies have proposed two mechanisms to explain the occurrence of cohesion fatigue following a prolonged metaphase arrest. The first proposes that a decreased level of cohesin proteins may reduce the structural integrity of the cohesin complex on the chromosomes and cause cohesion fatigue (Daum et al., 2012, 2009). In mitotic lysates of RHAMM-silenced cells, however, the levels of Rad21 and SMC2, two core components of the cohesin complex, were indistinguishable with those seen in the control-treated population (Fig. 4.19C). Confocal

images of metaphase cells also showed the correct localization of SMC2 along the entire chromosome volume in RHAMM-silenced and control-treated metaphase cells (Fig. 4.19D). Another model proposes that excess pulling forces along the mitotic spindle may simply rupture the cohesin complex, and induce asynchronous chromatid segregation (Gorbsky, 2013). This putative mechanism for cohesin fatigue may better align with my previous findings demonstrating an excess in outward forces present along the mitotic spindle in RHAMM-silenced cells.

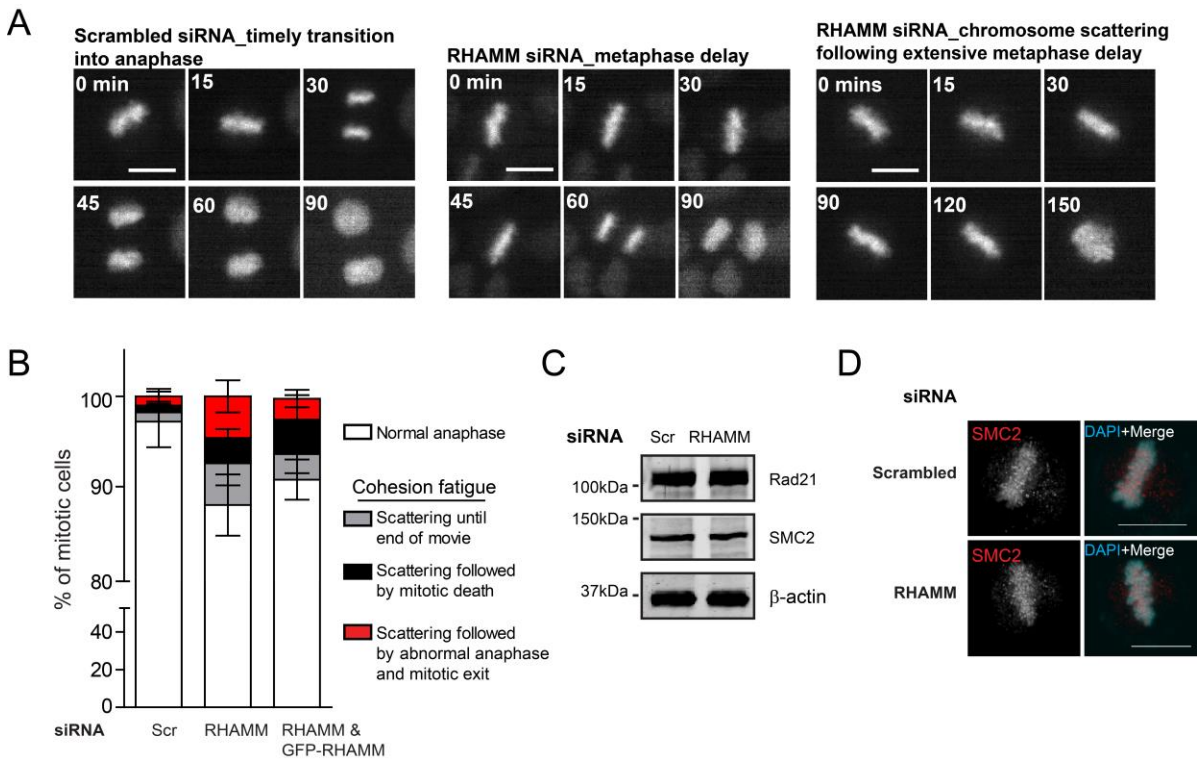

Figure 4.19 RHAMM silencing induces cohesion fatigue

A) Time-lapse microscopy of HeLa cells expressing mCherry Histone-H2B demonstrates chromosome scattering in RHAMM-silenced cells after prolonged metaphase delay. Scale bars= 10 μm.

B) Percentage of cells in experiments as in A) that underwent different mitotic fates. (mean ± s.d., 100-150 cells analyzed between 3 experiments).

C) HeLa cells were treated with either scrambled siRNA or siRNA targeting RHAMM, treated with a double thymidine block and released to early mitosis. Cell lysates were probed for cohesin complex proteins, Rad21 and SMC2. Equal loading was confirmed by probing for β-actin.

D) HeLa cells were treated with either scrambled siRNA or siRNA targeting RHAMM, treated with a double thymidine block and released to early mitosis. SMC2 localized to chromosomes in both treatment. Scale bars= 10 μm.

4.3 Key findings

1. Silencing RHAMM induces a sustained activation of the spindle checkpoint and delays mitotic progression into anaphase.
2. In RHAMM-silenced cells, Kt-MT attachments and inter-kinetochore tension are reduced, metaphase spindles are unfocused, but the localization of key checkpoint proteins to the kinetochore, Eg5 to mitotic microtubules, and Kif15 to the spindle pole is not affected.
3. In RHAMM-silenced cells, inhibitory TPX2-Eg5 complexes are significantly reduced, implicating hyperactive Eg5 activity as a putative cause for checkpoint delay. Consistently, addition of an Eg5 inhibitor to RHAMM-silenced cells establishes inter-kinetochore tension and promotes progression into anaphase.
4. Progression to anaphase requires RHAMM variants that encode the conserved bZip motif necessary for RHAMM-TPX2 interactions.
5. Prolonged metaphase arrest in RHAMM-silenced cells resolves through cohesion fatigue.

4.4 Discussion

The spindle checkpoint is a safety net that ensures successful mitosis by promoting mitotic exit only when equal chromosome segregation can be achieved. Thus, turning "on" the checkpoint signal is important to maintain genome fidelity, whereas turning "off" the checkpoint signal allows for entry into anaphase. Indeed, cells with weak checkpoint signals tend to slip out of mitosis with chromosome segregation errors (Bohers et al., 2008; Fang, 2002; Lampson and

Kapoor, 2005), while cells with sustained checkpoint activation undergo prolonged metaphase arrest (Lara-Gonzalez and Taylor, 2012). I found that the depletion of RHAMM increased the time needed to transition from metaphase to the onset of anaphase, which suggested sustained checkpoint activation. Consistently, the degradation of cyclin B1 was delayed in RHAMM-silenced cells. Sustained activation of the checkpoint occurred without evidence for changes in the abundance or location of key checkpoint proteins. Dunsch *et al* also observed a kinetic delay between nuclear envelope breakdown and the onset of anaphase without changes to the localization of BubR1 (Dunsch et al., 2012). However, Dunsch *et al* attributed this delay to spindle rotation that is normally prevented by a complex containing RHAMM, a spindle protein termed CHICA and dynein light chain 1 (Dunsch et al., 2012). Consequently, I analyzed spindle rotation in RHAMM-silenced cells but found the spindle oriented properly in half of the delayed mitotic cells. This prompted me to ask: Why do RHAMM-silenced cells with oriented and bipolar spindles exhibit sustained checkpoint activation?

A defining characteristic of metaphase spindle organization is the equilibrium established between opposing motor forces along the mitotic spindle. Dynein depletion, which removes inward forces on the spindle, results in unfocused spindles and delays chromosome alignment; when I silenced RHAMM, I observed phenotypes that approximated these observations. Indeed, the inhibition of the major outward force generator, Eg5, alleviated the mitotic delay induced in RHAMM-silenced cells. These findings are consistent with previous reports where inhibition of Eg5 restores bipolar spindle assembly in dynein-deficient cells (Mitchison et al., 2005; Tanenbaum et al., 2008). A series of papers identified Kif15 as a cooperative motor to Eg5 (Tanenbaum et al., 2009; Vanneste et al., 2009). Kif15 is not essential for bipolar spindle assembly during normal circumstances, but is required to partially rescue defects associated with

Eg5 inhibition (Tanenbaum et al., 2009; Vanneste et al., 2009). In accordance with those findings, I found that the inhibition of Eg5, but not Kif15, reduced the metaphase delay observed in RHAMM-silenced cells. Though it may be interesting to assess mitotic kinetics after inhibition of both kinesins in RHAMM-silenced cells, various other investigations had reported simultaneous inhibition of Eg5 and Kif15 to be unfeasible due to bipolar spindles collapsing to monopolar spindles (Tanenbaum et al., 2009; van Heesbeen et al., 2014).

Motor protein behavior is dependent on interactions with associated adapter proteins. These interactions determine motor protein localization, directionality, movement and function. TPX2 blocks the path of Eg5 on microtubule fibers via steric hindrance and functions as a potent inhibitor of Eg5 velocity by reducing its microtubule stepping activity (Balchand et al., 2015; Ma et al., 2011). Loss of this inhibitory action increases Eg5 movement towards microtubule plus ends, and the excess outward forces generated can cause astral microtubules to splay outward and produce unfocused spindle poles. These phenotypes are observed in RHAMM-silenced cells suggestive of excessive outward force at spindle poles. Indeed, my analyses of RHAMM-silenced mitotic cells indicate a reduction, but not complete loss, in the formation of inhibitory TPX2-Eg5 complexes (Balchand et al., 2015; Ma et al., 2011) as well as the disruption of co-localization between TPX2 and Eg5 specifically at spindle poles. Similar to the interaction between Aurora A and TPX2, TPX2-Eg5 complex formation was reduced even when the levels of TPX2 were restored by chemical inhibition of the proteasome. As RHAMM does not directly bind to Eg5, it may be needed to locate TPX2 to spindle poles to enable an interaction with Eg5 at this subcellular site. It is known that Eg5 localizes to poles through dynein and does not require TPX2 (Gable et al., 2012; Ma et al., 2011); consistently, Eg5 localized along spindle fiber and spindle poles in RHAMM-silenced cells. Thus, my results are consistent with a

requirement for RHAMM to promote a TPX2-Eg5 complex at the spindle pole; for this reason, the depletion of RHAMM does not completely disrupt TPX2-Eg5 complexes, which may still occur along the spindle fibers on the half-spindle. Collectively, my results indicate a net gain of outward force in RHAMM-silenced cells due to hyperactive Eg5 activity.

Force balance ensures chromosome attachment and alignment, which is required to complete the spindle checkpoint response. K-fibers are the main type of spindle microtubules needed to form stable Kt-MT attachments. TPX2-Eg5 complexes organize microtubules nucleated near kinetochores into functional K-fibers (Ma et al., 2011). For this reason, the expression of a truncated TPX2 construct (lacking the Eg5 binding domain) into TPX2-silenced cells did not affect microtubule nucleation near kinetochores but abolished cold-resistant organized K-fibers (Ma et al., 2011). Reduced TPX2-Eg5 complexes may mechanistically explain why stable Kt-MT attachments were not formed in RHAMM-silenced cells, as observed by Dunsch and colleagues (Dunsch et al., 2012). That is, my studies found cells lacking RHAMM are able to assemble K-fibers, albeit with reduced kinetics (i.e., non-centrosomal microtubule assembly was delayed but not abolished), but these fibers may be less stable due to a reduction in TPX2-Eg5 complexes.

Under normal circumstances in mitosis, metaphase is a brief stage, which reflects the transient nature of the spindle checkpoint. While a robust checkpoint signal is crucial to maintaining genome fidelity, failure to resolve the checkpoint signal can cause unscheduled mitotic exit and produce aneuploid progeny cells (C. Rieder and Maiato, 2004; Rossio et al., 2010; Weaver and Cleveland, 2005). Here, I show that prolonged metaphase arrest results in cohesion fatigue in a subset of RHAMM-silenced cells. Examination of key proteins within the cohesin complex revealed that the observed progressive chromatid separation may not be due to

reduced stability of the cohesin complex. I noted no differences in cohesin protein abundance and localization in the absence of RHAMM, suggesting chromatid cohesion is present. However, in a subset of metaphase delayed RHAMM-silenced cells, the excess outward forces created through hyperactive Eg5 may overcome the inward forces provided by chromatid cohesion and induce cohesion fatigue. Taken together, my findings show RHAMM acts as a brake on Eg5-dependent outward forces via targeting of TPX2 to spindle poles. This regulatory relationship is needed to facilitate correct chromosome segregation and prevent cohesion fatigue and aneuploid progeny.

Chapter 5: Mitotic success is dependent on the appropriate expression of RHAMM

5.1 Rationale and hypothesis

The immunodepletion of XRHAMM from *Xenopus* egg extracts blocked TPX2 concentration to spindle poles and disrupted spindle organization (Groen et al., 2004). Paradoxically, accumulation of XRHAMM, as achieved through the loss of BRCA1/BARD1, also disrupted TPX2 localization to spindle poles and affected spindle organization (Joukov et al., 2006). These findings imply that the dosage of RHAMM may be finely regulated during cell division. The results described in Chapters 3 and 4 consistently show that the construction and functionality of the mitotic spindle is negatively impacted when RHAMM is reduced. Thus, I hypothesize that the expression of RHAMM must be appropriately regulated within the dividing cell, and the over-expression of RHAMM may disrupt spindle architecture and the kinetics of mitosis.

5.2 Results

5.2.1 Overexpression of GFP-RHAMM results in aberrant spindle figures

To study the effects of excess RHAMM during mitosis in human cells, a HeLa sub-line was engineered with doxycycline-inducible expression of full-length GFP-RHAMM. In this model, GFP-RHAMM expression can be titrated by increasing induction time (Fig. 5.1A). After 24 hours of doxycycline induction, GFP-RHAMM expression was comparable to the level of endogenous RHAMM expression observed in nocodazole arrested mitotic cells (lane 1, Fig. 5.1A). Immunofluorescence quantification of fixed mitotic cells demonstrated a significant increase of aberrant spindle phenotypes with the induction of GFP- RHAMM expression (Fig. 5.1B).

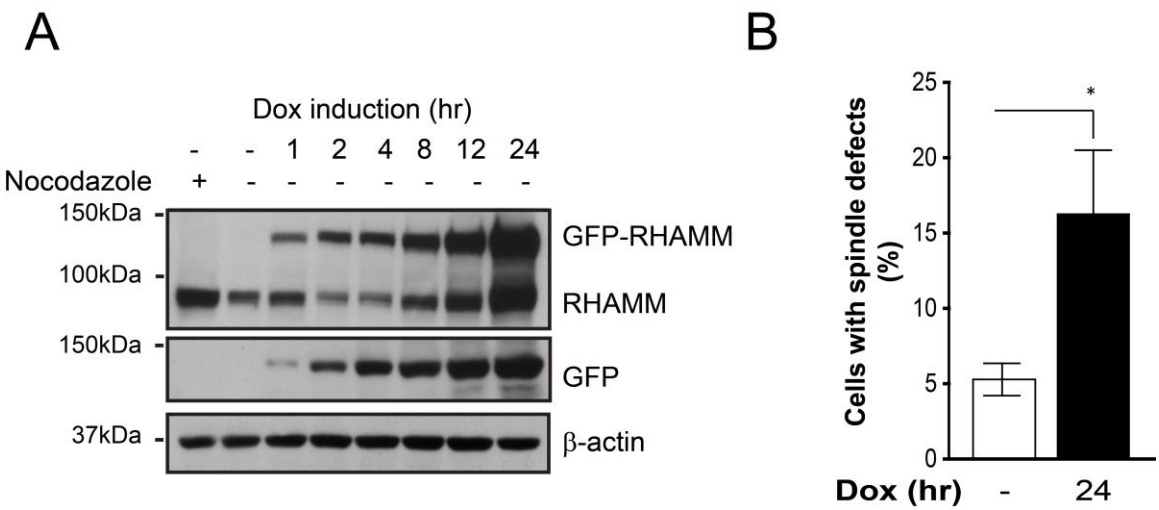

Figure 5.1 Doxycycline induced overexpression of GFP-RHAMM disrupts spindle organization

A) HeLa cells were treated with doxycycline for indicate durations to induce GFP-RHAMM overexpression, un-induced cells were treated with or without nocodazole for 12 hours. Analysis of lysates demonstrates GFP-RHAMM expression is titratable by increasing the duration of doxycycline treatment. At 24 hours induction, the level of GFP-RHAMM approximated the level of endogenous RHAMM in nocodazole arrested mitotic lysates. Equal loading was confirmed by probing for β-actin.

B) Overexpression of GFP-RHAMM after 24 hours of doxycycline induction significantly increased the incidence of aberrant mitotic spindles, such as multipolar spindle, unfocused and disorganized spindle. Spindle morphology was visualized by TUBB staining. (mean ± s.d., n= 4, >80 cells/treatment, *P< 0.05, t-test).

5.2.2 Overexpression of GFP-RHAMM results in aberrant division kinetics

I noted elevated levels of endogenous RHAMM expression after 24 hours of doxycycline induction, which likely reflects an associated delay in mitotic progression within the population of induced cells. In support of this hypothesis, I observed a similar increase in the levels of endogenous RHAMM in nocodazole treated cultures (Fig. 5.1A). To investigate whether GFP-RHAMM over-expression may also affect proper mitotic progression, I performed time-lapsed image analysis on living cells (Fig. 5.2A). HeLa cells were treated with doxycycline or DMSO for 24 hours, and then a Hoechst stain was added to visualize DNA. Interestingly, I found that GFP-RHAMM overexpression did not affect spindle assembly kinetics (prophase to metaphase), but significantly augmented the time needed to complete the spindle checkpoint (metaphase to anaphase) and the overall duration of mitosis (Fig.5.2B).

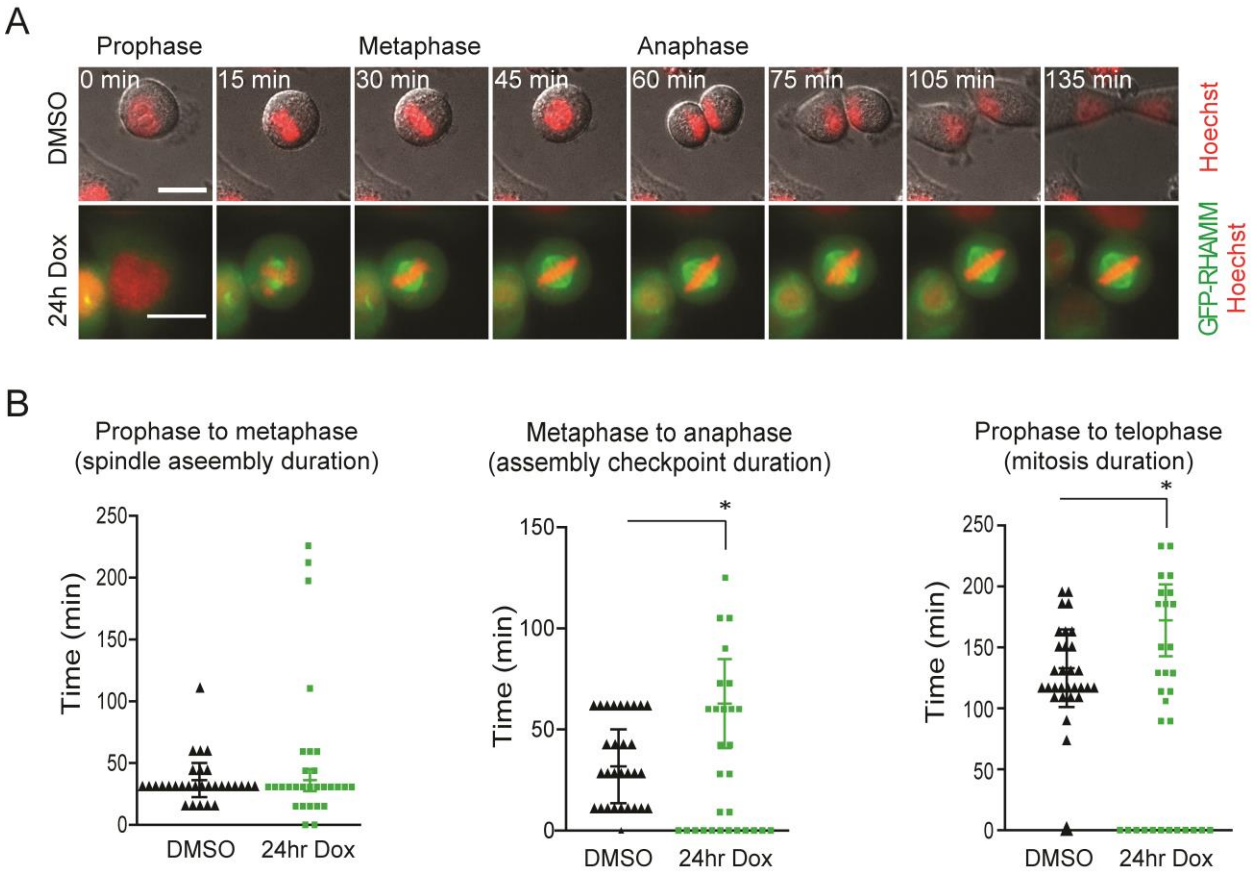

Figure 5.2 Overexpression of GFP-RHAMM results in aberrant mitosis kinetics

A) HeLa cells were treated with doxycycline for 24 hours to induce GFP-RHAMM overexpression, or with DMSO-vehicle control, and then labelled with Hoechst to visualize DNA, and followed by time-lapse microscopy as they transited through cell division. Scale bars= 10 μm.

B) The time needed for cells treated with doxycycline, or DMSO treated control cells, to transit from prophase to metaphase (spindle assembly duration), metaphase to anaphase (spindle checkpoint kinetics), or prophase to telophase (mitosis duration) is plotted. Cells that arrested at particular stage of mitosis were plotted at 0 minutes and were not included in the quantification of mitosis duration. (mean ± s.d., 30 cells/treatment, n= 6, **P*< 0.05, t-test).

5.2.3 GFP-RHAMM overexpression does not alter TPX2 and pAurora A localization or microtubule regrowth in HeLa cells

Live-cell image analysis suggested spindle assembly kinetics may not be affected by GFP-RHAMM overexpression. I used a microtubule regrowth assay to examine whether Aurora A-TPX2 mediated microtubule nucleation may be affected in cells expressing GFP-RHAMM (Fig. 5.3A). Comparison between DMSO-treated and doxycycline-treated cells revealed no difference in mitotic microtubule regrowth following release from nocodazole treatment. Moreover, microtubule regrowth asters stained positive for TPX2 and pAurora A, and were similar in size and abundance (Fig. 5.3A).

I localized TPX2 and pAurora A by immunofluorescence in non-synchronized mitotic HeLa cells after induction (Fig. 5.3B). In the doxycycline- induced cells, the spindles appear disorganized and compressed, which may indicate an imbalance in motor forces. However, the induced expression of GFP-RHAMM did not alter the localization of TPX2 along mitotic microtubules or the localization of pAurora A at the spindle poles (Fig. 5.3B).

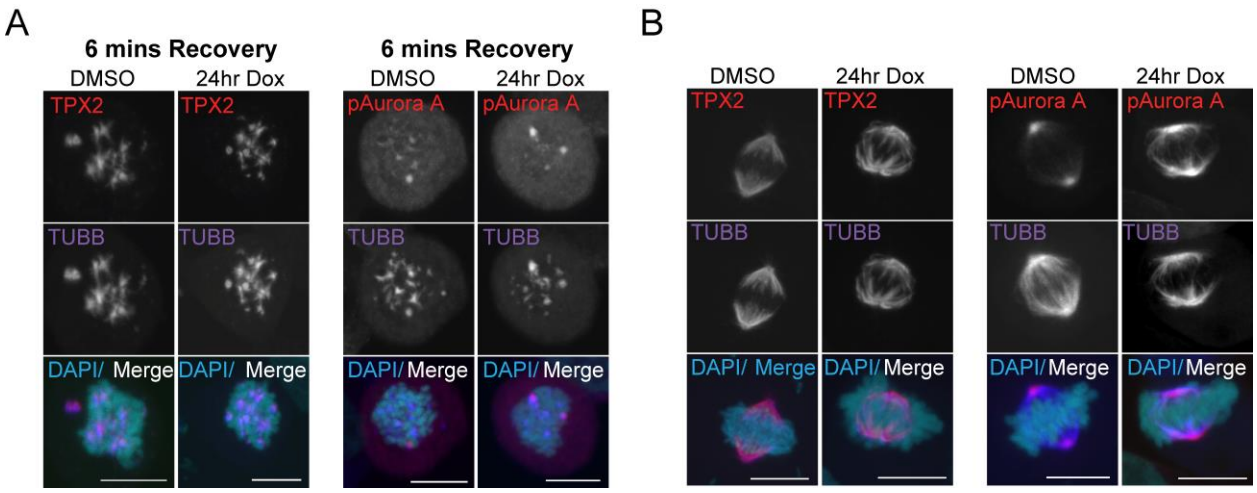

Figure 5.3 Overexpression of GFP-RHAMM does not alter TPX2 and pAurora A localization or microtubule regrowth in HeLa cells

A) Inducible GFP-RHAMM HeLa cells, pretreated with DMSO or doxycycline for 24 hours, were treated with nocodazole to depolymerize mitotic microtubules, released into fresh media to enable microtubule regrowth for six minutes, fixed and stained for TPX2 and pAurora A localization. Scale bars= 10 μm.

B) Asynchronously growing inducible GFP-RHAMM HeLa cells, pretreated with DMSO or doxycycline for 24 hours, were stained for TPX2 or pAurora A and beta-tubulin (TUBB) to locate the mitotic spindle. Scale bars= 10 μm.

5.2.4 Overexpression of GFP-RHAMM affects metaphase spindle positioning

When examining TPX2 and pAurora A localization in GFP-RHAMM expressing cells, I noted that many spindles were not centered, similar to a spindle positioning defect noted in RHAMM-silenced cells (Dunsch et al., 2012)(Fig. 4.3 and 4.4). To measure this effect, I analyzed spindle position and orientation during metaphase. After 24 hours of doxycycline induction, a substantial fraction of mitotic cells overexpressing GFP-RHAMM displayed off-center spindles (Fig. 5.4).

GFP-RHAMM expression in HeLa cells resulted in compressed, mis-positioned mitotic spindles and delayed mitotic progression to anaphase. Spindle assembly kinetics and TPX2-Aurora A mediated microtubule spindle nucleation remained unaffected. Thus, GFP-RHAMM expression may disrupt motor protein mediated spindle organization rather than mitotic spindle assembly.

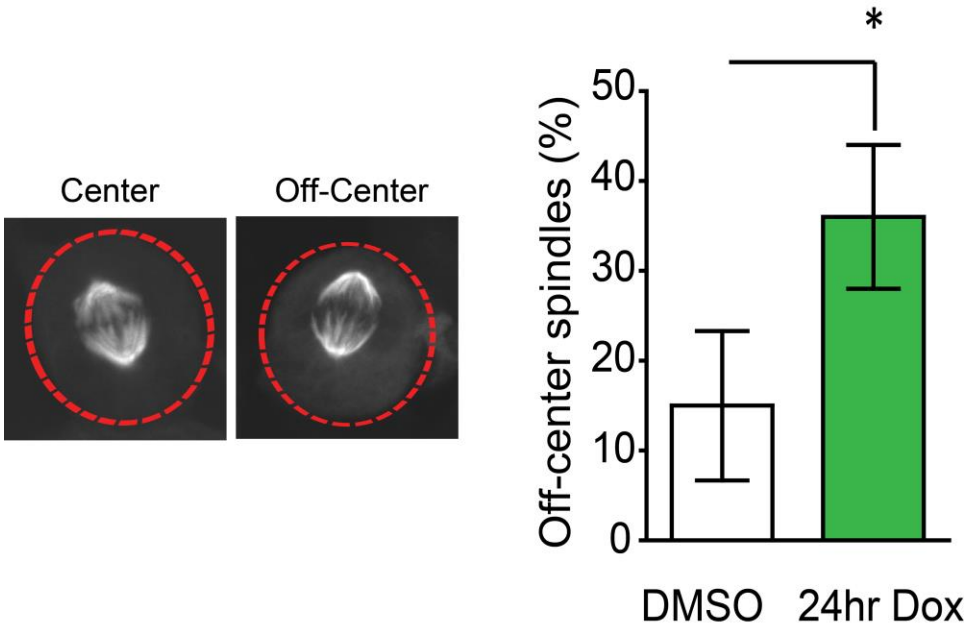

Figure 5.4 Proportion of cells with off-center spindles are significantly increased with GFP-RHAMM overexpression.

Asynchronously growing HeLa cells, pretreated with DMSO or doxycycline for 24 hours, were stained for TUBB to locate the mitotic spindle in dividing cells. Red dotted circle indicates periphery of the cell. Mean ± s.d. is plotted for 75 cells/treatment. (n= 3, *P< 0.05, t-test).

5.2.5 Chromosome translocation of the *HMMR* locus results in RHAMM overexpression in human fibroblast cells

A patient with a mosaic variegated aneuploidy-like phenotype, most commonly associated with mutations in the spindle checkpoint gene product BubR1 (Bohers et al., 2008; Hanks et al., 2006; Jacquemont et al., 2002; Matsuura et al., 2006; Suijkerbuijk et al., 2010), presented in Texas with a translocation between human chromosomes 5q33 and 12q24 (t(5;12)(q33.3;q24.31, personal communication to Dr. Maxwell). Unfortunately, tissue samples were not available from the patient. Since the translocation occurred proximal to the *HMMR*/RHAMM locus, 5q33.2-qter (Spicer et al., 1995), I hypothesized that a similar translocation may alter the abundance of RHAMM, thus producing a MVA-like phenotype by delaying chromosome segregation and, potentially, inducing cohesion fatigue. To investigate this hypothesis, I obtained, from the Coriell Biorepository, two untransformed fibroblast cell lines each with a t(5;12)(q33.3;q24.31): GM01536 (CC36) and GM01535 (CC35). CC36 was sampled from a 38 year old female, while CC35 was sampled from her daughter at 16 years of age. We also purchased from the ATCC (American Type Cell Collection) a control, untransformed fibroblast cell line with a normal diploid karyotype obtained from a newborn male, termed BJ CRL-2522 (BJ).

Karyotype analyses by The Coriell Biorepository showed that the CC36 cell line contains a balanced translocation with two breakpoints at 12q24 and 5q33. The CC36 cell line contains two copies of the 5q33 region and two copies of the 12q24 region. The CC35 cell line, however, contains a translocation with two derivative aneuploid segments at (-)12q24>12qter and (+)5q33>5qter. That is, the CC35 cell line contains three copies of the 5q33 region and a single

copy of the 12q24 region. Specifically, the amplified region of 5q33.3 is 161 Mb – 180.6 Mb, which contains the full *HMMR* gene (162.8 Mb – 162.9 Mb), while the deleted region of 12q24.33 (131.3 Mb – 132.3 Mb) contains the full *Ran* gene (131.35 Mb- 131.36 Mb).

To screen for genomic changes in the *HMMR* locus, I isolated DNA from the fibroblast cell lines and used three sets of primers (designed to recognize various intron-exon boundaries of the *HMMR* gene) to determine the copy-number of the *HMMR* gene (Fig. 5.5A). The relative expression of genomic DNA was normalized to levels identified in the diploid BJ fibroblast cell line. The copy number of the housekeeping gene, *TBP*, showed no difference between the three fibroblast cell lines and, therefore, these values were included as part of the delta-delta Ct analysis. Using these analysis parameters, an average 1.67 fold increase in *HMMR* gene dosage in CC35 relative to CC36 cells was revealed. I observed a similar fold increase in the abundance of RHAMM protein as determined through Western blot analysis of lysates of nocodazole-synchronized mitotic cells (Fig. 5.5B). However, the localization of RHAMM to the mitotic spindle and spindle pole was unchanged in the CC35 cells (Fig. 5.5C).

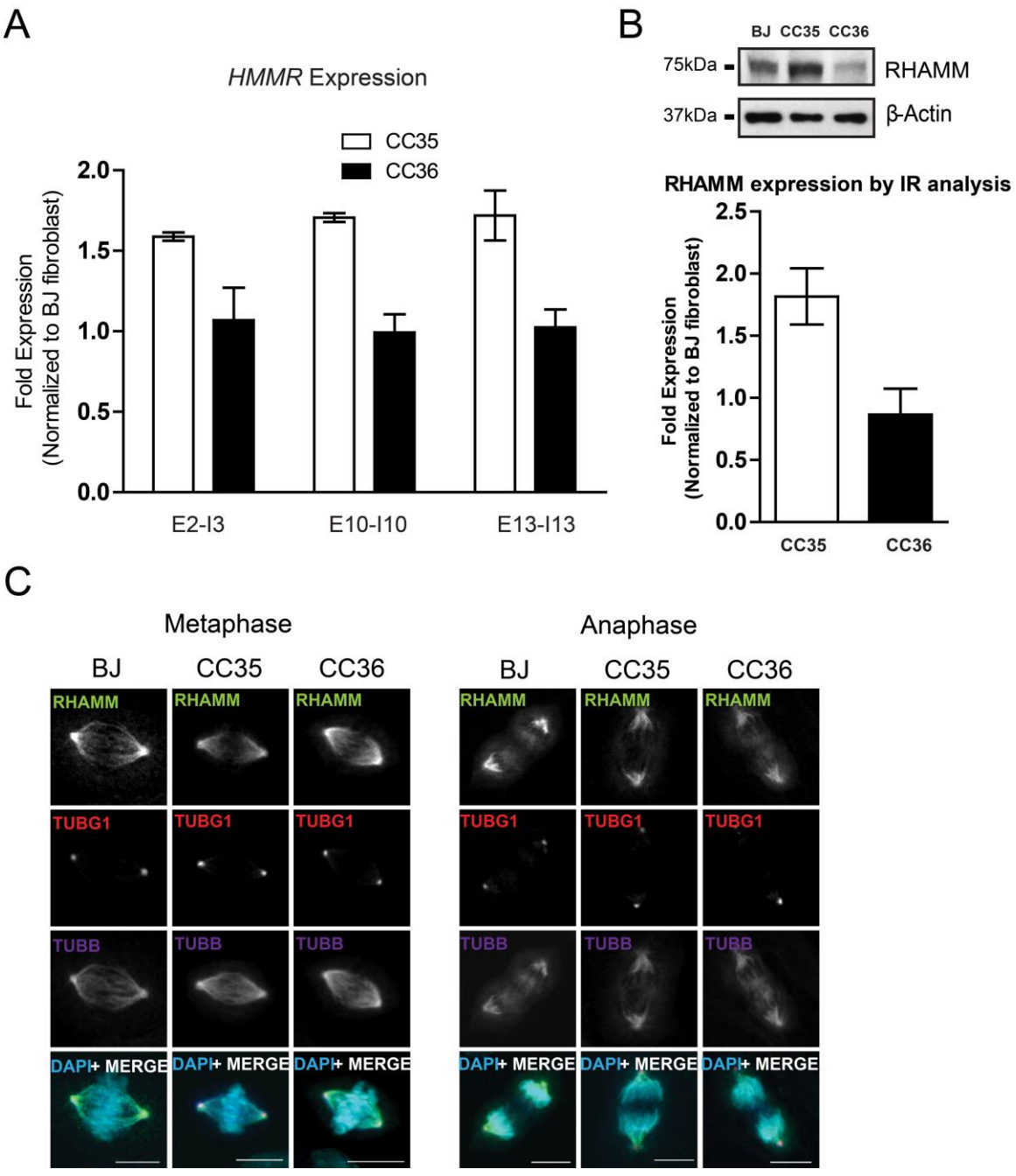
A
HMMR Expression
CC35
CC36
Fold Expression
(Normalized to BJ fibroblast)
2.0
1.5
1.0
0.5
0.0
E2-I3
E10-I10
E13-I13
B
BJ CC35 CC36
75kDa
RHAMM
37kDa
β-Actin
RHAMM expression by IR analysis
Fold Expression
(Normalized to BJ fibroblast)
2.5
2.0
1.5
1.0
0.5
0.0
CC35
CC36
C
Metaphase
Anaphase
BJ
CC35
CC36
RHAMM
TUBG1
TUBB
DAPI+ MERGE

Figure 5.5 RHAMM overexpression by chromosome translocation in human fibroblast cells

A) Quantitative PCR indicated copy numbers of the *HMMR* gene from IN genomic DNA extracted from Coriell fibroblast cells and normalized to levels obtained in diploid BJ fibroblasts. 3 sets of primers designed to recognize various intron-exon boundaries of the *HMMR* gene (mean ± s.d., n= 4)

B) Fibroblast cells were synchronized to mitosis by nocodazole, and RHAMM expression was measured by quantitative Western blot analysis. Protein bands were visualized by Licor imaging using IR fluorophore tagged secondary antibodies. Equal loading was confirmed with β-actin. Expression fold differences were first normalized to actin levels, then normalized to expression of RHAMM in BJ population. (mean ± s.d., n= 3)

C) Localization of RHAMM to spindle poles (indicated by TUBG1) and mitotic microtubules (indicated by TUBB) in asynchronous fibroblast cells. Scale bars= 10 μm.

5.2.6 Aberrant spindle figures are significantly increased in CC35 cells (+ RHAMM).

I quantified the proportion of cells displaying mitotic spindle defects, including abnormal bipolar spindles, multipolar spindles or anaphase segregation defects (Fig. 5.6A). The proportion of cells with aberrant spindle figures were significantly higher in CC35 cells compared to BJ cells, however, a comparison between CC35 and CC36 cells failed to produce any statistical difference. I then used time-lapse microscopy to analyze the mitotic kinetics of the different fibroblast populations (Fig. 5.6B). Mitosis duration was similar between the BJ cells and the CC36 cells, and I noted a slight delay in the completion of mitosis in the CC35 cell, though these changes were not statistically significant.

Untransformed human CC35 fibroblast cells containing a chromosome translocation that increases *HMMR* copy number served as an alternative model to study gain of RHAMM function. In CC35 cells, the localization of RHAMM is not affected but a significant increase in the frequency of aberrant mitotic spindles was noted although the kinetics of cell division were not significantly affected.

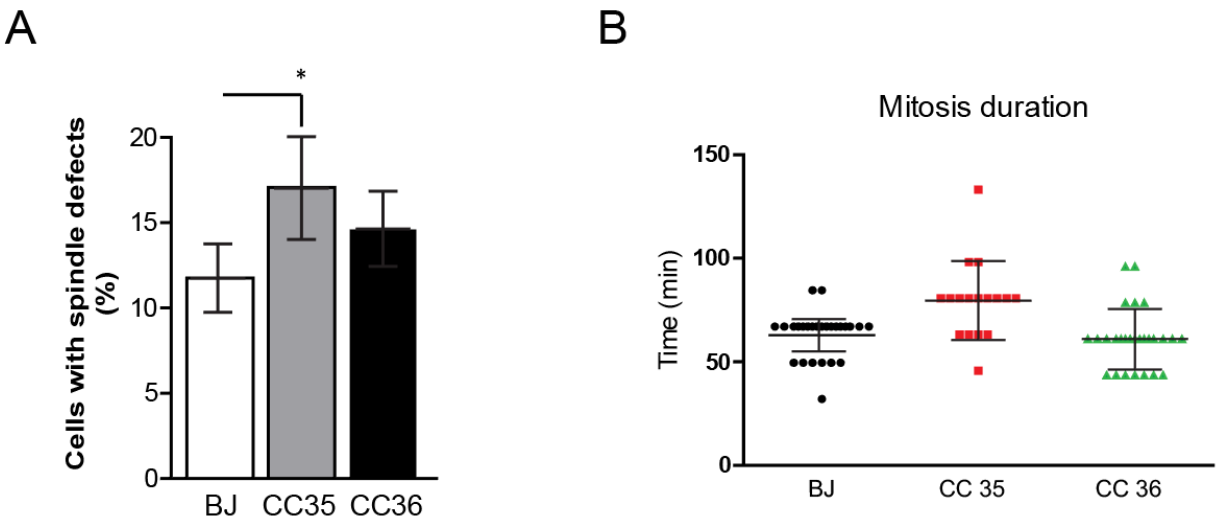

Figure 5.6 RHAMM overexpression results in aberrant spindle figures in human fibroblast cells

A) Quantification of abnormal bipolar spindles, multipolar spindles or anaphase segregation defects in fibroblast cells. Spindle morphology was visualized by TUBB staining. (mean ± s.d., n= 3, >120 cells/treatment, **P*< 0.05, ANOVA)

B) Fibroblast cells were labelled with Hoechst to visualize DNA and followed through mitosis by time-lapse microscopy. The time needed to complete mitosis in the different fibroblast populations. (mean ± s.d., >15 cells/treatment, n= 4, **P*< 0.05, ANOVA).

5.3 Key findings

1. Overexpression of GFP-RHAMM during mitosis results in aberrant mitotic spindle architecture, mispositioned bipolar spindles and delayed cell division kinetics.
2. Increased gene dose of *HMMR* in CC35 cells correlates with abnormal spindle structure.
3. Augmented RHAMM expression, whether exogenous expression of GFP-RHAMM or trisomy of the endogenous *HMMR* locus, disrupts mitotic outcomes in various cell model systems.

5.4 Discussion

Previous studies performed in *Xenopus* oocytes revealed contradictory findings regarding the necessity of RHAMM in targeting TPX2 to spindle poles and establishing a functional bipolar spindle (Groen et al., 2004; Joukov et al., 2006). The depletion of XRHAMM from egg extracts significantly inhibited both the abundance and size of microtubule asters, as well as reduced TPX2 localization at spindle poles (Groen et al., 2004). Joukov *et al* observed similar results by silencing the E3 ubiquitin ligase, tumor-suppressor complex, BRCA1-BARD1, which stabilizes and augments the levels of XRHAMM (Joukov et al., 2006). From this study, it was concluded that BRCA1-BARD1 contributed to anastral assembly in *Xenopus* cells by downregulating XRHAMM in mitosis, which is necessary for proper TPX2 localization (Joukov et al., 2006). Moreover, Joukov *et al* postulated that loss of BRCA1 may alter Aurora A activity downstream. Experiments performed in Chapter 3 and Chapter 4 utilize siRNA to silence endogenous RHAMM expression, and as a result, mitotic spindle structure and Aurora A activity

are negatively impacted, similar to the initial study performed in *Xenopus* cells (Groen et al., 2004).

In order to test the hypothesis that excess RHAMM may also have detrimental effects on mitotic spindle assembly and TPX2 localization, I first used HeLa cells with tetracycline-inducible expression of GFP-RHAMM. I observed that overexpression of GFP-RHAMM affects spindle architecture and metaphase spindle positioning. However, I did not observe alterations to TPX2 and Aurora A location as previously reported (Joukov et al., 2006). These findings suggest that excess GFP-RHAMM may not impede spindle microtubule nucleation but may negatively affect spindle organization. In line with these observations in fixed cells, time-lapse microscopy revealed a delay in spindle checkpoint completion with overexpression of GFP-RHAMM, during which spindle orientation is established. Indeed, other findings have demonstrated transient overexpression of GFP-RHAMM inhibits mitotic progression and affects spindle architecture in HeLa and 8226 cells (Maxwell et al., 2003).

As previously mentioned, the term spindle assembly encompasses both spindle microtubule nucleation and organization, which can be distinguished by performing a microtubule regrowth assay after depolymerizing by nocodazole. I examined TPX2 location along an intact spindle and during the recovery stage of a microtubule regrowth assay. Overexpression of GFP-RHAMM did not affect TPX2 localization in either scenarios: TPX2 is present at various microtubule nucleation sites, centrosomal and non-centrosomal, and TPX2 remained localized throughout the entire length of the intact metaphase spindle, despite gross defects in spindle morphology. Correspondingly, pAurora A localization mirrored that of TPX2 in both types of spindle.

HeLa cells with tetracycline-inducible expression of GFP-RHAMM allow the titration of GFP-RHAMM overexpression in the context of an aneuploid genome. The aforementioned MEF cells (refer to section 3.2.12) allow the study of wildtype and heterozygous gene dose responses. To complement these model systems, I utilized two untransformed human fibroblast cells, one of which harbored an unbalanced chromosome translocation of the *HMMR* locus and elevated expression of RHAMM at both mRNA and protein levels. Subsequent fixed and live cell mitosis analysis revealed delayed mitotic progression and aberrant spindle architecture in the fibroblast cell line with RHAMM overexpression similar to my findings observed in HeLa cells.

The studies in Chapters 3 and 4 focused on loss of function phenotypes observed after endogenous RHAMM depletion, while the studies presented in this chapter demonstrated the effects of RHAMM overexpression using various systems. Experiments performed after RHAMM silencing provide mechanistic insights into protein functions and interactions, while systems with RHAMM overexpression provide relevance to cancers described with elevated RHAMM expression (reviewed in Section 1.6.4). Aberrant mitosis structure and kinetics were observed with both depletion of endogenous RHAMM and RHAMM overexpression, which suggests that precise level of RHAMM expression is required for mitotic progression and genome stability.

Chapter 6: Discussion and conclusions

6.1 Summary and working models

The purpose of this study was to better understand the construction and organization of mitotic spindle microtubules into a functional structure that facilitates the faithful segregation of chromosomes during mitosis. My investigation is focused on the function of a novel mitotic regulator: the receptor for hyaluronan-mediated motility, RHAMM. Previously, RHAMM was thought to be an extracellular receptor for hyaluronan, a glycosaminoglycan, that promotes cell motility (Turley et al., 1987). However, the product of the full length *HMMR* gene was shown to be a cytoskeletal protein (Assmann et al., 1999, 1998; Hofmann et al., 1998) that stabilizes the spindle (Maxwell et al., 2005, 2003) and promotes anastral spindle assembly through the Ran-GTP pathway (Groen et al., 2004; Joukov et al., 2006; Sharp et al., 2011).

This study demonstrates that RHAMM contributes to both structural and biochemical signaling pathways that ensure bipolar spindle assembly and mitotic progression. Specifically, findings in **Chapter 3** show RHAMM targets TPX2 to both centrosome and non-centrosome sites for spindle assembly, where TPX2 promotes localized microtubule nucleation via activation of Aurora kinase A (Fig. 6.1). Using fixed and live cell assays, I show that RHAMM silencing delays the kinetics of spindle assembly, mislocalizes TPX2, reduces TPX2 stability and attenuates activation of Aurora kinase A. Consequently, the length of the mitotic spindle is reduced in RHAMM-silenced cells. Domain analyses uncovered that the RHAMM–TPX2 complex requires the C-terminal bZip motif in RHAMM and a domain that includes the nuclear localization signal in TPX2. Analysis of kinetic assays revealed a mitotic delay during spindle

checkpoint completion in RHAMM-silenced cells, which prompted a subsequent study investigating the functions of RHAMM during chromosome alignment and segregation.

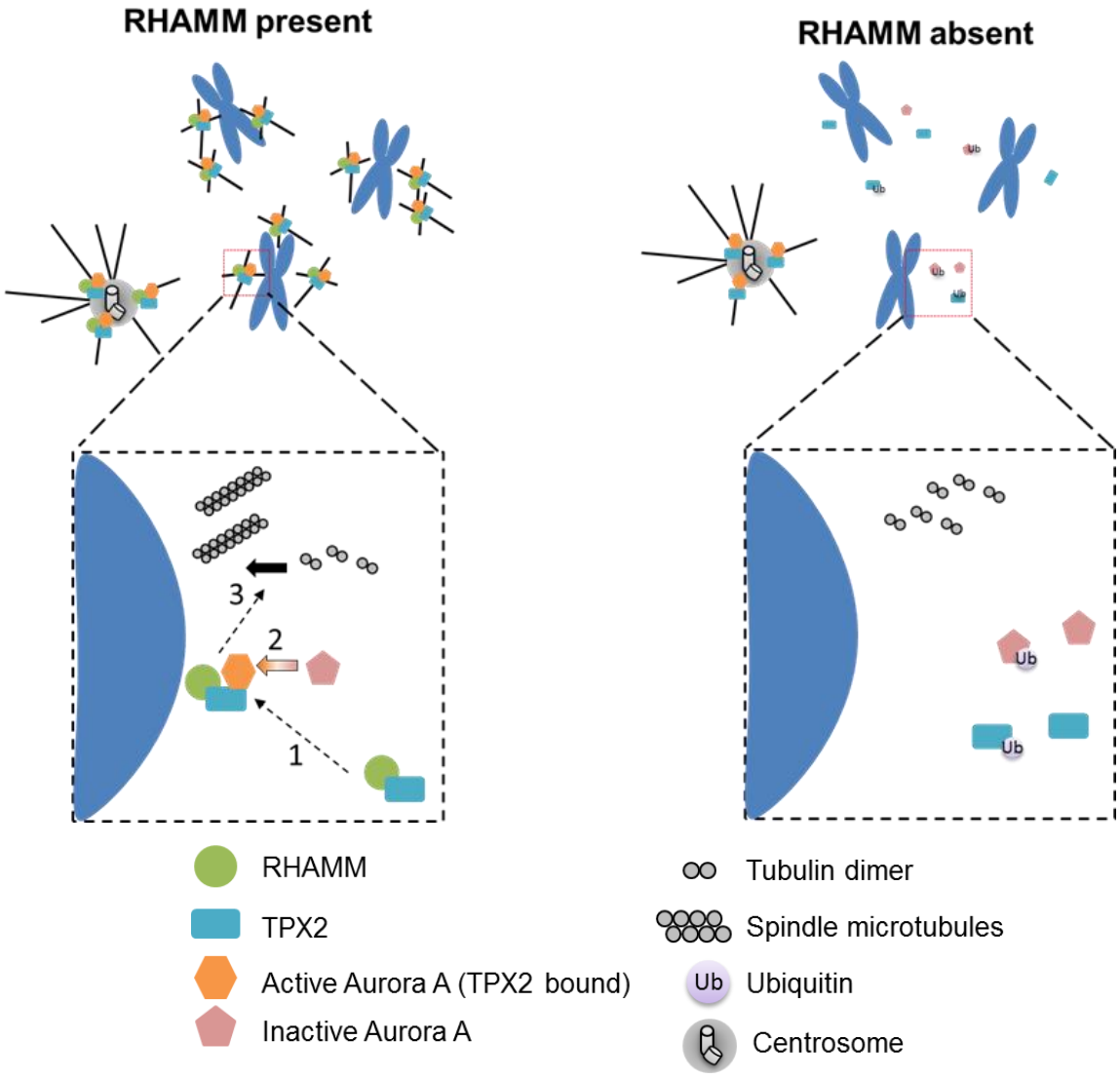

Figure 6.1 Spatial regulation of Aurora A activity during mitotic spindle assembly requires RHAMM to correctly localize TPX2

During prometaphase, in control-treated cells, RHAMM is located to sites of microtubule assembly at centrosomes and non-centrosome sites near kinetochores. For K-fiber assembly, (1) RHAMM targets TPX2 to spindle assembly sites near kinetochores, (2) where TPX2 promotes localized activation of Aurora kinase A, after which (3) the active kinase promotes spindle microtubule polymerization from tubulin dimers. In RHAMM-silenced cells, TPX2 is no longer targeted to K-fiber assembly sites and local Aurora A activation and microtubule nucleation are severely attenuated. Moreover, an interaction between RHAMM and TPX2 protects TPX2 and Aurora from ubiquitin-mediated proteasome degradation. Note, Aurora-TPX2 complex mediated microtubule nucleation at centrosomes is still present in RHAMM-silenced cells.

In **Chapter 4**, I show that RHAMM regulates the TPX2-Eg5 complex to balance motor forces necessary for chromosome attachment and segregation during the metaphase to anaphase progression. Silencing RHAMM induces aberrant spindle structures and erroneous chromosome segregation, and delays mitosis kinetics. At the molecular level, the formation of an inhibitory complex between TPX2 and Eg5 was severely reduced at spindle poles in these cells (Fig. 6.2).

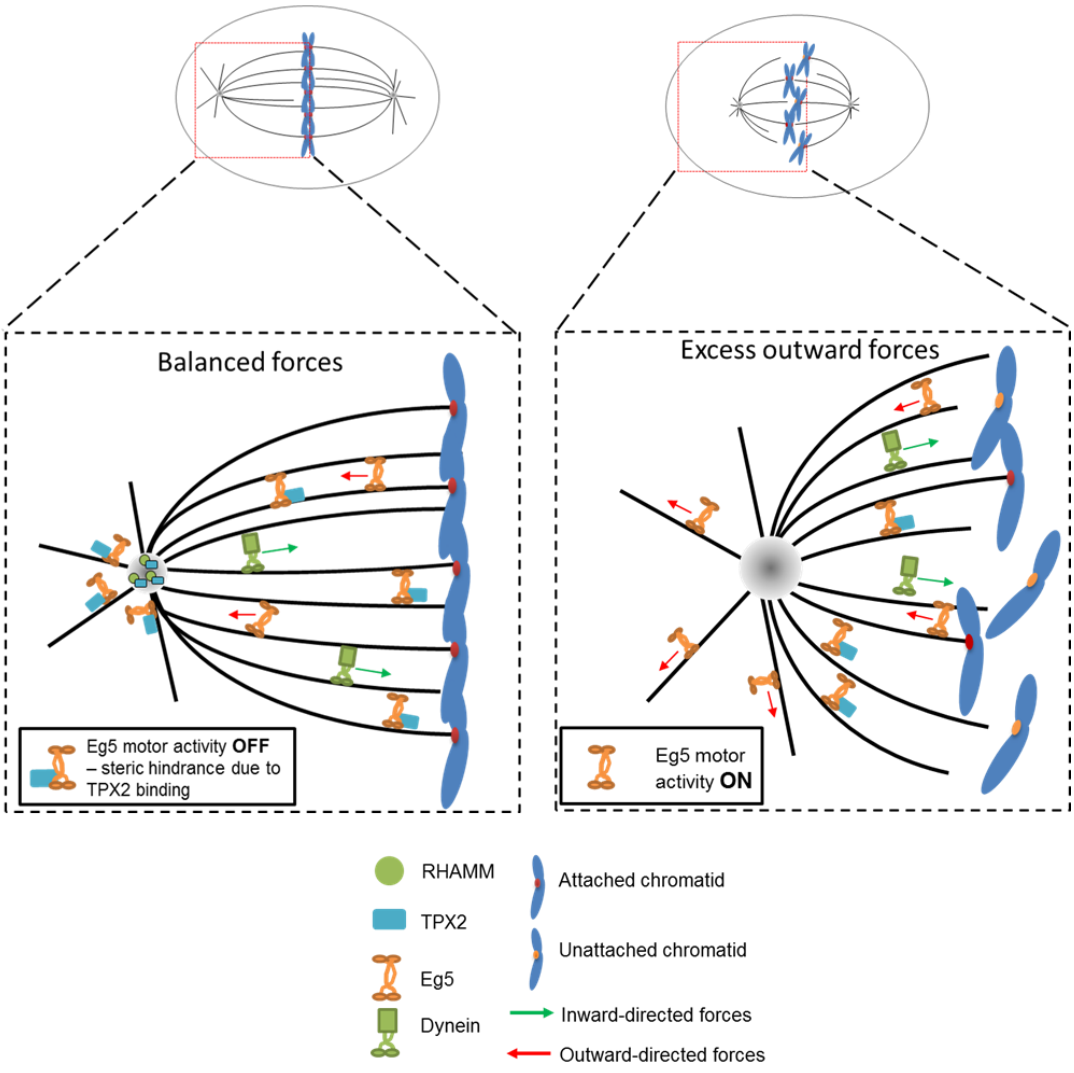

Figure 6.2 RHAMM balances motor forces needed to complete the spindle assembly checkpoint

During metaphase, in control-treated cells, RHAMM targets TPX2 to the spindle pole, where Eg5 activity is inhibited by an interaction with TPX2 to establish a force balance with the opposing motor dynein. Force balance along the mitotic spindle results in focused spindle poles, bipolar attachment of all chromosomes and completion of the spindle assembly checkpoint. In RHAMM-silenced cells, TPX2 is absent from the spindle poles, resulting in excess Eg5-mediated outward forces due to reduced formation of the inhibitory TPX2-Eg5 complex. Excess outward force along the mitotic spindle results in unfocused spindle poles, unattached chromosomes and delayed completion of the spindle assembly checkpoint. Note, the inhibitory TPX2-Eg5 complex is still formed along the half-spindle (between cell equator and spindle poles) in RHAMM-silenced cells.

Chapter 3 and Chapter 4 highlight that RHAMM regulates two distinct aspects of TPX2 function: 1) activating the mitotic kinase Aurora A during microtubule nucleation; and 2) regulating the kinesin motor Eg5 during metaphase spindle organization. In **Chapter 5**, I use various RHAMM overexpression model systems to address discrepancies observed in the literature, where both depletion of XRHAMM as well as accumulation of XRHAMM, through the loss of BRCA1, disrupted TPX2 localization and spindle architecture (Groen et al., 2004; Joukov et al., 2006). I show that augmenting RHAMM expression through genetic alterations or exogenous expression of GFP-RHAMM has detrimental effects on mitosis success in various animal and cell model systems, without associated evidence for mislocalization of TPX2 or the alteration of Aurora kinase (p-Aurora) activity.

6.2 RHAMM regulation of TPX2-Aurora A activity is cell-type and context dependent

Microtubule nucleation near kinetochores is essential for the construction of a functional bipolar spindle in cells with and without centrosomes. I found that microtubule nucleation at non-centrosome sites was significantly delayed but not eliminated in RHAMM-silenced cells. Thus, RHAMM is not essential for K-fiber assembly but enhances this process through Aurora A-TPX2 activation at these sites. Indeed, findings by Groen *et al* show that the addition of excess TPX2 (~4X the endogenous concentration) to XRHAMM depleted cells was able to rescue microtubule assembly defects (Groen et al., 2004). Groen *et al* concluded that RHAMM enhances the activity of TPX2 to promote Ran-GTP dependent microtubule nucleation, making spindle assembly more efficient in *Xenopus* systems (Groen et al., 2004). Immunoprecipitation experiments have revealed TPX2 interacts directly and indirectly with other motor and non-motor proteins that regulates mitotic spindle assembly (Wadsworth, 2015).

My findings, along with others (Groen et al., 2004; Scrofani et al., 2015), demonstrate that RHAMM plays a positive role in the correct location of TPX2 and the activation of Aurora A during spindle assembly, thus resolving previous findings in *Xenopus* systems (Groen et al., 2004; Joukov et al., 2006). However, I cannot discount the possibility that RHAMM may negatively regulate TPX2-Aurora A complex formation in other cell types during other cellular processes. For example, in interphase MCF10A cells, silencing RHAMM changes TPX2 location and leads to the accumulation of TPX2 at the nuclear envelope and in the cytoplasm (Maxwell et al., 2011). Consistent with this finding, I showed the minimal necessary binding domain for RHAMM (aa 40-319 in TPX2) overlaps with a primary nuclear localization signal and contains the motif recognized by importin-α for the nuclear import. Thus, RHAMM may regulate TPX2

shuttling between the nucleus and cytoplasm and, in doing so, alter TPX2-Aurora complex formation. In MPNST (malignant peripheral nerve sheath tumor) cells known to harbor genetic amplification of *HMMR*, silencing RHAMM by RNAi augmented Aurora A activity (Mohan et al., 2013). Thus, the elevated expression of RHAMM that resulted from genomic amplification was proposed to act as a molecular brake for Aurora A under these conditions (Mohan et al., 2013). Similarly, Aurora A activity is elevated in RHAMM$^{+/-}$ mouse embryonic stem cells relative to the wildtype counterparts (Jiang et al., 2013), which implies a negative regulatory role for RHAMM on kinase activity. These cells, with hemizygous mutation of *Hmmr*/RHAMM, undergo ectopic differentiation that can be reversed by small molecule inhibitors against Aurora A, as well as ERK1/2 (Jiang et al., 2013), suggesting, again, augmented kinase activity. Complicating these analyses is the fact that the abundance of RHAMM (and TPX2, and Aurora A) and kinase activity is strongly cell cycle regulated. Consequently, experimental manipulations that modulate cell cycle progression in a population of cells will indirectly affect protein abundance and kinase activities. It is for this reason that I quantified protein abundance and kinase activities in synchronized cell populations.

Lastly, the apparent discrepant responses to RHAMM overexpression between mammalian cells and *Xenopus* cells may be due to the fact that the non-centrosome spindle assembly pathway contributes to the overall spindle assembly process differently within the two systems. Specifically, Ran-GTP mediated K-fiber assembly is the predominant source of spindle microtubule nucleation in unfertilized *Xenopus* oocytes due to the lack of centrosomes. However, when sperm nuclei (containing centrosomes) are added to the egg extracts, the newly added centrosomes become the predominant site for microtubule nucleation (Heald et al., 1997; Sawin and Mitchison, 1991). This shows that there is a hierarchy of preference for different spindle

assembly pathways. Moreover, unlike cultured mammalian cells, chromosomes in *Xenopus* egg extracts are not enclosed in a nuclear membrane. Thus, TPX2 (normally nuclear) may be more accessible to XRHAMM and Aurora A, which are both located in the cytosol. This spatial separation may explain why my observations show microtubule nucleation at non-centrosome sites in cultured mammalian cells is only apparent during a microtubule regrowth assay, during which the nuclear envelope is absent. With these considerations in mind, a negative regulatory role for RHAMM on TPX2 location and Aurora A activity may be more apparent during spindle assembly in *Xenopus* extracts than it is during spindle assembly in human cells.

6.3 RHAMM regulates motor protein balance via TPX2

Mitosis is deemed successful when two genetically identical daughter cells are formed at the end of telophase. The spindle checkpoint is the safety mechanism that ensures faithful chromosome segregation during mitosis. The spindle checkpoint monitors structural cues on kinetochores, and elicits a cell-wide biochemical signaling cascade. A majority of the studies that examine the spindle checkpoint are focused on the various biochemical or structural pathways that occur at the kinetochores, such as Aurora B sensing attachment state (Ems-McClung et al., 2013; Fuller et al., 2008; Liu et al., 2012) or prevention of anaphase onset by the checkpoint complex (Fang, 2002; Ma and Poon, 2016; Sudakin et al., 2001). However, chromosome attachment is a cell-wide event during which the organization of spindle poles near the cell cortex dictates attachments at kinetochores at the cell equator. Less is known about how motor proteins that determine spindle dynamics contribute to the spindle checkpoint signal.

Forces along the spindle microtubules are carefully balanced: outward-directed forces mediated by Eg5 are antagonized by inward-directed forces exerted by dynein. My results indicate a net gain of outward force in RHAMM-silenced cells due to hyperactive Eg5 activity. Consistently, I was able to rescue RHAMM depletion phenotypes by chemical inhibition of Eg5 motor activity. Outward forces on the spindle are generated by two motors, Eg5 and Kif15. Kif15 is not essential for bipolar spindle assembly but its over-expression is able to rescue Eg5 inhibition (Tanenbaum et al., 2009; Vanneste et al., 2009). Structurally, RHAMM and Kif15 share a C-terminal bZip motif through which both proteins interact with TPX2. Thus, it is possible that RHAMM competes with Kif15 for binding to TPX2; however, I did not observe evidence supporting augmented Kif15-TPX2 interaction in the absence of RHAMM. Moreover,

the metaphase delay induced in RHAMM-silenced cells was not alleviated through co-depletion of Kif15. As Kif15 plays a minor role in the generation of outward force and is essential only in the absence of Eg5 (Tanenbaum et al., 2009; van Heesbeen et al., 2014), it is not surprising that Kif15 depletion was insufficient to restore force balance in RHAMM-silenced cells. While my results indicate a net gain of outward force in RHAMM-silenced cells, I cannot exclude the possibility that dynein-dependent inward forces are also reduced. Speaking against this hypothesis, however, I did not observe changes to the abundance of checkpoint complexes at the kinetochore, which would be expected to be augmented in an environment with reduced dynein-dependent stripping activity (Howell et al., 2001; Wojcik et al., 2001).

TPX2 was named for its action in targeting Kif15 to spindle poles (Wittmann et al., 1998). In RHAMM-silenced cells, the abundance of TPX2 was reduced, TPX2 localization was altered and yet the localization of Kif15 at unfocussed spindle poles was retained. The exact mechanism that targets and retains Kif15, a plus end directed motor, at centrosomes (microtubule minus ends) remains elusive but it is known to depend on poleward transport by dynein (Wittmann et al., 1998). In RHAMM-silenced cells, the reduced levels of TPX2 are sufficient for Kif15 localization to spindle poles but, as these were immunofluorescence studies of fixed cells, we do not know whether the kinetics of transport to, or retention at, spindle poles was altered. From my findings, I speculate: 1) TPX2 may promote dynein-dependent transport of Kif15 to spindle poles initially, but is not required for Kif15 retention subsequently; or, 2) TPX2 is involved in both the targeting and retention of Kif15 at spindle poles, and the reduced amount of spindle pole localized TPX2 present in RHAMM-silenced cells is sufficient for the retention of the kinesin at the poles. Further investigations are needed to answer these questions.

6.4 RHAMM balances forces needed for chromosome attachment at kinetochores

The spindle checkpoint signal is turned off when all chromosomes reach bipolar attachment orientation at their kinetochores. Here, I find in RHAMM-silenced cells a reduction in both stable Kt-MT attachments and TPX2-Eg5 complexes, which are known to promote functional K-fibers by organizing the microtubules nucleated near kinetochores (Ma et al., 2011). Attachment of K-fiber microtubules relies on the KMN (KNL1-Mis12-NDC80) network, as previously mentioned (section 1.3.1) (Cheeseman and Desai, 2008; Joglekar et al., 2010). Specifically, the NDC80 complex directly interacts with K-fibers (Alushin et al., 2010; Ciferri et al., 2008; Tooley et al., 2011). The elongated dumbbell-like shape of the NDC80 complex allows the protein complex sufficient flexibility to "search" for nearby microtubules (Alushin et al., 2010; Ciferri et al., 2008; Wang et al., 2008). Intuitively, in order for kinetochores to be successfully coupled to microtubule spindles during the "search" process, there must be a sufficient number of spindle fibers nearby to allow initial contact between NDC80 and microtubules. Thus, in RHAMM-silenced cells, if the number of stable K-fibers is reduced due to lower TPX2-Eg5 complexes, the probability of NDC80 complex coupling a nearby K-fiber will be reduced and the checkpoint will be delayed. Alternatively, RHAMM may be directly involved in stabilizing Kt-MT attachments via the NDC80 complex, which is suggested by a potential interaction between RHAMM and NDC80 identified in an IP/MS screen (Neumann et al., 2010). Though this interaction has not been confirmed, it does suggest an additional role for RHAMM at kinetochores during later stages of chromosome alignment.

6.5 RHAMM and hereditary cancers

My findings indicate an essential role for RHAMM, and the requirement for its tight regulation, during cell division. Given these findings, it is not surprising that alterations in RHAMM expression have been associated with rare, hereditary diseases and tumor predisposition syndromes.

6.5.1 Neurofibromatosis associated malignant peripheral nerve sheath tumors

Neurofibromatosis type I is an autosomal dominant cancer predisposition syndrome that causes the formation of benign dermal and plexiform tumors known as malignant peripheral nerve sheath tumors (MPNST) (Jett and Friedman, 2010). MPNSTs are aggressive malignancies that lack effective treatment with high rates of recurrence (Friedman, 1999; Jett and Friedman, 2010). Recently, two independent studies have demonstrated Aurora kinase inhibition is a promising target for MPNST therapy (Mohan et al., 2013; Patel et al., 2012). Specifically, Mohan *et al* demonstrated that the sensitivity of MPNST cell lines with genomic amplification of *Aurora A* depends upon kinase activity, which correlated with the expression of TPX2 and RHAMM (Mohan et al., 2013). In this study, a cell line with genomic amplification of *HMMR*/RHAMM was less sensitive to kinase inhibition, suggesting RHAMM acts as a molecular brake on kinase activity (Mohan et al., 2013). Silencing RHAMM, but not TPX2, sensitized these MPNST cells to an Aurora A inhibitor (Mohan et al., 2013).

6.5.2 Hereditary breast cancer associated with *BRCA1* mutations

HMMR/RHAMM is a breast cancer susceptibility gene, and different haplotypes that either elevate or reduce germline expression associate with an increased risk to develop breast cancer in Ashkenazi Jewish populations and in carriers of germline *BRCA1* mutations (Maxwell et al., 2011; Pujana et al., 2007). RHAMM is a substrate for BRCA1-BARD1–mediated polyubiquitination, and its proteolysis through this pathway controls centrosome numbers in breast tumor– and mammary epithelium–derived cell lines (Pujana et al., 2007). The regulation of centrosome number is vital to the maintenance of genome stability during mitosis, and increased centrosome numbers are intimately associated with tumorigenesis (Nigg, 2002). Maxwell *et al* demonstrated that the RHAMM-BRCA1 axis regulates apicobasal polarization of mammary epithelial cells (Maxwell et al., 2011). Specifically, apicobasal polarity requires reorganization of microtubules and centrosomes, and this is facilitated by the BRCA1-BARD1 complex and antagonized by the Aurora A-TPX2 complex (Maxwell et al., 2011). Dysregulation of this pathway may explain the expansion of primitive mammary cell subtypes in *BRCA1* mutation carriers (Lim et al., 2009; Proia et al., 2011). Lastly, I have shown RHAMM is needed to promote genome stability through the regulation of the spindle checkpoint. Thus, the control of the spindle checkpoint, along with the regulation of centrosome number and apical basal polarity, may be pathways through which RHAMM and BRCA1 interact to prevent mammary tumorigenesis.

6.5.3 Mosaic Variegated Aneuploidy (MVA)

MVA is an autosomal recessive disorder characterized by constitutional mosaic aneuploidies as a result of premature chromatid separation (Bohers et al., 2008; Hanks et al., 2004; Hanks and Rahman, 2005; Kajii et al., 2001; Kawame et al., 1999; Limwongse et al., 1999; Suijkerbuijk et al., 2010). MVA patients display a variety of trisomies and monosomies of different chromosomes with a proportion of aneuploid cells usually more than 25% (Hanks et al., 2004). 37% of MVA patients develop cancers, such as rhabdomyosarcoma, Wilms' tumor, and leukemia, within the first 3 years of life (Hanks and Rahman, 2005). In addition, individuals with MVA display a variety of developmental defects such as microcephaly, growth and mental retardation (Bohers et al., 2008; Hanks et al., 2004; Hanks and Rahman, 2005; Kajii et al., 2001; Kawame et al., 1999; Limwongse et al., 1999; Suijkerbuijk et al., 2010). Damaging mutations in an essential spindle checkpoint gene, *BubR1,* were identified to be causal for MVA (Bohers et al., 2008; Hanks et al., 2004; Hanks and Rahman, 2005; Kajii et al., 2001; Kawame et al., 1999; Limwongse et al., 1999; Suijkerbuijk et al., 2010). These mutations reduce the spindle checkpoint response and allow premature chromatid separation during mitosis (Bohers et al., 2008; Hanks et al., 2004; Hanks and Rahman, 2005; Kajii et al., 2001; Kawame et al., 1999; Limwongse et al., 1999; Suijkerbuijk et al., 2010). Recently, mutations in another mitotic protein, Cep57 (centrosome protein of 57kDa) have been suggested to cause MVA (Pinson et al., 2014; Snape et al., 2011). Cep57 is a structural protein of the mitotic spindle and promotes microtubule attachment to the centrosome (Pinson et al., 2014; Snape et al., 2011).

In Texas, a phenotypically normal female carrier of a t(5;12)(q33.3;q24.31) translocation carrying a female fetus with the same translocation was identified; routine analysis of 50

metaphases revealed 6 metaphases with distinct trisomies (extra copy of chromosome 2, 4, 7, 8, 22 and X, respectively) (personal communication to Dr. Maxwell). Samples were not available and so I obtained fibroblast cell lines with a similar chromosomal translocation. My analysis of one of these lines, which expressed elevated levels of RHAMM, revealed aberrant mitotic spindle figures and kinetics (section 5.2.5-5.2.6). Moreover, I observed that a subset of RHAMM-silenced cells underwent cohesion fatigue following a sustained checkpoint response (section 4.2.14). Cohesion fatigue may cause chromosome imbalances due to premature segregation of one or a few chromatids. Together, the findings of my thesis suggest that alterations in the expression of RHAMM may destabilize cell division and, through a prolonged spindle checkpoint, induce genome instability. In my studies of primary fibroblasts, it did not appear that elevated expression of RHAMM was sufficient to cause mosaic aneuploidies. But it is possible that, consistent with its modification of breast cancer risk, variation and/or mutation in *HMMR/*RHAMM may modify the incidence or severity of MVA associated with mutations in *BubR1* or *Cep57*. Currently, there are no published findings linking RHAMM to MVA but a detailed investigation is warranted.

6.6 Significance of study

Genome instability refers to increased alterations in the genome during the life cycle of a cell, which ranges from mutations in a specific gene to large-scale structural and numerical alterations of chromosomes. It is a major driving force for malignancy. The mitotic spindle is a cellular superstructure that controls division of the duplicated genome, and the spindle checkpoint is a critical tumor-suppressor mechanism. The results from my studies indicate that RHAMM contributes to both structural and biochemical signaling pathways that ensure bipolar spindle assembly and spindle checkpoint completion.

Aurora A kinase is the major regulator of mitotic spindle assembly (Barr and Gergely, 2007), and is frequently amplified in various cancers (Fraizer et al., 2004; Gritsko et al., 2003; Kamada et al., 2004; Sakakura et al., 2001; Sen et al., 2002; Tanaka et al., 1999), thus making it an attractive target in chemotherapy (Keen and Taylor, 2004; Kollareddy et al., 2012). Here, I provide new understanding of the regulation and activity of Aurora A by showing that RHAMM acts as a positive regulator for kinase activity through the targeting of its co-activator, TPX2. While building a functional bipolar spindle is critical for maintaining genome stability, the spindle checkpoint provides an additional safeguard that protects genome integrity by detecting and responding to errors in chromosome attachment. Here, I identify RHAMM as a new regulator for motor protein force and I show that RHAMM-mediated spindle organization is vital for correct chromosome attachment and segregation, and the disruption of this process, as induced by silencing RHAMM, delays mitotic exit and results in progeny cells with unstable genomes.

6.7 Caveats in study

6.7.1 Limitations in cell line models

The majority of the studies outlined in this thesis were carried out using HeLa cells as the model cell line. HeLa cells have predictable doubling times and are advantageous for studying mitotic processes due to their robust nature in tolerating various experimental manipulations. However, HeLa cells display extensive genomic and transcriptomic rearrangements, including hypertriploid chromosomes (Landry et al., 2013; Macville et al., 1999). Moreover, HeLa cells are p53 null (Berglind et al., 2016), which can affect Aurora kinase A activity and mitotic outcomes. Previous reports demonstrate p53 interacts with Aurora A and suppresses its oncogenic activity (Chen et al., 2002), while apoptosis is significantly suppressed with p53 deletion (Zhang et al., 2004). To overcome these limitations, I performed some of the experiments in parallel using other cell lines or primary human or mouse fibroblast cells.

The aim for my studies in Chapter 3 was to understand how K-fiber nucleation occurs using a mammalian somatic system, which relies on mitotic spindle assembly at both non-centrosome and centrosome sites. In HeLa cells, the assembly of mitotic microtubules near chromosomes is often difficult to visualize. To overcome this, I utilized a microtubule regrowth assay to monitor the spindle assembly process at multiple sites through time. With this assay, which can be performed in mammalian cells, the nuclear envelope has broken down, which allows the study of microtubule nucleation near the chromosomes.

Previous investigations of the role for *Xenopus* RHAMM in these processes were performed using *Xenopus* oocyte extracts (Groen et al., 2004; Joukov et al., 2006; Scrofani et al.,

2015), the immature egg cells of *Xenopus laevis*. This system also has its limitations: for example, these extracts lack centrosomes, thus isolating non-centrosome spindle assembly near chromosomes; these extracts contain excess protein, and are not representative of appropriate protein abundance as regulated in mammalian cells; and, 3) oocyte extracts contain a mixture of cytosolic and nuclear proteins, which are normally compartmentalized until prometaphase in mammalian cells. This lack of separation of protein fractions can potentially skew important regulation pathways involving protein translocation. In the specific case of my finding that RHAMM promotes microtubule assembly at non-centrosome sites through TPX2 localization and Aurora A activation presented in Chapter 3 (Chen et al., 2014), the robustness of this result is supported by subsequent findings from studies in *Xenopus* oocyte extracts that show XRHAMM-γTURC complexes anchor TPX2 and promote Ran-GTP dependent microtubule assembly (Scrofani *et al.,* 2015).

6.7.2 Limitations in experiments

Throughout this study, RHAMM protein expression is silenced by a pool of three siRNA constructs. This method is advantageous as these siRNA constructs target the untranslated regions of RHAMM mRNA, which enabled depletion of the endogenous protein and allowed for subsequent rescue experiments through transient expression of the wildtype transgene or truncation mutants. The exogenous RHAMM constructs are tagged with GFP at the N – terminus to allow for easy visual inspection and subsequent immunoprecipitation. Despite high transfection efficiency of the siRNA constructs, I was only able to reduce RHAMM protein by 80% as measured by quantitative Western blot analysis (section 3.2.3), suggesting incomplete

knockdown of the endogenous protein. Therefore, I cannot dismiss the possibility that the amount of residual protein may be sufficient to perform certain functions of RHAMM. A complete loss of endogenous RHAMM protein expression in HeLa cells can be achieved by utilizing the CRISPR-Cas9 (Clustered regularly interspaced short palindromic repeats-CRISPR associated protein 9). However, due to the fact that RHAMM is required for mitosis progression and cell cycle regulation, selected RHAMM knockout cell lines are often not viable (unpublished data). To overcome this limitation, I performed some of the experiments in parallel using *HMMR*$^{-/-}$ mouse embryonic fibroblast cells collected from a previously unpublished *HMMR*$^{-/-}$ C57BL/6N mouse model (Maxwell lab). *HMMR* gene expression and RHAMM mRNA and protein expressions in these cells and mice have been extensively characterized (3.2.12).

In Chapter 3, I utilized a characterized FRET-based probe for PLK1 activity to indirectly measure Aurora A activity (section 3.2.9). PLK1 is a substrate for Aurora A and depletion of Aurora A by siRNA is sufficient to attenuate PLK1 activity (Bruinsma et al., 2013; De Luca et al., 2006; Macurek et al., 2008). As there was no Aurora A specific FRET probe available at the time of my study, I choose to use the PLK1 FRET probe as an indirect measure for Aurora A activity. As the PLK1 FRET probe is fused with the kinetochore protein Hec1, this probe allowed the measurement of PLK1 activity specifically at non-centrosome assembly sites. Recently, an Aurora A specific FRET probe has been published (Bertolin et al., 2016), and it would be beneficial to further validate my findings using this novel construct. However, it is important to note that this Aurora A-FRET probe (Bertolin et al., 2016) is a cell-wide reporter, and, unlike the PLK1 FRET probe used in my study, is thus not able to distinguish Aurora A activity at specific assembly sites.

In Chapter 4, I utilized small molecule Eg5 inhibitor, STLC to rescue the metaphase delay imposed by RHAMM silencing, suggesting a net gain of outward force in RHAMM-silenced cells due to hyperactive Eg5 activity. Single particle tracking experiments (Gable et al., 2012) could be used to directly measure the velocity of Eg5 motor stepping and confirm a net gain of outward motor force in RHAMM-silenced cells.

6.8 Suggested future studies

My findings provide new insights into the processes of mitotic spindle assembly and the spindle checkpoint as well as the functions of RHAMM. While these studies answer several questions presented in the literature prior to this investigation (outlined in section 1.1.4), new questions were generated and warrant follow-up studies.

6.8.1 How does TPX2 regulate Kif15 localization at spindle poles?

TPX2 was named for its action in targeting Xklp2/Kif15 to spindle poles (Wittmann et al., 1998). It is curious then that TPX2 localization to spindle poles was lost in RHAMM-silenced cells and yet the localization of Kif15 at spindle poles was retained. The exact mechanism that targets and retains Kif15, a plus end directed motor, at centrosomes (microtubule minus ends) remains elusive but it is known to depend on poleward transport by dynein (Wittmann et al., 1998). Moreover, a C-terminus leucine zipper in Kif15 is required for its centrosome localization (Wittmann et al., 1998); this motif is homologous to the bZip motif in RHAMM, which I have shown to interact with TPX2. I hypothesize that TPX2 provides the two

essential requirements for Kif15 localization at spindle poles: 1) TPX2 promotes dynein-dependent transport of Kif15 to spindle poles initially and 2) TPX2 helps to retain Kif15 at spindle poles. In RHAMM-silenced cells, I found that the reduced levels of TPX2 at the spindle pole are sufficient for Kif15 localization. As my studies were immunofluorescence analyses of fixed cells, I could not determine whether the kinetics of transport to, or retention at, spindle poles was altered. To examine the kinetics of Kif15 transportation, I propose to track the location of exogenous fluorescent-tagged Kif15 truncation mutants that lack the bZip motif (involved in TPX2 binding) after silencing of endogenous Kif15. Alternatively, I propose to utilize fluorescent-tagged, full-length Kif15 along with fluorescent-tagged full-length TPX2, or a C-terminus truncation mutant that lack the Kif15 binding motif, in cells depleted of both endogenous Kif15 and TPX2, and follow the locations of these two exogenous constructs by time-lapse imaging. To examine whether TPX2 may play a role in the subsequent retention of Kif15 at spindle poles, I suggest utilizing: 1) fluorescence recovery after photobleaching studies to study the recovery into a bleached spindle pole of tagged-Kif15 (in the presence or absence of TPX2); and, 2) an inducible proteasome adaptor system (Wilmington and Matouschek, 2016) to regulate targeted rapid degradation of TPX2 through the ubiquitin pathway. In brief, a TPX2-specific proteasome adaptor would be transfected into the cell, which can mediate complex formation between the proteasome and TPX2 upon induction by rapamycin (Wilmington and Matouschek, 2016). Using this system, dividing cells would be arrested at metaphase first, followed by the addition of rapamycin to promote rapid degradation of TPX2 to allow the examination of whether Kif15 is retained at the spindle poles after it has been transported there. This method is advantageous in that it ensures proper TPX2 levels are present during early

mitosis for its proper functions, including the initial transportation of Kif15 to spindle poles and activation of Aurora A to promote spindle assembly.

6.8.2 Does RHAMM promote Kt-MT attachments directly at kinetochores?

I have shown RHAMM to be necessary for the proper balance of motor protein forces during metaphase spindle organization, which influences Kt-MT attachments at kinetochores. It would be interesting to examine whether RHAMM may potentially alter the function of kinetochore proteins during the spindle checkpoint response. In line with this, a previous IP/MS screen identified a potential interaction between RHAMM and NDC80 (Neumann et al., 2010), suggesting RHAMM may be directly involved in regulating Kt-MT attachments via the NDC80 complex. The NDC80 complex serves to connect chromosomes directly to microtubules, a process that is aided through clustering of several adjacent NDC80 complexes upon microtubule binding (Cheeseman et al., 2006; Ciferri et al., 2008; Tooley et al., 2011).

I hypothesize that RHAMM promotes proper Kt-MT attachments at kinetochores via regulation of the NDC80 complex. Given RHAMM is capable of crosslinking adjacent microtubules, I propose it may influence NDC80 clustering. To test this, I propose to use cryo-electron microscopy to examine whether clusters of NDC80 molecules are formed on microtubule lattices in the absence of RHAMM. Cryo-electron microscopy allows subnanometer resolution of protein structures, which can distinguish between a single molecule of NDC80 from a pair, or a cluster, of NDC80 proteins. Alternatively, phosphorylation of two tail segments in NDC80 by Aurora kinase B has been shown to cluster NDC80 proteins (Alushin et al., 2012). Thus, RHAMM assists NDC80 phosphorylation by Aurora B. To test this, I propose to examine

Aurora B activity at kinetochores in the absence of RHAMM, which can be monitored through the presence of its phosphorylated substrates by fixed cell analyses, or using a validated FRET biosensor (Fuller et al., 2008) by live cell analyses. Moreover, a variety of Aurora B specific small molecule inhibitors can be used to serve as controls to chemically inhibit kinase activity, such as ZM447439 and Hesperadin.

6.8.3 Does RHAMM modify the cancer predisposition syndrome mosaic variegated aneuploidy (MVA)?

Loss of function mutations in *BubR1* are causal for MVA (Bohers et al., 2008; Hanks et al., 2004; Hanks and Rahman, 2005; Kajii et al., 2001; Kawame et al., 1999; Limwongse et al., 1999; Suijkerbuijk et al., 2010). These mutations reduce BubR1 protein levels and induce a less robust spindle checkpoint response that results in premature chromatid separation during mitosis (Bohers et al., 2008; Hanks et al., 2004; Hanks and Rahman, 2005; Kajii et al., 2001; Kawame et al., 1999; Limwongse et al., 1999; Suijkerbuijk et al., 2010), similar to cohesion fatigue that follows metaphase arrest in RHAMM-silenced cells. Therefore, I hypothesize that alterations in the expression of RHAMM may destabilize cell division through alterations to the spindle checkpoint, which may associate with or modify the occurrence of MVA. In line with this postulate, a patient with a mosaic variegated aneuploidy-like phenotype (refer to section 5.2.5 and 6.6.3) presented with a germline translocation between chromosomes 5q33 and 12q24 (t(5;12)(q33.3;q24.31), which is proximal to the *HMMR*/RHAMM locus, 5q33.2-qter (Spicer et al., 1995). I examined two untransformed fibroblast cell lines, each with a t(5;12)(q33.3;q24.31),

to examine a potential link between RHAMM and MVA (section 5.2.5, 5.2.6 and 6.6.3). My preliminary findings show that increased *HMMR* copy number increases the frequency of aberrant mitotic spindles and delays the completion of mitosis (section 5.2.6). For a more detailed study of these cell lines, I propose to utilize time-lapse microscopy to monitor whether cohesion fatigue and chromosome segregation errors are present in these cells. It is possible that these events occur at a low baseline line frequency- lower that would be observed with *BubR1* mutations but sufficient to modify predisposition to the disease. In addition to a predisposition to cancers, MVA patients demonstrate a variety of developmental defects such as microcephaly, growth and mental retardation (Bohers et al., 2008; Hanks et al., 2004; Hanks and Rahman, 2005; Kajii et al., 2001; Kawame et al., 1999; Limwongse et al., 1999; Suijkerbuijk et al., 2010). These phenotypes have been recapitulated in mice carrying mono-allelic *BubR1* MVA mutation (Wijshake et al., 2012). Currently, Dr. Maxwell has generated a $HMMR^{-/-}$ C57BL/6N mouse model (unpublished), which has displayed microcephaly and stunted growth. Thus, these mice can be screened for the proportion of aneuploid cells and monitored for MVA associated malignancies.

6.9 Final remarks

This study identified new roles for RHAMM in the regulation of the Aurora A-TPX2 holoenzyme during mitotic spindle assembly and in the establishment of balanced motor forces needed to promote chromosome segregation and mitotic exit. These findings highlight RHAMM as a critical regulator of structural and biochemical processes during cell division and imply that the deregulation of RHAMM may associate with genome instability and rare, hereditary disease.

Bibliography

Abrieu, A., Kahana, J.A., Wood, K.W., Cleveland, D.W., 2000. CENP-E as an essential component of the mitotic checkpoint in vitro. Cell 102, 817–26.

Acquaviva, C., Pines, J., 2006. The anaphase-promoting complex/cyclosome: APC/C. J. Cell Sci. 119, 2401–2404.

Akhmedov, A.T., Frei, C., Tsai-Pflugfelder, M., Kemper, B., Gasser, S.M., Jessberger, R., 1998. Structural maintenance of chromosomes protein C-terminal fomains bind preferentially to DNA with decondary dtructure. J. Biol. Chem. 273, 24088–24094.

Akiyama, Y., Jung, S., Salhia, B., Lee, S., Hubbard, S., Taylor, M., Mainprize, T., Akaishi, K., van Furth, W., Rutka, J.T., 2001. Hyaluronate receptors mediating glioma cell migration and proliferation. J. Neurooncol. 53, 115–27.

Alushin, G.M., Musinipally, V., Matson, D., Tooley, J., Stukenberg, P.T., Nogales, E., 2012. Multimodal microtubule binding by the Ndc80 kinetochore complex. Nat. Struct. Mol. Biol. 19, 1161–7.

Alushin, G.M., Ramey, V.H., Pasqualato, S., Ball, D.A., Grigorieff, N., Musacchio, A., Nogales, E., 2010. The Ndc80 kinetochore complex forms oligomeric arrays along microtubules. Nature 467, 805–10.

Amato, A., Schillaci, T., Lentini, L., Di Leonardo, A., Rajagopalan, H., Lengauer, C., Pellman, D., Weaver, B., Cleveland, D., Kops, G., Weaver, B., Cleveland, D., Gimenez-Abian, J., Diaz-Martinez, L., Wirth, K., Andrews, C., Gimenez-Martin, G., Clarke, D., Pihan, G., Wallace, J., Zhou, Y., Doxsey, S., Cleveland, D., Mao, Y., Sullivan, K., Yuan, B., Xu, Y., Woo, J., Wang, Y., Bae, Y., Yoon, D., Wersto, R., Tully, E., Wilsbach, K., Gabrielson, E., Hanks, S., Coleman, K., Reid, S., Plaja, A., Firth, H., Fitzpatrick, D., Kidd, A., Mehes, K., Nash, R., Robin, N., Matsuura, S., Matsumoto, Y., Morishima, K., Izumi, H., Matsumoto, H., Ito, E., Tsutsui, K., Kobayashi, J., Tauchi, H., Kajiwara, Y., Cahill, D., Lengauer, C., Yu, J., Riggins, G., Willson, J., Markowitz, S., Kinzler, K., Vogelstein, B., Cimini, D., Pihan, G., Purohit, A., Wallace, J., Knecht, H., Woda, B., Quesenberry, P., Doxsey, S., Fukasawa, K., Zhou, H., Kuang, J., Zhong, L., Kuo, W., Gray, J., Sahin, A., Brinkley, B., Sen, S., Mundt, K., Golsteyn, R., Lane, H., Nigg, E., Kawamura, K., Izumi, H., Ma, Z., Ikeda, R., Moriyama, M., Tanaka, T., Nojima, T., Levin, L., Fujikawa-Yamamoto, K., Suzuki, K., Fukasawa, K., Bischoff, J., Anderson, L., Zhu, Y., Mossie, K., Ng, L., Souza, B., Schryver, B., Flanagan, P., Clairvoyant, F., Ginther, C., Chan, C., Novotny, M., Slamon, D., Plowman, G., Gray, P., Bearss, D., Han, H., Nagle, R., Tsao, M., Dean, N., Hoff, D. Von, Iovino, F., Lentini, L., Amato, A., Leonardo, A. Di, Lentini, L., Iovino, F., Amato, A., Leonardo, A. Di, Tarapore, P., Horn, H., Tokuyama, Y., Fukasawa, K., Oikawa, T., Okuda, M., Ma, Z., Goorha, R., Tsujimoto, H., Inokuma, H., Fukasawa, K., Olsson, A., Feber, A., Edwards, S., Poele, R. Te, Giddings, I., Merson, S., Cooper, C., Amato, A., Lentini, L., Schillaci, T., Iovino, F., Leonardo, A. Di, Hernando, E., Nahle, Z., Juan, G., Diaz-Rodriguez, E., Alaminos, M., Hemann, M., Michel, L., Mittal, V., Gerald, W., Benezra, R.,

Lowe, S., Cordon-Cardo, C., Wang, R., Yu, H., Deng, C., Tomonaga, T., Matsushita, K., Yamaguchi, S., Oohashi, T., Shimada, H., Ochiai, T., Yoda, K., Nomura, F., Weaver, B., Silk, A., Montagna, C., Verdier-Pinard, P., Cleveland, D., Salmon, E., Cimini, D., Cameron, L., DeLuca, J., Wang, I., Chen, Y., Hughes, D., Petrovic, V., Major, M., Park, H., Tan, Y., Ackerson, T., Costa, R., Hooser, A. Van, Ouspenski, I., Gregson, H., Starr, D., Yen, T., Goldberg, M., Yokomori, K., Earnshaw, W., Sullivan, K., Brinkley, B., Bunz, F., Dutriaux, A., Lengauer, C., Waldman, T., Zhou, S., Brown, J., Sedivy, J., Kinzler, K., Vogelstein, B., Kanda, T., Sullivan, K., Wahl, G., 2009. CENPA overexpression promotes genome instability in pRb-depleted human cells. Mol. Cancer 8, 119.

Anand, S., Penrhyn-Lowe, S., Venkitaraman, A.R., 2003. AURORA-A amplification overrides the mitotic spindle assembly checkpoint, inducing resistance to Taxol. Cancer Cell 3, 51–62.

Andrews, P.D., Ovechkina, Y., Morrice, N., Wagenbach, M., Duncan, K., Wordeman, L., Swedlow, J.R., 2004. Aurora B Regulates MCAK at the Mitotic Centromere. Dev. Cell 6, 253–268.

Assmann, V., Gillett, C.E., Poulsom, R., Ryder, K., Hart, I.R., Hanby, A.M., 2001. The pattern of expression of the microtubule-binding protein RHAMM/IHABP in mammary carcinoma suggests a role in the invasive behaviour of tumour cells. J. Pathol. 195, 191–6.

Assmann, V., Jenkinson, D., Marshall, J.F., Hart, I.R., 1999. The intracellular hyaluronan receptor RHAMM/IHABP interacts with microtubules and actin filaments. J. Cell Sci. 112 (Pt 2, 3943–54.

Assmann, V., Marshall, J.F., Fieber, C., Hofmann, M., Hart, I.R., 1998. The human hyaluronan receptor RHAMM is expressed as an intracellular protein in breast cancer cells. J. Cell Sci. 111 (Pt 1, 1685–94.

Asteriti, I.A., Rensen, W.M., Lindon, C., Lavia, P., Guarguaglini, G., 2010. The Aurora-A/TPX2 complex: a novel oncogenic holoenzyme? Biochim. Biophys. Acta 1806, 230–9.

Ayscough, K.R., 1998. In vivo functions of actin-binding proteins. Curr. Opin. Cell Biol. 10, 102–11.

Balchand, S.K., Mann, B.J., Titus, J., Ross, J.L., Wadsworth, P., 2015. TPX2 inhibits Eg5 by interactions with both motor and microtubule. J. Biol. Chem. 290, 17367–79.

Barr, A.R., Gergely, F., 2007. Aurora-A: the maker and breaker of spindle poles. J. Cell Sci. 120, 2987–96.

Barros, T.P., Kinoshita, K., Hyman, A.A., Raff, J.W., 2005. Aurora A activates D-TACC-Msps complexes exclusively at centrosomes to stabilize centrosomal microtubules. J. Cell Biol. 170, 1039–46.

Bayliss, R., Sardon, T., Vernos, I., Conti, E., 2003. Structural basis of Aurora-A activation by TPX2 at the mitotic spindle. Mol. Cell 12, 851–62.

Berdnik, D., Knoblich, J. a, 2002. Drosophila Aurora-A is required for centrosome maturation and actin-dependent asymmetric protein localization during mitosis. Curr. Biol. 12, 640–7.

Berglind, H., Pawitan, Y., Kato, S., Ishioka, C., Soussi, T., 2016. Analysis of p53 mutation status

in human cancer cell lines: a paradigm for cell line cross. Cancer Biol. Ther. 7, 699–708.

Beroukhim, R., Mermel, C.H., Porter, D., Wei, G., Raychaudhuri, S., Donovan, J., Barretina, J., Boehm, J.S., Dobson, J., Urashima, M., Mc Henry, K.T., Pinchback, R.M., Ligon, A.H., Cho, Y.-J., Haery, L., Greulich, H., Reich, M., Winckler, W., Lawrence, M.S., Weir, B.A., Tanaka, K.E., Chiang, D.Y., Bass, A.J., Loo, A., Hoffman, C., Prensner, J., Liefeld, T., Gao, Q., Yecies, D., Signoretti, S., Maher, E., Kaye, F.J., Sasaki, H., Tepper, J.E., Fletcher, J.A., Tabernero, J., Baselga, J., Tsao, M.-S., Demichelis, F., Rubin, M.A., Janne, P.A., Daly, M.J., Nucera, C., Levine, R.L., Ebert, B.L., Gabriel, S., Rustgi, A.K., Antonescu, C.R., Ladanyi, M., Letai, A., Garraway, L.A., Loda, M., Beer, D.G., True, L.D., Okamoto, A., Pomeroy, S.L., Singer, S., Golub, T.R., Lander, E.S., Getz, G., Sellers, W.R., Meyerson, M., 2010. The landscape of somatic copy-number alteration across human cancers. Nature 463, 899–905.

Bertolin, G., Sizaire, F., Herbomel, G., Reboutier, D., Prigent, C., Tramier, M., 2016. A FRET biosensor reveals spatiotemporal activation and functions of aurora kinase A in living cells. Nat. Commun. 7, 12674.

Bianconi, E., Piovesan, A., Facchin, F., Beraudi, A., Casadei, R., Frabetti, F., Vitale, L., Pelleri, M.C., Tassani, S., Piva, F., Perez-Amodio, S., Strippoli, P., Canaider, S., 2014. An estimation of the number of cells in the human body. Ann. Hum. Biol. 40, 463–71.

Bird, A.W., Hyman, A. a, 2008. Building a spindle of the correct length in human cells requires the interaction between TPX2 and Aurora A. J. Cell Biol. 182, 289–300.

Bischoff, J.R., Anderson, L., Zhu, Y., Mossie, K., Ng, L., Souza, B., Schryver, B., Flanagan, P., Clairvoyant, F., Ginther, C., Chan, C.S., Novotny, M., Slamon, D.J., Plowman, G.D., 1998. A homologue of Drosophila aurora kinase is oncogenic and amplified in human colorectal cancers. EMBO J. 17, 3052–65.

Blangy, A., Lane, H.A., D'Hérin, P., Harper, M., Kress, M., Niggt, E.A., 1995. Phosphorylation by p34cdc2 regulates spindle association of human Eg5, a kinesin-related motor essential for bipolar spindle formation in vivo. Cell 83, 1159–1169.

Bohers, E., Sarafan-Vasseur, N., Drouet, A., Paresy, M., Latouche, J.-B., Flaman, J.-M., Sesboüé, R., Frebourg, T., 2008. Gradual reduction of BUBR1 protein levels results in premature sister-chromatid separation then in aneuploidy. Hum. Genet. 124, 473–8.

Boleti, H., Karsenti, E., Vernos, I., 1996. Xklp2, a novel Xenopus centrosomal kinesin-like protein required for centrosome separation during mitosis. Cell 84, 49–59.

Booth, D.G., Hood, F.E., Prior, I.A., Royle, S.J., 2011. A TACC3/ch-TOG/clathrin complex stabilises kinetochore fibres by inter-microtubule bridging. EMBO J. 30, 906–19.

Bornens, M., 2012. The centrosome in cells and organisms. Science 335, 422–6.

Bruinsma, W., Macurek, L., Freire, R., Lindqvist, A., Medema, R.H., 2013. Bora and Aurora-A continue to activate Plk1 in mitosis. J. Cell Sci. 801–811.

Brunet, S., Sardon, T., Zimmerman, T., Wittmann, T., Pepperkok, R., Karsenti, E., Vernos, I., 2004. Characterization of the TPX2 domains involved in microtubule nucleation and spindle assembly in Xenopus egg extracts. Mol Biol Cell 15, 5318–5328.

Cahu, J., Olichon, A., Hentrich, C., Schek, H., Drinjakovic, J., Zhang, C., Doherty-Kirby, A., Lajoie, G., Surrey, T., 2008. Phosphorylation by Cdk1 increases the binding of Eg5 to microtubules In Vitro and in Xenopus egg extract spindles. PLoS One 3, e3936.

Calarco-Gillam, P.D., Siebert, M.C., Hubble, R., Mitchison, T., Kirschner, M., 1983. Centrosome development in early mouse embryos as defined by an autoantibody against pericentriolar material. Cell 35, 621–9.

Carmena, M., Ruchaud, S., Earnshaw, W.C., 2009. Making the Auroras glow: regulation of Aurora A and B kinase function by interacting proteins. Curr. Opin. Cell Biol. 21, 796–805.

Castro, A., Bernis, C., Vigneron, S., Labbe, J.-C., Lorca, T., 2005. The anaphase-promoting complex: a key factor in the regulation of cell cycle. Oncogene 24, 314–325.

Castro, A., Vigneron, S., Bernis, C., Labbé, J.-C., Prigent, C., Lorca, T., 2002. The D-Box-activating domain (DAD) is a new proteolysis signal that stimulates the silent D-Box sequence of Aurora-A. EMBO Rep. 3, 1209–14.

Caudron, M., Bunt, G., Bastiaens, P., Karsenti, E., 2005. Spatial coordination of spindle assembly by chromosome-mediated signaling gradients. Science (80-.). 309, 1373–1376.

Cazales, M., Schmitt, E., Montembault, E., Dozier, C., Prigent, C., Ducommun, B., 2005. CDC25B phosphorylation by Aurora-A occurs at the G2/M transition and is inhibited by DNA damage. Cell Cycle 4, 1233–8.

Chan, C.S., Botstein, D., 1993. Isolation and characterization of chromosome-gain and increase-in-ploidy mutants in yeast. Genetics 135, 677–91.

Chan, G.K., Jablonski, S. a, Sudakin, V., Hittle, J.C., Yen, T.J., 1999. Human BUBR1 is a mitotic checkpoint kinase that monitors CENP-E functions at kinetochores and binds the cyclosome/APC. J. Cell Biol. 146, 941–54.

Chan, G.K., Liu, S.-T., Yen, T.J., 2005. Kinetochore structure and function. Trends Cell Biol. 15, 589–98.

Chang, D.C., Xu, N., Luo, K.Q., 2003. Degradation of cyclin B is required for the onset of anaphase in mammalian cells. J. Biol. Chem. 278, 37865–37873.

Chang, L., Zhang, Z., Yang, J., McLaughlin, S.H., Barford, D., 2014. Molecular architecture and mechanism of the anaphase-promoting complex. Nature 513, 388–393.

Chao, W.C.H., Kulkarni, K., Zhang, Z., Kong, E.H., Barford, D., 2012. Structure of the mitotic checkpoint complex. Nature 484, 208–213.

Cheeseman, I.M., Chappie, J.S., Wilson-Kubalek, E.M., Desai, A., 2006. The Conserved KMN network constitutes the core microtubule-binding site of the kinetochore. Cell 127, 983–997.

Cheeseman, I.M., Desai, A., 2008. Molecular architecture of the kinetochore-microtubule interface. Nat. Rev. Mol. Cell Biol. 9, 33–46.

Chen, H., Mohan, P., Jiang, J., Nemirovsky, O., He, D., Fleisch, M.C., Niederacher, D., Pilarski, L.M., Lim, C.J., Maxwell, C.A., 2014. Spatial regulation of Aurora A activity during mitotic spindle assembly requires RHAMM to correctly localize TPX2. Cell Cycle 13, 2248–61.

Chen, S.-S., Chang, P.-C., Cheng, Y.-W., Tang, F.-M., Lin, Y.-S., 2002. Suppression of the STK15 oncogenic activity requires a transactivation-independent p53 function. EMBO J. 21, 4491–9.

Ciferri, C., Pasqualato, S., Screpanti, E., Varetti, G., Santaguida, S., Dos Reis, G., Maiolica, A., Polka, J., De Luca, J.G., De Wulf, P., Salek, M., Rappsilber, J., Moores, C.A., Salmon, E.D., Musacchio, A., 2008. Implications for kinetochore-microtubule attachment from the structure of an engineered Ndc80 Complex. Cell 133, 427–439.

Ciosk, R., Zachariae, W., Michaelis, C., Shevchenko, A., Mann, M., Nasmyth, K., 1998. An ESP1/PDS1 complex regulates loss of sister chromatid cohesion at the metaphase to anaphase transition in Yeast. Cell 93, 1067–1076.

Clarke, P.R., Zhang, C., 2008. Spatial and temporal coordination of mitosis by Ran GTPase. Nat. Rev. Mol. Cell Biol. 9, 464–77.

Clijsters, L., van Zon, W., Riet, B. ter, Voets, E., Boekhout, M., Ogink, J., Rumpf-Kienzl, C., Wolthuis, R.M.F., 2014. Inefficient degradation of cyclin B1 re-activates the spindle checkpoint right after sister chromatid disjunction. Cell Cycle 13, 2370–2378.

Clute, P., Pines, J., 1999. Temporal and spatial control of cyclin B1 destruction in metaphase. Nat Cell Biol 1, 82–87.

Cole, D.G., Saxton, W.M., Sheehan, K.B., Scholey, J.M., 1994. A "slow" homotetrameric kinesin-related motor protein purified from Drosophila embryos. J. Biol. Chem. 269, 22913–6.

Compton, D.A., 1998. Focusing on spindle poles. J. Cell Sci. 111 (Pt 1, 1477–81.

Compton, D.A., 2000. Spindle assembly in animal cells. Annu. Rev. Biochem. 69, 95–114.

Cox, D.G., Hankinson, S.E., Hunter, D.J., 2006. Polymorphisms of the AURKA (STK15/Aurora Kinase) gene and breast cancer risk (United States). Cancer Causes Control 17, 81–3.

Crainie, M., Belch, A.R., Mant, M.J., Pilarski, L.M., 1999. Overexpression of the Receptor for Hyaluronan-Mediated Motility (RHAMM) characterizes the malignant clone in multiple myeloma: identification of three distinct RHAMM variants. Blood 93, 1684–1696.

Crane, R., Kloepfer, A., Ruderman, J. V, 2004. Requirements for the destruction of human Aurora-A. J. Cell Sci. 117, 5975–83.

Daum, J.R., Potapova, T. a, Sivakumar, S., Daniel, J.J., Flynn, N., Rankin, S., Gorbsky, G.J., 2012. Cohesion fatiue induces chromatid separation in cells delayed at metaphase 21, 1018–1024.

Daum, J.R., Wren, J.D., Daniel, J.J., Sivakumar, S., McAvoy, J.N., Potapova, T. a., Gorbsky, G.J., 2009. Ska3 Is required for spindle checkpoint silencing and the maintenance of chromosome cohesion in mitosis. Curr. Biol. 19, 1467–1472.

De Luca, M., Lavia, P., Guarguaglini, G., 2006. A functional interplay between Aurora-A, Plk1 and TPX2 at spindle poles. Cell cycle 5, 296–303.

Dej, K.J., Orr-Weaver, T.L., 2000. Separation anxiety at the centromere. Trends Cell Biol. 10, 392–399.

Desai, A., Mitchison, T.J., 1997. Microtubule polymerization dynamics. Annu. Rev. Cell Dev. Biol. 13, 83–117.

Desai, A., Verma, S., Mitchison, T.J., Walczak, C.E., 1999. Kin I kinesins are microtubule-destabilizing enzymes. Cell 96, 69–78.

Dicioccio, R.A., Song, H., Waterfall, C., Kimura, M.T., Nagase, H., McGuire, V., Hogdall, E., Shah, M.N., Luben, R.N., Easton, D.F., Jacobs, I.J., Ponder, B.A.J., Whittemore, A.S., Gayther, S.A., Pharoah, P.D.P., Kruger-Kjaer, S., 2004. STK15 polymorphisms and association with risk of invasive ovarian cancer. Cancer Epidemiol. Biomarkers Prev. 13, 1589–94.

Dodson, C.A., Bayliss, R., 2012. Activation of Aurora-A kinase by protein partner binding and phosphorylation are independent and synergistic. J. Biol. Chem. 287, 1150–7.

Dodson, C.A., Kosmopoulou, M., Richards, M.W., Atrash, B., Bavetsias, V., Blagg, J., Bayliss, R., 2010. Crystal structure of an Aurora-A mutant that mimics Aurora-B bound to MLN8054: insights into selectivity and drug design. Biochem. J. 427, 19–28.

Doxsey, S., 2001. Re-evaluating centrosome function. Nat. Rev. Mol. Cell Biol. 2, 688–98.

Drechsler, H., McHugh, T., Singleton, M.R., Carter, N.J., McAinsh, A.D., 2014. The Kinesin-12 Kif15 is a processive track-switching tetramer. Elife 2014, 1–17.

Du, Y.-C.N., Chou, C.-K., Klimstra, D.S., Varmus, H., 2011. Receptor for hyaluronan-mediated motility isoform B promotes liver metastasis in a mouse model of multistep tumorigenesis and a tail vein assay for metastasis. Proc. Natl. Acad. Sci. U. S. A. 108, 16753–8.

Duncan, T., Wakefield, J.G., 2011. 50 ways to build a spindle: the complexity of microtubule generation during mitosis. Chromosome Res. 19, 321–33.

Dunsch, A.K., Hammond, D., Lloyd, J., Schermelleh, L., Gruneberg, U., Barr, F.A., 2012. Dynein light chain 1 and a spindle-associated adaptor promote dynein asymmetry and spindle orientation. J. Cell Biol. 198, 1039–54.

Eckerdt, F., Eyers, P. a., Lewellyn, A.L., Prigent, C., Maller, J.L., 2008. Spindle pole regulation by a discrete Eg5-interacting domain in TPX2. Curr. Biol. 18, 519–525.

Egan, K.M., Newcomb, P.A., Ambrosone, C.B., Trentham-Dietz, A., Titus-Ernstoff, L., Hampton, J.M., Kimura, M.T., Nagase, H., 2004. STK15 polymorphism and breast cancer risk in a population-based study. Carcinogenesis 25, 2149–53.

Ems-McClung, S.C., Hainline, S.G., Devare, J., Zong, H., Cai, S., Carnes, S.K., Shaw, S.L., Walczak, C.E., 2013. Aurora B inhibits MCAK activity through a phosphoconformational switch that reduces microtubule association. Curr. Biol. 23, 2491–9.

Enos, A., Morris, N.R., 1990. Mutation of a gene that encodes a kinesin-like protein blocks nuclear division in A. nidulans. Cell 60, 1019–1027.

Entwistle, J., Zhang, S., Yang, B., Wong, C., Li, Q., Hall, C.L., A, J., Mowat, M., Greenberg, A.H., Turley, E.A., 1995. Characterization of the murine gene encoding the hyaluronan receptor RHAMM, Gene.

Ewart-Toland, A., Briassouli, P., de Koning, J.P., Mao, J.-H., Yuan, J., Chan, F., MacCarthy-Morrogh, L., Ponder, B.A.J., Nagase, H., Burn, J., Ball, S., Almeida, M., Linardopoulos, S.,

Balmain, A., 2003. Identification of Stk6/STK15 as a candidate low-penetrance tumor-susceptibility gene in mouse and human. Nat. Genet. 34, 403–12.

Eyers, P.A., Churchill, M.E.A., Maller, J.L., 2005. The Aurora A and Aurora B protein kinases: a single amino acid difference controls intrinsic activity and activation by TPX2. Cell cycle 4, 784–9.

Eyers, P.A., Erikson, E., Chen, L.G., Maller, J.L., 2003. A novel mechanism for activation of the protein kinase Aurora A. Curr. Biol. 13, 691–697.

Eyers, P. a, Maller, J.L., 2004. Regulation of Xenopus Aurora A activation by TPX2. J. Biol. Chem. 279, 9008–15.

Fang, G., 2002. Checkpoint protein BubR1 acts synergistically with Mad2 to inhibit anaphase-promoting complex. Mol. Biol. Cell 13, 755–66.

Fededa, J.P., Gerlich, D.W., 2012. Molecular control of animal cell cytokinesis. Nat. Cell Biol. 14, 440–447.

Ferenz, N.P., Paul, R., Fagerstrom, C., Mogilner, A., Wadsworth, P., 2009. Dynein antagonizes eg5 by crosslinking and sliding antiparallel microtubules. Curr. Biol. 19, 1833–8.

Fieber, C., Plug, R., Sleeman, J., Dall, P., Ponta, H., Hofmann, M., 1999. Characterisation of the murine gene encoding the intracellular hyaluronan receptor IHABP (RHAMM). Gene 226, 41–50.

Florian, S., Mayer, T.U., 2012. The functional antagonism between Eg5 and dynein in spindle bipolarization is not compatible with a simple push-pull model. Cell Rep. 1, 408–16.

Foley, E.A., Kapoor, T.M., 2013. Microtubule attachment and spindle assembly checkpoint signalling at the kinetochore. Nat. Rev. Mol. Cell Biol. 14, 25–37.

Fraizer, G.C., Diaz, M.F., Lee, I.-L., Grossman, H.B., Sen, S., 2004. Aurora-A/STK15/BTAK enhances chromosomal instability in bladder cancer cells. Int. J. Oncol. 25, 1631–9.

Friedman, J.M., 1999. Epidemiology of neurofibromatosis type 1. Am. J. Med. Genet. 89, 1–6.

Fuller, B.G., Lampson, M. a, Foley, E. a, Rosasco-Nitcher, S., Le, K. V, Tobelmann, P., Brautigan, D.L., Stukenberg, P.T., Kapoor, T.M., 2008. Midzone activation of aurora B in anaphase produces an intracellular phosphorylation gradient. Nature 453, 1132–6.

Gable, A., Qiu, M., Titus, J., Balchand, S., Ferenz, N.P., Ma, N., Collins, E.S., Fagerstrom, C., Ross, J.L., Yang, G., Wadsworth, P., 2012. Dynamic reorganization of Eg5 in the mammalian spindle throughout mitosis requires dynein and TPX2. Mol. Biol. Cell 23, 1254–1266.

Gadde, S., Heald, R., 2004. Mechanisms and molecules of the mitotic spindle. Curr. Biol. 14, R797-805.

Gaglio, T., Saredi, A., Bingham, J.B., Hasbani, M.J., Gill, S.R., Schroer, T.A., Compton, D.A., 1996. Opposing motor activities are required for the organization of the mammalian mitotic spindle pole. J. Cell Biol. 135, 399–414.

Gaglio, T., Saredi, A., Compton, D.A., 1995. NuMA is required for the organization of microtubules into aster-like mitotic arrays. J. Cell Biol. 131, 693–708.

Garrett, S., Auer, K., Compton, D.A., Kapoor, T.M., 2002. hTPX2 is required for normal spindle morphology and centrosome integrity during vertebrate cell division. Curr. Biol. 12, 2055–9.

Giesecke, A., Stewart, M., 2010. Novel binding of the mitotic regulator TPX2 (target protein for Xenopus kinesin-like protein 2) to importin-alpha. J. Biol. Chem. 285, 17628–35.

Giet, R., McLean, D., Descamps, S., Lee, M.J., Raff, J.W., Prigent, C., Glover, D.M., 2002. Drosophila Aurora A kinase is required to localize D-TACC to centrosomes and to regulate astral microtubules. J. Cell Biol. 156, 437–51.

Giet, R., Uzbekov, R., Cubizolles, F., Le Guellec, K., Prigent, C., 1999. The Xenopus laevis aurora-related protein kinase pEg2 associates with and phosphorylates the kinesin-related protein XlEg5. J. Biol. Chem. 274, 15005–13.

Giubettini, M., Asteriti, I. a, Scrofani, J., De Luca, M., Lindon, C., Lavia, P., Guarguaglini, G., 2011. Control of Aurora-A stability through interaction with TPX2. J. Cell Sci. 124, 113–22.

Glotzer, M., 1997. The mechanism and control of cytokinesis. Curr. Opin. Cell Biol. 9, 815–823.

Glover, D.M., Leibowitz, M.H., McLean, D. a, Parry, H., 1995. Mutations in aurora prevent centrosome separation leading to the formation of monopolar spindles. Cell 81, 95–105.

Goldstein, L.S.., 2001. Molecular motors: from one motor many tails to one motor many tales. Trends Cell Biol. 11, 477–482.

Gorbsky, G.J., 2004. Mitosis: MCAK under the aura of Aurora B. Curr. Biol. 14, R346-8.

Gorbsky, G.J., 2013. Cohesion fatigue. Curr. Biol. 23, R986–R988.

Goss, J.W., Toomre, D.K., 2008. Both daughter cells traffic and exocytose membrane at the cleavage furrow during mammalian cytokinesis. J. Cell Biol. 181, 1047–54.

Greenan, G., Brangwynne, C.P., Jaensch, S., Gharakhani, J., Julicher, F., Hyman, A.A., 2010. Centrosome size sets mitotic spindle length in Caenorhabditis elegans embryos. Curr Biol 20, 353–358.

Greiner, J., Ringhoffer, M., Taniguchi, M., Schmitt, A., Kirchner, D., Krähn, G., Heilmann, V., Gschwend, J., Bergmann, L., Döhner, H., Schmitt, M., 2002. Receptor for hyaluronan acid–mediated motility (RHAMM) is a new immunogenic leukemia-associated antigen in acute and chronic myeloid leukemia. Exp. Hematol. 30, 1029–1035.

Grill, S.W., Hyman, A.A., 2005. Spindle positioning by cortical pulling forces. Dev. Cell 8, 461–5.

Gritsko, T.M., Coppola, D., Paciga, J.E., Yang, L., Sun, M., Shelley, S.A., Fiorica, J. V, Nicosia, S. V, Cheng, J.Q., 2003. Activation and overexpression of centrosome kinase BTAK/Aurora-A in human ovarian cancer. Clin. Cancer Res. 9, 1420–6.

Groen, A.C., Cameron, L.A., Coughlin, M., Miyamoto, D.T., Mitchison, T.J., Ohi, R., Carolina, N., Hill, C., 2004. XRHAMM functions in Ran-dependent microtubule nucleation and pole formation during anastral spindle assembly. Curr Biol 14, 1801–1811.

Groen, A.C., Needleman, D., Brangwynne, C., Gradinaru, C., Fowler, B., Mazitschek, R.,

Mitchison, T.J., 2008. A novel small-molecule inhibitor reveals a possible role of kinesin-5 in anastral spindle-pole assembly. J. Cell Sci. 121, 2293–300.

Gromley, A., Yeaman, C., Rosa, J., Redick, S., Chen, C.-T., Mirabelle, S., Guha, M., Sillibourne, J., Doxsey, S.J., 2005. Centriolin anchoring of exocyst and SNARE complexes at the midbody is required for secretory-vesicle-mediated abscission. Cell 123, 75–87.

Grosstessner-Hain, K., Hegemann, B., Novatchkova, M., Rameseder, J., Joughin, B.A., Hudecz, O., Roitinger, E., Pichler, P., Kraut, N., Yaffe, M.B., Peters, J.-M., Mechtler, K., 2011. Quantitative Phospho-proteomics to Investigate the Polo-like Kinase 1-Dependent Phospho-proteome. Mol. Cell. Proteomics 10, M111.008540-M111.008540.

Gruss, O.J., Carazo-Salas, R.E., Schatz, C. a, Guarguaglini, G., Kast, J., Wilm, M., Le Bot, N., Vernos, I., Karsenti, E., Mattaj, I.W., 2001. Ran induces spindle assembly by reversing the inhibitory effect of importin alpha on TPX2 activity. Cell 104, 83–93.

Gruss, O.J., Wittmann, M., Yokoyama, H., Pepperkok, R., Kufer, T., Silljé, H., Karsenti, E., Mattaj, I.W., Vernos, I., 2002. Chromosome-induced microtubule assembly mediated by TPX2 is required for spindle formation in HeLa cells. Nat. Cell Biol. 4, 871–9.

Gust, K.M., Hofer, M.D., Perner, S.R., Kim, R., Chinnaiyan, A.M., Rinnab, L., Rubin, M.A., Greiner, J., Schmitt, M., Kuefer, R., 2009. RHAMM (CD168) is overexpressed at the protein level and may constitute an immunogenic antigen in advanced prostate cancer disease 1. Neoplasia 11, 956–963.

Hall, C.L., Yang, B., Yang, X., Zhang, S., Turley, M., Samuel, S., Lange, L. a, Wang, C., Curpen, G.D., Savani, R.C., Greenberg, a H., Turley, E. a, 1995. Overexpression of the hyaluronan receptor RHAMM is transforming and is also required for H-ras transformation. Cell 82, 19–26.

Hanks, S., Coleman, K., Reid, S., Plaja, A., Firth, H., Fitzpatrick, D., Kidd, A., Méhes, K., Nash, R., Robin, N., Shannon, N., Tolmie, J., Swansbury, J., Irrthum, A., Douglas, J., Rahman, N., 2004. Constitutional aneuploidy and cancer predisposition caused by biallelic mutations in BUB1B. Nat. Genet. 36, 1159–61.

Hanks, S., Coleman, K., Summersgill, B., Messahel, B., Williamson, D., Pritchard-Jones, K., Strefford, J., Swansbury, J., Plaja, A., Shipley, J., Rahman, N., 2006. Comparative genomic hybridization and BUB1B mutation analyses in childhood cancers associated with mosaic variegated aneuploidy syndrome. Cancer Lett. 239, 234–8.

Hanks, S., Rahman, N., 2005. Aneuploidy-cancer predisposition syndromes 225–227.

Hardwick, C., Hoare, K., Owens, R., Hohn, H.P., Hook, M., Moore, D., Cripps, V., Austen, L., Nance, D.M., Turley, E. a, 1992. Molecular cloning of a novel hyaluronan receptor that mediates tumor cell motility. J. Cell Biol. 117, 1343–50.

Hardwick, K.G., Johnston, R.C., Smith, D.L., Murray, A.W., 2000. MAD3 encodes a novel component of the spindle checkpoint which interacts with Bub3p, Cdc20p, and Mad2p. J. Cell Biol. 148, 871–82.

Heald, R., Tournebize, R., Blank, T., Sandaltzopoulos, R., Becker, P., Hyman, A., Karsenti, E., 1996. Self-organization of microtubules into bipolar spindles around artificial chromosomes in Xenopus egg extracts. Nature 382, 420–5.

Heald, R., Tournebize, R., Habermann, A., Karsenti, E., Hyman, A., 1997. Spindle assembly in Xenopus egg extracts: respective roles of centrosomes and microtubule self-organization. J. Cell Biol. 138, 615–28.

Hirano, T., 2000. Chromosome cohesion, condensation, and separation. Annu. Rev. Biochem. 69, 115–144.

Hirota, T., Kunitoku, N., Sasayama, T., Marumoto, T., Zhang, D., Nitta, M., Hatakeyama, K., Saya, H., 2003. Aurora-A and an interacting activator, the LIM protein Ajuba, are required for mitotic commitment in human cells. Cell 114, 585–98.

Hoffman, D.B., Pearson, C.G., Yen, T.J., Howell, B.J., Salmon, E.D., 2001. Microtubule-dependent changes in assembly of microtubule motor proteins and mitotic spindle checkpoint proteins at PtK1 kinetochores. Mol. Biol. Cell 12, 1995–2009.

Hofmann, M., Fieber, C., Assmann, V., Göttlicher, M., Sleeman, J., Plug, R., Howells, N., von Stein, O., Ponta, H., Herrlich, P., 1998. Identification of IHABP, a 95 kDa intracellular hyaluronate binding protein. J. Cell Sci. 111, 1673–84.

Howell, B.J., McEwen, B.F., Canman, J.C., Hoffman, D.B., Farrar, E.M., Rieder, C.L., Salmon, E.D., 2001. Cytoplasmic dynein/dynactin drives kinetochore protein transport to the spindle poles and has a role in mitotic spindle checkpoint inactivation. J. Cell Biol. 155, 1159–72.

Hsu, J.-Y., Sun, Z.-W., Li, X., Reuben, M., Tatchell, K., Bishop, D.K., Grushcow, J.M., Brame, C.J., Caldwell, J.A., Hunt, D.F., Lin, R., Smith, M.M., Allis, C.D., 2000. Mitotic phosphorylation of Histone H3 is governed by Ipl1/aurora kinase and Glc7/PP1 phosphatase in budding yeast and nematodes. Cell 102, 279–291.

Hunter, A.W., Caplow, M., Coy, D.L., Hancock, W.O., Diez, S., Wordeman, L., Howard, J., 2003. The kinesin-related protein MCAK is a microtubule depolymerase that forms an ATP-hydrolyzing complex at microtubule ends. Mol. Cell 11, 445–457.

Inoué, S., Salmon, E.D., 1995. Force generation by microtubule assembly/disassembly in mitosis and related movements. Mol. Biol. Cell 6, 1619–40.

Ishigami, S., Ueno, S., Nishizono, Y., Matsumoto, M., Kurahara, H., Arigami, T., Uchikado, Y., Setoyama, T., Arima, H., Yoshiaki, K., Kijima, Y., Kitazono, M., Natsugoe, S., 2011. Prognostic impact of CD168 expression in gastric cancer. BMC Cancer 11, 106.

Jacquemont, S., Bocéno, M., Rival, J.M., Méchinaud, F., David, A., 2002. High risk of malignancy in mosaic variegated aneuploidy syndrome. Am. J. Med. Genet. 109, 17–21.

Jett, K., Friedman, J.M., 2010. Clinical and genetic aspects of neurofibromatosis 1. Genet. Med. 12, 1–11.

Jiang, J., Mohan, P., Maxwell, C.A., 2013. The cytoskeletal protein RHAMM and ERK1/2 activity maintain the pluripotency of murine embryonic stem cells. PLoS One 8, e73548.

Joglekar, A.P., Bloom, K.S., Salmon, E.D., 2010. Mechanisms of force generation by end-on kinetochore-microtubule attachments. Curr. Opin. Cell Biol. 22, 57–67.

Joukov, V., Groen, A.C., Prokhorova, T., Gerson, R., White, E., Rodriguez, A., Walter, J.C., Livingston, D.M., 2006. The BRCA1/BARD1 heterodimer modulates ran-dependent mitotic spindle assembly. Cell 127, 539–52.

Kadara, H., Lacroix, L., Behrens, C., Solis, L., Gu, X., Lee, J.J., Tahara, E., Lotan, D., Hong, W.K., Wistuba, I.I., Lotan, R., 2009. Identification of gene signatures and molecular markers for human lung cancer prognosis using an in vitro lung carcinogenesis system. Cancer Prev. Res. (Phila). 2, 702–11.

Kajii, T., Ikeuchi, T., Yang, Z.-Q., Nakamura, Y., Tsuji, Y., Yokomori, K., Kawamura, M., Fukuda, S., Horita, S., Asamoto, A., 2001. Cancer-prone syndrome of mosaic variegated aneuploidy and total premature chromatid separation: Report of five infants. Am. J. Med. Genet. 104, 57–64.

Kaláb, P., Pralle, A., Isacoff, E.Y., Heald, R., Weis, K., 2006. Analysis of a RanGTP-regulated gradient in mitotic somatic cells. Nature 440, 697–701.

Kamada, K., Yamada, Y., Hirao, T., Fujimoto, H., Takahama, Y., Ueno, M., Takayama, T., Naito, A., Hirao, S., Nakajima, Y., 2004. Amplification/overexpression of Aurora-A in human gastric carcinoma: potential role in differentiated type gastric carcinogenesis. Oncol. Rep. 12, 593–9.

Kapitein, L.C., Peterman, E.J.G., Kwok, B.H., Kim, J.H., Kapoor, T.M., Schmidt, C.F., 2005. The bipolar mitotic kinesin Eg5 moves on both microtubules that it crosslinks. Nature 435, 114–118.

Kapoor, T.M., 2001. Eg5 is static in bipolar spindles relative to tubulin: evidence for a static spindle matrix. J. Cell Biol. 154, 1125–1134.

Kardon, J.R., Vale, R.D., 2009. Regulators of the cytoplasmic dynein motor. Nat. Rev. Mol. Cell Biol. 10, 854–65.

Karsenti, E., Newport, J., Kirschner, M., 1984. Respective roles of centrosomes and chromatin in the conversion of microtubule arrays from interphase to metaphase. J. Cell Biol. 99, 47s–54s.

Kashina, A.S., Baskin, R.J., Cole, D.G., Wedaman, K.P., Saxton, W.M., Scholey, J.M., 1996. A bipolar kinesin. Nature 379, 270–2.

Katayama, H., Sasai, K., Kawai, H., Yuan, Z.-M., Bondaruk, J., Suzuki, F., Fujii, S., Arlinghaus, R.B., Czerniak, B. a, Sen, S., 2004. Phosphorylation by aurora kinase A induces Mdm2-mediated destabilization and inhibition of p53. Nat. Genet. 36, 55–62.

Kawame, H., Sugio, Y., Fuyama, Y., Hayashi, Y., Suzuki, H., Kurosawa, K., Maekawa, K., 1999. Syndrome of microcephaly, Dandy-Walker malformation, and Wilms tumor caused by mosaic variegated aneuploidy with premature centromere division (PCD): report of a new case and review of the literature. J. Hum. Genet. 44, 219–24.

Keen, N., Taylor, S., 2004. Aurora-kinase inhibitors as anticancer agents. Nat. Rev. Cancer 4, 927–36.

Khodjakov, A., Cole, R.W., Oakley, B.R., Rieder, C.L., 2000. Centrosome-independent mitotic spindle formation in vertebrates. Curr. Biol. 10, 59–67.

Khodjakov, A., Copenagle, L., Gordon, M.B., Compton, D.A., Kapoor, T.M., 2003. Minus-end capture of preformed kinetochore fibers contributes to spindle morphogenesis. J. Cell Biol. 160, 671–683.

Khodjakov, A., Pines, J., 2010. Centromere tension: a divisive issue. Nat. Cell Biol. 12, 919–23.

King, J.M., Hays, T.S., Nicklas, R.B., 2000. Dynein is a transient kinetochore component whose binding is regulated by microtubule attachment, not tension. J. Cell Biol. 151, 739–48.

Kinoshita, K., Noetzel, T.L., Pelletier, L., Mechtler, K., Drechsel, D.N., Schwager, A., Lee, M., Raff, J.W., Hyman, A. a, 2005. Aurora A phosphorylation of TACC3/maskin is required for centrosome-dependent microtubule assembly in mitosis. J. Cell Biol. 170, 1047–55.

Kirschner, M.W., Mitchison, T., 1986. Microtubule dynamics. Nature 324, 621.

Kiyomitsu, T., Cheeseman, I.M., 2012. Chromosome- and spindle-pole-derived signals generate an intrinsic code for spindle position and orientation. Nat. Cell Biol. 14, 311–7.

Kline, S.L., Cheeseman, I.M., Hori, T., Fukagawa, T., Desai, A., 2006. The human Mis12 complex is required for kinetochore assembly and proper chromosome segregation. J. Cell Biol. 173, 9–17.

Koffa, M.D., Casanova, C.M., Santarella, R., Köcher, T., Wilm, M., Mattaj, I.W., Carazo-Salas, R.E., Guarguaglini, G., Gruss, O.J., Segref, A., Karsenti, E., Mattaj, I.W., Askjaer, P., Galy, V., Hannak, E., Mattaj, I.W., Bamba, C., Bobinnec, Y., Fukuda, M., Nishida, E., Kalab, P., Pu, R.T., Dasso, M., Zhang, C., Hughes, M., Clarke, P.R., Wilde, A., Zheng, Y., Ohba, T., Nakamura, M., Nishitani, H., Nishimoto, T., Gruss, O.J., Carazo-Salas, R.E., Schatz, C.A., Guarguaglini, G., Kast, J., Wilm, M., Bot, N. Le, Vernos, I., Karsenti, E., Mattaj, I.W., Schatz, C.A., Santarella, R., Hoenger, A., Karsenti, E., Mattaj, I.W., Gruss, O.J., Carazo-Salas, R.E., Gruss, O.J., Wittmann, M., Yokoyama, H., Pepperkok, R., Kufer, T., Sillje, H., Karsenti, E., Mattaj, I.W., Vernos, I., Nachury, M.V., Maresca, T.J., Salmon, W.C., Waterman-Storer, C.M., Heald, R., Weis, K., Blower, M.D., Nachury, M., Heald, R., Weis, K., Enos, A.P., Morris, N.R., Hagan, I., Yanagida, M., Sawin, K.E., LeGuellec, K., Philippe, M., Mitchison, T.J., Kashina, A.S., Baskin, R.J., Cole, D.G., Wedaman, K.P., Saxton, W.M., Scholey, J.M., Kapitein, L.C., Peterman, E.J., Kwok, B.H., Kim, J.H., Kapoor, T.M., Schmidt, C.F., Miyamoto, D.T., Perlman, Z.E., Burbank, K.S., Groen, A.C., Mitchison, T.J., Wilde, A., Lizarraga, S.B., Zhang, L., Wiese, C., Gliksman, N.R., Walczak, C.E., Zheng, Y., Tsou, A.P., Yang, C.W., Huang, C.Y., Yu, R.C., Lee, Y.C., Chang, C.W., Chen, B.R., Chung, Y.F., Fann, M.J., Chi, C.W., Al., E., Carmena, M., Earnshaw, W.C., Bayliss, R., Sardon, T., Vernos, I., Conti, E., Eyers, P.A., Erikson, E., Chen, L.G., Maller, J.L., Tsai, M.Y., Wiese, C., Cao, K., Martin, O., Donovan, P., Ruderman, J., Prigent, C., Zheng, Y., Popov, A.V., Karsenti, E., Popov, A.V., Severin, F., Karsenti, E., Kinoshita, K., Habermann, B., Hyman, A.A., Bischoff, F.R., Klebe, C., Kretschmer, J., Wittinghofer, A., Ponstingl, H., Bischoff, J.R., Anderson, L., Zhu, Y., Mossie, K., Ng, L., Souza, B., Schryver, B., Flanagan, P., Clairvoyant, F., Ginther, C., Al., E., Meraldi, P., Nigg, E.A., Hsu, J.M., Lee, Y.C., Yu, C.T., Huang, C.Y., Kunitoku, N., Sasayama, T., Marumoto, T., Zhang, D., Honda, S., Kobayashi, O., Hatakeyama, K., Ushio, Y., Saya, H., Hirota, T., Yu, C.T., Hsu, J.M., Lee, Y.C., Tsou, A.P., Chou, C.K., Huang, C.Y., Nedelec, F., Mitchison, T.J., Anand, S., Penrhyn-Lowe, S., Venkitaraman, A.R., 2006. HURP is part of a Ran-dependent complex involved in spindle formation. Curr. Biol. 16, 743–754.

Kollareddy, M., Zheleva, D., Dzubak, P., Lepsik, M., Hajduch, M., 2012. Aurora kinase inhibitors : Progress towards the clinic. Invest New Drugs 6, 2411–2432.

Koshland, D., Strunnikov, A., 1996. Mitotic Chromosome Condensation. Annu. Rev. Cell Dev. Biol. 12, 305–333.

Kraft, C., Herzog, F., Gieffers, C., Mechtler, K., Hagting, A., Pines, J., Peters, J.-M., 2003. Mitotic regulation of the human anaphase-promoting complex by phosphorylation. EMBO J. 22, 6598–609.

Kschonsak, M., Haering, C.H., 2015. Shaping mitotic chromosomes: From classical concepts to molecular mechanisms. BioEssays 37, 755–766.

Kufer, T. a, Silljé, H.H.W., Körner, R., Gruss, O.J., Meraldi, P., Nigg, E. a, 2002. Human TPX2 is required for targeting Aurora-A kinase to the spindle. J. Cell Biol. 158, 617–23.

Kunitoku, N., Sasayama, T., Marumoto, T., Zhang, D., Honda, S., Kobayashi, O., Hatakeyama, K., Ushio, Y., Saya, H., Hirota, T., 2003. CENP-A Phosphorylation by Aurora-A in Prophase Is Required for Enrichment of Aurora-B at Inner Centromeres and for Kinetochore Function. Dev. Cell 5, 853–864.

Kwok, B.H., Yang, J.G., Kapoor, T.M., 2004. The Rate of Bipolar Spindle Assembly Depends on the Microtubule-Gliding Velocity of the Mitotic Kinesin Eg5. Curr. Biol. 14, 1783–1788.

Lampson, M.A., Kapoor, T.M., 2005. The human mitotic checkpoint protein BubR1 regulates chromosome-spindle attachments. Nat. Cell Biol. 7, 93–8.

Landry, J.J.M., Pyl, P.T., Rausch, T., Zichner, T., Tekkedil, M.M., Stütz, A.M., Jauch, A., Aiyar, R.S., Pau, G., Delhomme, N., Gagneur, J., Korbel, J.O., Huber, W., Steinmetz, L.M., 2013. The genomic and transcriptomic landscape of a HeLa cell line. G3 (Bethesda). 3, 1213–24.

Lara-Gonzalez, P., Taylor, S.S., 2012. Cohesion fatigue explains why pharmacological inhibition of the APC/C induces a spindle checkpoint-dependent mitotic arrest. PLoS One 7, 1–14.

Lara-Gonzalez, P., Westhorpe, F.G., Taylor, S.S., 2012. The spindle assembly checkpoint. Curr. Biol. 22, R966-80.

Lee, J.Y., Spicer, A.P., 2000. Hyaluronan: a multifunctional, megaDalton, stealth molecule. Curr. Opin. Cell Biol. 12, 581–586.

Li, H., Guo, L., Li, J.W., Liu, N., Qi, R., Liu, J., 2000. Expression of hyaluronan receptors CD44 and RHAMM in stomach cancers: relevance with tumor progression. Int. J. Oncol. 17, 927–32.

Li, X., Nicklas, R.B., 1997. Tension-sensitive kinetochore phosphorylation and the chromosome distribution checkpoint in praying mantid spermatocytes. J. Cell Sci. 110 (Pt 5, 537–45.

Liang, Y., Yu, W., Li, Y., Yu, L., Zhang, Q., Wang, F., Yang, Z., Du, J., Huang, Q., Yao, X., Zhu, X., 2007. Nudel Modulates Kinetochore Association and Function of Cytoplasmic Dynein in M Phase. Mol. Biol. Cell 18, 2656–2666.

Lim, E., Vaillant, F., Wu, D., Forrest, N.C., Pal, B., Hart, A.H., Asselin-Labat, M.-L., Gyorki, D.E., Ward, T., Partanen, A., Feleppa, F., Huschtscha, L.I., Thorne, H.J., kConFab, Fox, S.B., Yan, M., French, J.D., Brown, M.A., Smyth, G.K., Visvader, J.E., Lindeman, G.J., 2009. Aberrant luminal progenitors as the candidate target population for basal tumor development in BRCA1 mutation carriers. Nat. Med. 15, 907–13.

Limwongse, C., Schwartz, S., Bocian, M., Robin, N.H., 1999. Child with mosaic variegated aneuploidy and embryonal rhabdomyosarcoma. Am. J. Med. Genet. 82, 20–24.

Line, A., Slucka, Z., Stengrevics, A., Silina, K., Li, G., Rees, R., 2002. Characterisation of tumour-associated antigens in colon cancer. Cancer Immunol. Immunother. 51, 574–582.

Liu, D., Davydenko, O., Lampson, M.A., 2012. Polo-like kinase-1 regulates kinetochore-microtubule dynamics and spindle checkpoint silencing. J. Cell Biol. 198, 491–9.

Ma, H.T., Poon, R.Y.C., 2016. TRIP13 regulates both the activation and inactivation of the spindle-assembly checkpoint. Cell Rep. 14, 1086–1099.

Ma, N., Titus, J., Gable, A., Ross, J.L., Wadsworth, P., 2011. TPX2 regulates the localization and activity of Eg5 in the mammalian mitotic spindle. J. Cell Biol. 195, 87–98.

Macurek, L., Lindqvist, A., Lim, D., Lampson, M.A., Klompmaker, R., Freire, R., Clouin, C., Taylor, S.S., Yaffe, M.B., Medema, R.H., 2008. Polo-like kinase-1 is activated by aurora A to promote checkpoint recovery. Nature 455, 119–123.

Macville, M., Schröck, E., Padilla-Nash, H., Keck, C., Ghadimi, B.M., Zimonjic, D., Popescu, N., Ried, T., 1999. Comprehensive and definitive molecular cytogenetic characterization of HeLa cells by spectral karyotyping. Cancer Res. 59, 141–50.

Maney, T., Hunter, A.W., Wagenbach, M., Wordeman, L., 1998. Mitotic centromere-associated kinesin is important for anaphase chromosome segregation. J. Cell Biol. 142, 787–801.

Mantripragada, K.K., Spurlock, G., Kluwe, L., Chuzhanova, N., Ferner, R.E., Frayling, I.M., Dumanski, J.P., Guha, A., Mautner, V., Upadhyaya, M., 2008. High-resolution DNA copy number profiling of malignant peripheral nerve sheath tumors using targeted microarray-based comparative genomic hybridization. Clin. cancer Res. 14, 1015–24.

Maresca, T.J., Salmon, E.D., 2010. Welcome to a new kind of tension: translating kinetochore mechanics into a wait-anaphase signal. J. Cell Sci. 123, 825–35.

Marx, A., Hoenger, A., Mandelkow, E., 2009. Structures of kinesin motor proteins. Cell Motil. Cytoskeleton 66, 958–66.

Matsuura, S., Matsumoto, Y., Morishima, K., Izumi, H., Matsumoto, H., Ito, E., Tsutsui, K., Kobayashi, J., Tauchi, H., Kajiwara, Y., Hama, S., Kurisu, K., Tahara, H., Oshimura, M., Komatsu, K., Ikeuchi, T., Kajii, T., 2006. Monoallelic BUB1B mutations and defective mitotic-spindle checkpoint in seven families with premature chromatid separation (PCS) syndrome. Am. J. Med. Genet. A 140, 358–67.

Matthies, H.J., McDonald, H.B., Goldstein, L.S., Theurkauf, W.E., 1996. Anastral meiotic spindle morphogenesis: role of the non-claret disjunctional kinesin-like protein. J. Cell Biol. 134, 455–64.

Maxwell, C.A., Keats, J.J., Belch, A.R., Pilarski, L.M., Reiman, T., 2005. Receptor for Hyaluronan-Mediated Motility correlates with centrosome abnormalities in multiple myeloma and maintains mitotic integrity 65, 850–860.

Maxwell, C.A., Keats, J.J., Crainie, M., Sun, X., Yen, T., Shibuya, E., Hendzel, M., Chan, G., Pilarski, L.M., 2003. RHAMM is a centrosomal protein that interacts with dynein and maintains spindle pole stability. Mol. Biol. Cell 14, 2262–2276.

Maxwell, C.A., Rasmussen, E., Zhan, F., Keats, J.J., Adamia, S., Strachan, E., Crainie, M., Walker, R., Belch, A.R., Pilarski, L.M., Barlogie, B., Shaughnessy, J., Reiman, T., 2004. RHAMM expression and isoform balance predict aggressive disease and poor survival in multiple myeloma . Blood 104, 1151–1158.

Maxwell, C. a, Benítez, J., Gómez-Baldó, L., Osorio, A., Bonifaci, N., Fernández-Ramires, R., Costes, S. V, Guinó, E., Chen, H., Evans, G.J.R., Mohan, P., Català, I., Petit, A., Aguilar, H., Villanueva, A., Aytes, A., Serra-Musach, J., Rennert, G., Lejbkowicz, F., Peterlongo, P., Manoukian, S., Peissel, B., Ripamonti, C.B., Bonanni, B., Viel, A., Allavena, A., Bernard, L., Radice, P., Friedman, E., Kaufman, B., Laitman, Y., Dubrovsky, M., Milgrom, R., Jakubowska, A., Cybulski, C., Gorski, B., Jaworska, K., Durda, K., Sukiennicki, G., Lubiński, J., Shugart, Y.Y., Domchek, S.M., Letrero, R., Weber, B.L., Hogervorst, F.B.L., Rookus, M. a, Collee, J.M., Devilee, P., Ligtenberg, M.J., Luijt, R.B. Van Der, Aalfs, C.M., Waisfisz, Q., Wijnen, J., Roozendaal, C.E.P. Van, Easton, D.F., Peock, S., Cook, M., Oliver, C., Frost, D., Harrington, P., Evans, D.G., Lalloo, F., Eeles, R., Izatt, L., Chu, C., Eccles, D., Douglas, F., Brewer, C., Nevanlinna, H., Heikkinen, T., Couch, F.J., Lindor, N.M., Wang, X., Godwin, A.K., Caligo, M. a, Lombardi, G., Loman, N., Karlsson, P., Ehrencrona, H., Wachenfeldt, A. Von, Barkardottir, R.B., Hamann, U., Rashid, M.U., Lasa, A., Caldés, T., Andrés, R., Schmitt, M., Assmann, V., Stevens, K., Offit, K., Curado, J., Tilgner, H., Guigó, R., Aiza, G., Brunet, J., Castellsagué, J., Martrat, G., Urruticoechea, A., Blanco, I., Tihomirova, L., Goldgar, D.E., Buys, S., John, E.M., Miron, A., Southey, M., Daly, M.B., Schmutzler, R.K., Wappenschmidt, B., Meindl, A., Arnold, N., Deissler, H., Varon-Mateeva, R., Sutter, C., Niederacher, D., Imyamitov, E., Sinilnikova, O.M., Stoppa-Lyonne, D., Mazoyer, S., Verny-Pierre, C., Castera, L., de Pauw, A., Bignon, Y.-J., Uhrhammer, N., Peyrat, J.-P., Vennin, P., Fert Ferrer, S., Collonge-Rame, M.-A., Mortemousque, I., Spurdle, A.B., Beesley, J., Chen, X., Healey, S., Barcellos-Hoff, M.H., Vidal, M., Gruber, S.B., Lázaro, C., Capellá, G., McGuffog, L., Nathanson, K.L., Antoniou, A.C., Chenevix-Trench, G., Fleisch, M.C., Moreno, V., Pujana, M.A., 2011. Interplay between BRCA1 and RHAMM regulates epithelial apicobasal polarization and may influence risk of breast cancer. PLoS Biol. 9, e1001199.

McIntosh, J.R., 1991. Structural and mechanical control of mitotic progression. Cold Spring Harb. Symp. Quant. Biol. 56, 613–9.

Megraw, T.L., Kao, L.R., Kaufman, T.C., 2001. Zygotic development without functional mitotic centrosomes. Curr. Biol. 11, 116–20.

Meraldi, P., Nigg, E. a, 2002. The centrosome cycle. FEBS Lett. 521, 9–13.

Merdes, A., Ramyar, K., Vechio, J.D., Cleveland, D.W., 1996. A complex of NuMA and cytoplasmic dynein is essential for mitotic spindle assembly. Cell 87, 447–58.

Meunier, S., Vernos, I., 2011. K-fibre minus ends are stabilized by a RanGTP-dependent mechanism essential for functional spindle assembly. Nat. Cell Biol. 13, 1406–1414.

Meunier, S., Vernos, I., 2012. Microtubule assembly during mitosis - from distinct origins to distinct functions? J. Cell Sci. 125, 2805–2814.

Mitchison, T.J., Kirschner, M.W., 1984. Dynamic instability of microtubule growth. Nature 312, 237–42.

Mitchison, T.J., Maddox, P., Gaetz, J., Groen, A., Shirasu, M., Desai, A., Salmon, E.D., Kapoor, T.M., 2005. Roles of polymerization dynamics, opposed motors, and a tensile element in governing the length of Xenopus extract meiotic spindles. Mol. Biol. Cell 16, 3064–76.

Mohan, P., Castellsague, J., Jiang, J., Allen, K., Chen, H., Nemirovsky, O., Spyra, M., Hu, K., Kluwe, L., Pujana, M.A., Villanueva, A., Mautner, V.F., Keats, J.J., Dunn, S.E., Maxwell, C.A., 2013. Genomic imbalance of HMMR / RHAMM regulates the sensitivity and response of malignant peripheral nerve sheath tumour cells to aurora kinase inhibition . AbstrAct : 4, 80–93.

Mori, D., Yano, Y., Toyo-oka, K., Yoshida, N., Yamada, M., Muramatsu, M., Zhang, D., Saya, H., Toyoshima, Y.Y., Kinoshita, K., Wynshaw-Boris, A., Hirotsune, S., 2007. NDEL1 phosphorylation by Aurora-A kinase is essential for centrosomal maturation, separation, and TACC3 recruitment. Mol. Cell. Biol. 27, 352–67.

Musacchio, A., Salmon, E.D., 2007. The spindle-assembly checkpoint in space and time. Nat. Rev. Mol. Cell Biol. 8, 379–93.

Nasmyth, K., 2002. Segregating sister genomes: the molecular biology of chromosome separation. Science 297, 559–65.

Nasmyth, K., Peters, J.M., Uhlmann, F., Wilmut, I., Schnieke, A.E., McWhir, J., Kind, A.J., Campbell, K.H., Nurse, P., Hartwell, L.H., Weinert, T.A., Flemming, W., Watson, J.D., Crick, F.H.C., Maguire, M.P., Lin, D.C., Grossman, A.D., Nicklas, R.B., Ward, S.C., Mole-Bajer, J., Rieder, C.L., Palazzo, R.E., Izutsu, K., McNeill, P.A., Berns, M.W., Belar, K., Selig, S., Okumura, K., Ward, D.C., Cedar, H., Sumner, A.T., Rieder, C.L., Cole, R., Sigrist, S., Jacobs, H., Stratmann, R., Lehner, C.F., Vig, B.K., Goshima, G., Yanagida, M., Tippet, D.H., Pickett-Heaps, J.D., Leslie, R.L., Melander, Y., Comings, D.E., Murray, A.W., Szostak, J.W., Dinardo, S., Voelkel, K.A., Sternglanz, R.L., Koshland, D., Hartwell, L., Funabiki, H., Hagan, I., Uzawa, S., Yanagida, M., Downes, C.S., Mullinger, A.M., Johnson, R.T., Gorbsky, G.J., Maguire, M.P., Paredes, A.M., Riess, R.W., Davis, B.K., Goldstein, L.S.B., Kerrebrock, A.W., Moore, D.P., Wu, J.S., Orr-Weaver, T.L., Toth, A., Losada, A., Hirano, M., Hirano, T., Holloway, S.L., Glotzer, M., King, R.W., Murray, A.W., Irniger, S., Piatti, S., Michaelis, C., Nasmyth, K., King, R.W., Zachariae, W., Nasmyth, K., Yamamoto, A., Guacci, V., Koshland, D., Cohen-Fix, O., Peters, J.-M., Kirschner, M.W., Koshland, D., Funabiki, H., Ciosk, R., Michaelis, C., Ciosk, R., Nasmyth, K., Guacci, V., Koshland, D., Strunnikov, A., Furuya, K., Takahashi, K., Yanagida, M., Skibbens, R. V., Corson, L.B., Koshland, D., Hieter, P., Ciosk, R., Tanaka, T., Cosma, M.P., Wirth, K., Nasmyth, K., Blat, Y., Kleckner, N., Megee, P.C., Mistrot, C., Guacci, V., Koshland, D., Uhlmann, F., Nasmyth, K., Heemst, D. van, James, H., Pöggeler, S., Berteaux-Lecellier, V., Zickler, D., Denison, S.H., Kafer, E., May, G.S., Tanaka, K., Uhlmann, F., Lottspeich, F., Nasmyth, K., Hirano, T., Melby, T.E., Ciampaglio, C.N., Briscoe, G., Erickson, H.P., Akhmedov, A.T., Gross, B., Jessberger, R., Hirano, T., Mitchison, T.J., Saka, Y., Hirano, T., Kobayashi, R., Hirano, M., Kimura, K., Rybenkov, V. V., Crisona, N.J., Hirano, T., Cozzarelli, N.R., Surana, U., Zou, H., McGarry, T.J., Bernal, T., Kirschner, M.W., Saez, C., Pei, L., Melmed, S., Stratmann, R., Lehner, C.F., Yamamoto, A., Guacci, V., Koshland, D., Funabiki, H., Kumada, K., Yanagida, M., McGrew, J.T., Goetsch, L., Byers, B., Baum, P., May, G.S., McGoldrick, C.A., Holt, C.L., Denison, S.H.,

Chen, J.M., Rawlings, N.D., Stevens, R.A., Barrett, A.J., Klein, F., Kumada, K., Lica, L.M., Narayanswami, S., Hamkalo, B.A., Rattner, J.B., Fitzgerald, P.H., Pickering, A.F., Mercer, J.M., Miethke, P.M., Tomkins, D., Hunter, A., Roberts, M., Amon, A., Alexandru, G., Zachariae, W., Schleiffer, A., Nasmyth, K., Basu, J., Cahill, D.P., Weinstein, J., Shirayama, M., Zachariae, W., Ciosk, R., Nasmyth, K., Shteinberg, M., Protopopov, Y., Listovsky, T., Brandeis, M., Hershko, A., Kramer, E.R., Scheuringer, N., Podtelejnikov, A. V., Mann, M., Peters, J.-M., Khodjakov, A., Cole, R.W., Bajer, A.S., Rieder, C.L., 2000. Splitting the chromosome: cutting the ties that bind sister chromatids. Science 288, 1379–85.

Naumova, N., Imakaev, M., Fudenberg, G., Zhan, Y., Lajoie, B.R., Mirny, L.A., Dekker, J., Dekker, J., Fraser, P., Bickmore, W., Fudenberg, G., Getz, G., Meyerson, M., Mirny, L.A., Zhang, Y., McCord, R.P., Ho, Y.J., Lajoie, B.R., Hildebrand, D.G., Simon, A.C., Becker, M.S., Alt, F.W., Dekker, J., Hübner, M.R., Spector, D.L., Dekker, J., Rippe, K., Dekker, M., Kleckner, N., Lieberman-Aiden, E., Berkum, N.L. van, Williams, L., Imakaev, M., Ragoczy, T., Telling, A., Amit, I., Lajoie, B.R., Sabo, P.J., Dorschner, M.O., Sandstrom, R., Bernstein, B., Bender, M.A., Groudine, M., Gnirke, A., Stamatoyannopoulos, J., Mirny, L.A., Lander, E.S., Dekker, J., Markaki, Y., Gunkel, M., Schermelleh, L., Beichmanis, S., Neumann, J., Heidemann, M., Leonhardt, H., Eick, D., Cremer, C., Cremer, T., Dixon, J.R., Selvaraj, S., Yue, F., Kim, A., Li, Y., Shen, Y., Hu, M., Liu, J.S., Ren, B., Nora, E.P., Lajoie, B.R., Schulz, E.G., Giorgetti, L., Okamoto, I., Servant, N., Piolot, T., Berkum, N.L. van, Meisig, J., Sedat, J., Gribnau, J., Barillot, E., Blüthgen, N., Dekker, J., Heard, E., Sanyal, A., Lajoie, B.R., Jain, G., Dekker, J., Flemming, W., DuPraw, E.J., Bak, A.L., Zeuthen, J., Crick, F.H., Marsden, M.P., Laemmli, U.K., Swedlow, J.R., Hirano, T., Maeshima, K., Eltsov, M., Paulson, J.R., Laemmli, U.K., Maeshima, K., Laemmli, U.K., Sedat, J., Manuelidis, L., Belmont, A.S., Sedat, J.W., Agard, D.A., Nishino, Y., Eltsov, M., Joti, Y., Ito, K., Takata, H., Takahashi, Y., Hihara, S., Frangakis, A.S., Imamoto, N., Ishikawa, T., Maeshima, K., Marko, J.F., Kireeva, N., Lakonishok, M., Kireev, I., Hirano, T., Belmont, A.S., Dostie, J., Richmond, T.A., Arnaout, R.A., Selzer, R.R., Lee, W.L., Honan, T.A., Rubio, E.D., Krumm, A., Lamb, J., Nusbaum, C., Green, R.D., Dekker, J., Imakaev, M., Fudenberg, G., McCord, R.P., Naumova, N., Goloborodko, A., Lajoie, B.R., Dekker, J., Mirny, L.A., Simonis, M., Klous, P., Splinter, E., Moshkin, Y., Willemsen, R., Wit, E. de, Steensel, B. van, Laat, W. de, Fudenberg, G., Mirny, L.A., Rosa, A., Becker, N.B., Everaers, R., Lua, R., Borovinskiy, A.L., Grosberg, A.Y., Li, G., Sudlow, G., Belmont, A.S., Strukov, Y.G., Belmont, A.S., Marko, J.F., Siggia, E.D., Fussner, E., Maeshima, K., Hihara, S., Takata, H., Adachi, Y., Luke, M., Laemmli, U.K., Samejima, K., Samejima, I., Vagnarelli, P., Ogawa, H., Vargiu, G., Kelly, D.A., Alves, F. de L., Kerr, A., Green, L.C., Hudson, D.F., Ohta, S., Cooke, C.A., Farr, C.J., Rappsilber, J., Earnshaw, W.C., Sikorav, J.L., Jannink, G., Jackson, D.A., Dickinson, P., Cook, P.R., Earnshaw, W.C., Laemmli, U.K., Hirota, T., Gerlich, D., Koch, B., Ellenberg, J., Peters, J.M., Alipour, E., Marko, J.F., Kleckner, N., Zickler, D., Jones, G.H., Dekker, J., Padmore, R., Henle, J., Hutchinson, J., Sarge, K.D., Park-Sarge, O.K., Deng, W., Blobel, G.A., Follmer, N.E., Wani, A.H., Francis, N.J., Kadauke, S., Udugama, M.I., Pawlicki, J.M., Achtman, J.C., Jain, D.P., Cheng, Y., Hardison, R.C., Blobel, G.A., Strukov, Y.G., Wang, Y., Belmont, A.S., König, P., Braunfeld, M.B., Sedat, J.W., Agard, D.A., Zhang, Y., Heermann, D.W., 2013. Organization of the mitotic chromosome. Science 342, 948–53.

Negrini, S., Gorgoulis, V.G., Halazonetis, T.D., 2010. Genomic instability--an evolving hallmark of cancer. Nat. Rev. Mol. Cell Biol. 11, 220–8.

Neumann, B., Walter, T., Hériché, J.-K., Bulkescher, J., Erfle, H., Conrad, C., Rogers, P., Poser, I., Held, M., Liebel, U., Cetin, C., Sieckmann, F., Pau, G., Kabbe, R., Wünsche, A., Satagopam, V., Schmitz, M.H. a, Chapuis, C., Gerlich, D.W., Schneider, R., Eils, R., Huber, W., Peters, J.-M., Hyman, A. a, Durbin, R., Pepperkok, R., Ellenberg, J., 2010. Phenotypic profiling of the human genome by time-lapse microscopy reveals cell division genes. Nature 464, 721–7.

Neumayer, G., Belzil, C., Gruss, O.J., Nguyen, M.D., 2014. TPX2: of spindle assembly, DNA damage response, and cancer. Cell. Mol. Life Sci. 71, 3027–47.

Niault, T., Hached, K., Sotillo, R., Sorger, P.K., Maro, B., Benezra, R., Wassmann, K., 2007. Changing Mad2 levels affects chromosome segregation and spindle assembly checkpoint control in female mouse meiosis I. PLoS One 2, e1165.

Nigg, E.A., 2002. Centrosome Aberrations: Cause of Consequence of Cancer Progression? Nat. Rev. Genet. 3, 815–815.

Nigg, E.A., Stearns, T., 2011. The centrosome cycle: Centriole biogenesis, duplication and inherent asymmetries. Nat. Cell Biol. 13, 1154–60.

Ohtsubo, M., Kai, R., Furuno, N., Sekiguchi, T., Sekiguchi, M., Hayashida, H., Kuma, K., Miyata, T., Fukushige, S., Murotsu, T., 1987. Isolation and characterization of the active cDNA of the human cell cycle gene (RCC1) involved in the regulation of onset of chromosome condensation. Genes Dev. 1, 585–93.

Ohtsubo, M., Okazaki, H., Nishimoto, T., 1989. The RCC1 protein, a regulator for the onset of chromosome condensation locates in the nucleus and binds to DNA. J. Cell Biol. 109, 1389–97.

Ouchi, M., Fujiuchi, N., Sasai, K., Katayama, H., Minamishima, Y. a, Ongusaha, P.P., Deng, C., Sen, S., Lee, S.W., Ouchi, T., 2004. BRCA1 phosphorylation by Aurora-A in the regulation of G2 to M transition. J. Biol. Chem. 279, 19643–8.

Patel, A. V, Eaves, D., Jessen, W.J., Rizvi, T. a, Ecsedy, J. a, Qian, M.G., Aronow, B.J., Perentesis, J.P., Serra, E., Cripe, T.P., Miller, S.J., Ratner, N., 2012. Ras-driven transcriptome analysis identifies aurora kinase a as a potential malignant peripheral nerve sheath tumor therapeutic target. Clin. cancer Res. 18, 5020–30.

Peters, J.-M., 2002. The anaphase-promoting complex: proteolysis in mitosis and beyond. Mol. Cell 9, 931–43.

Pfarr, C.M., Coue, M., Grissom, P.M., Hays, T.S., Porter, M.E., McIntosh, J.R., 1990. Cytoplasmic dynein is localized to kinetochores during mitosis. Nature 345, 263–5.

Pfister, K.K., Shah, P.R., Hummerich, H., Russ, A., Cotton, J., Annuar, A.A., King, S.M., Fisher, E.M.C., 2006. Genetic analysis of the cytoplasmic dynein subunit families. PLoS Genet. 2, e1.

Pinson, L., Mannini, L., Willems, M., Cucco, F., Sirvent, N., Frebourg, T., Quarantotti, V., Collet, C., Schneider, A., Sarda, P., Geneviève, D., Puechberty, J., Lefort, G., Musio, A.,

2014. CEP57 mutation in a girl with mosaic variegated aneuploidy syndrome. Am. J. Med. Genet. Part A 164, 177–181.

Proia, T.A., Keller, P.J., Gupta, P.B., Klebba, I., Jones, A.D., Sedic, M., Gilmore, H., Tung, N., Naber, S.P., Schnitt, S., Lander, E.S., Kuperwasser, C., 2011. Genetic predisposition directs breast cancer phenotype by dictating progenitor cell fate. Cell Stem Cell 8, 149–63.

Pujana, M.A., Han, J.-D.J., Starita, L.M., Stevens, K.N., Tewari, M., Ahn, J.S., Rennert, G., Moreno, V., Kirchhoff, T., Gold, B., Assmann, V., Elshamy, W.M., Rual, J.-F., Levine, D., Rozek, L.S., Gelman, R.S., Gunsalus, K.C., Greenberg, R. a, Sobhian, B., Bertin, N., Venkatesan, K., Ayivi-Guedehoussou, N., Solé, X., Hernández, P., Lázaro, C., Nathanson, K.L., Weber, B.L., Cusick, M.E., Hill, D.E., Offit, K., Livingston, D.M., Gruber, S.B., Parvin, J.D., Vidal, M., 2007. Network modeling links breast cancer susceptibility and centrosome dysfunction. Nat. Genet. 39, 1338–49.

Raaijmakers, J.A., 2014. Mitotic spindle organization by dynein and kinetochores. Utrecht University.

Raaijmakers, J.A., van Heesbeen, R.G.H.P., Meaders, J.L., Geers, E.F., Fernandez-Garcia, B., Medema, R.H., Tanenbaum, M.E., 2012. Nuclear envelope-associated dynein drives prophase centrosome separation and enables Eg5-independent bipolar spindle formation. EMBO J. 31, 4179–90.

Rannou, Y., Troadec, M.-B., Petretti, C., Hans, F., Dutertre, S., Dimitrov, S., Prigent, C., 2008. Localization of aurora A and aurora B kinases during interphase: role of the N-terminal domain. Cell Cycle 7, 3012–20.

Rappaport, R., 1971. Cytokinesis in animal cells. Int. Rev. Cytol. 31, 169–213.

Rein, D.T., Roehrig, K., Schöndorf, T., Lazar, A., Fleisch, M., Niederacher, D., Bender, H.G., Dall, P., 2003. Expression of the hyaluronan receptor RHAMM in endometrial carcinomas suggests a role in tumour progression and metastasis. J. Cancer Res. Clin. Oncol. 129, 161–4.

Ribbeck, K., Groen, A.C., Santarella, R., Bohnsack, M.T., Raemaekers, T., Köcher, T., Gentzel, M., Görlich, D., Wilm, M., Carmeliet, G., Mitchison, T.J., Ellenberg, J., Hoenger, A., Mattaj, I.W., 2006. NuSAP, a mitotic RanGTP target that stabilizes and cross-links microtubules. Mol. Biol. Cell 17, 2646–60.

Rieder, C., Maiato, H., 2004. Stuck in Division or Passing through:\nWhat Happens When Cells Cannot\nSatisfy the Spindle Assembly Checkpoint. Dev. Cell 7, 637–651.

Rieder, C.L., Alexander, S.P., 1990. Kinetochores are transported poleward along a single astral microtubule during chromosome attachment to the spindle in newt lung cells. J. Cell Biol. 110, 81–95.

Rieder, C.L., Cole, R.W., Khodjakov, A., Sluder, G., 1995. The checkpoint delaying anaphase in response to chromosome monoorientation is mediated by an inhibitory signal produced by unattached kinetochores. J. Cell Biol. 130, 941–8.

Rieder, C.L., Maiato, H., 2004. Stuck in division or passing through: what happens when cells cannot satisfy the spindle assembly checkpoint. Dev. Cell 7, 637–51.

Roghi, C., Giet, R., Uzbekov, R., Morin, N., Chartrain, I., Le Guellec, R., Couturier, A., Dorée, M., Philippe, M., Prigent, C., 1998. The Xenopus protein kinase pEg2 associates with the centrosome in a cell cycle-dependent manner, binds to the spindle microtubules and is involved in bipolar mitotic spindle assembly. J. Cell Sci. 111, 557–72.

Rossio, V., Galati, E., Piatti, S., 2010. Adapt or die: how eukaryotic cells respond to prolonged activation of the spindle assembly checkpoint. Biochem. Soc. Trans. 38, 1645–1649.

Sakakura, C., Hagiwara, A., Yasuoka, R., Fujita, Y., Nakanishi, M., Masuda, K., Shimomura, K., Nakamura, Y., Inazawa, J., Abe, T., Yamagishi, H., 2001. Tumour-amplified kinase BTAK is amplified and overexpressed in gastric cancers with possible involvement in aneuploid formation. Br. J. Cancer 84, 824–831.

Salina, D., Bodoor, K., Eckley, D.M., Schroer, T.A., Rattner, J.B., Burke, B., 2002. Cytoplasmic dynein as a facilitator of nuclear envelope breakdown. Cell 108, 97–107.

Sankaran, S., Crone, D.E., Palazzo, R.E., Parvin, J.D., 2007. Aurora-A kinase regulates breast cancer associated gene 1 inhibition of centrosome-dependent microtubule nucleation. Cancer Res. 67, 11186–94.

Sankaran, S., Starita, L.M., Groen, A.C., Ko, M.J., Parvin, J.D., 2005. Centrosomal microtubule nucleation activity is inhibited by BRCA1-dependent ubiquitination. Mol. Cell. Biol. 25, 8656–68.

Sankaran, S., Starita, L.M., Simons, A.M., Parvin, J.D., 2006. Identification of domains of BRCA1 critical for the ubiquitin-dependent inhibition of centrosome function. Cancer Res. 66, 4100–7.

Santarella, R.A., Koffa, M.D., Tittmann, P., Gross, H., Hoenger, A., 2007. HURP Wraps Microtubule Ends with an Additional Tubulin Sheet That Has a Novel Conformation of Tubulin. J. Mol. Biol. 365, 1587–1595.

Sassoon, I., Severin, F.F., Andrews, P.D., Taba, M.R., Kaplan, K.B., Ashford, A.J., Stark, M.J., Sorger, P.K., Hyman, A.A., 1999. Regulation of Saccharomyces cerevisiae kinetochores by the type 1 phosphatase Glc7p. Genes Dev. 13, 545–55.

Satinover, D.L., Leach, C. a, Stukenberg, P.T., Brautigan, D.L., 2004. Activation of Aurora-A kinase by protein phosphatase inhibitor-2, a bifunctional signaling protein. Proc. Natl. Acad. Sci. U. S. A. 101, 8625–30.

Sawin, K.E., LeGuellec, K., Philippe, M., Mitchison, T.J., 1992. Mitotic spindle organization by a plus-end-directed microtubule motor. Nature 359, 540–3.

Sawin, K.E., Mitchison, T.J., 1991. Mitotic spindle assembly by two different pathways in vitro. J. Cell Biol. 112, 925–40.

Schatz, C.A., Santarella, R., Hoenger, A., Karsenti, E., Mattaj, I.W., Gruss, O.J., Carazo-Salas, R.E., 2003. Importin [alpha]-regulated nucleation of microtubules by TPX2. EMBO J 22, 2060–2070.

Schiel, J.A., Park, K., Morphew, M.K., Reid, E., Hoenger, A., Prekeris, R., 2011. Endocytic membrane fusion and buckling-induced microtubule severing mediate cell abscission. J. Cell Sci. 124, 1411–24.

Schumacher, J.M., Ashcroft, N., Donovan, P.J., Golden, A., 1998a. A highly conserved centrosomal kinase, AIR-1, is required for accurate cell cycle progression and segregation of developmental factors in Caenorhabditis elegans embryos. Development 125, 4391–402.

Schumacher, J.M., Golden, A., Donovan, P.J., 1998b. AIR-2: An Aurora/Ipl1-related protein kinase associated with chromosomes and midbody microtubules is required for polar body extrusion and cytokinesis in Caenorhabditis elegans embryos. J. Cell Biol. 143, 1635–46.

Scotto, L., Narayan, G., Nandula, S. V, Arias-Pulido, H., Subramaniyam, S., Schneider, A., Kaufmann, A.M., Wright, J.D., Pothuri, B., Mansukhani, M., Murty, V. V, 2008. Identification of copy number gain and overexpressed genes on chromosome arm 20q by an integrative genomic approach in cervical cancer: potential role in progression. Genes. Chromosomes Cancer 47, 755–65.

Scrofani, J., Sardon, T., Meunier, S., Vernos, I., 2015. Microtubule nucleation in mitosis by a RanGTP-dependent protein complex. Curr. Biol. 25, 131–40.

Sen, S., Zhou, H., Zhang, R.-D., Yoon, D.S., Vakar-Lopez, F., Ito, S., Jiang, F., Johnston, D., Grossman, H.B., Ruifrok, A.C., Katz, R.L., Brinkley, W., Czerniak, B., 2002. Amplification/overexpression of a mitotic kinase gene in human bladder cancer. J. Natl. Cancer Inst. 94, 1320–9.

Sharp, D.J., Brown, H.M., Kwon, M., Rogers, G.C., Holland, G., Scholey, J.M., 2000. Functional coordination of three mitotic motors in Drosophila embryos. Mol. Biol. Cell 11, 241–53.

Sharp, D.J., Yu, K.R., Sisson, J.C., Sullivan, W., Scholey, J.M., 1999. Antagonistic microtubule-sliding motors position mitotic centrosomes in Drosophila early embryos. Nat. Cell Biol. 1, 51–4.

Sharp, J.A., Plant, J.J., Ohsumi, T.K., Borowsky, M., Blower, M.D., 2011. Functional analysis of the microtubule-interacting transcriptome. Mol Biol Cell 22, 4312–4323.

Shi, Y., Reiman, T., Li, W., Maxwell, C.A., Sen, S., Pilarski, L., Daniels, T.R., Penichet, M.L., Feldman, R., Lichtenstein, A., 2007. Targeting aurora kinases as therapy in multiple myeloma. Blood 109, 3915–3921.

Shigeishi, H., Higashikawa, K., Takechi, M., 2014. Role of receptor for hyaluronan-mediated motility (RHAMM) in human head and neck cancers. J. Cancer Res. Clin. Oncol. 140, 1629–40.

Shim, S.Y., Perez de Castro, I., Neumayer, G., Wang, J., Park, S.K., Sanada, K., Nguyen, M.D., 2015. Phosphorylation of targeting protein for Xenopus kinesin-like protein 2 (TPX2) at threonine 72 in spindle assembly. J. Biol. Chem. 290, 9122–34.

Shrestha, R.L., Draviam, V.M., 2013. Lateral to end-on conversion of chromosome-microtubule attachment requires kinesins CENP-E and MCAK. Curr. Biol. 23, 1514–1526.

Silk, A.D., Holland, A.J., Cleveland, D.W., 2009. Requirements for NuMA in maintenance and establishment of mammalian spindle poles. J. Cell Biol. 184, 677–90.

Silva, P.M. a., Tavares, Á. a., Bousbaa, H., 2015. Co-silencing of human Bub3 and dynein highlights an antagonistic relationship in regulating kinetochore–microtubule attachments.

FEBS Lett. 589, 3588–3594.

Simpson-Lavy, K.J., Zenvirth, D., Brandeis, M., 2015. Phosphorylation and dephosphorylation regulate APC/C(Cdh1) substrate degradation. Cell Cycle 14, 3138–3145.

Snape, K., Hanks, S., Ruark, E., Barros-Núñez, P., Elliott, A., Murray, A., Lane, A.H., Shannon, N., Callier, P., Chitayat, D., Clayton-Smith, J., FitzPatrick, D.R., Gisselsson, D., Jacquemont, S., Asakura-Hay, K., Micale, M.A., Tolmie, J., Turnpenny, P.D., Wright, M., Douglas, J., Rahman, N., 2011. Mutations in CEP57 cause mosaic variegated aneuploidy syndrome. Nat. Genet. 43, 527–529.

Song, L., Rape, M., 2010. Regulated degradation of spindle assembly factors by the anaphase-promoting complex. Mol. Cell 38, 369–82.

Spicer, A.P., Roller, M.L., Camper, S.A., McPherson, J.D., Wasmuth, J.J., Hakim, S., Wang, C., Turley, E.A., McDonald, J.A., 1995. The human and mouse receptors for hyaluronan-mediated motility, RHAMM, genes (HMMR) map to human chromosome 5q33.2-qter and mouse chromosome 11. Genomics 30, 115–7.

Splinter, D., Tanenbaum, M.E., Lindqvist, A., Jaarsma, D., Flotho, A., Yu, K. Lou, Grigoriev, I., Engelsma, D., Haasdijk, E.D., Keijzer, N., Demmers, J., Fornerod, M., Melchior, F., Hoogenraad, C.C., Medema, R.H., Akhmanova, A., 2010. Bicaudal D2, dynein, and kinesin-1 associate with nuclear pore complexes and regulate centrosome and nuclear positioning during mitotic entry. PLoS Biol. 8, e1000350.

Steffen, W., Fuge, H., Dietz, R., Bastmeyer, M., Müller, G., 1986. Aster-free spindle poles in insect spermatocytes: evidence for chromosome-induced spindle formation? J. Cell Biol. 102, 1679–87.

Stehman, S.A., Chen, Y., McKenney, R.J., Vallee, R.B., 2007. NudE and NudEL are required for mitotic progression and are involved in dynein recruitment to kinetochores. J. Cell Biol. 178, 583–94.

Steuer, E.R., Wordeman, L., Schroer, T.A., Sheetz, M.P., 1990. Localization of cytoplasmic dynein to mitotic spindles and kinetochores. Nature 345, 266–8.

Stevens, D., Gassmann, R., Oegema, K., Desai, A., 2011. Uncoordinated loss of chromatid cohesion is a common outcome of extended metaphase arrest. PLoS One 6, e22969.

Stewart, S., Fang, G., 2005. Anaphase-Promoting Complex / Cyclosome Controls the Stability of TPX2 during Mitotic Exit 25, 10516–10527.

Sudakin, V., Chan, G.K., Yen, T.J., 2001. Checkpoint inhibition of the APC/C in HeLa cells is mediated by a complex of BUBR1, BUB3, CDC20, and MAD2. J. Cell Biol. 154, 925–36.

Suijkerbuijk, S.J.E., van Osch, M.H.J., Bos, F.L., Hanks, S., Rahman, N., Kops, G.J.P.L., 2010. Molecular causes for BUBR1 dysfunction in the human cancer predisposition syndrome mosaic variegated aneuploidy. Cancer Res. 70, 4891–900.

Syrovatkina, V., Fu, C., Tran, P.T., Dumont, S., Mitchison, T.J., Goshima, G., Scholey, J.M., Mogilner, A., Craig, E., Goshima, G., Wollman, R., Stuurman, N., Scholey, J.M., Vale, R.D., Saunders, W.S., Hoyt, M.A., Tanenbaum, M.E., Macůrek, L., Janssen, A., Geers, E.F., Alvarez-Fernández, M., Medema, R.H., Troxell, C.L., Sweezy, M.A., West, R.R.,

Reed, K.D., Carson, B.D., Pidoux, A.L., Cande, W.Z., McIntosh, J.R., Nabeshima, K., Nakagawa, T., Straight, A.F., Murray, A., Chikashige, Y., Yamashita, Y.M., Hiraoka, Y., Yanagida, M., Fu, C., Ward, J.J., Loiodice, I., Velve-Casquillas, G., Nedelec, F.J., Tran, P.T., Decottignies, A., Zarzov, P., Nurse, P., Tatebe, H., Goshima, G., Takeda, K., Nakagawa, T., Kinoshita, K., Yanagida, M., Garcia, M.A., Koonrugsa, N., Toda, T., West, R.R., Malmstrom, T., McIntosh, J.R., Erent, M., Drummond, D.R., Cross, R.A., Grissom, P.M., Fiedler, T., Grishchuk, E.L., Nicastro, D., West, R.R., McIntosh, J.R., Grishchuk, E.L., Efremov, A.K., Volkov, V.A., Spiridonov, I.S., Gudimchuk, N., Westermann, S., Drubin, D., Barnes, G., McIntosh, J.R., Ataullakhanov, F.I., Grishchuk, E.L., Spiridonov, I.S., Volkov, V.A., Efremov, A., Westermann, S., Drubin, D., Barnes, G., Ataullakhanov, F.I., McIntosh, J.R., Loïodice, I., Staub, J., Setty, T.G., Nguyen, N.P., Paoletti, A., Tran, P.T., Yamashita, A., Sato, M., Fujita, A., Yamamoto, M., Toda, T., Subramanian, R., Wilson-Kubalek, E.M., Arthur, C.P., Bick, M.J., Campbell, E.A., Darst, S.A., Milligan, R.A., Kapoor, T.M., Grishchuk, E.L., Spiridonov, I.S., McIntosh, J.R., Olmsted, Z.T., Riehlman, T.D., Branca, C.N., Colliver, A.G., Cruz, L.O., Paluh, J.L., Hagan, I., Yanagida, M., Casquillas, G.V., Fu, C., Berre, M. Le, Cramer, J., Meance, S., Plecis, A., Baigl, D., Greffet, J.J., Chen, Y., Piel, M., Tran, P.T., Blangy, A., Lane, H.A., d'Hérin, P., Harper, M., Kress, M., Nigg, E.A., Kapoor, T.M., Mayer, T.U., Coughlin, M.L., Mitchison, T.J., Saunders, A.M., Powers, J., Strome, S., Saxton, W.M., Kollu, S., Bakhoum, S.F., Compton, D.A., Lara-Gonzalez, P., Westhorpe, F.G., Taylor, S.S., Musacchio, A., Musacchio, A., Salmon, E.D., Vleugel, M., Hoogendoorn, E., Snel, B., Kops, G.J., Griffiths, K., Masuda, H., Dhut, S., Toda, T., Sanchez-Perez, I., Renwick, S.J., Crawley, K., Karig, I., Buck, V., Meadows, J.C., Franco-Sanchez, A., Fleig, U., Toda, T., Millar, J.B., West, R.R., Malmstrom, T., Troxell, C.L., McIntosh, J.R., Yamamoto, A., Hiraoka, Y., 2013. Antagonistic spindle motors and MAPs regulate metaphase spindle length and chromosome segregation. Curr. Biol. 23, 2423–9.

Tanaka, T., Kimura, M., Matsunaga, K., Fukada, D., Mori, H., Okano, Y., 1999. Centrosomal kinase AIK1 is overexpressed in invasive ductal carcinoma of the breast. Cancer Res. 59, 2041–4.

Tanenbaum, M.E., Macůrek, L., Galjart, N., Medema, R.H., 2008. Dynein, Lis1 and CLIP-170 counteract Eg5-dependent centrosome separation during bipolar spindle assembly. EMBO J. 27, 3235–45.

Tanenbaum, M.E., Macůrek, L., Janssen, A., Geers, E.F., Alvarez-Fernández, M., Medema, R.H., 2009. Kif15 cooperates with Eg5 to promote bipolar spindle assembly. Curr. Biol. 19, 1703–1711.

Tanenbaum, M.E., Medema, R.H., 2010. Mechanisms of centrosome separation and bipolar spindle assembly. Dev. Cell 19, 797–806.

Tang, Z., Sun, Y., Harley, S.E., Zou, H., Yu, H., 2004. Human Bub1 protects centromeric sister-chromatid cohesion through Shugoshin during mitosis. Proc. Natl. Acad. Sci. U. S. A. 101, 18012–7.

Terada, Y., Uetake, Y., Kuriyama, R., 2003. Interaction of Aurora-A and centrosomin at the microtubule-nucleating site in Drosophila and mammalian cells. J. Cell Biol. 162, 757–63.

Tolg, C., Hamilton, S.R., Morningstar, L., Zhang, J., Zhang, S., Esguerra, K. V, Telmer, P.G.,

Luyt, L.G., Harrison, R., McCarthy, J.B., Turley, E. a, 2010. RHAMM promotes interphase microtubule instability and mitotic spindle integrity through MEK1/ERK1/2 activity. J. Biol. Chem. 285, 26461–74.

Toole, B.P., 2001. Hyaluronan in morphogenesis. Semin. Cell Dev. Biol. 12, 79–87.

Toole, B.P., 2004. Hyaluronan: from extracellular glue to pericellular cue. Nat. Rev. Cancer 4, 528–39.

Tooley, J.G., Miller, S.A., Stukenberg, P.T., 2011. The Ndc80 complex uses a tripartite attachment point to couple microtubule depolymerization to chromosome movement. Mol. Biol. Cell 22, 1217–26.

Townsley, F.M., Ruderman, J. V, 1998. Proteolytic ratchets that control progression through mitosis. Trends Cell Biol. 8, 238–244.

Trokter, M., Mücke, N., Surrey, T., 2012. Reconstitution of the human cytoplasmic dynein complex. Proc. Natl. Acad. Sci. U. S. A. 109, 20895–900.

Tsai, M.-Y., Wiese, C., Cao, K., Martin, O., Donovan, P., Ruderman, J., Prigent, C., Zheng, Y., 2003. A Ran signalling pathway mediated by the mitotic kinase Aurora A in spindle assembly. Nat. Cell Biol. 5, 242–8.

Tsai, M.-Y., Zheng, Y., 2005. Aurora A kinase-coated beads function as microtubule-organizing centers and enhance RanGTP-induced spindle assembly. Curr. Biol. 15, 2156–2163.

Tulu, U.S., Fagerstrom, C., Ferenz, N.P., Wadsworth, P., 2006. Molecular requirements for kinetochore-associated microtubule formation in mammalian cells. Curr. Biol. 16, 536–41.

Turley, E.A., Austen, L., Vandeligt, K., Clary, C., 1991. Hyaluronan and a cell-associated hyaluronan binding protein regulate the locomotion of ras-transformed cells. J. Cell Biol. 112, 1041–7.

Turley, E. a, Moore, D., Hayden, L.J., 1987. Characterization of hyaluronate binding proteins isolated from 3T3 and murine sarcoma virus transformed 3T3 cells. Biochemistry 26, 2997–3005.

Uteng, M., Hentrich, C., Miura, K., Bieling, P., Surrey, T., 2008. Poleward transport of Eg5 by dynein-dynactin in Xenopus laevis egg extract spindles. J. Cell Biol. 182, 715–726.

Vale, R.D., 2003. The Molecular Motor Toolbox for Intracellular Transport. Cell 112, 467–480.

van Heesbeen, R.G.H.P., Tanenbaum, M.E., Medema, R.H., 2014. Balanced Activity of Three Mitotic Motors Is Required for Bipolar Spindle Assembly and Chromosome Segregation. Cell Rep. 8, 948–956.

van Zon, W., Ogink, J., ter Riet, B., Medema, R.H., te Riele, H., Wolthuis, R.M.F., 2010. The APC/C recruits cyclin B1-Cdk1-Cks in prometaphase before D box recognition to control mitotic exit. J. Cell Biol. 190, 587–602.

Vanneste, D., Takagi, M., Imamoto, N., Vernos, I., 2009. The role of Hklp2 in the stabilization and maintenance of spindle bipolarity. Curr. Biol. 19, 1712–7.

Varma, D., Monzo, P., Stehman, S. a, Vallee, R.B., 2008. Direct role of dynein motor in stable kinetochore-microtubule attachment, orientation, and alignment. J. Cell Biol. 182, 1045–54.

Varma, D., Wan, X., Cheerambathur, D., Gassmann, R., Suzuki, A., Lawrimore, J., Desai, A., Salmon, E.D., 2013. Spindle assembly checkpoint proteins are positioned close to core microtubule attachment sites at kinetochores. J. Cell Biol. 202, 735–46.

Venables, J.P., Klinck, R., Bramard, A., Inkel, L., Dufresne-Martin, G., Koh, C., Gervais-Bird, J., Lapointe, E., Froehlich, U., Durand, M., Gendron, D., Brosseau, J.-P., Thibault, P., Lucier, J.-F., Tremblay, K., Prinos, P., Wellinger, R.J., Chabot, B., Rancourt, C., Elela, S.A., 2008. Identification of alternative splicing markers for breast cancer. Cancer Res. 68, 9525–31.

Vink, M., Simonetta, M., Transidico, P., Ferrari, K., Mapelli, M., De Antoni, A., Massimiliano, L., Ciliberto, A., Faretta, M., Salmon, E.D., Musacchio, A., 2006. In vitro FRAP identifies the minimal requirements for Mad2 kinetochore dynamics. Curr. Biol. 16, 755–66.

Violin, J.D., Zhang, J., Tsien, R.Y., Newton, A.C., 2003. A genetically encoded fluorescent reporter reveals oscillatory phosphorylation by protein kinase C. J. Cell Biol. 161, 899–909.

Wadsworth, P., 2015. TPX2. Curr. Biol. 25, R1156-8.

Walczak, C.E., Cai, S., Khodjakov, A., 2010. Mechanisms of chromosome behaviour during mitosis. Nat Rev Mol Cell Biol 11, 91–102.

Walczak, C.E., Gan, E.C., Desai, A., Mitchison, T.J., Kline-Smith, S.L., 2002. The microtubule-destabilizing kinesin XKCM1 is required for chromosome positioning during spindle assembly. Curr. Biol. 12, 1885–9.

Walczak, C.E., Heald, R., 2008. Mechanisms of mitotic spindle assembly and function. Int. Rev. Cytol. 265, 111–58.

Walczak, C.E., Mitchison, T.J., Desai, A., 1996. XKCM1: a Xenopus kinesin-related protein that regulates microtubule dynamics during mitotic spindle assembly. Cell 84, 37–47.

Wang, C., Entwistle, J., Hou, G., Li, Q., Turley, E. a, 1996. The characterization of a human RHAMM cDNA: conservation of the hyaluronan-binding domains. Gene 174, 299–306.

Wang, C., Thor, A.D., Moore, D.H., Zhao, Y., Kerschmann, R., Stern, R., Watson, P.H., Turley, E.A., 1998. The overexpression of RHAMM, a hyaluronan-binding protein that regulates ras signaling, correlates with overexpression of mitogen-activated protein kinase and is a significant parameter in breast cancer progression. Clin. Cancer Res. 4, 567–76.

Wang, H., Brust-Mascher, I., Scholey, J.M., 2014. Sliding filaments and mitotic spindle organization. Nat. Cell Biol. 16, 737–9.

Wang, H.-W., Long, S., Ciferri, C., Westermann, S., Drubin, D., Barnes, G., Nogales, E., 2008. Architecture and Flexibility of the Yeast Ndc80 Kinetochore Complex. J. Mol. Biol. 383, 894–903.

Wang, X., Zhou, Y.-X., Qiao, W., Tominaga, Y., Ouchi, M., Ouchi, T., Deng, C.-X., 2006. Overexpression of aurora kinase A in mouse mammary epithelium induces genetic instability preceding mammary tumor formation. Oncogene 25, 7148–58.

Weaver, B.A.A., Cleveland, D.W., 2005. Decoding the links between mitosis, cancer, and chemotherapy: The mitotic checkpoint, adaptation, and cell death. Cancer Cell 8, 7–12.

Whitehead, C.M., Winkfein, R.J., Rattner, J.B., 1996. The relationship of HsEg5 and the actin

cytoskeleton to centrosome separation. Cell Motil. Cytoskeleton 35, 298–308.

Wijshake, T., Malureanu, L. a, Baker, D.J., Jeganathan, K.B., van de Sluis, B., van Deursen, J.M., 2012. Reduced life- and healthspan in mice carrying a mono-allelic BubR1 MVA mutation. PLoS Genet. 8, e1003138.

Wilmington, S.R., Matouschek, A., 2016. An Inducible System for Rapid Degradation of Specific Cellular Proteins Using Proteasome Adaptors. PLoS One 11, e0152679.

Wittmann, T., Boleti, H., Antony, C., Karsenti, E., Vernos, I., 1998. Localization of the kinesin-like protein Xklp2 to spindle poles requires a leucine zipper, a microtubule-associated protein, and dynein. J Cell Biol 143, 673–685.

Wittmann, T., Hyman, A., Desai, A., Planck, M., Cell, M., Dresden, D.-, 2001. The spindle : a dynamic assembly of microtubules and motors. Nat. Cell Biol. 3, 28–31.

Wittmann, T., Wilm, M., Karsenti, E., Vernos, I., 2000. TPX2, A novel xenopus MAP involved in spindle pole organization. J. Cell Biol. 149, 1405–18.

Wojcik, E., Basto, R., Serr, M., Scaërou, F., Karess, R., Hays, T., 2001. Kinetochore dynein: its dynamics and role in the transport of the Rough deal checkpoint protein. Nat. Cell Biol. 3, 1001–7.

Wollman, R., Cytrynbaum, E.N., Jones, J.T., Meyer, T., Scholey, J.M., Mogilner, A., 2005. Efficient chromosome capture requires a bias in the “search-and-capture” process during mitotic-spindle assembly. Curr. Biol. 15, 828–32.

Wong, J., Fang, G., 2006. HURP controls spindle dynamics to promote proper interkinetochore tension and efficient kinetochore capture. J. Cell Biol. 173, 879–91.

Woodcock, S.A., Rushton, H.J., Castañeda-Saucedo, E., Myant, K., White, G.R.M., Blyth, K., Sansom, O.J., Malliri, A., 2010. Tiam1-Rac signaling counteracts Eg5 during bipolar spindle assembly to facilitate chromosome congression. Curr. Biol. 20, 669–75.

Wordeman, L., Mitchison, T.J., 1995. Identification and partial characterization of mitotic centromere- associated kinesin, a kinesin-related protein that associates with centromeres during mitosis. J. Cell Biol. 128, 95–104.

Xu, X., Wang, X., Xiao, Z., Li, Y., Wang, Y., 2011. Two TPX2-Dependent Switches Control the Activity of Aurora A. PLoS One 6, e16757.

Yamada, Y., Itano, N., Narimatsu, H., Kudo, T., Hirohashi, S., Ochiai, A., Niimi, A., Ueda, M., Kimata, K., 1999. Receptor for hyaluronan-mediated motility and CD44 expressions in colon cancer assessed by quantitative analysis using real-time reverse transcriptase-polymerase chain reaction. Jpn. J. Cancer Res. 90, 987–92.

Yamano, Y., Uzawa, K., Shinozuka, K., Fushimi, K., Ishigami, T., Nomura, H., Ogawara, K., Shiiba, M., Yokoe, H., Tanzawa, H., 2008. Hyaluronan-mediated motility: a target in oral squamous cell carcinoma. Int. J. Oncol. 32, 1001–9.

Yang, B., Yang, B.L., Savani, R.C., Turley, E.A., 1994. Identification of a common hyaluronan binding motif in the hyaluronan binding proteins RHAMM, CD44 and link protein. EMBO J. 13, 286–96.

Yang, B., Zhang, L., Turley, E. a, 1993. Identification of two hyaluronan-binding domains in the

hyaluronan receptor RHAMM. J. Biol. Chem. 268, 8617–23.

Yang, C.W., Su, J., Tsou, A.P., Chau, G.L., Liu, H.L., Chen, C.H., Chien, C.Y., Chou, C.K., 2005. Integrative genomics based identification of potential human hepatocarcinogenesis-associated cell cycle regulators: RHAMM as an example. Biochem. Biophys. Res. Commun. 330, 489–497.

Yao, X., Abrieu, A., Zheng, Y., Sullivan, K.F., Cleveland, D.W., 2000. CENP-E forms a link between attachment of spindle microtubules to kinetochores and the mitotic checkpoint. Nat. Cell Biol. 2, 484–91.

Zeng, K., Bastos, R.N., Barr, F.A., Gruneberg, U., 2010. Protein phosphatase 6 regulates mitotic spindle formation by controlling the T-loop phosphorylation state of Aurora A bound to its activator TPX2. J. Cell Biol. 191, 1315–1332.

Zhang, D., Hirota, T., Marumoto, T., Shimizu, M., Kunitoku, N., Sasayama, T., Arima, Y., Feng, L., Suzuki, M., Takeya, M., Saya, H., 2004. Cre-loxP-controlled periodic Aurora-A overexpression induces mitotic abnormalities and hyperplasia in mammary glands of mouse models. Oncogene 23, 8720–8730.

Zhang, X., Ems-mcclung, S.C., Walczak, C.E., 2008. Aurora A Phosphorylates MCAK to Control Ran-dependent Spindle Bipolarity 19, 2752–2765.

Zheng, Y., Wong, M.L., Alberts, B., Mitchison, T., 1995. Nucleation of microtubule assembly by a gamma-tubulin-containing ring complex. Nature 378, 578–83.

Zhou, H., Kuang, J., Zhong, L., Kuo, W.L., Gray, J.W., Sahin, A., Brinkley, B.R., Sen, S., 1998. Tumour amplified kinase STK15/BTAK induces centrosome amplification, aneuploidy and transformation. Nat. Genet. 20, 189–93.

Zhou, J., 2002. Attachment and tension in the spindle assembly checkpoint. J. Cell Sci. 115, 3547–3555.

Zhu, C., Zhao, J., Bibikova, M., Leverson, J.D., Bossy-Wetzel, E., Fan, J.-B., Abraham, R.T., Jiang, W., 2005. Functional analysis of human microtubule-based motor proteins, the kinesins and dyneins, in mitosis/cytokinesis using RNA interference. Mol. Biol. Cell 16, 3187–99.

Zlobec, I., Terracciano, L., Tornillo, L., Günthert, U., Vuong, T., Jass, J.R., Lugli, A., 2008. Role of RHAMM within the hierarchy of well-established prognostic factors in colorectal cancer . Gut 57, 1413–1419.

Zur, A., Brandeis, M., 2001. Securin degradation is mediated by fzy and fzr, and is required for complete chromatid separation but not for cytokinesis. EMBO J. 20, 792–801.